

# Probabilistic Safety Assessment of Multi-functional Flood Defences



**Juan Pablo Aguilar López**

# **Probabilistic Safety Assessment of Multi-functional Flood Defences**

Promotion committee:

Prof. dr. ir. G.P.M.R. Dewulf  
Prof. dr. S.J.M.H. Hulscher  
Dr. J.J. Warmink  
Dr. R.M.J. Schielen

University of Twente, Chairman/Secretary  
University of Twente, Promotor  
University of Twente, Co-promotor  
University of Twente, Co-promotor

Prof.dr.ir. M. Kok  
Prof. ir. A.C.W.M. Vrouwenfelder  
Prof.dr. M. van der Meijde  
Prof.dr. R.W.M.R.J. Ranasinghe

Technical University of Delft  
Technical University of Delft  
University of Twente  
University of Twente

Other members:

dr. J.B. Sellmeijer



This research is supported by the Dutch Technology Foundation STW, which is part of the Netherlands Organisation for Scientific Research (NWO), and which is partly funded by the Ministry of Economic Affairs (Project number: P10-28/12178).



This research is part of the program on Integral and Sustainable Design of Multifunctional Flood Defences.

Cover design: Juan Pablo Aguilar López

Copyright © 2016 by Juan Pablo Aguilar López, Enschede, the Netherlands.

All rights reserved. No part of this book may be reproduced, stored in a retrieval system, or transmitted in any form or by any means, without the written permission of the author.

Printed by Gildeprint

DOI: 10.3990/1.9789036542586

ISBN 978-90-365-4258-6



**PROBABILISTIC SAFETY ASSESSMENT  
OF MULTI-FUNCTIONAL FLOOD DEFENCES**

**DISSERTATION**

to obtain  
the degree of doctor at the University of Twente,  
on the authority of the rector magnificus  
Prof.dr. T.T.M. Palstra,  
on account of the decision of the graduation committee,  
to be publicly defended  
on Friday the 9<sup>th</sup> of December 2016 at 16:45hrs

by

**Juan Pablo Aguilar López**

born on the 9<sup>th</sup> of December 1981  
in Bogotá, Colombia

This thesis was approved by:

Prof. dr. S.J.M.H. Hulscher

Dr. J.J. Warmink

Dr. R.M.J. Schielen

Promotor

Co-promotor

Co-promotor

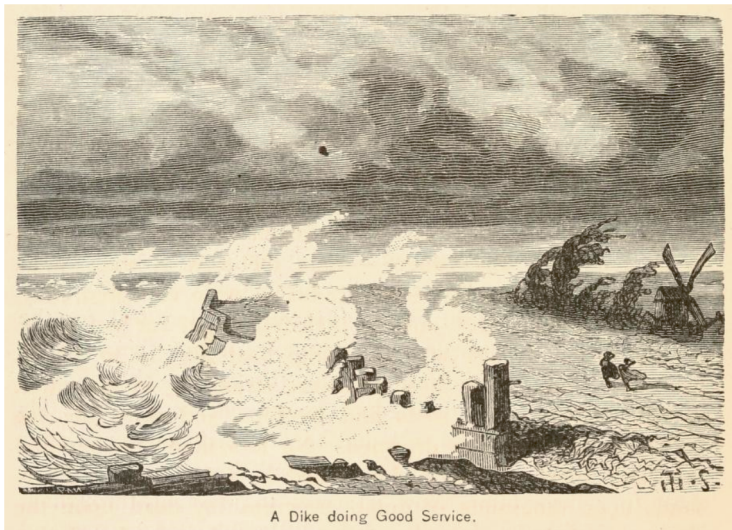
*'By three methods we may learn wisdom: First, by reflection, which is the noblest; Second, by imitation, which is the easiest; and third by experience, which is the bitterest.'*

*Confucius (551 BC - 479 BC)*



# Preface

The children's book called "Hans Brinker or the silver skates" was written by the American author Mary Mapes Dodge and first time published in 1865. The main plot developed around the story of a poor and honourable young boy named Hans Brinker and his younger sister Gretel who eagerly wanted to participate in December's great ice skating race on the frozen canals. The book was originally subtitled as a "story of life in Holland" and aimed to depict the Dutch life on the 1800's to the young American readers. The author dedicates chapter number two, to try to describe in detail, the atypical and yet fascinating landscapes and daily life of what she refers to as *Contrary-land*. A place which has a vast portion of the land, laying below the level of the sea. Where dikes, ditches and canals are everywhere to be seen. Where often the keels of floating ships are higher than the roofs of the dwellings. And she questions: "Which is Holland? The shores or the water?". Since those early times, it was already acknowledged that living in the Netherlands meant to have the blue colour always present in the lower parts of the landscape as well. In the same manner, this same landscape could be suddenly split in two by a green and brownish stripe where people tend to go whenever the waters got angry.



Storm Illustration extracted from "Hans Brinker or the Silver Skates, Dodge (1876)"

“*Angry*” was the expression used by the father of the main character in “The Hero of Haarlem”, a child’s story taught as lesson 62 in school during the English reading class in the same Novel.

This inner story described how a little boy saved the town of Haarlem by putting his finger inside a leak of a dike in order to avoid an imminent catastrophe. He spent the whole night in the freezing cold retaining water flow until he was found in the next morning by a clergyman who was walking back home on a trail located over the dike. In that way, the little boy saved the town and the story inspired the young readers in the novel.



**Hero of Haarlem. Illustration extracted from “Hans Brinker or the Silver Skates, Dodge (1876)”**

The story tells, that Mr. Raff Brinker had been employed for several years for the maintenance of the dikes which kept the city safe during the angry water times. After identifying a weak leakage spot near the Veermyk sluice, the midst of a severe storm impaired the worker’s vision making him fall from a scaffolding. In this sense, the story also reflects the importance of the dikes to the Dutch community and how since the early days of Dutch history flood risk has represented a major threat to life. Nevertheless, the early Dutch way of living did not succumb to fear but on the contrary it has defied the “angry waters” by using the dikes as habitable spaces and/or access pathways as well. Both traits are also described by Dodge, who also stated in her book that: “*Sometimes the dikes give way or spring a leak, and the most disastrous results ensue. Yet, They*

*are high and wide, and the tops of some of them are covered with buildings and trees. They have even fine public roads on them, from which horses may look down upon wayside cottages”.*

After all previous highlights of all sort of flood defence technicalities, is natural that the young reader’s mind will be intrigued by one main question:

*“If dikes had structures of considerable size such as buildings and roads embedded, what are the chances that the whole flood defence reliability can be changed by one kid’s finger ?“*

The present study aims to elucidate a very small and yet significant part of this complex question which directly relates to the influence of structural embedments, in the probabilistic design and assessment of a multi-functional flood defence. Note that the fundamental support for the idea of expressing a system performance in terms of a probabilistic measure comes from the acknowledgement of its uncertain nature.

The book of Hans Brinker on its own becomes a large source of uncertainty if taken into account that the author had never visited the Netherlands before publishing the novel.



# Contents

Preface .....	vii
Contents .....	xi
Summary.....	xv
Samenvatting .....	xviii
<b>1. Introduction .....</b>	<b>1</b>
1.1 Multi-functional flood defences (MFFD's).....	1
1.2 Failure mechanisms .....	4
1.2.1 State of the art of piping erosion .....	6
1.2.2 State of the art of overtopping .....	6
1.2.3 State of the art of slope stability.....	7
1.3 Probabilistic design of flood defences .....	8
1.3.1 Probabilistic design versus probabilistic assessment.....	8
1.3.2 Limit state design .....	9
1.3.3 Reliability Methods.....	10
1.3.4 Fault tree analysis of flood defences.....	12
1.3.5 Dutch flood safety standards.....	13
1.4 Structural embedments .....	15
1.5 Design choices and their impact on the structural safety.....	17
1.5.1 Model selection for probabilistic design and assessment.....	19
1.5.2 Emulation of models.....	20
1.5.3 Correlation and spatial variability modelling .....	21
1.6 Problem definition .....	22
1.7 Objective and research questions.....	24
1.8 Methodology .....	24
1.9 Thesis outline.....	26
<b>2. Soil stochastic parameter correlation impact in the piping erosion safety assessment.....</b>	<b>27</b>
2.1 Introduction.....	28
2.2 Limit State Safety Assessment Method.....	31
2.2.1 PE Sellmeijer revised limit state equation.....	31
2.2.2 Hydraulic conductivity by Kozeny-Carman equation.....	34
2.2.3 Copula correlation models.....	35
2.2.4 Goodness of fit tests.....	37
2.2.5 Reliability method: Monte Carlo with copula random sampling.....	39
2.3 Case study: Lekdijk.....	39

2.3.1	Stochastic parameters.....	40
2.3.2	PE and Uplift/Heave probability estimation.....	40
2.3.3	Complementary data sets.....	41
2.4	Results: Correlation degree between K and $d_{70}$ .....	41
2.5	Results: Copula model selection and validation.....	44
2.5.1	Graphical method.....	44
2.5.2	Root mean square error (RMSE).....	45
2.5.3	Formal statistical goodness of fit test.....	46
2.6	Results: Correlation impact in the reliability assessment.....	47
2.6.1	Impact in the limit state marginal distribution.....	47
2.6.2	Impact in the tail located events.....	49
2.6.3	Reliability Index ( $\beta$ ).....	50
2.7	Discussion.....	51
2.7.1	Research question 1.....	51
2.7.2	Research question 2.....	53
2.7.3	Research question 3.....	54
2.8	Conclusions and recommendations.....	56
2.9	Acknowledgements.....	57
<b>3.</b>	<b>Piping erosion safety assessment of flood defences founded over sewer pipes.....</b>	<b>59</b>
3.1	Introduction.....	60
3.2	IJkdijk full scale experiment.....	62
3.3	Method.....	63
3.3.1	Piping erosion model.....	65
3.3.2	Sellmeijer limit state recalibrated equation.....	69
3.3.3	Deterministic safety assessment.....	70
3.3.4	Probabilistic safety assessment.....	70
3.4	Data.....	72
3.4.1	Stochastic distributions of input variables.....	72
3.4.2	FEM emulator training data set.....	73
3.5	Results and discussions.....	74
3.5.1	Optimal erosion channel shape and size.....	74
3.5.2	Deterministic safety assessment for structural embedment.....	77
3.5.3	Probabilistic safety assessment.....	80
3.6	Conclusions.....	87
3.7	Acknowledgements.....	88

<b>4.</b>	<b>Wave overtopping probabilistic safety assessment of flood defences with roads on top .....</b>	<b>89</b>
4.1	Introduction.....	90
4.2	Theoretical erosion background.....	93
	4.2.1 Shear stress excess ( <b>T</b> ).....	93
	4.2.2 Erosion model as a function of <b>T</b> .....	95
4.3	Millingen aan de Rijn Wave Overtopping experiment with a road.....	96
	4.3.1 Millingen experiment part I: Scouring measurements.....	97
	4.3.2 Millingen experiment part II: Flow depths and velocity measurements.....	98
4.4	CFD emulation for probabilistic analysis.....	98
	4.4.1 CFD models.....	100
	4.4.2 Emulator surfaces construction.....	103
	4.4.3 <b>CE</b> functions .....	104
	4.4.4 Probabilistic safety assessment .....	106
4.5	Results .....	110
	4.5.1 Effects on the excess shear stress.....	110
	4.5.2 $C_E$ curves from Millingen measurements.....	112
	4.5.3 Scouring depth profiles.....	113
	4.5.4 Probability of failure.....	116
4.6	Discussion.....	119
4.7	Conclusions.....	123
4.8	Acknowledgements.....	124
<b>5.</b>	<b>Discussion .....</b>	<b>125</b>
5.1	Applicability of correlation modelling for piping erosion MFFD design (Chapter 2).....	125
5.2	Applicability of the fictitious permeability method (Chapter 3) .....	129
5.3	Applicability of the shear stress excess method (Chapter 4).....	134
5.4	Effects derived from other structural embedments .....	137
5.5	Applicability of emulation techniques for safety assessments.....	140
5.6	MFFD's safety assessment in an international context .....	141
5.7	Quantification of the effect of the design choices in the MFFD safety.....	141
5.8	Additional effects from the design choices.....	145
<b>6.</b>	<b>Conclusions and recommendations.....</b>	<b>147</b>
6.1	Research question 1 .....	147
6.2	Research question 2.....	148
6.3	Research question 3.....	149
6.4	Synthesis.....	150

6.5	Final Recommendations.....	151
<b>7.</b>	<b>References .....</b>	<b>153</b>
<b>8.</b>	<b>Appendices.....</b>	<b>165</b>
A.1	GCDM Crest validation.....	165
A.2	Landward slope validation.....	167
A.3	Overtopping times validation.....	168
A.4	Friction loss coefficients ( $\beta_i$ ) for different cross sections.....	169
A.5	Sellmeijer modified limit state function 2011.....	170
<b>9.</b>	<b>List of Figures.....</b>	<b>171</b>
<b>10.</b>	<b>List of Tables .....</b>	<b>173</b>
<b>11.</b>	<b>List of Symbols .....</b>	<b>175</b>
<b>12.</b>	<b>List of Publications .....</b>	<b>179</b>
<b>13.</b>	<b>Acknowledgments.....</b>	<b>181</b>
<b>14.</b>	<b>About the Author .....</b>	<b>183</b>

# Summary

The state of the art related to flood defences design and assessment show that the most common adaptation measures for tackling the uncertainties regarding climate change and demographic explosion, often involve an increase in size of these water-retaining structures. The shortage of habitable areas in the deltaic zones and the required increase in dimensions gave birth to the multifunctional flood defence concept. The main idea behind the multifunctional flood defences is that the extra space that results from almost inevitable increase in dimensions can be exploited by including additional non-water retaining functions such as commercial, recreational, ecological and habitational space. The inclusion of these new functions will also allow these defences to be financially feasible as their marginal cost reduces due to the expected benefits from the additional function allocation. The addition of functions will require structural embedments for connecting them to the transport, sewage, water supply, and electricity networks. Flood defences are exposed to deterioration processes known as “failure mechanisms” which may be triggered during flood events. The embedment of hard structures derived from the connecting requirements to the different infrastructure networks will have an impact on these processes and their frequency of occurrence.

In the last decades, due to the advance in computing capability, the structural design discipline has migrated towards the implementation of probabilistic safety assessments for existing structures and for new designs. Moreover, probabilistic target values are now being included in the latest flood risk policies and normative codes. Yet, most of these values are defined based on the results of probabilistic assessments performed for flood defences which have no other function besides the water retaining one. The inclusion of non-water retaining structures will have an impact in most of the failure mechanisms and consequently their safety estimated values.

In the particular case of the Netherlands, the VNK project which is the largest national flood risk assessment study, concluded that despite the large number of potential failure mechanisms only a few of them account for most of the estimated failure probability given the actual state of the flood defence system. Especially, the ones which were described by an erosive process such as piping and wave overtopping grass cover failure. This does not mean that only these two failure mechanisms are important to assess or that they are the most frequently registered cases. It also means that the associated uncertainty to these failure mechanisms may be larger when compared to the uncertainty associated with other failure mechanisms.

Consequently, the scope narrowing approach of the present thesis is based on the assumption that the design choices for multifunctional flood defences that directly influence the erosion-based failure mechanisms may have the largest impact the flood

defence reliability. Consequently, they should be prioritized for a deeper study over the ones that influence non-erosion based failure mechanisms. Yet, it is acknowledged that all failure mechanisms are important. As a result, the objective of the present thesis is “*To determine and quantify the effects in the probabilistic design and safety assessment of erosion based failure mechanisms of MFFD’s, derived from the foundation and the embedment of hard structures*”.

The research was divided in two main components. The first part aimed to study the effects derived from the design and assessment choice of reducing the associated uncertainty of the materials involved in the failure mechanisms modelling. The second part aimed to study the effects derived from geometrical design choices of the embedded structure such as size and location. In order to do that, one case studies was used for the first part and two more for the second part.

In Chapter 2, the first case study correspond to the assessment of the effects on the probabilistic safety assessment from reducing the material uncertainty by including the “potential” correlation effect between the representative grain size  $d_{70}$  and the foundation aquifer hydraulic conductivity variable  $K$ . This is done for the piping erosion failure mechanism assessed via the revised Sellmeijer limit state equation. The results showed that correlation between  $d_{70}$  and  $K$  has a significant effect on the failure probability of structures for the case of piping erosion. This is because it increases the probability of having small  $d_{70}$  grains in combination with large hydraulic conductivity values which analogously reduces the probability high conductivity values in combination with small  $d_{70}$  grain diameters. These effects are even more important for multifunctional flood defences as they can help to reduce the minimum required seepage length for achieving its safety target values.

The second case study is presented in Chapter 3 and corresponds to the assessment of the effects on the probabilistic safety assessment for piping erosion from embedding a sewer pipe under a flood defence. This assessment is done by implementing a finite element model in combination with emulation techniques which allow the modification of the sewer pipe characteristics for assessing the effects of size and location. The results showed that for the studied case, the embedment of sewer pipes inside the aquifer foundation of multifunctional flood defences will always represent an increase in safety against piping erosion. The degree of improvement of the safety is conditioned to the location of the pipe, the size of the pipe, the aquifer depth, the aquifer confinement and the aquifer equivalent hydraulic conductivity.

The third and final case study is presented in Chapter 4. This case study consists of the assessment of a flood defence exposed to wave overtopping which threatens its safety due to the erosion of the grass cover. The effects on the failure probability due to these failure mechanisms are assessed by including the change in the overtopped wave’s hydrodynamics from computational modelling in combination with emulation

techniques. In addition, the grass cover quality spatial variability is also included in the analysis which allows to determine which zones are more prone to failure for dikes with and without a road. The results showed that the presence of asphalt roads will reduce the safety against grass cover erosion due to wave overtopping. This reduction is explained by the change in superficial material roughness and the presence of superficial profile irregularities which increase the likelihood of localized failures. In addition, it is also observed how the grass quality spatial variability and the stochastic nature of the localized resistance variables are more important indicators of potential failure for dikes with roads on top.

In Chapter 5, the applicability of the methods and the implications of the assumptions were further discussed. In terms of implications it is shown that the correlation omission may result in wider structures. In addition, the implementation of the new Sellmeijer limit state equation may not be suitable in its actual state for assessing defences with sewer pipes underneath. In relation with the grass erosion due to overtopping, the erodability values of grass should be represented as functions of the critical shear stress for different grass qualities instead of constant values for each grass quality. In order to compare the importance of each choice in the total safety of the flood defence, the change in the reliability index was estimated for each choice.

Finally in Chapter 6, the main conclusions are compiled and further recommendations are listed. The main outcome of this thesis is that the inclusion of hard structures in the flood defence have significant effects in their reliability which is not negligible. These effects are derived from design uncertainties associated to the materials and the dimensioning of the multifunctional flood defences. Furthermore, it was observed that these effects may be either positive or negative in percentages of as much as 20% for the studied cases, with respect to the case of an identical flood defence which doesn't have an embedded structure. Therefore, it is recommended to include this effects in the future safety assessments of multifunctional flood defences and to update the actual design tools so that the additional embedded structures may be included.

# Samenvatting

Het tekort aan bewoonbare gebieden in delta's en de vereiste toename in afmetingen van waterkeringen gezien klimaatverandering, heeft geleid tot het ontstaan van het multifunctionele waterkering (MFWK) concept. Het belangrijkste idee achter dit concept is dat de extra ruimte, die gecreëerd wordt als gevolg van de quasi onvermijdelijke toename in afmetingen van toekomstige waterkeringen, geëxploiteerd kan worden met extra niet-waterkerende functies zoals commerciële, recreatieve, ecologische en woonruimte. De opname van deze extra functies maakt grotere waterkeringen financieel haalbaar aangezien marginale kosten verminderen door de verwachte voordelen van deze extra functies. Deze extra functies vereisen echter ook structurele inbeddingen en funderingen om deze ruimte aan te sluiten op het vervoer, riolering, waterleiding, en elektriciteitsnetwerken. Deze extra verankering zal de veiligheid van de multifunctionele waterkering veranderen ten opzichte van conventionele waterkeringen van dezelfde afmetingen.

Als gevolg van de toegenomen reken capaciteit, is structureel ontwerp als discipline in de laatste decennia gemigreerd naar de uitvoering van probabilistische veiligheidsbeoordelingen van structuren. Bovendien worden probabilistische streefwaarden nu ook opgenomen in beleid rond overstromingsrisico en in normatieve codes gezien de nood aan officiële risico-gebaseerde veiligheidsnormen. Deze evaluaties bestaan uit het inschatten van de faalkans van structuren of systemen opgebouwd uit structuren als gevolg van hun belangrijkste faalprocessen. Deze processen zijn bekend als "faalmechanismen" die geactiveerd kunnen worden tijdens overstromingen. Het opnemen van structuren naast de waterkeringen zelf, zal een impact hebben op het optreden van deze faalmechanismen en bijgevolg op de geschatte veiligheidswaarden. Voor het specifieke geval van Nederland, hebben verschillende studies rond overstromingsrisico geconcludeerd dat ondanks het grote aantal potentiële faalmechanismen slechts een paar mechanismen instaan voor het grootste deel van de geschatte faalkans gezien de werkelijke toestand van de waterkering. Het gaat dan vooral over faalmechanismen die toegeschreven worden aan een erosief proces, zoals "piping" en falen van grasmatten door golfoverslag. De scope van de huidige studie is bijgevolg verfijnd, gebaseerd op de veronderstelling dat ontwerpkeuzes die de erosie gerelateerde faalmechanismen direct beïnvloeden, de grootste gevolgen zouden hebben op de totale betrouwbaarheid van de multifunctionele waterkering. Daarom moeten deze ontwerpkeuzes geprioriteerd worden voor een diepere studie boven ontwerpkeuzes die niet-erosie gerelateerde faalmechanismen beïnvloeden. Toch wordt erkend dat alle faalmechanismen belangrijk zijn.

Als gevolg daarvan is het doel van dit proefschrift "*Het determineren en kwantificeren van de effecten van erosie-gerelateerde faalmechanismen van MFWK's, afkomstig van de fundering en inbedding van harde structuren, op het probabilistische ontwerp en de veiligheidsbeoordeling*".

Het onderzoek is opgesplitst in twee hoofdonderdelen. Het eerste deel bestudeert het effect van ontwerp en evaluatie keuzes gericht op het verminderen van de onzekerheid in materialen bij het modelleren van faalmechanismen. Het tweede deel bestudeert het effect van geometrisch ontwerp keuzes van de ingebedde structuren, zoals de grootte en de locatie. Hiervoor werden casus studies gebruikt; een voor het eerste deel en twee voor het tweede deel.

In hoofdstuk 2, wordt in de eerste casus het effect bestudeerd van verminderde materiaalonzekerheid op de probabilistische veiligheidsbeoordeling door inbegrip van het "potentiele" correlatie effect tussen korrelgrootte  $d_{70}$  en de fundering aquifer geleidbaarheid variabele  $K$ . Dit is gedaan voor het faalmechanisme gerelateerd aan pijperosie dat geëvalueerd wordt met de herziene Sellmeijer grenstoestand vergelijking. De resultaten tonen aan dat de correlatie tussen  $d_{70}$  en  $K$  een significant effect heeft op de faalkans van structuren bij pijperosie. Dit is omdat het de kans op kleine  $d_{70}$  korrels in combinatie met grote  $K$  waarden verhoogt en in analogie de kans op hoge  $K$  in combinatie met kleine diameters  $d_{70}$  korrel vermindert. Deze effecten zijn nog belangrijker voor multifunctionele waterkeringen aangezien ze de minimaal vereiste kwelweglengte voor het bereiken van de veiligheid streefwaarden kunnen helpen verminderen.

De tweede casus wordt gepresenteerd in hoofdstuk 3 en betreft de beoordeling van het effect van een onder de waterkering ingebedde rioolbuis op de probabilistische veiligheidsbeoordeling voor pijperosie. Deze beoordeling gebeurt op basis van een eindige elementen model in combinatie met emulatietechnieken die variatie van de rioolbuis kenmerken toelaten om de effecten van grootte en locatie te evalueren. De resultaten tonen aan dat voor de onderzochte casus, de inbedding van rioolbuizen in de aquifer fundering van multifunctionele waterkeringen altijd een toegenomen veiligheid tegen pijperosie vertegenwoordigt. De mate waarin de veiligheid toeneemt, wordt geconditioneerd door de locatie van de buis, de diameter van de buis, de aquifer diepte, de aquifer begrenzing en de aquifer equivalente geleidbaarheid.

De derde en laatste casus wordt gepresenteerd in hoofdstuk 4. In deze casus wordt een waterkering geëvalueerd die blootgesteld wordt aan golfoverslag waarbij de veiligheid wordt bedreigd als gevolg van de erosie van de grasmat. De effecten van deze faalmechanismen op de faalkans worden beoordeeld met inbegrip van de veranderende hydrodynamica van de overslaande golf op basis van computermodellen in combinatie met emulatie technieken. Bovendien wordt de ruimtelijke variatie in grasmat kwaliteit ook opgenomen in de analyse, waardoor het mogelijk wordt om te bepalen welke zones

meer kans op falen hebben en dit voor dijken met en zonder weg. De resultaten tonen aan dat de aanwezigheid van asfaltwegen de veiligheid tegen grasmat erosie door golfoverslag zal verminderen. Deze daling wordt verklaard door de verandering in ruwheid van het oppervlakte materiaal en de aanwezigheid van onregelmatigheden in het oppervlakte profiel waardoor de kans op falen gelokaliseerd verhoogt. Daarnaast wordt ook waargenomen dat de ruimtelijke variabiliteit in graskwaliteit en de stochastische aard van gelokaliseerde resistentie variabelen belangrijke indicatoren zijn voor mogelijk falen van dijken waarop wegen lopen.

In hoofdstuk 5 worden de toepasbaarheid van de methoden en de gevolgen van de aannames verder besproken. Wat betreft gevolgen van aannames, wordt aangetoond dat het weglaten van correlatie tussen korrelgrootte en geleidbaarheid kan leiden tot bredere structuren. Bovendien blijkt dat de nieuwe Sellmeijer grenstoestand vergelijking in zijn huidige vorm mogelijk niet geschikt is voor de beoordeling van waterkeringen waaronder rioolbuizen lopen. Wat betreft graserosie door golfoverslag, moet de erosiegevoeligheid van gras weergegeven worden als functie van de kritische schuifspanning voor verschillende graskwaliteit in plaats van te werken met constante waarden voor elke graskwaliteit. Om het belang van elke keuze te vergelijken in de totale waterkering veiligheid, werd de verandering in de betrouwbaarheidsindex geschat voor elke keuze.

Tot slot worden in hoofdstuk 6 de belangrijkste conclusies gecompileerd en verdere aanbevelingen opgenomen. Het belangrijkste resultaat van dit proefschrift is dat de opname van harde structuren in de waterkering een significant effect hebben op hun betrouwbaarheid en dit effect is niet te verwaarlozen. Dit significant effect stamt uit ontwerp onzekerheden rond de materialen en de dimensionering van de multifunctionele waterkeringen. Voorts werd opgemerkt dat deze effecten zowel positief als negatief kunnen zijn en dit tot in 20% van de onderzochte gevallen, in vergelijking met een identieke waterkering zonder toegevoegde structuur. Daarom verdient het aanbeveling om deze effecten op te nemen in de toekomstige veiligheidsbeoordeling van multifunctionele waterkeringen en om de gebruikte ontwerptools bij te werken, zodat de extra ingebedde structuren erin opgenomen kunnen worden.

# Chapter 1

## Introduction

### 1.1 Multi-functional flood defences (MFFD's)

Multifunctional flood defences (MFFD's), are being conceived as an innovative and yet robust solution where flood defence components can be safely combined with non-water retaining components (Van Loon-Steensma and Vellinga, 2014). Sea level rise and climate change have proven to reduce the effectiveness of flood defence structural measures and consequently increase the risk of flooding (Klijn et al., 2015). The increase of dimensions is the most common adaptation measure for tackling the uncertainties that affect the safety of flood defences. This statement is the backbone of flood defence concepts such as the Delta dike (Knoeff and Ellen, 2011) or the “Un-breachable” dike (Vellinga et al., 2009) which intended to increase the safety by making defences sufficiently large so that the probability of failure is close zero. To achieve it, it was proposed that the current safety standards should be reduced by a factor of 100 to cope with climate change and the increasing demographic explosion (Silva and Van Velzen, 2008). Despite the fact that this value is not necessarily correct, it does reflect the necessity of flood risk management practitioners for developing longer-term adaptation strategies which may also account for the different future uncertainties. For the case of flood defences which are specially designed for coping with sea level rise for example, the heightening of the structures is the most recurrent adaptation measure as the marginal cost per capita is significantly reduced as a function of population density (Nicholls et al., 2011). For geotechnical related uncertainties, the increase in seepage lengths and slopes became the preferred adaptation measures. Note that all mentioned strategies will require an increase in the flood defence area allocation in the future planning. This “extra space” may be more efficiently used if additional functions besides the water retaining one are included as it will not only allow to reduce the population density but it will make these solutions more financially feasible.

This is better understood from the optimal cost-benefit perspective in which the acceptable level of risk can be formulated as an economic decision problem (Jonkman et al., 2004). For a conventional flood defence, the optimal design in economic terms is

represented by the point with the lowest total costs of the cost-benefit curve. This total cost is determined as the sum of the costs of the flood defence plus the expected value of the economic damage which the flood defence avoids. For significantly larger MFFD's, an additional term should be added (with a negative sign) to the total cost function, in order to include the added value of having the flood defence plus additional function(s) such as recreation, urban areas, commercial developments and etc. A good example of this larger structures is the “Super-Levee” (Stalenberg and Kikumori, 2008) located in Japan along the Arakawa river in the city of Tokyo (Figure 1-1). The former dike was widened and heightened for increasing its reliability. The extra generated space was urbanized so that this kind of solution becomes feasible from an economic point of view.



Figure 1-1 “Super Levee” board in Oshima Komatsugawa Park, Tokyo (Japan Times, (Brasor, 2010))

If the Dutch MFFD's are also intended to reduce the failure probabilities by a factor of 100, a significant increase in the dimensions of the flood defence is expected (e.g. height and width). Specifically for the Netherlands, the safety standards are quite high (between 1/100,000 years and 1/300 years) with respect to other countries like for example the U.S. in which post-Katrina standards were set to flooding return periods of 1/500 years (Link, 2010). The Dutch standards are set like this as almost 60% of the country is flood prone. To achieve even stricter standards as the ones intended for the Un-breachable dike for example, massive flood defences are required which may only become economically viable by including highly profitable additional functions. Despite these facts, the present thesis is developed around the idea that MFFD's should not be framed solely in the concept of massive financially feasible dunes, quay walls or embankments as this is just a side effect derived from the required reduction of failure probabilities.

The main idea of MFFD's then, must be defined as *“flood defences that can have additional functions while not compromising the main water retaining one”*. With this definition, a dike with a bicycle path on top which was strengthened by sheet piling for improving its resistance is a clear and existent example of a multifunctional flood defence. Note that, the sheet pile measure can change its failure probability by a factor of 100 without increasing its original dimensions or affecting its total flooding damage cost “significantly” plus the bicycle path represents a non-water retaining function which not necessarily generates enough profit to affect the cost benefit analysis. This kind of MFFD has additional functions which are not costly or beneficial enough (in monetary terms) so that they are worth to be included either on the flood defence cost or the resultant economic damage. Nevertheless, the inclusion of this additional functions does have an important effect in their structural safety as they may interfere with the deterioration processes that occur during a flood event. These processes are commonly referred to as failure mechanisms (Vrijling, 2001). Failure mechanisms can either occur on the flood defence or its foundation. Analogously, functions are located on either the flood defence or its foundation (see Figure 1-2).



**Figure 1-2 House and road in the Lekdijk in Vianen – Utrecht province**

For developing the additional functions of the MFFD's, the inclusion of hard structures inside their main “body” will be almost inevitable. Furthermore, these additional functions will require to be connected to the main infrastructure systems such as energy, sewage, communication and transport among others.

Despite the MFFD's concept is relatively new and not yet widely implemented, the inclusion or presence of structural embedments in the flood defences is a common issue all over the world (Allsop et al., 2007; Kanning et al., 2007; Danka and Zhang, 2015; Hoffmans et al., 2015). These foreign structures are referred along this thesis as “structural embedments”.

## 1.2 Failure mechanisms

Failure mechanisms are modelled based on the physical phenomena that better represents the deterioration process. In the year 2007, the FLOODSITE project (Allsop et al., 2007) compiled a large inventory of case specific sets of failure mechanisms of flood defences, with the aim to improve the available knowledge. Despite the fact that all possible failure mechanisms have a chance to occur, different studies have shown that only few of them account for most of the failure registered cases (Danka and Zhang, 2015). The most relevant are overflow, wave overtopping, inner slope stability and piping erosion (Figure 1-3).

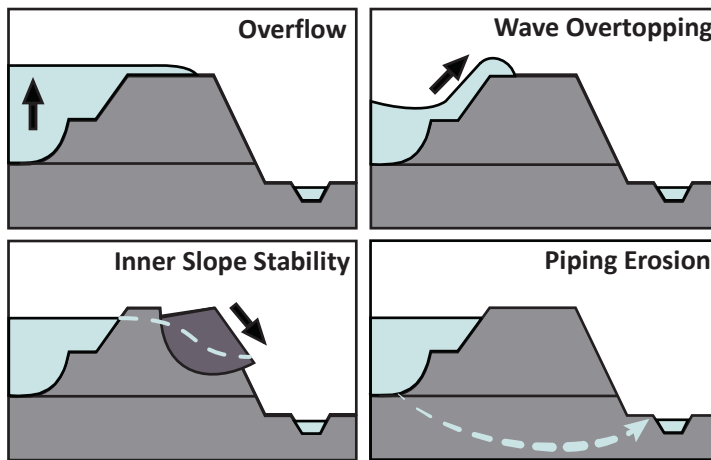


Figure 1-3 Schematics of the most dominant failure mechanisms

**Overflow:** Inflow of water towards the protected area due to an extreme water level event that exceeds the height of the flood defence.

**Wave Overtopping:** inflow of water volumes due to wave run-up process which may result in erosion of the crest and landward slope.

**Inner Slope Stability:** rotational soil mass displacement due to reduction of inner shear strength of the soil also referred to as “Macro-stability”. It can be triggered during high water events due to the variation of the phreatic level inside the flood defence.

**Piping Erosion:** loss of bearing capacity of the flood defence foundation due to cavity formation originated from soil transport due to high seepage flows.

From a historical point of view, the work of Van Baars and Van Kempen (2009) showed that, storm surges and high water levels account for 77% of the failure drivers of the historical registered dike breach events in the Netherlands between the years 1134

and 2006. Such drivers trigger different failure mechanisms which may result in dike failure during high water events. For example, erosion of the slopes and crest due to wave overtopping corresponded to 67% of the total registered dike failures. Inner slope stability of the landward slope accounted for 5% and internal backward erosion of the foundation (also known as piping erosion) accounted for 1% of the total registered failure.

The study by Vorogushyn et al. (2009) showed that these last four failure mechanisms were also the most dominant for dike breach events in Hungary for the period between 1954 and 2004, and for the Saxony province in Germany during the flood event of August 2002. Both of these observations are partially in agreement with the ones presented by Van Baars and Van Kempen (2009) in which overtopping derived failure mechanisms (overflow, wave overtopping and wave impact) accounted for 73% of the total failures.

However, 20% in the Hungarian case and 9.5% in the German case are observed for piping erosion with respect to the 1% observed in the Dutch case. This change in percentage can be explained by the facts that flood defences have been increased in height during the last 3 decades and also some of the piping evidence was wrongly attributed to animal induced failures. A more recent study by Danka and Zhang (2015) about worldwide dike failure statistics, resulted in very similar percentages for slope stability and overtopping with respect to both Hungarian and German cases. Yet this study was based on updated data which also includes an additional 3% for failure of hard structures embedded in the flood defences and 5.8% attributed to human or animal activities among others.

While all previously mentioned studies reiteratively conclude that a large portion of the total failure probability is attributable to only four dominant failure mechanisms, it is even more remarkable how much of this portion can be attributed to erosion based failure mechanisms solely. For the study of Van Baars and Van Kempen (2009), 68% of the total failures can be attributed to piping erosion and wave overtopping. For the study of Vorogushyn et al. (2009), 89% for the Hungarian case study and 79.7% for the Saxony case study may be attributed for the same failure mechanisms. For the study of Danka and Zhang (2015), 83%. For the VNK study, the percentages depend on which dike ring system is the statistic taken into account. However, one of the general conclusions of the study is that piping failure of riverine flood defences is more important than what they estimated in the past.

## 1.2.1 State of the art of piping erosion

For design and assessment of piping erosion, the methods have evolved over time as more experience has been acquired from field and experimental work (Hoffmans, 2014b). Nevertheless, most of these tools consist in simplified equations with no strong physical background to support them (Bligh, 1910; Lane, 1935). In the recent years, the piping erosion state of the art has also improved significantly (Sellmeijer et al., 2011; Van Esch et al., 2013; Van Beek, 2015). More detailed description of the state of the art of these failure mechanisms is also presented in Chapters 2 and 3. Yet, this failure mechanism still lacks of through investigation for cases where structural embedments are present.

## 1.2.2 State of the art of overtopping

For overtopping derived failure mechanisms (either by increase of the still water level or by wave overtopping), Edelman in 1954 (Van der Meer, 2009) noticed that dikes would fail by overtopping if:

1. The crest was too low so erosion and/or flooding may occur ;
2. The quality of the materials was bad so that infiltration happened too fast resulting in slope stability;
3. The inner slope was too steep which may lead to an inner slope stability or grass cover failure;

Hence, the countermeasures taken against wave overtopping consisted in ensuring inner slopes of at least 1:3 and heightening of the dikes to a level equivalent to the wave run-up height which occurs less than 2% of the time. Due to these measures and the actual strict flood safety standards, overtopping and overflowing are nowadays the less probable failure mechanisms in the actual flood defence system according to the results of the VNK2 (VNK2, 2014). However, in the past 30 years, the overtopping derived failure mechanisms have redrawn the attention of the flood risk community due to climate change and the risk-based national policy migration (Van der Most et al., 2014). Both require a better understanding of the processes so that future measures become more cost efficient. Hence, Dutch (Van der Meer, 2002; Hoffmans et al., 2008; Van der Meer et al., 2008) and international (Pullen et al., 2007; Dean et al., 2010; Thornton et al., 2011) research initiatives were developed with the aim of increasing the knowledge in the understanding, modelling and prediction of wave overtopping effects on flood defences.

The effects derived from the inclusion of embedded structures in the wave overtopping process has become a recent research interest as significant amount of the flood defences along the Dutch and international landscapes include different transitions and structural embedments (Verheij et al., 2012; Steendam et al., 2014). The next step is to develop methods which allow to include the effects of these transitions and/or structural embedments for flood risk reduction. A first approach known as the “cumulative hydraulic load method” for wave overtopping is already in development (Hoffmans, 2015). A significant part of the development of this method is related to the grass quality of the cover.

### **1.2.3 State of the art of slope stability**

With regard to the inner slope stability failure mechanism, greater advance has been achieved in the knowledge of this kind of failure as this deterioration process is of “paramount” importance not only for dikes but also for many other soil composed structures such as railway embankments, dams, road cuts and landfills. For the specific case of dikes, two primary adaptation measures are commonly implemented for avoiding inner slope stability failure due to high water events: the reduction of the slope and implementation of an inner berm. Note that both measures are oriented towards adding extra weight to the inner side so that the rotational mass displacement is less probable. These solutions are typically designed and tested by three main calculation methodologies: limit equilibrium, displacement based and resistance reduction methods (Weigao, 2015). The first method is the oldest of the three of them and therefore a larger amount of applications can be found in literature with respect to the other two. They are preferred by designers as their implementation is less complex with respect to Finite Element Model (FEM) based methods. For the specific case of slope stability assessments with structural embedments, the work of Paul and Kumar (1997) is an example of the implementation of limit equilibrium methods. Their results showed that failure can either occur from the localized failure of the interface between soil and structure or by a larger slip surface that includes the whole structure inside the collapsed soil mass. For the specific case of flood defences, the master research thesis of Jongerius (2016) aimed to quantify the effects on the failure probability derived from an structural house embedment. His study assessed the safety of the flood defence by assuming a limit equilibrium method conditioned to the collapsation of the embedded structure.

Both studies are important stepping stones towards the fully probabilistic assessment, but the circular failure surface and the inner pressure assumptions might not be correct for assessing these complex structures.

## **1.3 Probabilistic design of flood defences**

In the Netherlands, dikes were designed in the middle ages based on the most extreme water level registered in time plus one meter of freeboard in terms of height. After a disastrous flood event in 1953, a statistical approach was chosen, which allowed to extrapolate storm surge levels for flood defence design. In the later years and with the development of reliability theory in the 1980's, the Dutch hydraulic engineers developed and implemented assessment guidelines which allowed to quantify the flooding risks taking into account the different failure mechanisms (Vrijling, 2001). From the design philosophy point of view, structures can be designed and assessed either by the allowable stress design (ASD) criteria or by the limit state design (LSD) criteria (Vrouwenvelder, 2001). The ASD ensures that the exerted stresses of the structure due to service loads do not exceed the allowable stress of the materials of which the structure is composed so that the service state is satisfied (state in which the structures still fulfil its desired function). The way to cope with the uncertainty in the material is by the use of partial safety factors (Elishakoff, 2012). The LSD uses the ultimate load and resistance criteria to ensure that both service state and limit state (state of the structure before failure of one or more of the structural components) are fulfilled. This last one acknowledges the uncertainty of both load and resistance by including partial safety factors, model uncertainty factors or even the probabilistic description of the inputs for the more advanced probabilistic methods.

### **1.3.1 Probabilistic design versus probabilistic assessment**

The distinction between probabilistic design and probabilistic assessment has been difficult to determine as both terms are used indiscriminately in most of the reliability related literature. One of the main reasons for this lack of term distinction is that both the design of an unconstructed structure and an existent structured may have their safety "assessed". In other words, both the design and structure can be checked in order to determine if they comply with the legislative or recommended safety standards. Nevertheless the paper of Arangio (2012) clearly defines the distinction between the terms design and assessment by associating them to either non-existent and existent structures and the stage in which they are located inside the structural life cycle. This distinction applies to deterministic, semi-probabilistic and fully probabilistic implementation of both designs and assessments. For the present research, both terms were defined and used as:

**Probabilistic design:** Determination of the required dimensions, materials and safety factors to cope with the associated uncertainties of a *future* structure construction, operation and maintenance for achieving a required level of safety. The correct design choices and their inherent uncertainty representations should minimize the structural and operational costs while ensuring an associated target safety level.

**Probabilistic assessment:** Determination of the level of safety of an *existing* structure due to its operation, maintenance and deterioration given the actual set of load and resistance conditions which are expressed in a probabilistic manner. The assessment aims to determine the actual safety level of the structure which may or not comply with its associated target safety level.

Both probabilistic design and probabilistic assessment in the present research are implemented under a limit state philosophy which ensures that the performance of a structure is evaluated until achieving its failure state.

### 1.3.2 Limit state design

The LSD design philosophy is widely used for the risk-based design and assessment of structures (Vrouwenvelder, 2002), as it allows to define the general limit state in a mathematical form, i.e. :

$$Z = Z(x_1, x_2, x_3 \dots x_n) \quad \text{Eq. 1-1}$$

This general equation describes the failure state of a structure due to a certain deterioration process. In many situations, it is more convenient to separate it in two terms as:

$$Z = R(x_1, x_2, x_3 \dots x_n) - S(y_1, y_2, y_3 \dots y_n) \quad \text{Eq. 1-2}$$

where  $S$  represents the solicitation or “load” exerted by the structure,  $R$  represents the resistance of the structure against such load and  $x_{1\dots n}$  and  $y_{1\dots n}$  represent the input variables for estimating both  $R$  and  $S$ . The  $Z$  term represents the marginal resistance against the represented failure mechanism. When positive, the state of the structure is assumed as “not failed” whereas if negative it is assumed to be “failed”. For most of the structural designs and in particular for flood defences, the load term  $S$  represents the environmental/climatological drivers that trigger the occurrence of the failure mechanism. The increase or decrease in the probability of the failure mechanisms to occur is highly influenced by the likelihood of the environmental/climatological drivers to occur as well (e.g. wind speeds, storm surges, ice drifts and rainfall). However, the

uncertainty of these drivers is not possible to reduce. In consequence, the materials, the geometrical features and/or the operational guidelines become the most important tools for designers for reducing the flood risk until acceptable levels (Vrijling et al., 1998). These tools are normally reflected in the resistance term  $R$ . Adaptation to climate change and/or sea level is tackled with these tools but larger uncertainty in the likelihood of the water levels is also expected in the future (Voortman and Vrijling, 2004). Consequently, both  $R$  and  $S$  are uncertain which makes  $Z$  uncertain as well and therefore the limit state function can be expressed in terms of vectors  $\mathbf{X}$  and  $\mathbf{Y}$  of random variables as:

$$Z = R(\mathbf{X}_1, \mathbf{X}_2, \mathbf{X}_3 \dots \mathbf{X}_n) - S(\mathbf{Y}_1, \mathbf{Y}_2, \mathbf{Y}_3 \dots \mathbf{Y}_n) \quad \text{Eq. 1-3}$$

It is common to find that  $R$  and  $S$  may range from simple equations to highly complex computational models which may also include an stochastic component themselves (Yen, 1988). Examples of limit state equations for a significant number of different failure mechanisms of flood defences are presented in the report T04-06-01 of the FLOODsite project (Allsop et al., 2007).

### 1.3.3 Reliability Methods

The acknowledgement and complexity associated with the failure process uncertainty, represents the division line between choosing a deterministic or a probabilistic design. In particular, probabilistic design is the basis of the structural reliability discipline which aims to quantify the failure probability of structures and/or systems of structures. This is done by considering the associated uncertainties in their materials, loading conditions and operation. The “reliability” of a structure can be estimated by different methods depending on the amount of knowledge of the system; e.g. parameters stochastic nature, limit state definition and reliability function topology. In addition, there is also an obliged trade-off between accuracy and calculation time which also affects the reliability estimation (Koduru and Haukaas, 2010). With this in mind, the reliability discipline has grouped these design methods by levels (Thoft-Cristensen and Baker, 2012):

**Level I:** Deterministic values of  $R$  and  $S$  are multiplied by partial safety coefficients. These coefficients are calibrated from fully probabilistic analysis so that level I methods represent a semi-probabilistic design basis.

**Level II:** Probabilistic distributions are associated to the uncertainty variables ( $\mathbf{X}_1, \mathbf{X}_2, \mathbf{X}_3 \dots \mathbf{X}_n$  and  $\mathbf{Y}_1, \mathbf{Y}_2, \mathbf{Y}_3 \dots \mathbf{Y}_n$ ). Later, they are evaluated in an “idealized”

failure surface for obtaining an approximation of the failure probability ( $P_f$ ) and/or the reliability index ( $\beta$ ). These methods are also known as “approximated” methods.

**Level III:** Use of detailed numerical simulations based on the specific probabilistic distributions associated to the input uncertain variables ( $\mathbf{X}_1, \mathbf{X}_2, \mathbf{X}_3 \dots \mathbf{X}_n$  and  $\mathbf{Y}_1, \mathbf{Y}_2, \mathbf{Y}_3 \dots \mathbf{Y}_n$ ), for constructing the multi-variable joint probability density function. This type of methods allows to calculate the failure probability ( $P_f$ ) and/or the reliability index ( $\beta$ ) from based on an “exact” failure surface.

The reliability index ( $\beta$ ) is a common measure to express the level of reliability of a structure. Hasofer and Lind (1974) proposed to transform the  $Z$  function into an standardized U-space form which allowed to produce an invariant reliability  $\beta$  index. For these U-space methods, this index is be defined as the minimum distance between the origin of the bivariate ( $R$  and  $S$ ) distribution and the failure surface  $Z$ . Such combination of  $R$  and  $S$  has the highest likelihood of failure.

This index is widely used in the structural reliability design and assessment as most of problems are solved by implementing level II reliability methods (approximated methods) due to their inherent computational burden. That is also one of the main reasons why reliability based design guidelines are defined in terms of target indexes in the  $\beta$  form. Note that all  $\beta$  indexes may be directly related to failure probability values estimated from a normal standardized Gaussian distribution ( $\Phi$ ). Hence, it is also possible to express the obtained failure probability of the level III methods in terms of  $\beta$  indexes as  $\Phi^{-1}(P_f)$ . It is also possible to compare them with the target reliability  $\beta$  indexes contained in the reliability design codes or legislative standards.

Level II methods are based on assumptions that the limit state function can be approximated to a linear or a second order quadratic function by means of a Taylor expansion approach (Karadeniz and Vrouwenvelder, 2003). For these methods, iterative procedures are often required in order to find the closest distance to the most probable failure point (also known as design point). The main reason for implementing these approximate methods is that they are significantly less expensive in computational terms with respect to Level III methods.

For the level III methods, the most commonly used is the Monte Carlo failure estimation in which the failure point is found by sampling the variables and/or modelling of the system according to their stochastic nature, in order to find a more exact failure probability than with level II methods. This last method in its most basic form does not require any prior knowledge of the limit state function topology. Hence,

a level III method is a better initial choice when analysing systems that may present discontinuities of the limit state function or even more important of its first derivatives which are the basis for the implementation of level II methods. It is expected that for complex structures such as MFFD's for which the inclusion of hard structures in soft soil may result in unforeseen discontinuities of the limit state functions and therefore, only level III methods were implemented in the present thesis.

### 1.3.4 Fault tree analysis of flood defences

In order to estimate the total probability of failure of a structure while considering the most relevant failure mechanisms, it is common to implement a “Fault tree” method. This method allows to include the logical relationship between a series of events that may lead to the total failure of a system (Barlow, 2004). The events are linked depending on the type of relation (e.g. and, or, if) between events as seen in Figure 1-4.

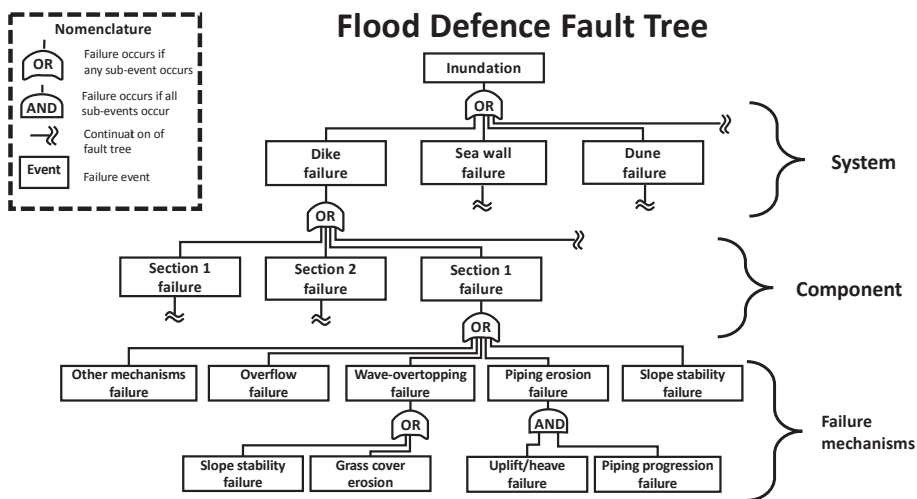


Figure 1-4 Fault tree of flood defence

For flood defence systems, the system level of the fault tree is composed of structures (Vrijling, 2001). The component level is composed of representative structure sections and these sections fail due to their correspondent failure mechanisms per section. For the latest statutory assessment tools (WBI-2017, 2015) of the Dutch flood safety system, percentages of the maximum allowable failure probability per component were defined per failure mechanism based on the results of the VNK2 project (Jongejan and Calle, 2013). These failure probability budgets are referred to as “ $\omega$  factors” and will be implemented in the new Dutch safety standards law of 2017 as:

Table 1-1. Failure probability budget factors per failure mechanism (WBI-2017, 2015)

Type of Flood Defence	Failure Mechanism	$\omega$ factors per max. allowable $P_f$	
		Sandy Coast	Other
Dike	Wave Overtopping	0	0.24
	Uplift and Piping	0	0.24
	Slope stability of inner slope	0	0.04
	Revetment failure and erosion	0	0.10
Hydraulic structures	Non-Closure	0	0.04
	Piping	0	0.02
	Structural failure	0	0.02
Dune	Erosion	0.70	0.0/0.10
Other	-	0.30	0.30/0.20
<b>TOTAL</b>		1.0	1.0

From the suggested  $\omega$  values for defining the maximum allowable probability it can be observed how the wave overtopping, uplift and piping and revetment failures account for 58% of the total maximum allowable failure probability. All three represent the erosion based failure mechanisms of a dike. Ideally, dikes should be designed so that the failure mechanisms probability is as low as possible and yet the coefficients are still relatively high with respect to other failure mechanisms. This may be explained by the associated uncertainty in the estimation of this failure mechanisms.

### 1.3.5 Dutch flood safety standards

After the major flooding event of 1953, a system of safety standards was developed and proposed by the Dutch Delta Committee. These standards (exceedance frequencies related to optimal design water levels) were obtained from the economic optimization between investment costs in flood safety and the resultant benefits of the damage reduction (Vrijling, 2001). The optimal frequency's obtained for the primary flood defences ranged from 1/10,000 for coastal areas to higher frequencies in riverine areas between 1/1250 and 1/2000. The population growth, economic development and possible effects of climate change called for a revision of these safety standards. In the year 2006, the Ministry of Infrastructure and Environment, the Association of Regional Water Authorities and the Association of Provincial Authorities had the initiative of implementing a fully probabilistic safety assessment for all major levee systems in the Netherlands in the VNK project (Jongejan and Maaskant, 2013). One of the main conclusions of this project was that the effects of additional structures or objects in the

flood defence reliability were not possible to include in a probabilistic manner and that new tools should be developed for this purpose (VNK2, 2014).

More recently, a new updated cost-benefit analysis was developed in the project “WV21: water safety of the 21<sup>st</sup> century” (Kind, 2011). The results of this study allowed to redefine the required optimal safety levels of the primary flood defences. By the year 2015, a new set safety standards were available and were defined by segment instead of by dike ring as shown in Figure 1-5:



**Figure 1-5 New flood standards by segment according to the Deltaprogram 2015, (Kuijken, 2015)**

These standards have been formally proposed by the Deltaprogram 2015 (Kuijken, 2015), and later included approved by Dutch parliament on March 23 of 2016 as an amendment to the National Water Act. These new standards were derived taking into account factors such as the individual risk of becoming a victim of flooding ( $< 1/100,000$  per year), the societal disruption due to flooding and the economic efficiency of future investments in flood protection (Van der Most et al., 2014).

## 1.4 Structural embedments

Structures like trees, buildings and cables are the most often encountered in the actual Dutch landscape and their influence on the flood defence safety has been acknowledged by the national authorities (VTV2006, 2007). In the current Dutch legislation, it is preferred to have a safe buffer zone in which additional structures should be avoided as much as possible (Zwanenburg et al., 2013). However, there are safety assessment guidelines (Beijersbergen and Spaargaren, 2009) for non-water retaining objects (NWO's – *niet waterkerende objecten* in Dutch) which allow to determine if these additional structures may or not compromise the main functions of a flood defence (STOWA, 2000; VTV2006).

The method consists of elaborated flow charts in which the characteristics of the flood defence and the structural embedment are evaluated based on yes/no questions which result in a safe or unsafe definition. The method is elaborated for assessing the most typical embedments such as small buildings, trees, pipelines, cables among other random objects. An interesting characteristic of this method is that it initially evaluates the safety depending on the type of structure which is embedded. This can be interpreted as a safety philosophy approach which prioritizes the risk of the embedded structure to fail over the risk of the flood defence to fail. However, such an approach is quite understandable as the additional structures tend to be founded in the same locations of the flood defence, e.g. roads over the crest, houses inside or nearby, cables and pipes underneath or beside. Hence, the safety philosophy behind the method is to ensure that these external elements do not compromise the stability of the main elements of the flood defence such as the slopes, the crest or the core.

Different dike failure studies have also shown that the inclusion of hard structures and/or transitions between the earthen embankments and other structures originate “weak spots” in which erosion tends to start first (Kanning et al., 2007; Verheij et al., 2012; Hoffmans et al., 2015). Yet, these transitions are not explicitly included in design codes or regulations in terms of suggested design factors or safety values. By including the derived effects of the embedments in the failure mechanisms processes, it is expected to obtain better failure probability estimations of the flood defence systems while also allowing to include the embedment reliability effects in the complete safety assessments.

Flood defence failure mechanisms have specific zones of occurrence on the flood defence which allow intuiting that the location of the additional structure allow determining which failure mechanisms will be directly affected by the embedment. The

present thesis is developed around the idea that structural embedments may be first classified by their location with respect to the flood defence so that is easier to identify which failure mechanisms they affect directly. Based on examples from the Dutch landscape, the identified influence zones were on top of the defence, inside of the body of the defence and below the flood defence (Figure 1-6). The most interesting examples of embedments by each location were identified as roads, constructions and sewer pipes respectively.

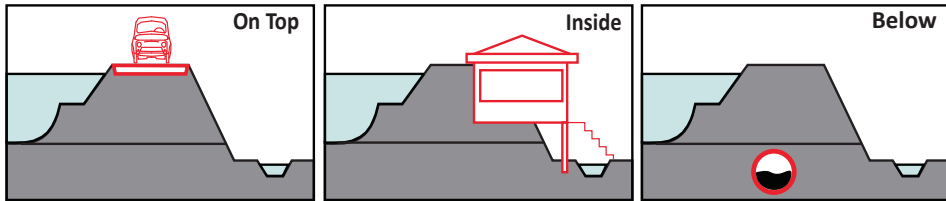


**Figure 1-6 Influence zones of structural embedments**

The effect of the embedment is not always related to one single failure mechanism only. For example, a house embedded inside the flood defence which may be founded deeper than the flood defence bottom will not only compromise the slope stability of the defence but will also have a significant effect on the occurrence of other failure mechanisms such as seepage through the dike, piping erosion and grass cover erosion due to wave overtopping.

Some failure mechanisms also have variable uncertainties in common derived from either the material or the geometrical characteristics which may induce correlation in their occurrence likelihood. Nevertheless, as an initial approach, it is chosen to identify cases in which one single failure mechanism is affected by one single structural embedment, or one expected correlated event affects one single failure mechanism for the sake of simplicity. For the specific cases of erosion based failure mechanisms it is acknowledged that piping erosion occurs in the foundation (“below” influence zone, Figure 1-6) whereas overtopping occurs over the flood defence (on top influence zone, Figure 1-6).

Erosion based failure mechanisms are less commonly studied with respect to deformation or retaining capacity failure mechanisms as the later ones are also found in dam engineering. This knowledge gap becomes more evident for studies related to structural embedments and erosion based failure mechanisms. Nevertheless, this information is required for the future implementation of MFFD’s.

## 1.5 Design choices and their impact on the structural safety

During the design process, geometrical and material choices are what define the structural resistance against failure. These choices are required for both flood defence and structural embedment. However, it is expected that the design process follows the logical order of first designing the flood defence for ensuring the primary water retaining function, later include the embedment and finally assess the design. Based on this design order, the embedment of structures will change the probabilistic distribution of the  $R$  and  $S$  terms of the limit state equations, with respect to the initial case of the flood defence of the same dimensions and materials which has no structural embedment. The piping erosion failure mechanism is a good example of this situation as the presence of discontinuities changes the flow resistance of the aquifer and consequently the inner pressure distribution (Wang et al., 2014). Hence, the probabilistic distribution of the  $R$  term will change and consequently the flood defence reliability. This is also the case of the inner slope stability safety in which the embedment of a hard structure inside the flood defence will directly affect the equilibrium state during a flood event. From this last example, it is noted that the mechanical properties of the embedded structure may contribute as well in a positive way to the flood defence stability it may add an extra resisting component against the rotational failure.

The selection and reduction of the associated variable uncertainties involved in the estimation of the load and resistance terms of a failure mechanism will also have an impact in the structure's reliability. For example, there are failure mechanisms in which the load term  $S$  statistical distribution is affected by the geometrical and geo-mechanical properties of the structure. This is the case of wave overtopping in which the overtopped water volumes erode the protecting grass cover in the landward side of a dike. If a structure is present on top of the profile, the hydrodynamics will be affected and consequently the erosion patterns will change. Or for the case of wave impact on buildings in which the dimensions of the flood defence and embedded structure may define the loading condition on the dike (Chen et al., 2015) and its probabilistic distribution (Chen et al., 2016).

For the design of MFFD's, it is important to understand the derived effects of the structural embedment in the likelihood of the failure mechanisms. This knowledge will allow to define the degree of integration (Van Veelen et al., 2015) between structures since the initial design stage resulting in more cost effective structures. Operation and maintenance are also part of the design process and may also be affected by the

inclusion of embedded structures. However, their influence in the MFFD as it is out of the scope of this thesis. Hence, the remaining choices for a structural design can be classified into two groups; the material and the dimensional choices. Both design choice groups may be represented as uncertainties in the probabilistic design (Diamantidis, 1987). Based on this classification, it is defined that the most important design choices of an MFFD's can be characterized as:

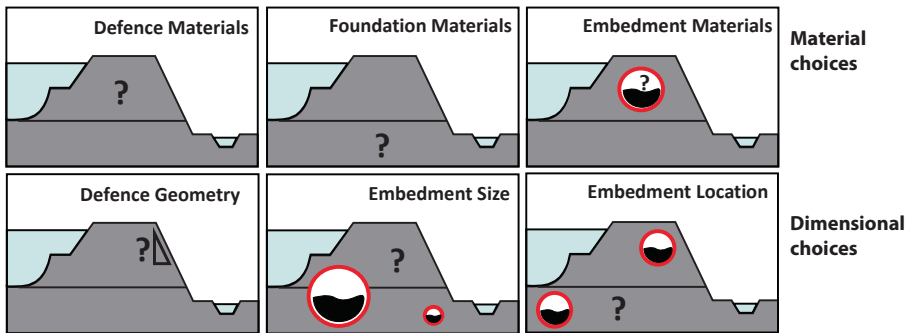


Figure 1-7 Design choices

Depending on the design choice, it is expected that a reduction of the failure probability for one or more failure mechanism may be achieved by:

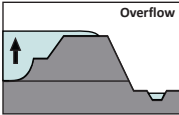
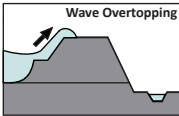
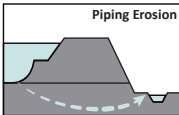
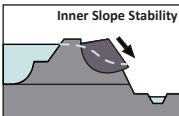
1. Improving the resistance of the **materials** of the **flood defence**
2. Improving the resistance of the **materials** of the **foundation**
3. Improving the resistance of the **materials** of the **embedded structure**
4. Changing the **geometry** of the **flood defence**
5. Changing the **geometry** of the **embedded structure**
6. Changing the **location** of the **embedded structure**
7. Combinations of all of the above

The optimal selection and uncertainty assumption of each of the choices can be used for accurately estimating and improving the MFFD safety. For riverine dikes, piping erosion and wave overtopping are influenced by all 7 design choices.

## 1.5.1 Model selection for probabilistic design and assessment

The selection of the model that represents the failure situation better represents another important design choice. Nowadays, numerical models are capable of representing reality in different levels of complexity. Models are representations of physical processes in which assumptions allow to simplify (or increase) their computational complexity (Brooks and Tobias, 1996). Model complexity depends on the number of processes involved, their time dependency, the interaction between processes and the number of spatial dimensions in which the processes are modelled, among others. According to the study of Wainwright and Mulligan (2005), models may be classified based on their complexity as empirical, conceptual and physically based. For the four main flood defence failure mechanisms, reference studies in which different modelling complexities are implemented are summarized in Table 1-2. After the fast advance of computational intelligence, a new kind of modelling approach emerged which is formerly known as “data driven”. In this type of modelling, the processes are recreated based only on algorithms built based on the input and output collected data of the physical process, disregarding the physical representation of the process itself (Solomatine et al., 2009).

**Table 1-2. Failure mechanisms modelling studies with different complexities**

Failure mechanism	Empirical models	Conceptual models	Physically based models	Data Driven models
	-	(Hewlett et al., 1987)	(Pontillo et al., 2010)	(Aguilar-López et al., 2014)
	(Van der Meer, 2002)	(Schüttrumpf and Oumeraci, 2005)	(Quang and Oumeraci, 2012) and (Aguilar-López et al Chapter 4)	(van Gent et al., 2007)
	(Lane, 1935) and (Sellmeijer et al., 2011)	(Sellmeijer, 1988)	Wang et al. (2014); (Aguilar-López et al., 2016a)	(Kaunda, 2015; Aguilar-López et al., 2016a)
	(Johnson et al., 1999)	(Van et al., 2005)	(Moellmann et al., 2011)	(Kingston, 2011)

An additional modelling uncertainty is derived from the choice of reliability method (see section 1.3.3). Uncertainty factors regarding the model selection are also included in the latest statutory assessment tools (WBI-2017, 2015) based on the level of complexity of the models. Yet, these model factors are calibrated for semi-probabilistic assessments based on fully probabilistic assessments of conventional flood defences. This shows how fully probabilistic methods (Level III) are considered as the most accurate way to estimate the structural reliability. For implementing such reliability methods, the model choice is always a difficult one. For the design of MFFD's, it is expected that detailed numerical solutions (e.g. finite element modelling) will reduce the initial uncertainty derived from the lack of safety factors required for implementing level II reliability methods. Furthermore, these methods allow to develop the tailor made MFFD's models required for each particular case as the structural embedment combinations are infinite. However, probabilistic finite element modelling in particular, is constrained by factors such as the “curse” of dimensionality (Hurtado, 2013) in which the computational burden is not only increased by the number of variable uncertainties and by the required calibration and validation process but also by the number of structural elements to solve.

## 1.5.2 Emulation of models

A way to reduce the computational burden, is by imitating the original models used for representing the  $R$  and  $S$  for estimating the limit state function. In that manner, it is possible to implement complex models such as FEM's in level III reliability methods. Emulators (also referred to as surrogate models or meta-models) are pseudo models built from the input-output datasets produced by the more complex original model. These models allow to capture highly non-linear relations while remaining computationally efficient. Such models are widely used in reliability studies after the advance in the fields of machine learning, support vector machines and response surface fitting techniques during the last 20 years (Sundar and Shields, 2016). Yet, two main challenges must be tackled for achieving their robust implementation; the first is the efficient selection of training data sets. The second is the correct selection of the algorithm used to recreate the input-output relation function (Forrester et al., 2008). Most of the times the two challenges are dependent on each other making their implementation a matter of trial and error. The accuracy of these models depends on both choices but only the first one is affected by the computational burden of the model to be “emulated”. After the training procedure is performed, emulators are tested and validated. Once approved based on their performance evaluation, they can be

implemented in any of three reliability levels. The main advantage of these models is that they allow to assess different stochastic scenarios until certain bounded extrapolation ranges without having to re-run the original complex models.

For specific cases of flood defence emulation, different failure mechanisms have been emulated in the past (Sellmeijer, 2006; Kingston, 2011; Pyayt et al., 2011; Razavi, 2012; Schoefs et al., 2013; Aguilar-López et al., 2014; Yazdi and Salehi Neyshabouri, 2014). On one hand, the approaches explained in these studies allowed to implement fully probabilistic safety assessments in all cases. On the other hand, none of them included the derived effects of additional non-water retaining structures in the structural reliability. Nevertheless, they proved that emulation is a good solution for the implementation of probabilistic safety assessment in level III reliability methods for structures that may present highly non-linear responses to the loading conditions. It is expected that this is the case for MFFD's in which structural embedments may represent a discontinuity point in the limit state functions.

### **1.5.3 Correlation and spatial variability modelling**

Variable inter and auto dependency is a modelling choice which is related to the input variables. This choice becomes another source of uncertainty as it will directly affect the estimated structural reliability of the flood defence in unknown ways. While including a certain degree of dependency in the input variables may not seem like a design choice per se, the correct selection of mathematical functions for representing the correct topological relation within themselves is also simulation choice and consequently a design choice. Correlation between variables is an important modelling choice as it may have a significant influence on the reliability estimation of the structure. Other probabilistic studies have aimed to include the possible correlations between variables in the load term of the limit state function. More specifically, the hydro-climatological variables which define the water levels (Van Gelder, 2000; Grimaldi and Serinaldi, 2006; Diermanse and Geerse, 2012). However, little is known about the effects of intra-variable correlation for erosive process derived failure mechanisms. In particular for the piping erosion Sellmeijer limit state equation (Sellmeijer et al., 2011) which will be included in the new statutory assessment tools in the year 2017.

With regard to the spatial autocorrelation of variables for the reliability estimation of flood defences, Vrouwenvelder (2006) explains these effects were modelled and included in the PC-RING assessment tool. The autocorrelation of variables in  $x$  and in  $x$  and  $y$  directions along the dike are modelled to represent the expected change in the statistical properties that represent the soil characteristics. The PC-RING tool includes

these spatial correlation effects for dike design variables such as height, soil angle of friction and the cohesion. Furthermore, a method based on a Bayesian inference approach was also presented by Vrouwenvelder and Calle (2003) which allows to determine the scale of fluctuation (auto-correlation parameter) of the decay functions when few samples are available. The scale of fluctuation is a very important factor for accurately determining the failure probability of flood defences, especially because they are longitudinal structures in which the probability of finding a weaker location increases with the increase of their length. This is referred to as the “length-effect” and becomes more important with the increase of the uncertainty of the variables that describe the failure mechanisms, in particular for erosive process based failure mechanisms such as piping. This failure mechanism has proven to be highly influenced by the length effect as shown by Vrijling (2010). His study concludes that the failure probability of piping erosion may be underestimated by factors that range between 5 and 10 times when not included in the safety assessment. In the research of Kanning (2012), a new 2D model developed based on random fields, Bayesian theory and groundwater flow allowed to estimate the influence of the scale of fluctuation of the  $d_70$  parameter in space.

From all earlier studies, it can be concluded that the spatial variability of the parameters of piping erosion has been thoroughly studied and that it may have a significant effect on the flood defence reliability. This may also be important the case for wave overtopping in which the parameters that describe the resistance against erosion process may also vary in space. Yet no relevant literature has been found which allows to understand the influence of the spatial variability for these particular failure mechanism. This becomes even more important for the case of the design of MFFD’s in which the inclusion of additional structures may represent a significant change in the spatially distributed resistance and superficial roughness the flood defence cover.

## **1.6 Problem definition**

Flood defences which allocate other functions are already present in the flood defence systems all over the world. The challenge for MFFD’s implementation in terms of safety is the inclusion of the structural embedments derived effects in their probabilistic flood defence safety assessments (Van Ree et al., 2011). Recent flood risk studies such as FloodProbe, Floodsite and VNK2 have reiteratively concluded that it is of paramount importance to develop modelling tools which allow to determine and include the reliability of combined flood defences for their safety assessments (Morris et al., 2008; Van Ree et al., 2011; VNK2, 2014). However, it is not effective to develop separate methods for all types of structural embedments in all possible failure mechanisms.

From the allocation of maximum target failure probabilities presented in Table 1-1, it is observed that erosion based failure mechanisms represent the largest threat to flood defences and therefore the inclusion of embedded structures in their influence zones may also increase the risk of failure of the flood defence. More specifically, the inclusion of structures founded under and over the flood defence as they will directly affect the failure mechanisms of piping erosion and wave overtopping erosion.

With the present thesis it is intended to address knowledge gaps for design and assessment of MFFD's with respect to the two most threatening erosive processes such as:

1. The lack of information about the influence of correlation between variables for designing or assessing a flood defence seepage length for piping erosion. Especially with the Sellmeijer revised limit state function to be included in the new assessment tools.
2. The lack of information about the derived effects of the flood defence reliability against piping erosion from the inclusion of pipes in the foundation. Most of the literature is concerned about the reliability of the embedded structure while disregarding the influence in the physical piping erosion processes.
3. The lack of information about the reliability effects derived from locating roads on flood defences or the effects derived from the grass resistance uncertainty and its spatial distribution. The available studies are mostly about experimental results or the ongoing developments for the cumulative hydraulic load.

In the actual state of the art of failure mechanisms modelling, it is possible to achieve a great degree of detail in the tailor-made models for combined structures such as MFFD's with complex numerical solutions like finite element methods. Level III methods are more suitable for assessing complex structures when no prior knowledge of the limit state function is available, but the resultant computational burden makes them difficult to implement.

## 1.7 Objective and research questions

The objective of this research is:

**“To determine and quantify the effects in the probabilistic design and safety assessment of erosion based failure mechanisms of MFFD’s, derived from the foundation and the embedment of hard structures”**

To do that, three main research questions have been posed as:

**Q1.** How does correlation between  $K$  and  $d_{70}$  influence the probabilistic design and assessment of a multifunctional flood defence?

**Q2.** How does an embedded pipe under a multifunctional flood defence influences the probabilistic design and assessment of the piping erosion failure mechanism?

**Q3.** How does the presence of a road on top of the crest of a multifunctional flood defence influence the probabilistic design and assessment for wave overtopping grass cover erosion failure mechanism?

## 1.8 Methodology

The research methodology for answering the first 3 questions consist on comparing the reliability of two detailed models; one which includes a certain design choice and one that doesn't. This same approach was taken for all 3 cases included in each of the next three chapters of this thesis. The first step consists in a literature review of for finding the most detailed and updated information about the physical process that underlies beneath the failure mechanism to be studied. In addition, literature about the modelling of such processes, and the stochastic nature of the variables involved is also done. This will allow to produce numerical models with high detail so that the design choice may be included in an accurate way. The second step consists in collecting and processing data from full-scale experiments for building the detailed models. The third step consists on building and validating the models while considering the features that may directly influence the failure mechanism physical process for a given design choice. The fourth step consists in generating data from the original models and using it for training emulators. Once these emulators are trained and verified, they can be used in the fifth and final step which consists in performing the safety assessment with a level III reliability method. In this step, failure scenarios are defined which are reflected in the stochastic distributions associated to the input variables of the emulators.

Afterwards, random samples for each scenario are generated and propagated through the emulators, which are used for a Monte Carlo reliability assessment. As a result, each scenario is related to its failure probability which allows to compare them to each other and with respect to the maximum allowable probabilities included in the Dutch assessment tools. The relation and inner sequences are in the flowchart presented in Figure 1-8.

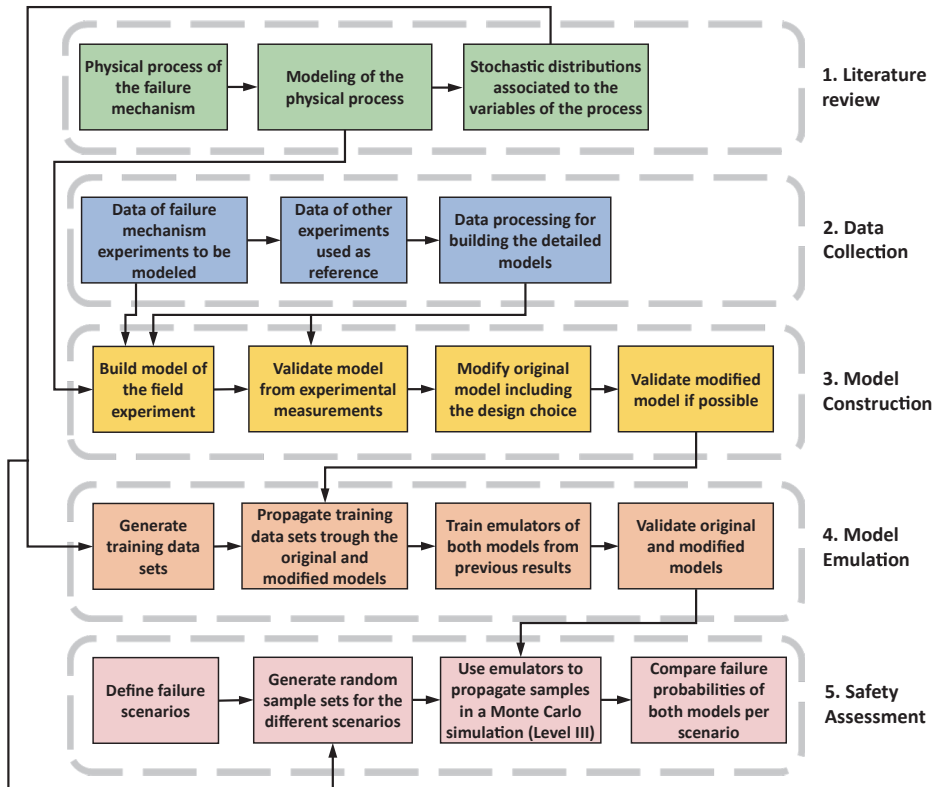


Figure 1-8 General thesis research methodology

The last research question is answered by the integration of the failure probabilities of the three different cases in a simple fault tree analysis based on the maximum allowable failure probabilities included in the new Dutch flood safety assessment tools (WBI-2017, 2015).

## 1.9 Thesis outline

Three different cases were studied for answering each of the first three research questions. In each case, the different design choices have a direct influence on the occurrence of the assessed failure mechanism.

The first case presented in Chapter 2, corresponds to a flood defence prone to fail by piping erosion. The material foundation uncertainty has an influence on both conventional flood defences and MFFD's likelihood of this failure mechanism to occur. The variables  $d_{70}$  and  $K$  have a strong influence in the reliability assessment of piping erosion when performed with the Sellmeijer limit state revised equation. The choice of including the correlation between these two variables is an important choice during the design and assessment process of an MFFD. This single choice may define the feasibility of the design as it has a strong influence on the resultant space that can be used for the future functions and structural embedments. This case allowed to answer the first research question.

The second case presented in Chapter 3, correspond to another hypothetical flood defence prone also to piping erosion. The model used for assessing this case is based on the piping erosion results of the full-scale experiment known as the "IJKdijk". In this case, the effects derived from the choice of founding structures underneath the flood defences is presented. Specifically, for the case of the embedment of a sewer pipe inside the MFFD granular foundation. Factors like the size and location of the sewer pipe with respect to the midpoint of the flood defence are investigated. The results of this study were used to answer the second research question.

The third case is presented in Chapter 4, corresponds to a flood defence with a road on top of the crest. The presence of roads is often observed in the Dutch and international flood defended landscape. This design choice is quite recurrent as polders need to be accessed and dike crests are good locations for this kind of longitudinal structures. Yet, their presence may have a significant effect on the wave overtopping failure mechanism. In addition, the spatial variation of the resistance against the erosion of the grass and soil is another determining factor for failure. The results of this study allowed to answer the third research question.

The advantages, shortcomings, and implications derived from the different design choices of MFFD's are further discussed in Chapter 5. In addition, the obtained failure probabilities for the three different choices are evaluated in a simple fault tree analysis.. Finally, the answer to each of the three research questions is included in Chapter 6.

# Chapter 2

## Soil stochastic parameter correlation impact in the piping erosion safety assessment

### Abstract

Piping erosion has been proved to be one of the failure mechanisms that contributes the most to the total probability of failure on the Dutch flood defence systems. The present study aimed to find the impact of correlation and tail dependence between soil parameters present in the Sellmeijer revised limit state equation for piping safety assessment. Particularly between the grain size and hydraulic conductivity parameters. A copula based random sampling method was used as a tool to include this effect in the probabilistic estimation of this type of failure. The method was framed in a real case study for a flood defence along the Lek river, in the Netherlands. The results showed that inclusion of correlation between the two parameters reduces the variance of the limit state marginal distribution by almost 10% when compared to the uncorrelated case. This effect changes the tail values sampling frequency and therefore reduces the probability of failure by a factor of 1.7. The omission of correlation between the two parameters for safety assessment based on the Sellmeijer limit state function may result in over dimensioned structures.

**This chapter is published as:** Aguilar-López, J.P., Warmink, J.J., Schielen, R.M.J., Hulscher, S.J.M.H., 2016. Soil stochastic parameter correlation impact in the piping erosion failure estimation of riverine flood defences. *Structural Safety*, 60: 117-129. DOI: 10.1016/j.strusafe.2016.01.004

## 2.1 Introduction

In the Netherlands, large flood risk assessment projects such as the VNK2 (Jongejan et al., 2013) have devoted great attention to develop and improve more robust probabilistic estimation methods for the safety assessment of their levee systems. One of the main results from this study was the prioritization of the different failure mechanisms that contribute the most to the total failure probability ( $P_f$ ) of the levee systems. Reiteratively, piping erosion (PE) was found to be a major threat in most of the components of the system. This type of failure consists in a progressive erosion channel under the flood defence foundation which will eventually start a breaching process due to the loss of stability of the structure. This type of failure can be simulated by the numerical model developed by Sellmeijer (Sellmeijer and Koenders, 1991). For safety assessment, a revised limit state equation (LSE) (Sellmeijer et al., 2011) was derived based on this same model. This equation describes the safety state of the system given the most sensitive variables involved in the process for the occurrence of this particular failure mechanism. Limit state equations are implemented in probabilistic safety assessments as they can be used to express the loads experienced by the flood managing structure as a function of the water level probabilistic distribution. The resistance of the structure against these loads can also be represented as a probabilistic marginal distribution.

It is common in practice to assume that the random variables used for the limit state evaluation are represented by univariate probability density functions. Hence, they are commonly assumed as uncorrelated when no evidence is available. The omission of possible statistical dependence or correlation between different state variables is one major source of error in the failure estimation of reliability of a system when such variables are highly sensitive for the model probabilistic outcome. Correlation analysis is not only concerned about the degree of dependence but also the temporal and spatial distribution of the correlated random variables (Jongejan et al., 2013). Extensive research has been done about the effect of spatial correlation of load and resistance of flood defences in the Netherlands (Van Noortwijk et al., 1999; Vrouwenvelder, 2006; Kanning, 2012). Yet, the correlations were analysed considering how a variable depends on itself (autocorrelation) along space and time and not within each other. The importance of variable correlation for flood defence structures was demonstrated in the study by Diermanse and Geerse (Diermanse and Geerse, 2012) where the influence of bivariate correlation modelling between two hydro climatological variables required for dike safety assessment was studied. One case study was done by modelling the inflows from the IJssel River and the water levels in the IJssel Lake, and another one for

modelling the wind speeds and water levels in the North Sea coast correlated as well. Both case studies showed the influence that correlation modelling can have in the safety assessment of flood defences. Yet, the correlation impact was only studied in the variables involved for estimating the marginal distributions of the loads applied to the flood defences.

With this study it is intended to quantify the influence of correlation in failure estimation between two parameters present in the erosion model for piping assessment, in particular for a “single” cross section in a riverine flood defence when assessed by the revised Sellmeijer LSE (Sellmeijer et al., 2011). This equation includes, the representative aquifer grain size parameters ( $d_{70}$ ) and the hydraulic conductivity parameter (K) which can be correlated for different models as presented by (Rosas et al., 2014). For the design and safety assessment of flood defences in the Netherlands, the dependence of these two parameters is considered by the empirical equation present in (Förster et al., 2012). The drawbacks of this equation are that it is only valid for sands with  $d_{10} < 0.06$  mm and it also depends on a qualitative factor associated to the packing density of the particles in situ. Hence, the implementation of such equation in a fully probabilistic assessment (correlation inclusion) becomes unreliable. Note that the correlation addressed with this kind of equations (grain size versus hydraulic conductivity) represent the chance that the two variables are dependent disregarding their location (spatial correlation) in time and space (non-stationary process).

Despite including the dependence of these two parameters, the correlation degree between the two of them is not constant for all quantiles either. Based on the sample distribution, a higher correlation is expected for sands with larger percentages of smaller grains. Such variability of the correlation is known as tail dependence. This is also not included in the actual probabilistic assessment methods for flood defence reliability of PE and can have an important effect if the structure reliability.

During the PE process, only the most upper part of the aquifer is eroded which means that the  $d_{70}$  statistical distribution should be representative of mainly that zone. It is common to find finer grain distributions in the upper layer of the aquifers which will imply a lower correlation degree between  $d_{70}$  and the K parameters. When the grain distribution of the most upper layer of the aquifer is significantly different and finer with respect to the one associated to the whole aquifer average distribution, the measured representative conductivity values for the whole aquifer can be assumed as uncorrelated.

However, in the actual practice a detailed sampling procedure of only the upper layer of grain size and permeability is not practical for such longitudinal structures. Hence, the  $d_{70}$  and  $K$  statistical descriptors are estimated by indirect methods.

Despite the fact the upper layer may have a distinct granulometric distribution, this doesn't imply that no correlation or neither tail dependence exists between  $d_{70}$  and  $K$ . It will only mean that the degree of dependence between the two parameters is lower than expected. Yet, this degree of correlation and tail dependence might change the probabilistic outcome if found significant enough. It is also important to state that not all variables involved in this process necessarily should be considered as correlated, despite the fact that significant correlation can be estimated from their dataset. Sufficient physical evidence of the origin of the correlation should be proven before deciding to include its effect in a structural reliability assessment. In other words correlation does not necessarily implies causation.

For the data of an existent river flood defence located in the Netherlands along the Lek River, the correlation and its physical origin were studied. In order to structure the research, three main questions were addressed:

1. Is there considerable correlation between the representative grain size ( $d_{70}$ ) and the hydraulic conductivity ( $K$ )?
2. How to select and validate a correlation bivariate model (Copula family) for the failure estimation due to piping?
3. How important is the impact of correlation between  $d_{70}$  and  $K$  in the failure probability estimation due PE when estimated by Sellmeijer revised limit state equation?

The outline of the paper consist in the physical process of the PE failure mechanism and its limit state function which are explained in detail in section 2.2, plus the implementation of the copula functions for generating the correlated random samples. In section 2.3 the case study and the input data used for the failure estimation are described. Section 2.4 describes the results obtained from estimating correlation from the field collected data. In section 2.5 the selection and validation of a model that describes best the soil behaviour is presented. In section 6, the results of the correlation effect on the limit state function marginal distribution and failure probabilities are presented. In section 2.7, the results of each research question are discussed and finally the main conclusions of the study are presented in section 2.8.

## 2.2 Limit State Safety Assessment Method

For the present study, the random variables involved in the Sellmeijer revised LSE are sampled and propagated by a Monte Carlo reliability method. As a proposed tool to assess the effect of correlation between the sensitive random variables in PE estimation, the statistical bivariate joint distribution method for correlated sampling known as “copula” (Sklar, 1959) was implemented. Copula joint distribution models are capable of inducing correlation between two univariate marginal distributions while maintaining their statistical moments fixed. Different copula functions can be found in the literature according to which topological behaviour is desired when tail dependence representation is required (Nelsen, 2006).

The degree of correlation is one of the copula main input parameters. Therefore, it also allows to generate  $n$  random samples with a particular desired degree of dependence. The final product consists of a table of failure probabilities as function of the degree of correlation estimated for each of the chosen copula models.

### 2.2.1 PE Sellmeijer revised limit state equation

PE is also known as backward erosion, and consists in the loss of stability of the flood defence structure due to the erosion of the granular foundation stratum (Figure 2-1). In order for PE to happen, a previous failure mechanism called “uplift” must have occurred as well.

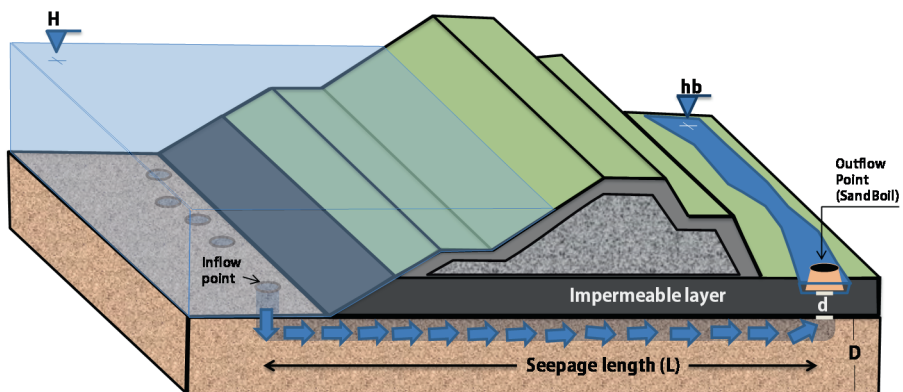


Figure 2-1. PE process under flood defence

This mechanism consists in the lifting and breakage of the impervious layer between the body and the foundation of the dike, due to a high hydrostatic pressure. Afterwards, the water movement inside the aquifer from the river side towards the inland side, transports fine grains which originate a longitudinal void also referred as “pipe”. Once the pipe has developed for a length equal or greater than the width (L) of the flood defence (Figure 2-1), it is assumed to be in failure state. Nevertheless, the breaching of the flood defence may not necessarily occur in that exact instant. Several empirical and numerical models (equations) for estimating the critical head of PE have been developed since the early 20th century, such as Bligh and Lane (Ojha et al., 2008). A more robust conceptual numerical model and LSE was developed in the Netherlands by Sellmeijer and Koenders (1991).

Recently, the LSE was re-calibrated with the obtained results of several experiments at different scales (Sellmeijer et al., 2011). The LSE is presented in Eq. 2-1 to Eq. 2-5.

$$Z_p = H_c - (H - h_b - 0.3d) \quad \text{Eq. 2-1}$$

$$H_c = m_p(F_G)(F_R)(F_S)L \quad \text{Eq. 2-2}$$

$$F_S = \frac{d_{70m}}{\sqrt[3]{\left(\frac{vK}{g}\right)L}} \left(\frac{d_{70}}{d_{70m}}\right)^{0.4} \quad \text{Eq. 2-3}$$

$$F_R = \eta \frac{\gamma'_s}{\gamma_w} \tan(\theta) \quad \text{Eq. 2-4}$$

$$F_G = 0.91 \left(\frac{D}{L}\right)^{\left(\frac{0.28}{\left(\frac{D}{L}\right)^{2.8} - 1} + 0.04\right)} \quad \text{Eq. 2-5}$$

<b>Z<sub>p</sub></b>	<b>[m]</b>	Residual resistance (Limit State function)
<b>η</b>	<b>[-]</b>	Sand drag force factor (0.25)
<b>γ<sub>s</sub></b>	<b>[kN/m<sup>3</sup>]</b>	Unitary weight of submerged sand particles
<b>γ<sub>w</sub></b>	<b>[kN/m<sup>3</sup>]</b>	Unitary weight of water
<b>θ</b>	<b>[deg]</b>	Bedding angle of sand grains
<b>d<sub>70</sub></b>	<b>[m]</b>	70 percent quantile value grain size distribution of sand layer
<b>d<sub>70m</sub></b>	<b>[m]</b>	Calibration reference value (2.08 x 10 <sup>-4</sup> m)
<b>ν</b>	<b>[m<sup>2</sup>/s]</b>	Kinematic viscosity of water at 20 °C
<b>K</b>	<b>[m/s]</b>	Hydraulic conductivity of sand
<b>g</b>	<b>[m/s<sup>2</sup>]</b>	Gravitational acceleration (9.81m/s <sup>2</sup> )
<b>D</b>	<b>[m]</b>	Average thickness of sand layer
<b>mp</b>	<b>[-]</b>	Modelling uncertainty factor
<b>F<sub>R</sub></b>	<b>[-]</b>	Resistance factor
<b>F<sub>S</sub></b>	<b>[-]</b>	Scale factor
<b>F<sub>G</sub></b>	<b>[-]</b>	Geometric factor
<b>H<sub>c</sub></b>	<b>[m]</b>	Critical PE resistance head
<b>L</b>	<b>[m]</b>	Seepage length from entrance point to sand boil water exit
<b>H</b>	<b>[m]</b>	Water level in the riverside of the flood defence (annual maximum)
<b>h<sub>b</sub></b>	<b>[m]</b>	Water level at hinterside outflow point
<b>d</b>	<b>[m]</b>	Impermeable layer thickness at the sand boil exit point

Note: the product of the hydraulic permeability of soil and kinematic viscosity divided by the gravitational acceleration is equal to the intrinsic permeability  $k$  [m<sup>2</sup>] (noted as lower case k).

In many cases, a small water ditch is located behind the dike (Figure 2-1) which serves as a drainage and irrigation control structure. Then, the hydraulic head exerted by the flood defence is calculated as the difference between the riverside withstanding water level (H) and the landside ditch water level (h<sub>b</sub>) plus an additional resistance margin estimated as 30% of the aquitard layer thickness. This margin takes into account the additional flow resistance from the vertical flow through the crack in the impermeable layer (Koelewijn, 2009).

## 2.2.2 Hydraulic conductivity by Kozeny-Carman equation

The Kozeny-Carman equation estimates the hydraulic conductivity based on the soil representative diameter and the porosity, which is commonly used in studies where in situ measurements are scarce. Its applicable to large range of grain and several types of soil as presented by Chapuis (Chapuis, 2012), which makes it suitable for stochastic sample generation. Mazzoleni et al. (2014) also used the Kozeny-Carman equation for PE evaluation along the Po river where the porosity showed to be an important parameter which can be also used for the failure prediction.

$$K = \frac{\rho g}{\mu} \frac{n^3}{(1-n)^2} \frac{d_m^2}{180} \quad \text{Eq. 2-6}$$

Where:

$K$	[m/s]	: Hydraulic conductivity
$\rho$	[kg/m <sup>3</sup> ]	: Water density
$g$	[m/s <sup>2</sup> ]	: Gravitational acceleration (9.81m/s <sup>2</sup> )
$\mu$	[kg·s/m]	: Water dynamic viscosity
$n$	[-]	: Porosity
$d_m$	[m]	: Representative diameter

When measured values of porosity are not available, Vukovic and Soro (Vukovic and Soro, 1992) present an empirical formula to calculate these parameter as a function of the ratio between the  $d_{60}$  and  $d_{10}$ , according to:

$$n = 0.255(1 + 0.83\frac{d_{60}}{d_{10}}) \quad \text{Eq. 2-7}$$

The Kozeny-Carman equation it can be implied that the porosity term has a significant influence in the hydraulic conductivity estimation. Hence, its uncertainty is also an important factor in the accuracy of the hydraulic conductivity estimation. This uncertainty will be reflected in the measured values or can be represented as an additional term affecting equation 7. However, information of these uncertainty related to the empirical regression is limited and is beyond the scope of the present study. Therefore it was not included in the calculations.

## 2.2.3 Copula correlation models

Copula functions can be used for generating correlated values during a random sampling process. They allow to build joint distributions from two or more variables while maintaining the statistical properties of their marginal distributions (Billar and Gunes Corlu, 2012). All types of possible copulas (families) are derived from the Sklar theorem which states that every probability function can be written as a copula multivariate function of the uniformly transformed marginal values (Sklar, 1959). The most common families are the “Gaussian” and the “Archimedean” functions (e.g. Gumbel, Frank or Clayton).

For the bivariate case, the general copula cumulative probability function can be written as Eq. 2-8:

$$F_{X,Y}(x, y) = C[F_X(x), F_Y(y); \theta] \quad \text{Eq. 2-8}$$

Where  $F_X(x)$  and  $F_Y(y)$  represent the cumulative distribution functions of the random variables  $x$  and  $y$ . The  $\theta$  symbol represents the general correlation copula parameter which describes the degree of dependence between variables  $x$  and  $y$  and  $F_{X,Y}$  is the joint probability function given  $x$  and  $y$ . For continuous marginal distributions, there is always a unique  $C$  matrix that relates  $x$  and  $y$ . Their probability marginal are always contained inside the unit square  $[0,1]^2$  for the case of bivariate joint distributions.

Tail dependence is an additional feature of correlated variables which is defined as the probability that extreme values of the variable  $x$  are achieved given large values of the variable  $y$ . Full correlation means that variable  $x$  has a one to one relation with variable  $y$  and that the probability of any other value to be associated with  $x$  is equal to 0. Conversely, fully uncorrelated variables have probability of any other value to be associated with  $x$  equal to 1. In general, bivariate variables can have the same degree of correlation with different tail dependencies. The Gaussian copulas for example are built as a function of the normal distribution and allow equal degrees of positive and negative correlation. However, they will not induce any tail dependence. Tail dependence is important for reliability assessment as the occurrence of two extreme values at the same time might either increase or reduce the probability of failure to occur in comparison to the cases where no tail dependence and no correlation is present.

The Archimedean copulas such as “Gumbel” or “Clayton” on the other hand allow to generate the samples correlated with a stronger dependence in either of the two tails of the bivariate joint distribution.

Copula families are built based on mathematical descriptions that relate the different marginal distributions of the univariate  $x$  and  $y$  distributions via different functions known as “generators” (Table 2-1) as a function of their correlation parameter  $\theta$ .

**Table 2-1. Copula families and generator functions**

Family Type	Gaussian	Archimedean	
	Gauss	Gumbel	Clayton
Copula $C(u, v)$	$\Phi_\rho(\Phi^{-1}(u), \Phi^{-1}(v))$	$\exp(-[(-\ln u)^\alpha + (-\ln v)^\alpha]^{1/\alpha})$	$\max[(u^{-\alpha} + v^{-\alpha} - 1), 0]^{1/\alpha}$
Correlation parameter ( $\theta$ )	“ $\rho$ ” Pearson correlation coefficient normal distribution $\Phi^{-1}$ .	$\alpha \in [1, \infty)$	$\alpha \in [0, \infty)$

Every generator function will originate a copula type based on its convexity and monotonic behaviour. The general sampling algorithm for all copula models consist in generating two uncorrelated sets of uniformly distributed samples as  $(0,1]$ . Each of these sets are assumed to be equivalent to the random cumulative probability values ( $u$  and  $v$ ). Afterwards, the copula value  $C$  for each pair of samples  $u$  and  $v$  is calculated with its correspondent generator function and the chosen degree of correlation. As a result, a third set of samples is generated, which represents the copula bivariate function. Finally, this Copula function which is also bounded in  $(0,1]$  can be inverse sampled with the help of two additional auxiliary random uniformly generated sets bounded and the original generator function. Note that a larger data set of the initial sampling procedure will ensure a “smoother” sampling. In the present study, the random copula generation tools included in the MATLAB program where implemented as they are optimized for efficient sampling of large random value sets.

Copulas are generated taking into account the dependence represented by the correlation parameters ( $\alpha$ ) for the Archimedean family and “ $\rho$ ” Pearson’s coefficient for the Gaussian family (Table 2-1). The “ $\alpha$ ” and “ $\rho$ ” parameters at the same time, can be expressed i the Kendall’s correlation coefficient. Kendall’s rank correlation measures the degree of dependence based on how many data points are concordant compared with the ones that are not concordant when ordered from smallest to greatest. This condition ensures that the dependence degree will not be affected by any transformation in the original dataset, especially when any of the variables is not normally distributed (Dobrić and Schmid, 2007). Regardless of the correlation coefficient selection, the dependence degree can be expressed in terms of the generator correlation parameter (Attoh-Okine, 2013) as shown in Table 2-2.

**Table 2-2. Equivalence expressions between dependence Copula generator parameters and Kendall’s ranking correlation coefficient ( $\tau$ ).**

Gaussian	Gumbel	Clayton
$\tau = \frac{2\arcsin(\rho)}{\pi}$	$\tau = 1 - \frac{1}{\alpha}$	$\tau = \frac{\alpha}{2 + \alpha}$

This equivalence allows to model the correlation for three different type of copulas while inducing the same degree of dependence during the random sampling process. Hence it is possible to compare the different results as a function of the correlation degree for each copula type. The tail dependency between variables will also change according to a correlation parameter.

## 2.2.4 Goodness of fit tests

In order to validate the (synthetical) type of copula and its selection criteria, several types of goodness of fit tests were performed. First, one joint probability surface copula was constructed from the available dataset, as a benchmark for validation. This kind of bivariate models are also known as “empirical copula” models (Nelsen, 2006). They are built based on the univariate marginal probabilities of each of the correlated variables. The accuracy of the empirical copula cannot be judged unless additional data from the location becomes available for validation. Afterwards, a joint probability distribution surface was generated for each of the different copula models. Bivariate distributions can be represented as three dimensional surfaces where each point has as coordinates its parameter value for the x and y axis and its joint cumulative probability in the z axis. Finally, the empirical surface was compared with each of the copula surfaces in order to determine the goodness of fit of each of the copula families. The available methods range from graphical, over different residual error estimators to more formal statistical methods as it was stated by Vandenberghe et al. (2010). Any of these three different type of methods might result in different conclusions if analysed solely. Therefore, a copula selection should only be done after performing more than one of the methods.

The graphical method consisted in generating contours from the four pre built surfaces and plotting them on top of each other. Afterwards a visual examination was performed in order to evaluate which synthetic copula looks more similar to the empirical one. As an additional check, the SAPE method is proposed in order to explain the fitting error based on the amount of available data. A second way to estimate the goodness of fit of a model is by measuring the difference between the observed data and the predicted

one. For an average value the rooted mean squared error (Eq. 2-9) is a suitable approach for interpolated surfaces.

$$RMSE = \sqrt{\frac{1}{n} \sum_{i=1}^n (C_{emp}(u_i, v_i) - C_{family}(u_i, v_i))^2} \quad \text{Eq. 2-9}$$

The third goodness of fit test corresponds to a statistical one. Different studies (Dobrić and Schmid, 2007; Genest et al., 2009; Vandenberghe et al., 2010) have recommended to use the Anderson Darling goodness of fit method for copula selection over methods such Kolmogorov-Smirnov or Cramér von-Mises. This test is rank based and therefore gives more importance to the tail dependency. It is also non-parametric. Initially the test was developed to prove normality of sample populations. The two sample Anderson Darling test statistic ( $AD^2$ ) is calculated as a function of the marginal probabilities of the sampled dataset with  $n$  samples. Afterwards  $AD^2$  calculated statistic value (Eq. 2-10) is compared to the  $AD^2$  equivalent value of the standardized normal distribution with a desired degree of significance.

$$AD^2 = -n - \frac{1}{n} \sum_{i=1}^n (2i - 1) \ln(F(x_{(i)})) + \ln(1 - (F(x_{(n+1-i)}))) \quad \text{Eq. 2-10}$$

In 1987 Scholz and Stevens (Scholz and Stephens, 1987) developed a generalization of the two sample Anderson-Darling test ( $AD^2_{kN}$ ) applicable for any type of statistical distribution (Eq. 16). The major drawback of this generalization is that the threshold statistic value is sample size dependent. Therefore, it needs to be calculated for every time the test is performed with the formula:

$$AD^2_{kN} = \frac{1}{N} \sum_{i=1}^k \frac{1}{n_i} \sum_{j=1}^{N-1} \frac{(NM_{ij} - jn_i)^2}{j(N-j)} \quad \text{Eq. 2-11}$$

The main goals of this test is to try to reject the null hypothesis that states that a certain observed sample comes or behaves like a pre-defined theoretical sample.  $M_{ij}$  represents the number of observations in the  $i$ th sample which are smaller than  $K_j^{\text{th}}$  value. In our case the null hypothesis will try to answer if the empirical copula behaves like the other three synthetic copula models.

## 2.2.5 Reliability method: Monte Carlo with copula random sampling

Monte Carlo method was chosen as the reliability estimation method for this study, as it allows to implement copula models in an easier way compared to more common reliability methods such as SORM or FORM (Steenberghen et al., 2004). The first phase of the method consists in generating the random samples of each of the parameters. The parameters are divided in two groups. The first group random samples is generated by a classical inverse CDF transform method. The second group is also generated with a CDF inverse transform method but instead of generating random uncorrelated values from a uniform distribution between zero and one, they are generated with a random copula sampling method (Biller and Gunes Corlu, 2012) to a chosen “tau” degree of correlation. The correlated sets were generated for 10 different correlation coefficient degrees ( $\tau$ ) ranging from almost 0 until 0.99. This process was repeated for the three copula types. The second phase of the procedure consists in evaluating the correlated and uncorrelated sample set groups in the Sellmeijer LSE. If the critical resistance head ( $H_c$ ) is smaller than the sampled hydraulic head ( $h-h_b-0.3d$ ), then it is accounted as failed sample. In the third and last phase after evaluating all the generated combination samples, the probability of failure is estimated as the ratio between the number of failed samples and the total number of evaluations. The probability density function of the limit state can also be constructed from all the results obtained by each  $Z_{p_i}$  evaluation, represented afterwards a probability density function.

## 2.3 Case study: Lekdijk

The riverine flood defence called the “Lekdijk” located along the Lek river in the province of Utrecht was used as a case study. For this particular location, the VNK2 project (VNK2 et al., 2014) recommended a strengthening measure as the defence didn’t comply with the safety standard. The field sampled “Lek” dataset is composed of 76 soil gradation samples which include  $d_{10}$ ,  $d_{60}$  and  $d_{70}$  measured in the lab. No hydraulic conductivity measurements were available. Hence the  $K$  values were estimated from  $d_{60}$  and  $d_{10}$  by the Kozeny-Carman indirect method (section 2.2.2). The estimated uncertainties (mean, standard deviation and type of distribution) of  $d_{70}$  and  $K$  are presented in Table 2-3.

### 2.3.1 Stochastic parameters

The prior marginal distributions used as input data are presented in Table 2-3.

**Table 2-3. Input data for stochastic failure estimation of PE.**

Variable	Unit	Distribution	Mean	CV	Source
n	[-]	Deterministic	0.25	-	VNK (VNK2 et al., 2014)
$\gamma_s$	[kN/m <sup>3</sup> ]	Normal	26.5	0.1	VNK (VNK2 et al., 2014)
$\gamma_w$	[kN/m <sup>3</sup> ]	Deterministic	9.81	-	-
$\theta$	[deg]	Deterministic	37	-	VNK (VNK2 et al., 2014)
d <sub>70</sub>	[m]	Log-normal	0.000333	0.15	Field
d <sub>70m</sub>	[m]	Deterministic	0.000208	-	VNK (VNK2 et al., 2014)
K	[m/s]	Log-normal	0.000302	1	Kozeny-Carman
g	[m/s <sup>2</sup> ]	Deterministic	9.81	-	-
D	[m]	Log-normal	65	0.1	Field
mp	[-]	Log-normal	1	0.12	VNK (VNK2 et al., 2014)
L	[m]	Log-normal	70	0.1	Field
H*	[m]	Gumbel	a=4.357	b=0.288	HR2006(Rijkswaterstaat, 2007)
h <sub>b</sub>	[m]	Normal	0.5	0.1	Field
d	[m]	Log-normal	4.3	0.3	Field

\* The load term H is assumed to fit a Gumbel extreme distribution with shape and location parameters equal to a and b.

Most of the soil derived mean and variation coefficients were obtained from field samples which were further analysed in the lab. For the non-measured parameters and their associated distribution type functions, recommended values were obtained from VNK (VNK2 et al., 2014). For the extreme distribution fitting of the water levels (loads), information contained in the boundary conditions report for primary water defences assessment was used (Rijkswaterstaat, 2007).

### 2.3.2 PE and Uplift/Heave probability estimation

For the estimation of PE failure probability it is also required to calculate the probability of uplift/heave (Schweckendiek et al., 2014). Both failure mechanisms need to occur in order to ensure the progression of PE as explained in section 2.2.1. For this particular study, the correlation between d<sub>70</sub> and K does not influence the estimated probability of uplift and therefore remains constant for all simulations ( $P_{f_{\text{uplift/heave}}} = 0.621$ ). Note that from the system reliability point of view, uplift and PE are treated as a fully independent failure in parallel which means that the failure probability is calculated as:

$$Pf = P(\text{Uplift/Heave} \cap PE) = P(\text{Uplift/Heave})P(PE) \quad \text{Eq. 2-12}$$

### 2.3.3 Complementary data sets

For benchmarking the results obtained from the Lekdijk dataset, the samples and measurements presented in the studies of the datasets presented by Vienken and Dietrich (Vienken and Dietrich, 2011) and by Van Beek et al. (2011) were used. The first one corresponds to a field campaign of an Aquifer in Bitterfeld Germany. The dataset includes borehole sampling of  $d_{10}$ ,  $d_{60}$  and its correspondent slug test measurements of hydraulic conductivity. The second one corresponds to different Dutch sand samples used for different scale experiments. The data set includes  $d_{70}$  grain sizes and their correspondent hydraulic conductivity lab measurements. This data set is mostly composed of heterogeneous sands.

## 2.4 Results: Correlation degree between $K$ and $d_{70}$

Sellmeijer et al. (Sellmeijer et al., 2011) also showed that the hydraulic conductivity and the  $d_{70}$  representative diameter have the highest relative predictive importance for the Sellmeijer revised limit state equation. Consequently, the present study only considered the effect of correlation of these two parameters. For the present case study, samples from the aquifer stratum were analysed and characterized in order to determine their  $d_{10}$ ,  $d_{60}$  and  $d_{70}$  representative values. Ideally, conductivity in situ measurements will ensure that the estimated correlation is closest to the real one. However, for the present study there is not sufficient measured data in terms of hydraulic conductivity. By the use of the Kozeny-Carman equation, it was possible to estimate the hydraulic conductivity for each soil sample. From the obtained results 2 major aspects can be highlighted. The first one is that the value for the mean univariate marginal distribution of the generated hydraulic conductivity ( $2.87 \times 10^{-4}$  m/s), is similar to the one used in the VNK2 study ( $2.5 \times 10^{-4}$  m/s). Their coefficient of variation (0.98 and 1.0) are very similar as well. This shows that the results by the VNK and the ones obtained from this study are comparable. The second aspect is concerned about the possible inducement of spurious correlation from the fact that the hydraulic conductivity was also calculated from the grain sampled data. The correlation between the grain size quantiles and the estimated conductivities estimated by Kendall's method for the Lek dataset are presented in Table 2-4.

**Table 2-4. Kendall's correlation coefficient between variables.**

<b>Kendall's <math>\tau</math></b>	<b><math>d_{10}</math> [mm]</b>	<b><math>d_{60}</math> [mm]</b>	<b><math>d_{70}</math> [mm]</b>	<b>K [m/s]</b>
<b><math>d_{10}</math> [mm]</b>	1.00	0.786	0.764	0.930
<b><math>d_{60}</math> [mm]</b>	-	1.00	0.968	0.714
<b><math>d_{70}</math> [mm]</b>	-	-	1.00	0.692
<b>K [m/s]</b>	-	-	-	1.00

The Kozeny-Carman model estimates the conductivity values as a function of the  $d_{10}$  and the porosity. At the same time, the porosity is estimated from the  $d_{10}$  and  $d_{60}$ . Nevertheless,  $d_{10}$ ,  $d_{60}$  and  $d_{70}$  represent 3 independent lab measurements. For the Lekdijk dataset, the obtained Kendall coefficient of correlation between  $d_{70}$  and K is 0.692 (Table 2-4). The three different datasets (Lekdijk, Bitterfield and Dutch Sands) correspond to heterogeneous, highly heterogeneous, and homogeneous (Lab and real scale experiments) aquifers measured in different conditions (saturation, temperature, and compaction) which can have a significant effect in the correlation analysis of each of the sets. Nevertheless, the main goal of analysing the three datasets is to find out the order of magnitude of potential correlation while using three different methods of conductivity measurement (indirect Kozeny-Carman computed values, in situ slug test and direct flow measurement from the experimental set up). The first dataset contained grain size values for a highly heterogeneous unconsolidated aquifer located in Germany. From their dataset,  $d_{10}$  and  $d_{60}$  values were measured for 108 samples where a Kendall's  $\tau$  of 0.723 was obtained. This value can also be validated from the statistical significance point of view by the p-value test. This test represents the probability of obtaining this same correlation coefficient while the null hypothesis remains true ( $d_{70}$  and K are uncorrelated). The p-value with significance 0.05 was  $9.9 \times 10^{-19}$  for this dataset. Additionally, 17 samples were presented in the same study with their correspondent in situ hydraulic conductivity measurement. From this set, a Kendall's  $\tau$  of 0.5396 with a p-value of 0.0014 is obtained. The second dataset from the study of van Beek et al. (Van Beek et al., 2011) is composed by values of  $d_{70}$  and K of 50 samples of different Dutch sands used in small, medium and real scale experiments for PE. The Kendall's  $\tau$  obtained for this dataset is 0.522 with a p-value of  $5.1 \times 10^{-7}$  which shows that the estimated tau value is statistically significant.

The tail dependence is another important issue to be studied in reliability assessment of structures as extreme tail values become more important when correlated with other variable extreme values during failure estimation. For the Lekdijk dataset, one may think that based on the plotting of the actual variable values (Figure 2-2.a), a stronger left tail correlation might be evident.

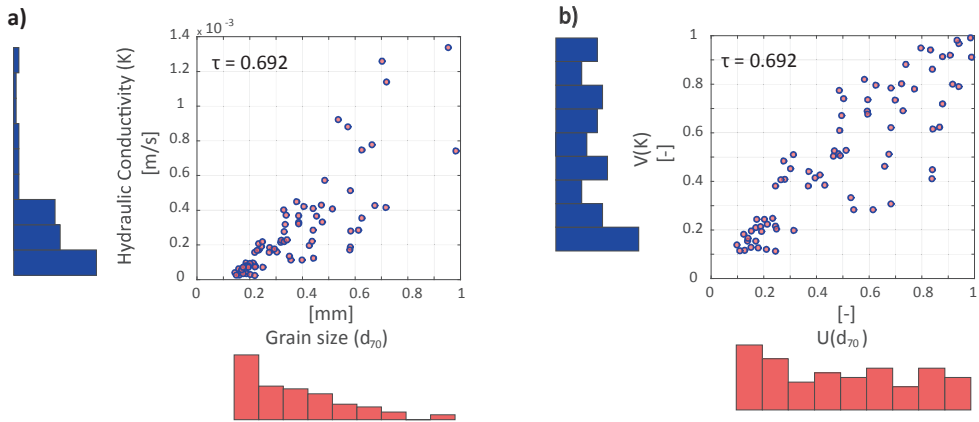


**Figure 2-2. a)  $d_{70}$  vs K and b) marginal probabilities  $U(d_{70})$  vs  $V(K)$**

While this might be true, it is also important to stress out that correlation of variables is measured between its probability marginal and not by the correlation between the actual variable values. In that sense it can be observed in Figure 2-2.b, the dataset presents strong tail dependence in the left tail and mild tail dependence in the right side when plotted in terms of the variable marginal probabilities. There is also higher scattering of the data points around the mean value area of both variables compared to their tails, which implies that a tail dependent model is suitable for representing the relationship. For the datasets from the previously mentioned studies presented by Vienken and Dietrich (Vienken and Dietrich, 2011) and by van Beek et al. (Van Beek et al., 2011), only the last one showed potential left tail dependence (visual inspection).

## 2.5 Results: Copula model selection and validation

### 2.5.1 Graphical method

From the obtained empirical surface, contours were extracted, each spaced by 0.1 joint probability units. Next, the 3 copula surfaces (Gumbel, Gauss and Clayton) were generated while maintaining the same Kendall's correlation coefficient from the dataset ( $\tau=0.692$ ).

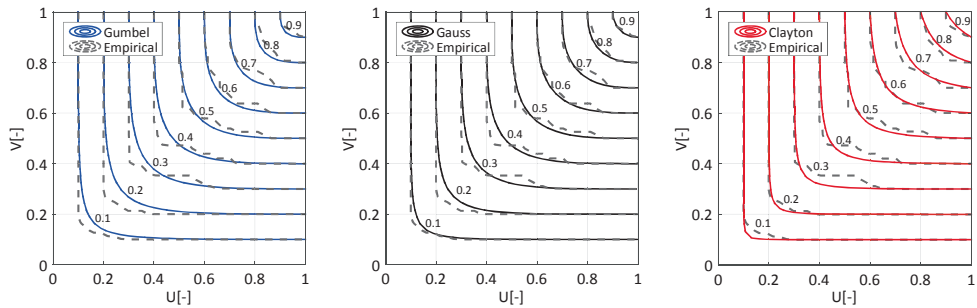


**Figure 2-3. Generated empirical probability contours (dashed) vs Gumbel, Gauss and Clayton copula probability contours with rank correlation coefficient  $\tau=0.692$ .**

After plotting the generated contours (Figure 2-3) it is evident that the three copulas do not outstand between each other in their general performance. As the sampled data does not present a smooth behaviour, the points located in the vertex of the empirical copula are not smoothly curved as the theoretical ones. The available dataset does not cover uniformly and sufficiently the unit space. Therefore, the observed rough edges are a result of the linear interpolation method. From the results of this method, the Gumbel copula can be discarded as the “empirical” contours are always farther from the fitted ones.

As these contours were generated from interpolated surfaces, it is possible to visualize the regions which present higher errors by estimating the spatial absolute percentual error (SAPE):

$$SAPE_{ij} = \left( \frac{|C_{family}(u_i, v_i)|}{C_{emp}(u_i, v_i)} - 1 \right) \quad \text{Eq. 2-13}$$

This type of error is an indicator of the spatial distribution and goodness of fit of the copula models. It is interpreted as the percentage of discrepancy between the empirical copula and the other copula types associated in the space (Figure 2-4). The marginal probabilities  $u$  and  $v$  are correspondent to the variables  $d_{70}$  and  $K$  respectively.

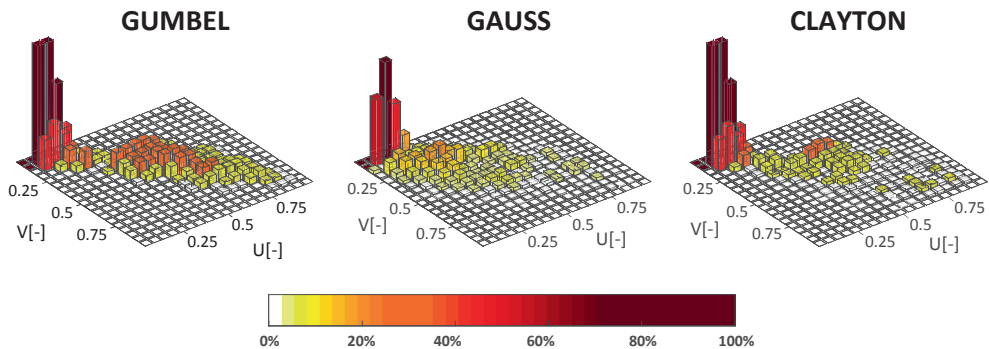


**Figure 2-4. SAPE of the three different copula functions.**

From the SAPE results shown in Figure 2-4, it can be observed that the Gumbel copula presents errors in almost 30% around the mean value area ( $U=0.5, V=0.5$ ), whereas the Gauss and Clayton copulas present errors that are lower than 10%. In the case of the right tail dependence, the two models with higher scattering (Figure 2-2.a) for right tail values represent better the soil behaviour as they present a lower SAPE.

From the left tail dependence, the Clayton copula performs better despite the fact that the extreme value representation is less accurate compared with the other two. This can be explained as the empirical copula surface does not have sufficient data for representing (interpolating) correctly the left tail dependence. In addition, it can be observed (Figure 2-2.b) that the left lower corner area ( $U \leq 0.1, V \leq 0.1$ ) has no available points that represent extreme left tail values in the dataset. This is the main reason why all copulas present higher errors in that area. Furthermore, the Clayton copula surface is steeper around that area. Then, the difference between the empirical and the Clayton surfaces is higher around that area as it is shown in Figure 2-4.

## 2.5.2 Root mean square error (RMSE)

The RMSE is calculated for each of the 76 sampled points used for the copula fitting. The best performance was obtained for the actual calculated tau correlation coefficient ( $\tau = 0.692$ ) with a Gauss copula (Figure 2-5). For low  $\tau$  values, the Clayton copula always performs better. For higher values, both Gumbel and Gaussian copulas present almost the same value of RMSE.

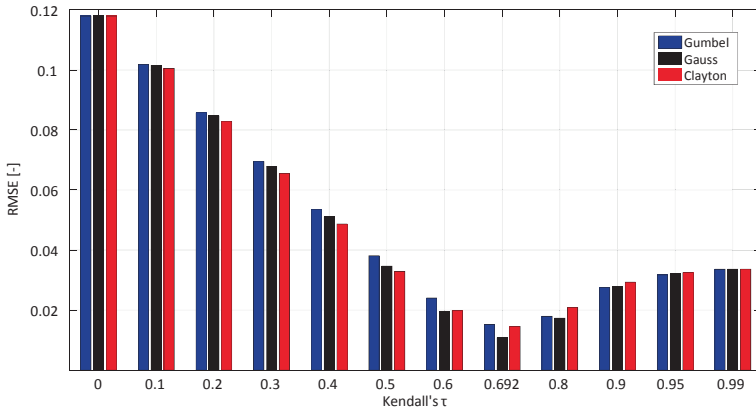


**Figure 2-5. Root mean square errors for different Kendall's rank correlation coefficients estimated from the 76 samples.**

The results presented in Figure 2-5 show that for all copula families,  $\tau = 0.692$  results in the minimum RMSE value for each copula fitting. This value is chosen based on the results presented in Table 2-4 obtained from the Lek dataset. Note that the trend was represented by evaluating values every 0.1 measures of  $\tau$ . Nevertheless, the lowest RMSE for each copula might be achieved in different but very close values to 0.692. Hence it was replaced instead of the 0.7 in Figure 2-5.

From this plot it can also be concluded that neglecting correlation ( $\tau = 0$ ) may result in higher errors despite the exact representation of the tail dependence. For example when comparing the RMSE value found for the correlation value estimated for the Lek dataset (Table 2-4,  $d_{70}$  versus K is  $\tau = 0.692$ ) the error is 0.0107 with respect to the 0.118 obtained for the 100% uncorrelated case ( $\tau = 0$ ).

### 2.5.3 Formal statistical goodness of fit test

For the present study, the generalized Anderson-Darling test ( $AD^2_{kN}$ ) was implemented using the 76 empirical copula values of U and V coordinates, against the copula values of the three copula families for the exact same marginal probability coordinates (U,V). The results in Table 2-5 show that the three synthetic copula families are capable of representing the empirical surface since  $AD^2_{kN}$  statistic value is lower than the critical value. However, the p-value of the test shows that the probability of achieving a better distribution fitting than the Clayton copula is the lowest.

**Table 2-5 Anderson Darling test results for the three Copula fittings**

<b>Copula family</b>	<b>Null Hypothesis <math>H_0</math> <math>C_{emp} = C_{family\ type}</math></b>	<b>Probability of p 5% significance</b>	<b><math>AD^2_{kN}</math> Statistic</b>	<b><math>AD^2_{kN}</math> Critical value</b>
<b>Gumbel</b>	Failed to reject	0.3801	0.9574	2.4948
<b>Gaussian</b>	Failed to reject	0.3479	1.0176	2.4948
<b>Clayton</b>	Failed to reject	0.2304	1.3059	2.4948

## **2.6 Results: Correlation impact in the reliability assessment**

When including correlation of variables in the limit state function evaluation, a change in the marginal distribution variance is expected. However, this amount of change is directly related to how sensitive the limit state function is with respect to the correlated variables.

### **2.6.1 Impact in the limit state marginal distribution**

Left tailed correlated joint distributions will represent higher probability of sampling a lower conductivity value and low grain size  $d_{70}$  diameter in comparison with an uncorrelated joint distribution (Figure 2-6). As a first guess, it is obvious to imply that bigger  $d_{70}$  grains are more difficult to drag and consequently structures founded in sand with greater diameters are less prone to suffer PE processes. Yet according to the Sellmeijer PE failure model, for lower conductivity values a lower probability of structural failure is expected. As the rolling resistance of the grains is less probable to be exceeded for lower conductivity values (less flow inside the cavity), correlation will imply also that a higher frequency of smaller  $d_{70}$ 's (Figure 2-6) is a sign of a safer structure. Therefore, correlation of these two variables will always represent a safer combination state of the structure compared to the uncorrelated case.

Note that the variance of the K parameter in Sellmeijer model has a much greater impact in the total variance of the PE limit state equation than the variance of the  $d_{70}$  according to (Sellmeijer et al., 2011).

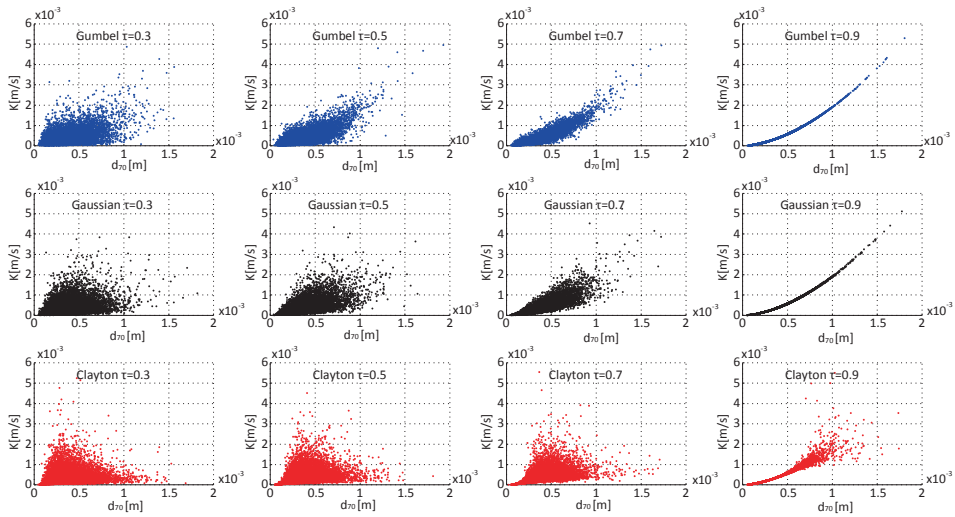


**Figure 2-6. Generated copula samples of  $d_{70}$  representative grain size diameter versus hydraulic conductivity for different correlation degrees (Kendall's tau coefficient).**

This additional safety obtained from correlation is explained from a probabilistic point of view by a combined effect of a mean and variance reduction of the limit state marginal distribution. The first one is very mild and will make the structure less safe in average terms. However, the variance reduction has a much stronger positive effect making the distribution less spread (Table 2-6) and consequently safer. The overall effect is translated in a safer structure as it can be concluded from the reduction in the coefficient of variation no matter the copula correlation model used. It's also observed from the variation coefficients for each copula family how the marginal effect of the variance reduction is greater for low correlation values.

**Table 2-6 Obtained Standard deviation of  $Z_p$  for different rank correlation copulas.**

Tau	GUMBEL			GAUSS			CLAYTON		
	Mean [m]	Std [m]	CV [%]	Mean [m]	Std [m]	CV [%]	Mean [m]	Std [m]	CV [%]
0.00	4.710	2.490	53	4.710	2.490	53	4.710	2.490	53
0.30	4.661	2.308	50	4.656	2.284	49	4.650	2.240	48
0.50	4.628	2.191	47	4.628	2.166	47	4.620	2.128	46
0.70	4.606	2.095	45	4.602	2.075	45	4.605	2.061	45
0.90	4.592	2.031	44	4.590	2.029	44	4.599	2.030	44
0.95	4.589	2.024	44	4.589	2.021	44	4.594	2.028	44
0.99	4.591	2.019	44	4.591	2.022	44	4.589	2.023	44

## 2.6.2 Impact in the tail located events

For failure, the zone bounded between  $-\infty$  and 0 (tails zoom)

Figure 2-7) is the one of more interest as its integral represents the probability of the flood defence to fail due to PE. The bars in

Figure 2-7 represent the histogram of the limit state function obtained from an uncorrelated stochastic estimation. The other three lines represent the obtained limit state probability density function for the three copula families with different degree of rank correlation.

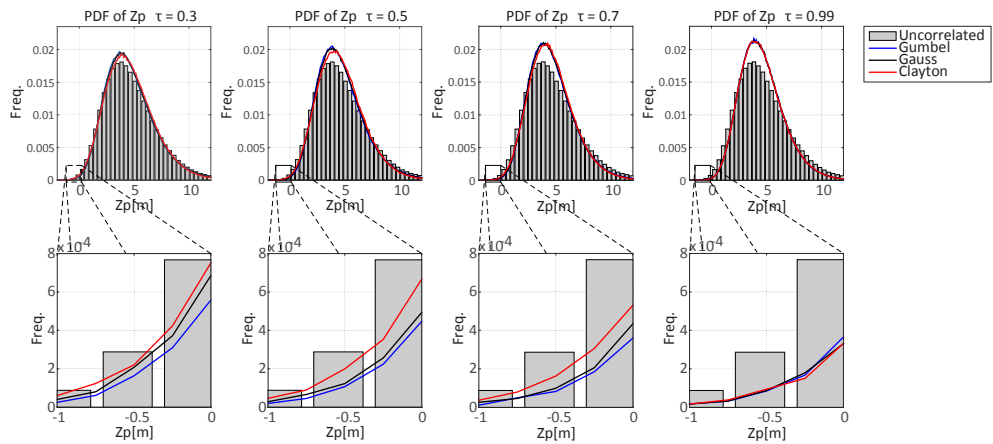


**Figure 2-7. Probability density functions of LSE for different copulas with different correlation.**

From the tail zoom, it can be observed that the rate of change of probability of failure is also different. For example, the Clayton copula gives a higher probability of failure for a low rank correlation. It can also be observed that every time the induced correlation is increased, the frequency peak of the pdfs increases as well. This is expected as the reduction of the variance due to correlation will redistribute the area as the density function becomes steeper in the tails.

Even though there is a significant change in the total variance of the model, it cannot be concluded that this change is attributed solely to these two variables. The other variables included in the Sellmeijer limit state equation are also fluctuating along their uncertainty ranges and therefore the variance of the LSE will also be affected by them in a minor scale.

### 2.6.3 Reliability Index ( $\beta$ )

In the Dutch regulation, the minimum return periods that flood defences need to have are clearly defined for each of the main flood defence systems inside the country. In the case of the Lekdijk, a minimum return period of 2000 years is required for river flood defences located in the dike ring 16. This value is equivalent to the total probability of all possible types of failure mechanisms combined for all the flood system components (e.g. representative cross sections). For each copula function, the total (PE/Uplift) failure probability was estimated by inducing different degrees of correlation between  $d_{70}$  and  $K$ . The results with their correspondent 95% confidence intervals (dashed lines) are presented in Figure 2-8. These intervals are calculated from the different probability estimations from the Monte Carlo simulation for each degree of correlation.

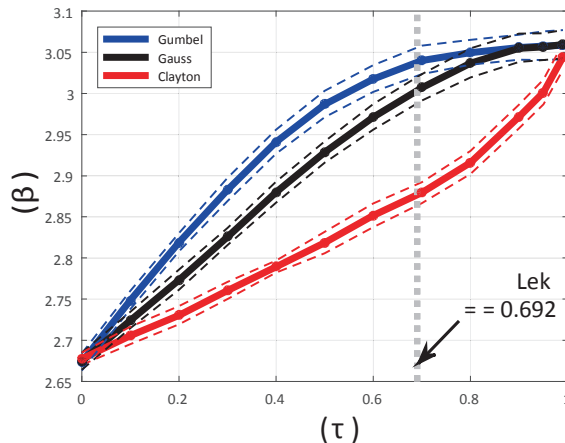


**Figure 2-8. PE/Uplift  $\beta$  index of the Lekdijk flood defence as a function of rank correlation coefficient ( $\tau$ ) with 95% confidence bounds**

For reliability assessment of structures it is common practice to refer to the Hasofer-Lind reliability index ( $\beta$ ) to define the structure safety instead of the failure probability. This is a more comprehensible measure in terms of failure for designers who are guided by legislative design codes.

The VNK2 study concluded that for the Lekdijk flood defence in Vianen. The return period associated solely to PE (PE/Uplift) in the specific location for this study is 280 years ( $P_f = 3.5 \times 10^{-3}/\text{year}$ ). This is equivalent to a reliability index ( $\beta$ ) of 2.69. For our study, for the uncorrelated case ( $\tau=0$ ) the  $\beta$  reliability index obtained is equal to 2.675 (Figure 2-8). This is equivalent to a return period of 267 years ( $P_f = 3.74 \times 10^{-3}/\text{year}$ ). The small difference in reliability indexes between the VNK value and the present study can be attributed to the different LSE used (non-revised versus revised Sellmeijer) and

the more detailed field values used for representing the parameter uncertainties in this study. Also the analysis is done for a single cross section where the seepage length is selected based on possible inflow and outflow points observed in the field. The dashed line represents the best correlation estimate between  $d_{70}$  and  $K$  (Table 2-4,  $\tau = 0.692$ ) obtained from the soil sampled dataset (Figure 2-8). In this case the  $\beta$  index will differ significantly with respect to the uncorrelated case no matter which copula model is chosen.

From three models, the Clayton copula is the most conservative as it will always result in lower reliability indexes with respect to the Gaussian and the Gumbel copulas. The explanation for this behaviour can be deduced from the combined inclusion of the  $d_{70}$  and  $K$  parameters in the  $F_S$  term (equation 3) of the Sellmeijer limit state function. The hydraulic conductivity is powered to  $1/3$  whereas the  $d_{70}$  is powered to  $2/5$ . A smaller power of a small number will always be greater than a larger power of the same small number. This means that the denominator will be greater than the numerator in average. The Clayton copula induces higher tail dependency for left tail values (low permeability and low representative diameter) and consequently higher probability of sampling them at the same time. Conclusively, the  $F_S$  term probability distribution of a Clayton copula has higher probability of having a smaller mean value than the other two and consequently a lower critical head mean value ( $H_c$ ) with respect to the other two.

## 2.7 Discussion

### 2.7.1 Research question 1

Is there any considerable correlation between the representative grain size ( $d_{70}$ ) and the hydraulic conductivity?

First, it's important to note that the hydraulic conductivity values for this study were calculated and not measured. For the Lekdijk soil investigation, three different independent values were used to generate the marginal distribution of the hydraulic conductivity. More explicitly, the  $d_{70}$ ,  $d_{60}$  and  $d_{10}$  values are obtained from the gradation curves of each sample which are measured by passing the collected soil through different incremental sieves. While one sample contains all grain sizes and knowing that  $d_{60}$  and  $d_{70}$  are quite similar for well graded soils, they are still measured as independent values. Kozeny-Carman equation only uses  $d_{10}$  and  $d_{60}$  values for the hydraulic conductivity estimation. Hence, the correlation found between  $d_{10}$  and  $d_{60}$  is independent of the correlation found between  $K$  and  $d_{70}$ . This can be observed in the Kendall's correlation

values presented in Table 2-6. Nevertheless, the obtained values must also be analysed by comparing their results with other studies in order to clarify if they are feasible.

The obtained values for mean and standard deviation from the sampled data for  $d_{70}$  and  $K$  in the present study are in fully agreement with the ones used for the VNK study (V NK2 et al., 2014). This suggests that implementing the Kozeny-Carman equation gives a good approximation value in terms of the order of magnitude and statistical characterization when compared to the measured values in the field. Consequently, it proves to be a powerful tool when no field measurements are available. The correlation between  $d_{60}$  and  $d_{70}$  is normally quite high for granular soils and even more for this dataset in particular. Therefore, when calculating  $K$  as a function of  $d_{10}$  and  $d_{60}$  and then estimating the correlation degree from the  $d_{70}$  values obtained from the same samples, the expected degree of dependence is higher than calculated from independent measured values. Nevertheless, the actual Dutch methodology even accounts for this correlation degree by including an “alpha” coefficient in the method used for estimating the hydraulic conductivity (Calle and Weijers, 1994). The optimal situation would be if for each borehole sample, an in situ measurement of the local hydraulic conductivity was performed instead of calculating them via Kozeny-Carman model. Yet, this kind of data was not available for the present study. In addition, the aleatory uncertainty associated to the measurement of the hydraulic conductivity is large in comparison to the one associated to the  $d_{70}$ . In the present reliability method this issue is addressed by the selection of the coefficient of a variation (CV, Table 2-3) for the two variables during the random sampling. The influence of this uncertainty is case dependent and cannot be generalized. Still, a sensitivity analysis of the coefficient of variance is a helpful tool to estimate its influence in the failure probability value for a fixed correlation degree. In contrast, the epistemic uncertainty derived from the simplification of assuming an equivalent hydraulic conductivity value for the whole aquifer (Sellmeijer limit state function) can be quantified by implementing the complete Sellmeijer numerical solution in which the hydraulic conductivity can be represented in more detail with a layered aquifer for example.

In order to determine if the high correlation value obtained between  $d_{60}$  and  $K$  in the present study ( $\tau = 0.714$ , Table 2-4) is a feasible value, the sample dataset from the research paper from Vienken and Dietrich (Vienken and Dietrich, 2011) was used. Their study is presented with a dataset that contains  $d_{60}$  values with their correspondent in situ measurements of slug testing for hydraulic conductivity. The Kendall's rank correlation between  $d_{60}$  and  $K$  obtained for their dataset is  $\tau = 0.5396$  ( $\rho=0.64$ ). These samples were obtained from a highly heterogeneous unconsolidated aquifer in

Bitterfield, Germany. Measurements from less heterogeneous sands presented by van Beek et al. in (Van Beek et al., 2011) were also analysed resulting in a  $d_{60}$  versus  $K$  correlation  $\tau = 0.522$  ( $\rho=0.671$ ). This results show that the correlations obtained for the Lekdijk (Table 2-4,  $d_{60}$  versus  $K$   $\tau = 0.714$  and  $d_{70}$  versus  $K$   $\tau = 0.692$ ) is not impossible to obtain but is significantly different to the one obtained for this research case study. Both studies can also be assumed as highly reliable given the sampling techniques employed for the conductivity measurement. The Bitterfield dataset presented Vianken et al. is composed of in situ measurements only which makes it more realistic but the significance can be quite low as only 22 slug tests were done in 4 different boreholes. Then the same dataset contains 108 core samples which were characterized for this sampling campaign as well. The rank correlation coefficient obtained for this larger dataset between  $d_{10}$  and  $d_{60}$  is equal to  $\tau = 0.608$ . This value is closer to the one found for Lekdijk case (Table 2-4,  $\tau = 0.786$ ). Despite the differences found for all Bitterfield, Dutch sands and Vianen aquifer, all show either left tail dependence (section 2.5) and/or significant correlation.

## 2.7.2 Research question 2

How to select and validate a correlation bivariate model (Copula family) to correctly include its effect in the failure estimation due to PE?

In principle, if no data was available for deriving any quantitative conclusion, porous media theory suggests that the soils with smaller representative diameter values tend to present higher correlation in the resistance of water to flow inside them, Bear and Buchlin (Bear et al., 1991) explain how these two parameters are correlated according to Darcy's law, if inertial effects are included in its differential form. If so, a new quadratic term appears in the equation which expresses the exponent relation between the grain size and the flow velocity in presence of a porous matrix. The study presented by Chapuis (Chapuis, 2012) shows that most relevant empirical models for predicting conductivity from grain sizes are based on this exponent relation. In fact, it can also be concluded that models are majorly built based on values of the smaller representative particle sizes from the sand samples while their representative hydraulic conductivity values range between  $1 \times 10^{-2}$  to  $1 \times 10^{-14}$  m/s. Hence it can be concluded that the bivariate joint distribution should have a stronger left tail dependence (smaller grain sizes) which allows to discard the "Gumbel" copula function from the start. However, it was included in the present study as a measure of probabilistic bounding for understanding the consequences of assuming the wrong model. From the point of view of the obtained results of the different goodness of fit of the copula models, the Clayton

performed better than the Gaussian in two of the three tests. Nevertheless, the results do not reflect an extreme over performance between the two remaining models. In addition, all three models had difficulty representing the left tail dependence. Most likely to be originated from the fact that the empirical copula surface lacks information in the left tail corner area. Therefore, the SAPE test is a more reliable performance method for assessing copula goodness of fit when low tail data coverage is observed.

From all the results presented in this study, the Clayton copula better represent the soil behaviour based on the literature and the available soil data. Nevertheless, the results of this study cannot be used to recommend one over the other one for the general case. Yet for the Lekdijk case study, the Clayton copula is recommended as a first choice if no additional information is available.

### 2.7.3 Research question 3

How important is the impact of correlation between  $d_{70}$  and  $K$  in the reliability assessment against PE?

The two main observed effects are the reduction of the variance and the “no effect” in the average marginal resistance value of the structure due to PE. As it was stated, the mean resistance of the structure is not affected at all. However, the variance reduction originated from the correlation and tail dependence represents a more reliable structure with respect to the uncorrelated case. This also can be explained from a physical point of view as a greater conductivity allows the water to flow easier in the aquifer which makes it less safe. However, for conductivity to increase there has to be a larger porosity which can only be achieved by the increasing the percentage of bigger grains in the grain distribution. These larger grains are more difficult to drag and therefore they make the aquifer less prone to be eroded. Consequently, both extreme tail values are counteracting with each other, reducing their importance reflected in the estimated resistance value in the limit state marginal distribution evaluation.

The results for the Lekdijk field data suggest that  $d_{70}$  and  $K$  are correlated with  $\tau=0.692$  (Table 2-4) with left tail dependence which is better represented by a Clayton copula function. With these characteristics, the probability of having PE is  $2.01 \times 10^{-3}$ /year. This is equivalent to have a return period of 498 years or a  $\beta = 2.877$ . For assessing the impact in the safety assessment of PE, the error is estimated as the difference in failure probabilities between the resultant reliability indexes of any correlation assumption compared to these results. Therefore, three different scenarios can be derived:

Scenario 1:  $d_{70}$  and  $K$  are 100% correlated.

This is a highly unrealistic scenario but it can be used to understand what assumption impacts the failure estimation the most. The reliability index for any 100% correlated copula model is equal to 3.05 which is equivalent to a  $P_f$  of  $1.14 \times 10^{-3}$ /year. The error that one can incur by assuming the model to be completely correlated is 43% of overestimation. This means that the flood defence will be assumed as 43% safer.

Scenario 2:  $d_{70}$  and  $K$  are correlated in  $\tau=0.692$  while assuming a wrong copula model.

This scenario will be equivalent to choose the results obtained for a Gumbel copula correlated with the “correct” degree of dependence. The estimation of failure probability due to PE would be equal to  $1.19 \times 10^{-3}$ /year ( $\beta = 3.04$ ). Therefore, the assessment of the flood defence is 40.7% safer against PE.

Scenario 3:  $d_{70}$  and  $K$  are 100% uncorrelated (Actual assumption in these type of assessments).

In the actual procedure for PE failure estimation,  $d_{70}$  and  $K$  are assumed as 100% uncorrelated which means that the Lekdijk probability of failing because of PE is  $3.71 \times 10^{-3}$ /year ( $\beta = 2.677$ ). That would represent an underestimation of 85% in the reliability of the flood defence towards PE. In other words, the flood defence is assumed as 85% less safe than what it can actually be. Such results may drive decision makers towards strengthening policies which might not be required. Or at least not until a more robust soil investigation is performed.

For the system that includes the Lekdijk (Dike ring 16) it was found that according to the VNK safety assessment results, 79.4% of the total failure probability could be attributed solely to the PE failure mechanism. According to the Dutch regulation, the Lekdijk defence must have at most a total failure probability of  $5 \times 10^{-4}$ /year. Therefore, the minimum allowable failure probability of the Lekdijk due to PE is  $0.794 \times 5 \times 10^{-4}$ /year which equals  $3.97 \times 10^{-4}$ /year ( $\beta = 3.35$ ). For design purposes, the percentage of failure budget (maximum allowable probability of failure due to an specific failure mechanism) is even more strict as presented in (Jongejan and Calle, 2013). In their study, the failure budget allocated for estimating the maximum allowable failure probability is 35% of the total failure probability ( $3.97 \times 10^{-4}$ /year or  $\beta = 3.58$ ). Consequently, no matter the correlation degree, the Lekdijk must be strengthened as its estimated reliability index obtained by including the effect of correlation with the best fitting copula model is  $\beta = 2.877$ . Nevertheless, if correlation is included in the strengthening measures

design (flood defence width, berm or sheet pile), a less expensive design will be obtained.

As a final remark, it was observed that this method can also be used for probability bounding. More kinds of copulas are available but for the present study, only the ones that showed dependence degrees in each of the tails and non-tail dependence (Gaussian) were selected. It is also acknowledged by the authors that large amounts of samples are required in order to have a reliable estimate of the degree of correlation between  $d_{70}$  and  $K$  and best copula model selection.

## 2.8 Conclusions and recommendations

Strong evidence that significant correlation degree between  $d_{70}$  and  $K$  is feasible is concluded from the results obtained from the Lekdijk case study and from the complementary datasets provided by other authors. Nevertheless, it is also acknowledged that for the present case study, the high correlation degree originates from the high intrinsic correlation structure present between the  $d_{10}$  and  $d_{70}$  values for the Lek dataset in particular.

Based on the Lekdijk dataset, the Clayton copula model is capable of describing the bivariate behaviour and the physics of the soil in this location better than the Gumbel or the Gauss copula. Therefore, the Clayton copula or any other copula model with stronger left tail dependence is recommended as it can represent statistically and physically better the behaviour of the correlation between the  $d_{70}$  representative grain size and hydraulic conductivity.

No matter which copula type is chosen, the correlation inclusion in the Sellmeijer LSE shows always a reduction in the failure probability of PE. This is a result of the monotonic variance reduction in the limit state marginal density function that results from joint effect of including  $k$  and  $d_{70}$  as correlated in the LSE method.

The present study showed that the assumption of uncorrelated variables implemented in the actual safety assessment for PE performed in the Netherlands might be conservative. The assumption of no correlation between  $d_{70}$  and  $K$  will be translated to higher probabilities of failure when the structure is assessed with the Sellmeijer revised equation.

The assumption of any tail dependent model with any correlation degree will result in a smaller error in the estimation of the failure probability due to PE when compared to the 100% uncorrelated case.

Correlation assessment for the Sellmeijer PE model is recommended as for the Lekdijk case study the failure probability is overestimated by a factor of 1.84 ( $P_{f_{\text{correlated}}} = 2.01 \times 10^{-3}/\text{year}$ ,  $P_{f_{\text{un-correlated}}} = 3.71 \times 10^{-3}/\text{year}$ ) when assuming the two parameters to be 100% uncorrelated.

Solutions like wider cross sections, sheet piling or berms are common ways to cope with PE. For probabilistic design of flood defences, the omission of correlation can result in less cost effective designs by adding this kind of measures when they might be not needed. Therefore, a more detailed soil investigation is recommended in locations where failure is expected or in locations where the historical performance of the structure differs significantly with the expected limit state.

All goodness of fit methods are derived from the interpolation of copula surfaces. Therefore, the optimization of discretization criteria for the interpolation is recommended.

## 2.9 Acknowledgements

“This research is supported by the Dutch Technology Foundation STW, which is part of the Netherlands Organisation for Scientific Research (NWO), and which is partly funded by the Ministry of Economic Affairs.” The authors would like to thank the STW foundation, Raymond van der Meij and the flood risk department from Deltares, Doctor Mireia Romaguera from ITC Twente Faculty, the anonymous reviewers of this journal and the Integral and sustainable design of Multi-functional flood defences program for the help and support.



# Chapter 3

## Piping erosion safety assessment of flood defences founded over sewer pipes

### Abstract

Piping erosion is one of the major causes of failure of flood defences. The occurrence of this failure mechanism is difficult to predict and it can be triggered by a flood event. The inclusion of hard structures under flood defences will change the probability of occurrence of this erosion process. The present study aimed at understanding the effect of an embedded sewer pipe under the flood defence foundation in its safety assessment for piping erosion failure. This was done by setting a probabilistic analysis framework based on emulation of finite element models of porous media flow and the fictitious permeability approach. The effects of size and location of the sewer pipe were evaluated via a deterministic stability factor approach. Later, emulators of the safest and most unsafe finite element models were trained and used for probabilistic assessments. For the case without a sewer pipe, the emulator approach showed good results when compared to the Sellmeijer limit state revised function. The results showed that the embedment of a sewer pipe in the flood defence foundation has a significant effect on its safety. The magnitude of the effect is highly dependent on the size and location of the sewer pipe. Furthermore, the foundation permeability uncertainty shows a conditional effect with respect to the sewer pipe size and location.

**This chapter is published as:** Aguilar-López, J.P., Warmink, J.J., Schielen, R.M.J., Hulscher, S.J.M.H., 2016a. Piping erosion safety assessment of flood defences founded over sewer pipes. *European Journal of Environmental and Civil Engineering*: 1-29. DOI:10.1080/19648189.2016.1217793

### 3.1 Introduction

Piping erosion is a deterioration process that threatens flood defences by compromising their structural stability during a flood event. This failure consists in the progression of erosion “channels” underneath the flood defence granular foundation due to water movement. It is originated from the head difference between the water body and the protected side when the water level raises. Recently, large interest has emerged in the modelling, prediction and uncertainty assessment of this failure mechanism. More specifically, in the probabilistic estimation of the occurrence of this kind of failure (Hoffmans, 2014a). The inclusion of an embedded structure located underneath the flood defence will change the groundwater flow patterns and consequently will have an effect in the piping erosion failure prediction and uncertainty as well. Flood risk managers and urban planners are inclining towards solutions such as multifunctional flood defences (Van Loon-Steensma and Vellinga, 2014; Van Veelen et al., 2015) given climate change and demographic explosion in urban areas. If so, the combination of flood defence strategies and additional embedded infrastructure such as sewer pipes will become an option instead of an exception.

Probabilistic assessment of structural deterioration processes (failure mechanisms) consists in the propagation of variable uncertainties through a model which is later used to assess the probability of occurrence of an event. For the particular case of piping erosion and sewer pipes, the model used for the uncertainty propagation should be capable of predicting whether the piping erosion progresses or not. At the same time, it should include the effects of the additional structure on the ground water flow.

The most relevant modelling approaches for piping erosion were grouped into three categories based on the type of representation of the process (Wang et al., 2014). The first category is composed of models which represent the piping zone as a less impermeable soil. They consider the pore pressure distribution in the whole foundation during the modelling process. The application of this kind of models has been found in 3 different piping erosion studies (Jianhua, 1998; Bersan et al., 2013; Vandenboer et al., 2014b). The second category consists of models that are capable of representing the mixture of water and soil flow inside the progressing channel. This is done by combining the numerical solution of the Darcy (fully saturated) or Darcy-Brinkman’s (partially saturated) equations for the porous media domain with the Navier-Stokes equations for the pure water domain. At the same time, particles are modelled individually based on a particle tracing trajectory numerical solution. Such methods are quite detailed and allow to describe the erosion progression in time, but are computationally demanding

given the individual particle modelling. Examples of these models (El Shamy and Aydin, 2008; Lominé et al., 2013) show promising results as well. The third category includes the models (Sellmeijer and Koenders, 1991; Lachouette et al., 2008; Zhou et al., 2012) where soils are divided into phases with different erosion models which are governed by different physic laws. The numerical model used in the present study for uncertainty propagation correspond to the first category.

The uncertainty in the water levels and the soil characteristic values will highly influence the safety assessment of piping failure (Sellmeijer et al., 2011). For the particular case in which a sewer pipe is embedded in the foundation, the combined effects of the earlier mentioned uncertainties plus the “atypical” behaviour in the groundwater flow due to the inclusion of the hard structure will make safety assessment even less accurate. Then, the probabilistic methods become a more suitable type of assessment as they can include the most relevant uncertainties for the system. To our knowledge, there is no available literature that presents the probabilistic effect on piping erosion originated from the presence of hard structures embedded in the foundation of the flood defence. The only study found which included structural embedment (Wang et al., 2014) recreated the progression of piping erosion in time with a cut-off wall under a flood defence. The drawback of this method is its demanding numerical solution which requires an iterative process that makes it computationally expensive and unreliable for probabilistic safety assessments. Note that the propagation of the variables uncertainty implies a large number of simulations which in some cases may be computationally unfeasible.

In reliability science, it is common practice to use model simplifications, which only determines the state of the system based on the most relevant “state variables” instead of modelling the physical process. These models are represented in the form of “limit state functions”. These functions represent the difference between the resistance ( $R$ ) of the structure against a failure mechanism and its solicitation load ( $S$ ). This type of modelling is more suitable for probabilistic safety assessment as they are easier to evaluate (reduced computational burden) and can be built based on more complex numerical solutions if required. In the case of piping erosion failure, several notable examples of limit state equations are commonly used for either levee or large dam safety assessment (Bligh, 1910; Lane, 1935; Terzaghi et al., 1996; Ojha et al., 2008; Sellmeijer et al., 2011). These models do not allow to explicitly include the effects of embedded structures in the ground water flow. Hence, the uncertainty of their application in safety assessments increases when embedded structures are present underneath.

The present study aimed at developing a methodology that allows to understand and quantify the effect on the safety assessment of piping erosion derived from placing a hard structure underneath a flood defence. As a realistic example, we use the embedment of a sewer pipe inside a granular foundation of a dike. The models used in the present study for performing the different assessments are based on the results obtained from the IJkdijk real scale experiment for piping erosion (Koelewijn et al., 2014). In order to do that, three main research questions were formulated for assessing the safety of the flood defence:

1. How can we model the process of piping erosion while including an embedded sewer pipe and the soil uncertainties at the same time?
2. What are the effects of the sewer pipe characteristics such as size and location in the flood defence safety?
3. What are the effects of the water loads and soil uncertainty in the safety assessment of a flood defence with a sewer pipe embedded in its foundation?

The present paper explains the methodology used for solving these three research questions. First, the IJkdijk experiment is explained in section 3.2. Afterwards, the steps of the methodology used to for building the FEM models for the deterministic and probabilistic assessments are explained in section 3.3. This part allows to solve the research question 1. The data and stochastic distributions (parametric uncertainties) used for building the model emulators and performing both (deterministic and probabilistic) safety assessments are presented in section 3.4. The results of both safety assessments are presented in section 3.5 which are used to solve the second and third research questions. Finally, the conclusions of the study are compiled in section 3.6.

## **3.2 IJkdijk full scale experiment**

Full scale experiments for levee failures were performed as part of the “IJkdijk” Dutch research project (initiated in the year 2005). The project (Sellmeijer et al., 2011; Koelewijn et al., 2014) aimed at testing monitoring techniques and improving the knowledge on geotechnical failure mechanisms of flood defences in real scale structures. For the case of piping erosion, the experiment consisted in monitoring the erosion process inside the foundation of a real scale flood defence due to an incremental water load, until achieving the complete failure process. Four tests were performed in flood defences built with the exact same cross section as the one shown in Figure 3-1. Each of the four experiments was composed of an impermeable levee founded in a different type of sand.

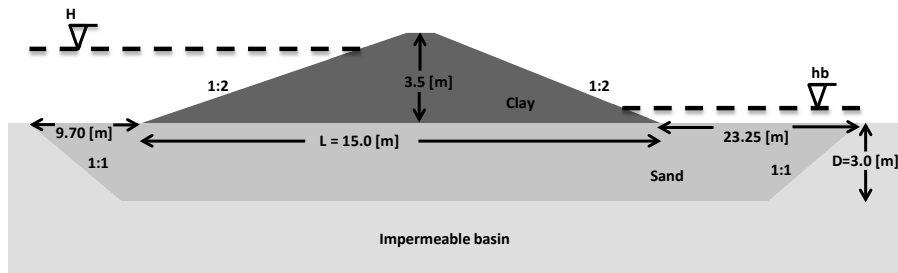


Figure 3-1 IJkdijk cross section for piping erosion test (not in scale)

For the present study, the experiment number 3 performed in 2009 was selected as there was no clogging of the erosion channel during the test. The measured characteristics and results from the experiment (Koelewijn et al., 2014) are shown in Table 3-1.

Table 3-1 IJkdijk experiment 3 parameters and results

Parameter	Value	Unit
Aquifer permeability ( $k$ )	1.07E-11	[m <sup>2</sup> ]
Representative grain diameter ( $d_{70}$ )	180.0	[ $\mu$ m]
Potential seepage length ( $L$ )	15.0	[m]
Aquifer depth thickness ( $D$ )	3.0	[m]
Critical head difference to failure ( $H_c$ )	2.1	[m]

### 3.3 Method

In short, the method consists in building and calibrating a detailed finite element model (FEM) of a conventional flood defence based on the measured conditions from the “IJkdijk” piping real scale experiment presented in section 3.2. The grain equilibrium concept for piping erosion (Sellmeijer, 1988), was used for building all FEM models built in this study. To simplify the numerical solution, a fictitious permeability equivalence was implemented (Bersan et al., 2013). The most important aspects for calibrating this model are the erosion channel average size and shape. To our knowledge, there is no literature available for predefining these characteristics of the erosion channel in a model. Hence the first part of the study consisted of a sensitivity analysis of this parameter for determining the best choice based on the IJkdijk experimental results. After defining the size and shape of the erosion channel, the aquifer depth and permeability influence in the erosion capacity were also studied in this analysis. The rest of the parameters were available from the reports of the experiment. This calibration and validation procedure corresponds to the first part of the study.

The second part of the study consisted in modifying the initial model by including an embedded sewer pipe. This process is repeated several times for different sizes and locations of the embedded structure in order to assess its effect on the stability factor of the structure. This part corresponds to the “deterministic” safety assessment of the structure.

For the third part of the present study, the most safe and unsafe configurations found in the deterministic assessment are selected for further analysis. For each of these cases, an artificial neural network (ANN) emulator was built (referred as surrogate models in Chojaczyk et al. (2015)). This was done by generating training data from the original FEM models. These models were later used for failure probability estimation. This analysis corresponds to the probabilistic safety assessment. The order of the steps taken for each section is presented in the methodology flow chart of Figure 3-2.

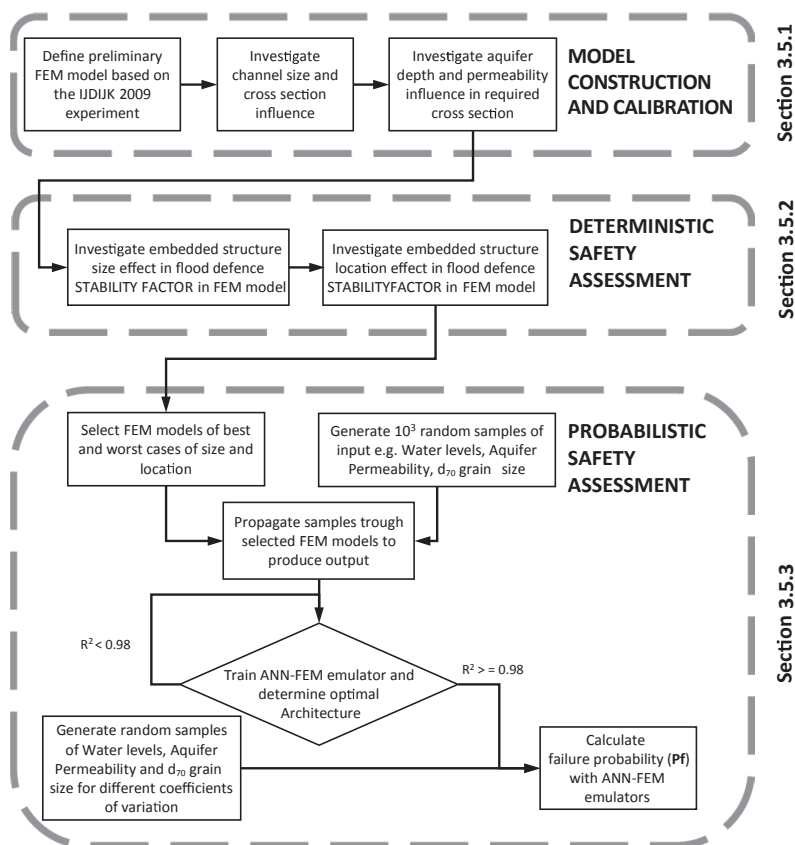


Figure 3-2 Methodology flow chart

### 3.3.1 Piping erosion model

The numerical solution for the present study corresponds to a multiphase piping erosion type of model. Two different configurations of FEM models were built for the present study for the safety assessment as presented in Figure 3-3.

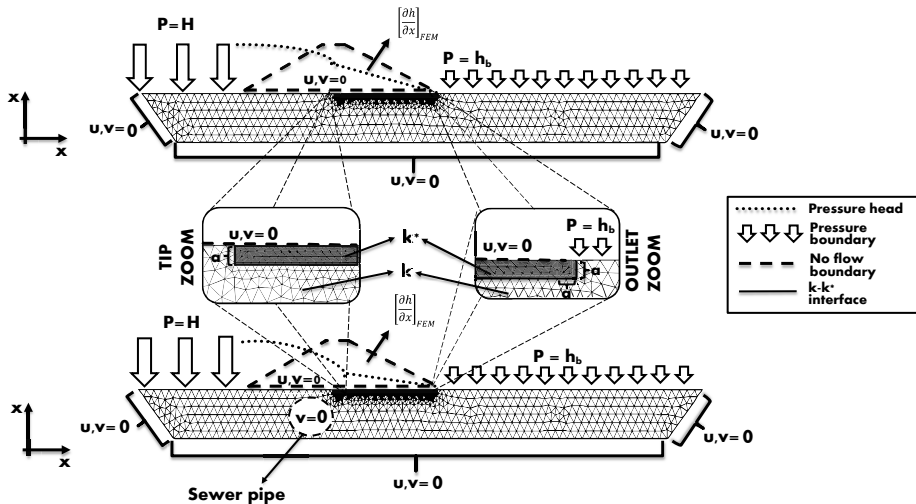


Figure 3-3 IJkdijk cross section and boundary conditions of FEM models with and without embedded sewer pipe

The first model corresponds to the case of a flood defence with no sewer pipe embedded in the foundation aquifer. The second model includes an embedded sewer pipe (a hollow circle boundary with no inflow or outflow) inside the foundation aquifer. Later the size and location of the sewer pipe are changed and a new model is produced. All models were built based on the “IJkdijk” experimental flood defence dimensions presented in (Koelewijn et al., 2014). Both have the same external boundary condition definition. The boundaries with pressure distributions allow water inflow towards the porous media whereas the ones with null velocity component represent the absence of inflow as presented in Figure 3-3.

According to Sellmeijer’s conceptual model (Sellmeijer, 1988), the equilibrium condition of piping erosion is defined by the horizontal pressure gradient ( $\left[\frac{\partial h}{\partial x}\right]_{FEM}$ ) exerted inside the erosion channel and the rolling grains resistance. This condition is represented by a two forces limit equilibrium assumption. According to experimental findings (Sellmeijer and Koenders, 1991), it is assumed that this equilibrium condition becomes critical once the erosion channel has progressed until approximately the midpoint of the flood

defence. If the pressure gradient becomes larger than the rolling resistance at this particular point, the erosion progression will continue indistinctively from the loading conditions of the structure until the failure of the flood defence foundation. This condition is predefined in the FEM model by the inclusion of the erosion channel until the exact midpoint, as it can be observed in Figure 3-3. The thick dashed line represents the impermeable flood defence body.

### **Load Term (S): Erosion channel inner pressure gradient**

The pressure gradient ( $\left[\frac{\partial h}{\partial x}\right]_{FEM}$ ) inside the predefined erosion channel (Figure 3-3) is the only required output from the model for assessing the occurrence of the piping erosion failure. Both FEM models are solved for a steady state condition of the system. This choice is correct for systems where the “limit state” condition do not include any time dependencies as the one presented in this study. Hence, the flow inside the porous media can be solved by the steady state Darcy’s law (Eq. 3-1):

$$u = -\frac{k}{\mu}(\rho g \nabla H) \quad \text{Eq. 3-1}$$

The equation is used to estimate the flow velocity ( $u$ ) of the water through the porous medium as a function of the soil permeability ( $k$ ) and the hydraulic gradient ( $\nabla H$ ). In terms of the flow inside the erosion channel, the Navier-Stokes equations would be the most correct approach. However, the solution of the combined equation system (Darcy and Navier-Stokes) becomes difficult as the boundary conditions of both models are dependent on each other. If so, the solution of the model becomes an iterative process until both boundary conditions are satisfied. This process is computationally demanding when a large number of simulations is required as in the case of probabilistic assessment.

The fictitious permeability method (also referred as continuum solution for fracture flow (Bear and Verruijt, 1987; Liedl et al., 2003; Samardzioska and Popov, 2005; Chen et al., 2012) allows to avoid the boundary iteration by assuming that the erosion channel is filled with a porous material of high permeability value ( $k^*$ ). Hence all domains (aquifer and erosion channel) can be solved with Eq. 3-1 only. A comparison study (Bersan et al., 2013) for piping modelling concluded, that no major implications are derived from this assumption when compared to the complete solution of the Navier-Stokes and Darcy-Brinkman numerical solution for two and three dimensions. Similar approaches were used in the study (Zhou et al., 2012; Wang et al., 2014) that included the sheet pile effect. The simplification is derived from the Darcy-Weisbach equation

(Mott et al., 2006) for the head loss pressure gradient  $\left(\frac{\partial h}{\partial x}\right)$  inside a closed conduit of hydraulic diameter ( $D_h$ ) is presented in Eq. 3-2:

$$\frac{\partial h}{\partial x} = \frac{f u^2}{2gD_h} \quad \text{Eq. 3-2}$$

If a vertical segment was added to the erosion channel, the resistance in the y direction should also be included in the model (Wang et al., 2014). For the present study is assumed that the resistance of flow inside the channel is only significant in the x direction given the relation of height versus length of the erosion channel. The permeability coefficient inside the foundation is assumed to be the same in x and y directions.

The flow friction factor ( $f$ ) (Muzychka and Yovanovich, 2009) can be written as a function of its Reynolds number ( $Re$ ) and a ( $\beta_{fi}$ ) factor and only depends on the cross section shape as presented in equation Eq. 3-3:

$$f = \frac{\beta_{fi}}{Re} \quad \text{Eq. 3-3}$$

Additionally, the Reynolds number of a close conduit is expressed in terms of the hydraulic diameter and the fluid characteristics (density ( $\rho$ ) and dynamic viscosity ( $\mu$ )) as:

$$Re = \frac{u\rho D_h}{\mu} \quad \text{Eq. 3-4}$$

When substituting Eq. 3-3 and Eq. 3-4 in Eq. 3-2, the velocity ( $u$ ) inside a pipe can be expressed in terms of Darcy flow as:

$$u = \left(\frac{2D_h^2}{\beta_{fi}}\right) \left(\frac{g\rho}{\mu}\right) \frac{\partial h}{\partial x} \quad \text{Eq. 3-5}$$

Assuming that the flow velocity and pressure gradients are equivalent inside a pipe filled with water that flows in a laminar regime, it can be concluded that the required fictitious permeability ( $k^*$ ) in Eq. 3-1 can be written as:

$$k^* = -\frac{2D_h^2}{\beta_{fi}} \quad \text{Eq. 3-6}$$

The  $\beta_{fi}$  coefficient for fully laminar developed flow is dependent on the cross section shape (Muzychka and Yovanovich, 2009). Different coefficients are presented in Appendix A.4 for each type of geometrical cross section. The most relevant and updated piping erosion modelling literature (Sellmeijer and Koenders, 1991; Lachouette et al., 2008; Zhou et al., 2012; Bersan et al., 2013; Van Esch et al., 2013; Vandenboer et al., 2014b; Wang et al., 2014) assumes a prior knowledge of the size and/or shape of the erosion channel. For the fictitious permeability solution, the channel geometry becomes great source of uncertainty as there is no literature that recommends how to predetermine it. Hence five different cross section geometries presented in appendix A.4 were tested in different sizes, in order to calibrate the model and suggest a tentative choice for other modelers. Note that the calibration of this parameter also depends on the soil parameters which are assumed as the most relevant by Sellmeijer. Hence in this study, the size of the channel was denoted in terms of the variable ( $n_g$ ) which allows to express the erosion channel in terms of the representative grain size ( $d_{70}$ ) and the erosion channel height ( $a$ ) included in Sellmeijer model.

$$n_g = \frac{a}{d_{70}} \quad \text{Eq. 3-7}$$

The findings and remarks about erosion channel height based on Sellmeijer model (Van Esch et al., 2013; Van Beek et al., 2014) were also expressed in terms of  $n_g$  and were used for the validation of the present 2D modelling. The  $a$  and  $\beta_{fi}$  values obtained for the experimental conditions of the “Ijkdijk” (Koelewijn et al., 2014) are also used for all other cases present in this study. This means that the models where no structure is present are modified only by including an additional boundary condition inside the aquifer for representing the presence of a hard structure inside the flood defence foundation.

### **Resistance Term (R): Two forces equilibrium**

Once the pressures inside the aquifer and the erosion channel are known, it is required to check if the resultant inner pressure gradients are high enough so that the grains can be eroded. This can be estimated based on the equilibrium of forces acting on a single grain (Figure 3-4). The contact area of the grain is expressed as a function of the White’s ( $\eta=0.25$ ) sand packing coefficient (White, 1940) and the representative particle diameter ( $d$ ).

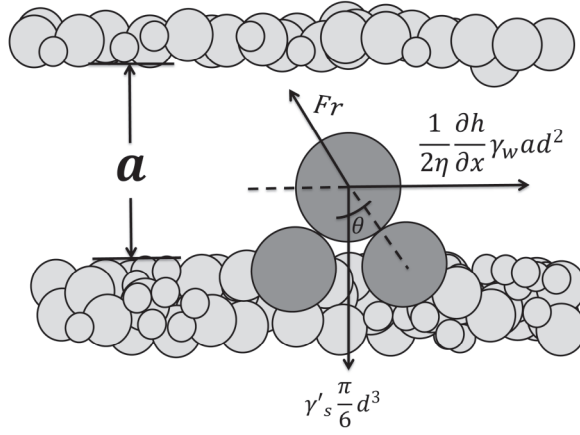


**Figure 3-4 Two forces grain equilibrium model inside the erosion channel.**

Solving the system in equilibrium of forces (Van Esch et al., 2013) it is possible to conclude that:

$$\left[ \frac{\partial h}{\partial x} \right]_{critical} = \frac{\pi \gamma_s'}{3 \gamma_w} \frac{d \eta \tan(\theta)}{a} \quad \text{Eq. 3-8}$$

In reality, the representative  $d_{70}$  grain size can be correlated to the aquifer permeability variable included in the load term (S). This correlation can be induced during the sampling process of both  $d_{70}$  and  $k$ . Despite the fact that this correlation effect can have a significant impact in the probabilistic assessment of piping erosion (Aguilar-López et al., 2016b), it is out of the scope of this study and therefore it is not considered.

### 3.3.2 Sellmeijer limit state recalibrated equation

Due to the complexity of the numerical model, Sellmeijer developed a complementary limit state equation (Sellmeijer and Koenders, 1991) from curve fitting for design purposes of conventional flood defences. In 2011 this equation was modified and calibrated (Sellmeijer et al., 2011) based on the two forces approach explained previously in section 3.3.2. The equation was recalibrated again with additional experimental correction factors via multivariate analysis as presented by Van Beek in (Van Beek, 2015). These results differ significantly from the theoretical modelling results for extreme values. Hence, the 2011 equation (Sellmeijer et al., 2011) is selected for validation of the obtained failure probabilities from the emulators as it is more reliable for stochastic modelling. The equation is presented in appendix A.5.

### 3.3.3 Deterministic safety assessment

The main output of the FEM model is the resultant pressure gradient  $\left(\left[\frac{\partial h}{\partial x}\right]_{FEM}\right)$  inside the erosion channel for a specific set of boundary conditions and soil characteristics (e.g. permeability, aquifer depth, specific weight, etc.). This pressure gradient represents the solicitation (S) or “load” of the system. The resistance (R) of grains to roll can be also expressed as a critical pressure gradient  $\left(\left[\frac{\partial h}{\partial x}\right]_{critical}\right)$  as explained in Eq. 3-8. In reliability studies, the ratio between the resistance term (R) and the load (S) is commonly referred as the stability factor. For the present study, the stability factor (**SF**) for piping erosion is defined as :

$$SF = \frac{R}{S} = \frac{\left(\left[\frac{\partial h}{\partial x}\right]_{critical}\right)}{\left(\left[\frac{\partial h}{\partial x}\right]_{FEM}\right)} \quad \text{Eq. 3-9}$$

For the second part of the study, both terms R and S are assumed as deterministic. The resistance term is defined by the critical pressure gradient which represents the threshold pressure value required for the grains to roll. This value is derived from the two forces limit state equilibrium concept (section 0). The safe condition is defined by  $SF > 1$  and conversely unsafe if  $SF \leq 1$ .

### 3.3.4 Probabilistic safety assessment

When the model parameters are expressed as uncertainties in the form of random variables, their load (S) and resistance (R) can be expressed as uncertainties as well. This representation is more convenient for assessing the safety state of the structure in a probabilistic manner. However, the safety state is now defined by the safety margin instead of the stability factor. This notation form allows to include the cases where the solicitation is equal to zero. This kind of notation is referred to as limit state function and its general form is expressed as:

$$Z = R(\mathbf{X}_i) - S(\mathbf{Y}_i) \quad \text{Eq. 3-10}$$

In which X and Y are vectors of random variables used as inputs of R and S models in each model ith model run. In order to estimate  $P(Z < 0)$  from the resultant Z distribution, a large number of model runs are required in order to ensure that the extreme events located in the tail of the distribution are also generated.

Normally these events correspond to the failure state. Such procedure becomes computationally unfeasible when FEM models are to be used for propagating uncertainties due to the computational burden. In those cases, first and second order reliability methods (FORM and SORM; Low (2014)) become a more attractive choice as they require a significantly lower number of models runs of the FEM's when compared to a Monte Carlo reliability method. The problem with FORM and SORM methods is that prior knowledge of the failure functions is required in order to linearize them. This requirement makes both methods difficult to implement if no prior knowledge of the functions is available. This is the case for porous media flows with large heterogeneities. Therefore, an artificial neural network emulation methodology (Chojaczyk et al., 2015) was implemented for replicating the FEM numerical solution for the probabilistic analysis. Emulating (metamodelling or also known as surrogate modelling) is a common practice in reliability studies where high precision approximations of an original model are required for calculating large amounts of simulations with low computational costs (Bucher and Most, 2008; Forrester et al., 2008; Li et al., 2011; Lü and Low, 2011; Schoefs et al., 2013; Shamekhi and Tannant, 2015; Zhang et al., 2015). Such models consist in propagating different input combinations through a complex model such as a FEM to produce a significant amount of input-output data sets. These are later used for building an approximation of the original model. The multilayer perceptron artificial neural network algorithm was selected as it has proven to be successful in approximating nonlinear behaviour of different type of structures (Cho, 2009; Kingston, 2011; Yazdi and Salehi Neyshabouri, 2014; Chojaczyk et al., 2015; Kaunda, 2015). For the case of piping erosion based on Sellmeijer conceptual model, a robust network was trained (Sellmeijer, 2006) for cases where no additional structure was embedded. This method proved to be sufficiently accurate for predicting the critical head but the training set was quite large (16807 samples) and based on the Mseep software numerical solution (Sellmeijer, 1988) which requires an iterative method for solving the boundary conditions as mentioned previously. The fictitious permeability method presented in the present study allows to implement the method in any FEM groundwater software that allows fine meshing generation inside the potential erosion channel. For the present study the emulator (denoted by  $\Omega$ ) is defined as an approximation function of the original FEM model as follows:

$$\Omega((H - h_b), k) \approx \left[ \frac{\partial h}{\partial x} \right]_{FEM} ((H - h_b), k) \quad \text{Eq. 3-11}$$

Where  $H$  corresponds to the water level in the river side of the flood defence,  $h_b$  corresponds to the water level in the hinterside and  $k$  corresponds to the permeability value of the aquifer foundation. These two inputs were selected as the only stochastic parameters for the emulators as they account for most of the model variability (Sellmeijer et al., 2011). These inputs are also propagated as uncertainties in the original FEM model. After propagating the samples through the FEM and training the emulators, the limit state functions can be defined as:

$$Z_{FEM} = \left[ \frac{\partial h}{\partial x} \right]_{critical} - \left[ \frac{\partial h}{\partial x} \right]_{FEM} ((H - h_b), k) \quad \text{Eq. 3-12}$$

$$Z_{Emulator} = \left[ \frac{\partial h}{\partial x} \right]_{critical} - \Omega(H, k) \quad \text{Eq. 3-13}$$

Note that the FEM model calculates the pressure gradient as a function of the head difference whereas the emulator is trained based on the total water load height ( $H$ ). The critical pressure gradient is also stochastic as it is a function of the  $d_{70}$  stochastic variable. Note that this function is independent of the  $\Omega$  function.

## 3.4 Data

### 3.4.1 Stochastic distributions of input variables

For the probabilistic assessment, the parameters presented in Table 3-1 become stochastic random variables. Their statistical distributions and coefficient of variation ( $CV$ ) were extracted from the study of Schweckendiek et al. (2014) as presented in Table 3-2. The IJkdijk experiment does not represent any specific site and therefore there were no hydraulic boundary conditions associated to this structure. The IJkdijk experiment has a 3.5 height as shown in Figure 3-1. Based on the future safety standards of the Netherlands, the lowest safety value for this kind of structures correspond to a 100 years return period. In practice, it is recommended to have at least 0.5 meters of freeboard for riverine dikes. Therefore, the boundary condition for the water levels ( $H$ ) is fitted arbitrarily to a Gumbel distribution with two fitting parameters ( $a$ ,  $b$ ) for a 100 years return period corresponding to a 3 meter water level. In addition, a piping model factor ( $m_p$ ) is included for accounting for the uncertainty of the Sellmeijer model.

**Table 3-2 Prior distributions of random variables for FEM models and Sellmeijer limit state equation**

Variable	Unit	Distributed	Mean	CV	$\lambda$
$k$	[m <sup>2</sup> ]	Log-normal	1.07e-11	1.0	1.5
$d_{70}$	[ $\mu$ m]	Log-normal	180	0.15	1.5
$L$	[m]	Deterministic	15	-	-
$D$	[m]	Deterministic	*	-	*
$H^{**}$	[m]	Deterministic	a=1.569	b=0.311	1.5
Additional parameters required for Sellmeijer 2011 (Appendix A.5)					
$\eta$	[-]	Deterministic	0.25	-	-
$\gamma_s$	[kN/m <sup>3</sup> ]	Deterministic	26.5	-	-
$\gamma_w$	[kN/m <sup>3</sup> ]	Deterministic	9.81	-	-
$\theta$	[deg]	Deterministic	37	-	-
$m_p$	[-]	Log-normal	1	0.12	-
$h_b^{**}$	[m]	Deterministic	0.1	-	-
$d$	[m]	Deterministic	0	-	-

**Notes:**

\* 4 different aquifer models were tested with depths of 3,5,8,30 meters

\*\*  $H$  and  $h_b$  are relative to the NAP reference vertical datum.

### 3.4.2 FEM emulator training data set

Ten thousand variable samples were generated randomly following the statistical distributions presented in Table 3-2. Afterwards, they were propagated through the original FEM. This number of samples ensures that the expected standard error in the Monte Carlo simulation remains close to 1%. Finally, input and output sets constitute the basis for training and validating the neural networks. It is possible that after training these models, the new generated samples used for the future probabilistic analysis are sampled outside the training data set. If so, the emulators will have to extrapolate for those combinations of inputs and consequently large errors may be induced. To avoid this kind of errors, the initial training random samples were generated maintaining the mean value of the original models but increasing their “spreading”. In other words, the original coefficient of variance ( $CV$ ) from the distributions presented in Table 3-2 were modified. This was done by multiplying the  $CV$  values by an amplification factor ( $\lambda$ , Table 3-2) before generating the training data samples used as input in the FEM. This ensures that the model is trained for values located further in the tail which reduce the probability of extrapolation.

## 3.5 Results and discussions

### 3.5.1 Optimal erosion channel shape and size

According to Sellmeijer conceptual model (Sellmeijer, 1988), the groundwater parameters that contribute most to the inflow of the erosion channel are the aquifer depth and the aquifer permeability. In that order of ideas, the erosion channel geometry and its inner pressure loss will also have a significant effect on the amount of inner inflow. For this reason, the influence in the progression capacity from these three parameters was tested for their implementation in the models used for the safety assessment.

#### 3.5.1.1 Erosion channel cross section shape

The hydraulic gradients inside the erosion channel for the different cross section sizes were estimated as presented in Figure 3-5. The critical head value ( $H_c$ ) obtained during the IJkdijk experiment (Table 3-1) was used for all models as a fixed boundary condition. The grain number coefficient  $n_g$  (Eq. 3-7) allows to calculate both the exerted inner pressure gradient and the critical one (2 forces dashed line, Figure 3-5) in terms of the erosion channel height. The intersection between the two lines defines the maximum channel height threshold required for building sufficient pressure inside the channel to drag the representative sand particle.

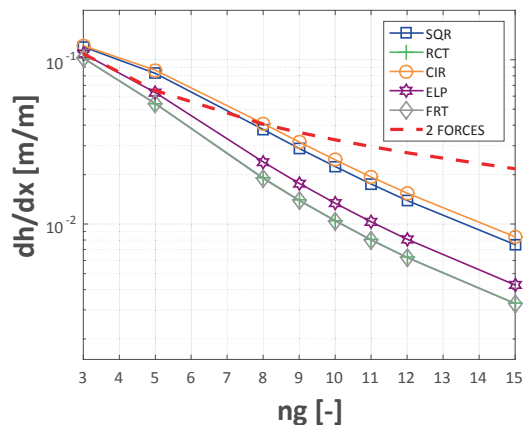


Figure 3-5 Required erosion channel height (in terms of  $n_g$ ), for different cross section geometries.

Channels with larger diameters will not generate sufficient inner pressure gradients for dragging the grains towards the outlet. For the case of the circular cross section, a  $n_g$  equal to 8.2 is obtained which is close to the 10 grain approximate size reported in the modelling study (Van Esch et al., 2013) and very close when compared the one obtained in a latest experimental study (Van Beek et al., 2014).

Other cross section geometries such as the square and elliptical present lower thresholds whereas the rectangular and fracture ones present no eroding capacity at all for any given channel height. The results in terms of height of the erosion channel are consistent with the literature experimental findings. In the case of the width size, there is no agreement between the different authors (Van Beek et al., 2011; Zhou et al., 2012; Bersan et al., 2013; Vandenboer et al., 2014b; Wang et al., 2014).

For the present study, a single 2D erosion channel with constant circular cross section was assumed. The results from the study by Van Beek et al. (2014) showed that when the cross section size was represented as an average value for the whole length, the width/depth ratio tends to be closer to the unity for one of the experiments (width/depth=3.5mm/3.2mm) and 2.5 times (width/depth=8.4mm/3.3mm) for a second experiment. From the previous mentioned studies and the results presented in Figure 3-5, the fracture flow approach can be discarded for modelling piping erosion. Note that piping erosion is a three dimensional process which includes an erratic meandering progression, multiple derivation of secondary channels and non-uniform cross section. Hence, the measured pressure loss inside the channel of an experimental setup is greater than the one obtained in a two dimensional model with a cross section that is significantly wider with respect to its depth. The fictitious permeability approach allows to compensate for this additional pressure loss by producing a narrower cross section with a width depth ratio closer to 1. This statement agrees with the results obtained for the circular and square sections of the present study.

In addition, the results presented in Van Beek et al. (2014) for FEM modelling showed that an equivalent conductivity value of 0.5 m/s (the conductivity can be estimated as a function of the soil permeability and fluid properties as explained in the note of appendix A.5) inside the erosion channel gave the best fit for representing the experimental data. For the present study, the resultant equivalent fictitious conductivity of the circular cross section with a height of 8.2  $n_g$  is 0.49 m/s whereas for the square cross section is 0.54 m/s. Based on these results, a circular cross section with an  $n_g$  coefficient of 8.2 is chosen. All models are built with this same geometry except for the ones studied in section 3.5.3.4 and 3.5.3.5 where the  $n_g$  (channel height) was modified

as a function of the aquifer depths given the results presented in section 3.5.1.3. Nevertheless, the results show that a square section can be implemented as well.

### 3.5.1.2 Aquifer permeability effect on the cross section size

Several permeability values were tested between 0.01 and 100 times corresponding to highly impermeable and highly permeable soils (Bear and Verruijt, 1987). The permeability value of the aquifer foundation from the IJkdijk experiment corresponds to a fine sand of good permeability. Figure 3-6 shows that for very low permeability values (representative of very fine sands), the system will not be able to build a sufficiently high pressure gradient inside the erosion channel so that the grain particle can be dragged.

For the IJkdijk case (high permeability aquifers of clean sand) and larger  $d_{70}$  grains (10 times  $k$  in Figure 3-6), the results agree with the reported experimental findings (Van Esch et al., 2013) which stated that values of  $n_g = 10$  in experimental setup and  $n_g = 30$  in field surveys for coarser sands were observed.

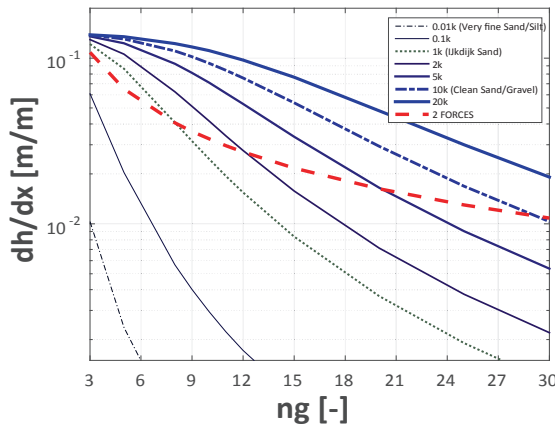


Figure 3-6 Required erosion channel height (in terms of  $n_g$ ), for different aquifer permeability ( $k$ ) values.

Based on these results it is concluded that the aquifer permeability has a very large influence in the eroding capacity and therefore it should be represented as a random variable instead of a calibration value for the probabilistic assessment.

### 3.5.1.3 Aquifer depth effect on the cross section size

Four different aquifer depths were tested (3, 5, 8 and 30 meters). The results showed that from 3 to 8 meters depth, the variation of the required erosion height fluctuated between 8 and 10 grains. For thicker aquifers ( $D > 8$  meters), there is no additional depth related effect observed as the pressure gradient lines are overlapping (see Figure 3-7).

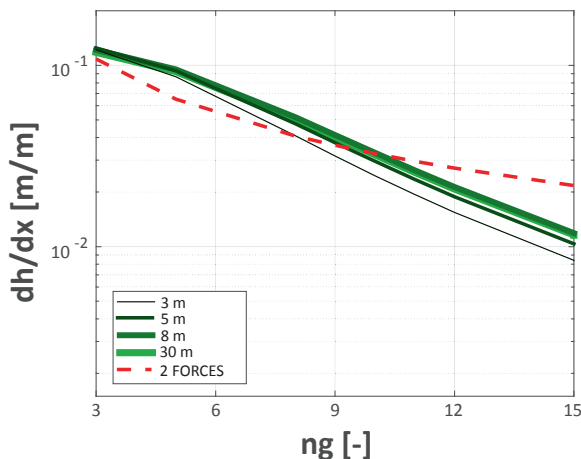


Figure 3-7 Required erosion channel height (in terms of  $n_g$ ), for different aquifer depths.

The model is not highly sensitive to the aquifer depth variation and it stops being sensitive to after 8 meters depth. Therefore the range of variation of this parameter can be bounded. Hence, this characteristic was not represented as a stochastic parameter in the probabilistic safety assessment. Instead, several aquifer depths with their correspondent erosion channel height were tested.

## 3.5.2 Deterministic safety assessment for structural embedment

Three different commercial size sewer pipes were selected for this analysis. Diameters of 0.8, 1.0 and 1.2 meters were selected assuming that such sizes will have a significant effect in the flow paths inside the aquifer. In terms of the sewer pipe position, 8 locations in the horizontal direction and 3 in the vertical location were modelled. Their corresponding stability factor value was obtained based on Eq. 3-9 evaluated with the mean characteristic values of the soil presented in Table 3-2. In Figure 3-8, the obtained stability factor values are written in the exact location corresponding to the center of the assessed sewer pipe. For the most critical and favourable locations, the perimeter of the sewer pipe is plotted with a dashed line while preserving the scale. The erosion channel is represented by a thicker dashed line along the bottom of the flood defence.

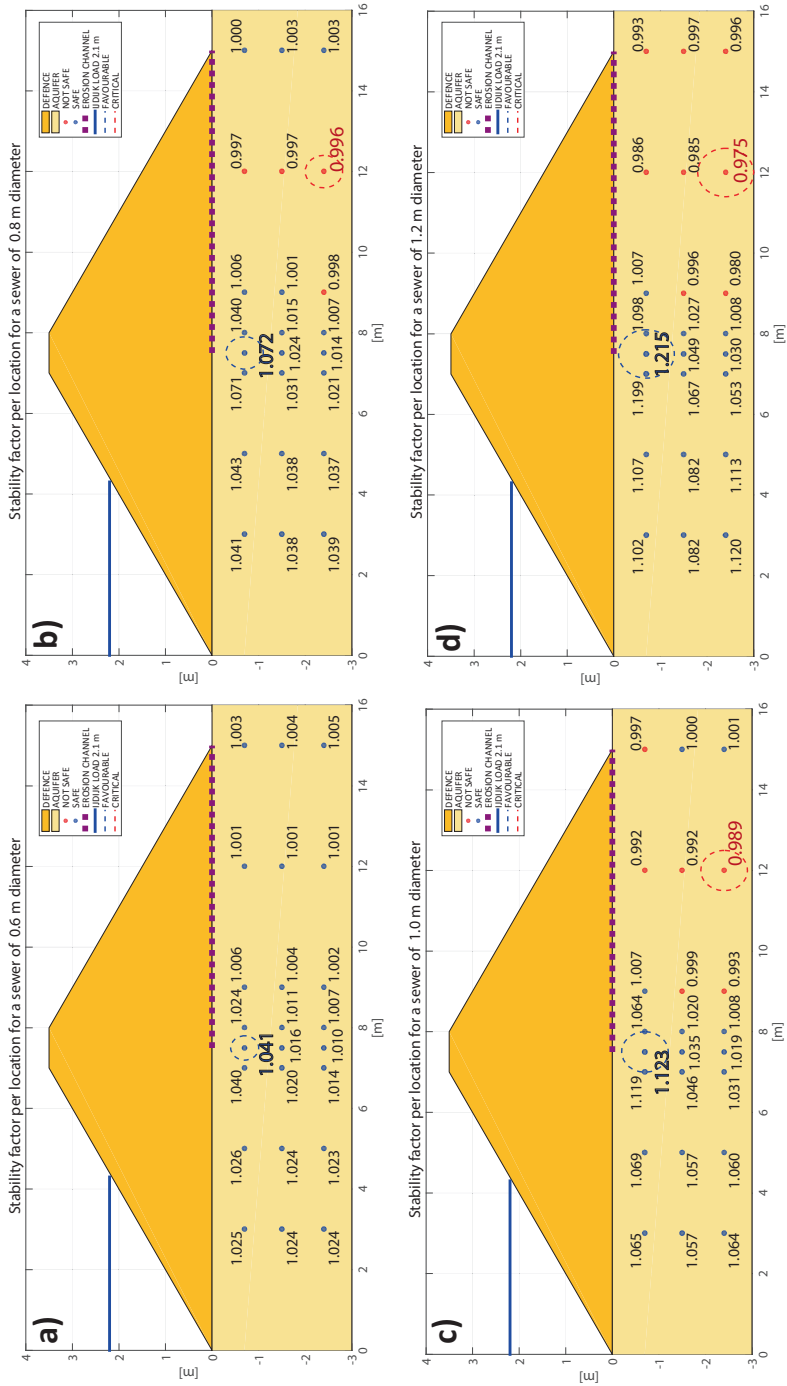


Figure 3-8 Stability factor as a function of location for a) 0.5 m diameter, b) 0.8 m diameter, c) 1.0 m diameter, d) 1.2 m diameter

From the obtained results five main observations can be highlighted. The first observation is that for all studied diameters, the highest stability factors were obtained for the shallow locations. In other words, the safest location for all studied diameters will always be located in the most upper location between the aquifer and the bottom of the flood defence.

The second observation is that the increase in diameter is proportional to the increase in stability factor. The highest stability factor (1.215) for all the 4 different diameters was obtained for the largest pipe diameter (1.2 m). The explanation for this result is the diversion of the incoming flow in two separated portions. One portion of the flow is heading upwards in the direction of the erosion channel whereas the other one is flowing downwards to the bottom of the sewer pipe. After this last portion flows all the way along the perimeter of the sewer pipe, it will try to flow again upwards. In consequence, a higher pressure loss will occur resulting in a lower pressure gradient inside the erosion channel in comparison to the case where no sewer pipe is embedded.

The third observation is that regardless of the diameter of the sewer pipe, the safest condition can will always be found when the sewer pipe is located exactly in the midsection of the flood defence, just below the tip of the erosion channel. This can be explained based on the resultant soil filled gap located between the sewer pipe and the impermeable base of the flood defence. This gap determines the amount of flow going directly towards the tip of the erosion channel. This means that the diversion effect is not only a function of the size of the sewer pipe but also of the amount of space left in between the impermeable 'roof' and the hard structure. If this space is equal to zero, the embedded structure will work in the same manner as a cut-off wall.

The fourth observation is that there is always a positive effect in terms of safety no matter the size of the sewer pipe, if located anywhere in front of the tip of the erosion channel. The inclusion of a discontinuity before the tip of the erosion channel will always work as an obstacle (energy loss) for the water flowing towards it.

The last observation is that if the sewer pipe is located behind the tip of the erosion channel, it can also have negative effects, especially when located near the bottom of the aquifer (for the IJkdijk case). This corresponds to the critical cases indicated with dashed line pipes with stability factor values lower than 1. This observation is explained by the fact that the IJkdijk flood defence was founded over a shallow aquifer on top of an impermeable basin. In case a large diameter pipe is embedded in the bottom of such a small aquifer it can also redirect the lower flow upwards in the direction of the erosion channel. Hence, the pressure gradient inside the erosion channel will increase

augmenting the erosion capacity. From this it can be concluded that the relative depth of the aquifer with respect to the structure vertical dimension can have an important effect in the flood defence safety as well.

Based on these five observations, it is recommended to locate future sewer pipes (if possible) in the zone in front of the erosion channel tip towards the river side of the flood defence while trying to reduce the “gap” between the bottom of the flood defence and the sewer pipe as much as possible. The size of this gap determines the amount of flow that goes directly towards the erosion channel tip and bottom. If the gap is completely closed, the whole system (flood defence and sewer pipe) will behave similarly to the case where a cut-off wall is present. Analogously, the vertical dimension of the embedded structure is equivalent to the cut-off wall depth. As a final remark, it is important to note that the locations considered unsafe are described by stability factors which are very close to 1 whereas for the safe conditions, the change in stability factor can be as much as 20%. Therefore there is not sufficient evidence to state that sewer pipes have a negative effect in the piping erosion progression.

### 3.5.3 Probabilistic safety assessment

The results obtained in sections 3.5.1.1 to 3.5.1.3 show that the erosion channel characteristics and the aquifer depth have significantly less influence on the variability of the erosion capacity compared to the aquifer permeability (section 3.5.1.2). Therefore, the training data was defined only by the water level ( $H$ ) and the aquifer permeability ( $k$ ) random variables.

#### 3.5.3.1 FEM emulation method

Artificial neural networks (ANN) used as  $\Omega$  functions in the present study, were trained to predict the pressure gradient inside the erosion channel. The optimal ANN architecture is defined by the combination of number of samples ( $N$ ) and the number of hidden neurons (HN) (Chojaczyk et al., 2015). This combination is referred as the ANN architecture. Different ANN architectures were tested to find the optimal one which corresponds to the combination which requires less samples and less number of HN and still achieves high performance. By performance it is referred to as the criteria in which the accuracy of the prediction of the model is evaluated. In our case, the selected performance indicator is the coefficient of determination ( $R^2$ ) which indicates the proportion of the variance from the dependent variable(s) that is explained from the independent variables in a function or model. The emulators were trained for 100, 400, 1000, 2500 and 10,000 samples given that their expected standard error from a

Monte Carlo simulation is 10%, 5%, 3.2%, 2% and 1% respectively. The set of  $N$  samples were randomly splitted allocating 70% for training and 30% for validating for all architectures. The performance results for the different architectures is presented in Figure 3-9.

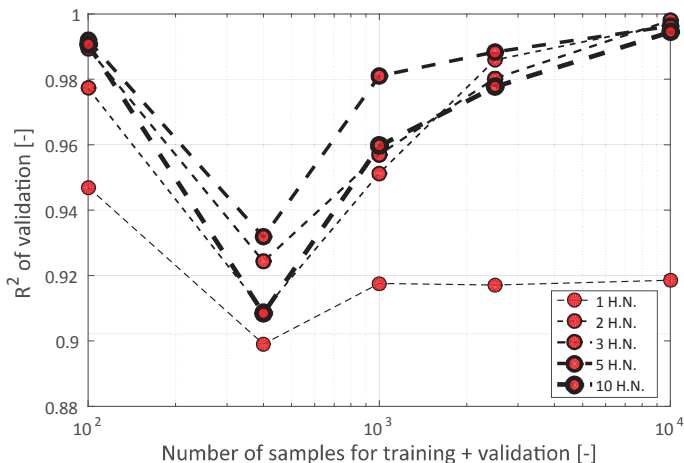


**Figure 3-9 ANN emulator architectures R2**

The results show that the 400 samples architectures has the highest difficulty in reproducing the results of the FEM (Figure 3-9) whereas the 100 samples architecture performs better. This contradiction is expected for the case where highly nonlinear processes are being captured as more data represents more information available for training but also more scattering in the data sets. In that case, an increase in the HN is useful as long as the increase does not imply overfitting of the model. Hence, overfitting was checked by comparing the error obtained between training a validation for each architecture (Piotrowski and Napiorkowski, 2013). If the error obtained for the training set is very high (high predictive capacity) and significantly different than the error obtained during validation it means that the model is over fitted (low generalization capacity).

For the ANN model of non-embedded structure, the architecture that requires less training input and less hidden neurons is composed by 5 hidden neurons and 1000 samples. This configuration achieves the highest  $R^2$  (0.982). A value of 0.98 for the  $R^2$  is high for general model validation, but for the case of emulator training, such a high value is desirable given the fact that it is always possible to afford additional training data.

### 3.5.3.2 FEM emulator probabilistic validation

The Sellmeijer 2011 limit state equation (Appendix A.5) was used for validating the FEM model and emulator limit state functions without embedded sewer pipe. The resulting pdf's (Figure 3-10) for the three different limit state functions were built based on the 10,000 initially generated input data set.

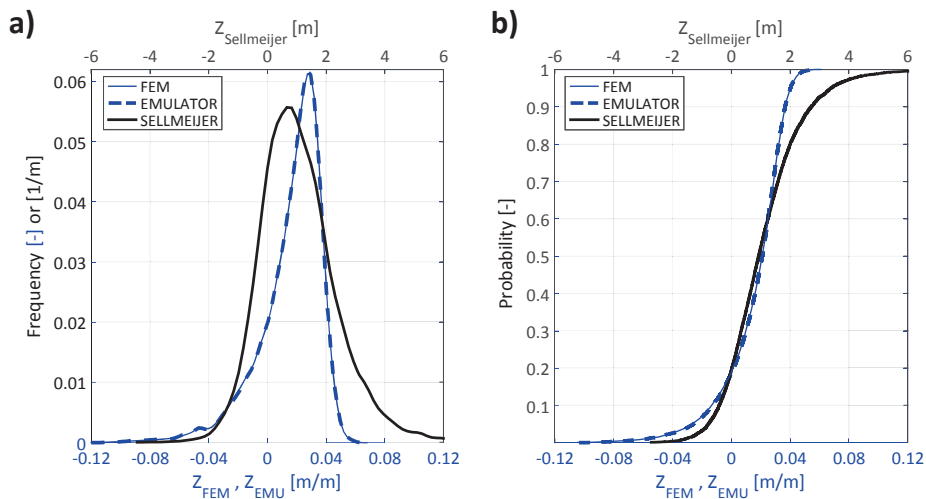


**Figure 3-10 a) PDF of Z for the Sellmeijer revised equation (Thick black line), FEM (Thin blue line) and Emulator (Dashed line). b) CDF of Z for the Sellmeijer revised equation (Thick black line), FEM (Thin blue line) and Emulator (Dashed line).**

The probability functions for the three models are presented in Figure 3-10b with two different horizontal axis. Note that the Sellmeijer limit state is expressed in different units with respect to the FEM and Emulator distributions. The Emulator and FEM are expressed in terms of pressure gradients inside the erosion channel whereas the Sellmeijer limit state function is expressed terms of total head difference. The distribution generated with the Sellmeijer limit state function presents a Gaussian type of shape whereas the emulator and FEM distributions presents a negatively skewed distribution. On one hand, the Sellmeijer limit state equation calculates the residual strength in terms of the total head. On the other hand, the FEM and the emulator calculate the limit state as the residual resistance in terms of pressure gradients [m/m] inside the erosion channel. However, they are still comparable as the general form of the limit state equations allows to define the failure threshold ( $Z \leq 0$ ) no matter the limit state function. In other words, the failure probability is defined for all models by the exact same point where the resistance is equal to or less than the load. In Figure 3-10b it can be observed how the three functions intersect in two common points including

the failure threshold ( $Z \leq 0$ ). The corresponding probabilities of failure value from FEM, emulator and Sellmeijer are equal to 0.189, 0.186 and 0.193 respectively. Note that this high failure probabilities are not representative of the actual dikes as the IJkdijk experiment was designed to fail on purpose. Consequently, it is concluded that the emulator can be used for failure probability estimation as for the case of non-structural embedment is producing very close values of failure probability when compared to the revised Sellmeijer limit state equation.

### 3.5.3.3 FEM emulator sensitivity analysis

The emulators were trained for distributions modified by the ( $\lambda$ ) as explained in section 3.4.2. However, the interpolation and extrapolation capacity from the emulator was tested. The tests consisted in calculating the probability of failure for different  $CV$  for the three main parameters assumed as stochastic. For each parameter test, one single variable was sampled for different  $CV$  values while fixing the other two as constant with mean value presented in Table 3-2. The results are presented in Figure 3-11.

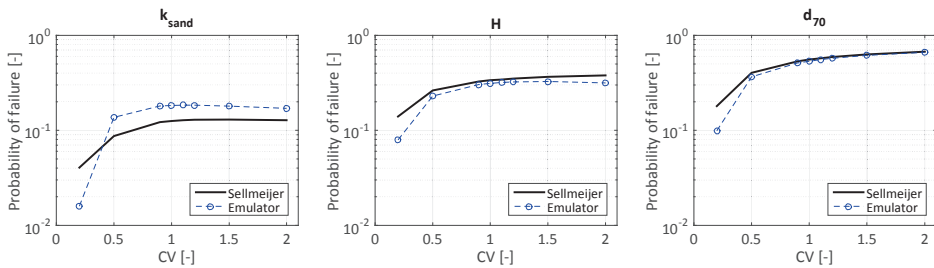


**Figure 3-11 Failure probabilities as a function of the main random variables with different  $CV$**

In terms of extrapolation, the emulator performs very well for large  $CV$  values. For less spreaded distributions of the parameters, the emulator results in larger difference in the estimated failure probabilities with respect to Sellmeijer function. In particular, for the case of the sand permeability where the Sellmeijer limit state gives a failure probability of 0.0406 whereas the emulator results in 0.16. After comparing the change in failure probability for three main parameters, it can be concluded that the sand permeability is the one that accounts for the largest variability (change by order of magnitude for smallest and largest  $CV$ ) in the estimated failure probability for both Sellmeijer and the emulator. Hence, the emulator will only be implemented for  $CV$ 's between 0.5 and 1.5.

### 3.5.3.4 FEM emulation with structural embedment

In the previous section, it was shown that the two forces equilibrium concept and the Darcy flow with fictitious permeability model are consistent with the Sellmeijer limit state equation (Appendix A.5) when representing the no-embedment case. It is assumed that the inclusion of an embedded structure is equivalent to a change in the aquifer permeability and flow pattern behaviour but the failure concept still holds. Hence, the same emulation methodology was used for the cases where structural embedment is present.

Twelve different ANN emulators were trained based on 1000 samples propagated through their original FEM models. Each FEM model corresponds to one of the three selected aquifer depths ( $D$ ). For nine of the twelve cases, a sewer pipe of 1.2 meters is used in different locations. The three remaining ones correspond to the case where no structure is embedded. A cover of 30 centimetres below the flood defence at a burial depth of 1.5 meters to the bottom of the pipe was chosen. All models were trained with 70% of the training data and validated with the remaining 30% with a fixed  $N$  set of 1000 samples. Therefore, the results presented in Table 3-3 correspond to the average  $R^2$  value obtained after training each emulator a 100 times. Note that the size of the erosion channel ( $n_g$ ) is varied as a function of the aquifer depths based on the results presented in section 3.5.1.3.

**Table 3-3 Validation results of emulators ( $\Omega$ ) versus FEM output as a function of different number of hidden layers (H.L.)**

Sewer pipe	X [m]	Y [m]	GAP [m]	D [m]	ng [-]	R <sup>2</sup> for $\left[\frac{\partial h}{\partial x}\right]_{FEM}$ vs. $\left[\frac{\partial h}{\partial x}\right]_{EMU}$				
						1 H.L	2 H.L	3 H.L	4 H.L	5 H.L.
No	-	-	0.3	3	8.2	0.91	0.98	0.99	0.99	0.998
Yes	0	-0.9	0.3	3	8.2	0.91	0.98	0.99	0.99	0.996
Yes	7.5	-0.9	0.3	3	8.2	0.91	0.97	0.99	0.99	0.998
Yes	15	-0.9	0.3	3	8.2	0.91	0.97	0.99	0.99	0.998
No	-	-	0.3	5	9.4	0.91	0.98	0.99	0.99	0.997
Yes	0	-0.9	0.3	5	9.4	0.91	0.98	0.99	0.99	0.997
Yes	7.5	-0.9	0.3	5	9.4	0.92	0.98	0.99	0.99	0.997
Yes	15	-0.9	0.3	5	9.4	0.91	0.98	0.99	0.99	0.997
No	-	-	0.3	8	10	0.92	0.98	0.99	0.99	0.996
Yes	0	-0.9	0.3	8	10	0.91	0.97	0.99	0.99	0.996
Yes	7.5	-0.9	0.3	8	10	0.92	0.97	0.99	0.99	0.997
Yes	15	-0.9	0.3	8	10	0.92	0.97	0.99	0.99	0.997

Table 3-3 shows that in average, 3 hidden nodes represent the most optimal architecture in general while satisfying  $R^2 \geq 0.98$ . We found that it is possible to obtain high predictive capacity with only 1000 training samples for both embedded and non-embedded cases reducing the computational burden significantly.

### 3.5.3.5 Reliability index ( $\beta$ ) for structural embedment

The safety of each flood defence was quantified based on the Hasofer-Lind reliability index ( $\beta$ ) (Hasofer, 1974) instead of the failure probability. A higher  $\beta$  index represents a safer structure. This index is equivalent to the reduced standardized variable that corresponds to the structure failure probability in the standardized normal distribution. To quantify the combined effect of the embedded sewer pipe and the permeability uncertainty, the defence safety was assessed for different  $CV$ 's for the twelve trained emulators (Table 3-3) as presented in Figure 3-12.

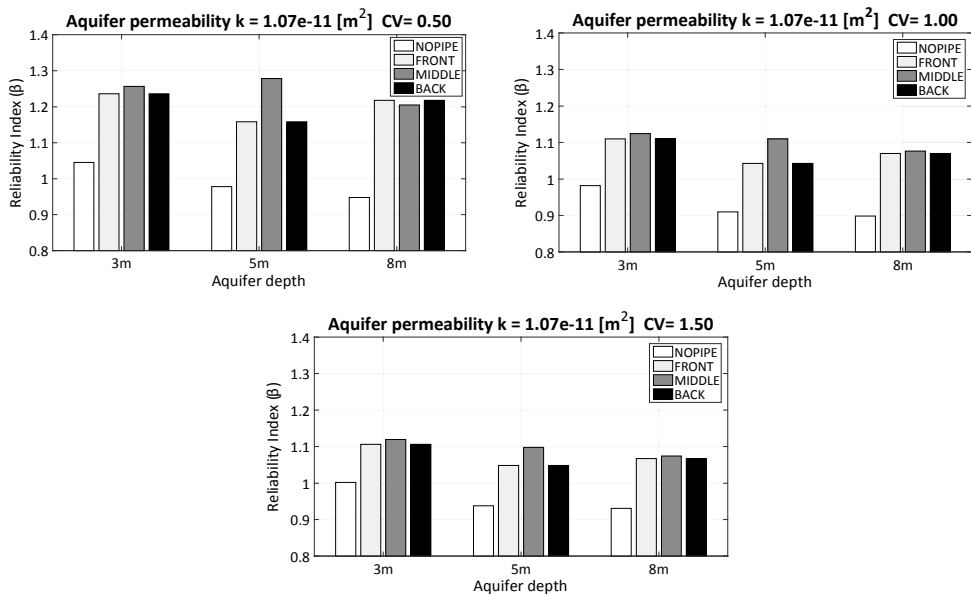


Figure 3-12  $\beta$  indexes for different aquifer depths and permeability  $CV$ 's

These results show how locating the sewer pipe in the midsection will always be safer than in the other two locations, despite the heterogeneity ( $CV$  of permeability) of the soil. Furthermore, the marginal effect (difference between no sewer pipe and with sewer pipe) increases with the increment in aquifer depth. For aquifers equal or deeper than 8 meters, the increment in  $\beta$  index with respect to the case of no embedded sewer pipe will be very similar despite the location of the sewer pipe.

These results show that the aquifer depth has a significant influence on the safety of the structure and consequently the assumption of representing it as a deterministic value might change the assessment. Yet, the effect is only relevant until a certain depth and therefore the random distribution should be bounded based on the results presented in section 3.5.1.3.

All 3 assessments for locations with sewer pipes show that the inclusion of the hard structure inside the foundation will always improve the safety with respect to the case of non-structural embedment no matter the degree of heterogeneity of the soil permeability. This result differs with the conclusion obtained from the deterministic location in section 3.5.2, where it was observed that most structures located in the hinterside resulted in unsafe situations. This difference can be explained due to the fact that once the permeability factor becomes a random variable, the changes in the inner pressures of the aquifer are not equally affected by the embed sewer pipe. This cannot be observed under deterministic conditions. Additionally, the uncertainty in the aquifer permeability is the one that has the highest impact in the variability of the resultant failure probability.

In case of a less heterogeneous soil represented by a  $CV$  of 0.5, the maximum difference in  $\beta$  indexes is obtained for an aquifer of 5 meters. In this case, the non-sewer embedment results in a  $\beta$  index of 0.978 whereas the one with the sewer pipe located in the middle results in a  $\beta$  index of 1.28. If compared to the cases where the pipe is located in front and in the back of the tip of the erosion channel, the effect is less significant but still positive as both produce a  $\beta$  index of 1.16. Note that the results of this analysis reflect low beta indexes or in other words in very “Unsafe“ situations .

In a more “complete” piping erosion assessment, the total failure probability is conditional to the failure mechanisms of heave and/or uplift (Schweckendiek et al., 2014). As a consequence, the resultant safety  $\beta$  index will be higher (safer structure) as the probability of the total failure mechanism is conditional on the occurrence of the other two failure mechanisms. In the Netherlands, flood defences are designed for  $\beta$  indexes of 3 and above depending on the associated flood risk (Lopez De La Cruz et al., 2011). In those cases, the failure probabilities will be located more towards the left tail of the  $Z$  reliability PDF and consequently higher beta indexes are expected. If so, it is expected that the difference in safety between the case of embedment and non-embedment will be more significant than the ones encountered in this study.

### 3.6 Conclusions

A limit state piping erosion FEM modelling methodology has been developed and validated against the obtained results from the same conditions evaluated in the Sellmeijer 2011 limit state equation (Appendix A.5). This methodology allows to include the effect on safety originated from sewer pipes under flood defences. The methodology was implemented for both deterministic and probabilistic safety assessments which allowed to answer the three main research questions. The main and general conclusion of the present study is that the presence of sewer pipes under flood defences has a significant effect on the safety of the flood defence in terms of piping erosion. This conclusion holds for both deterministic and probabilistic safety assessments. The results also indicate that it can even have beneficiary effects in terms of safety depending on the location and relative size with respect to the aquifer depth. For the three research questions it can be stated that:

The fictitious permeability approach for FEM modelling proves to be a reliable method for assessing piping erosion in steady state conditions. A value of 8.2 times of the  $d_{70}$  particle size diameter for the average erosion channel height was obtained based on the experimental conditions for the IJkdijk experiment. This value agrees with other experimental findings and it is recommended as an initial guess for implementing the fictitious permeability approach for limit state piping erosion modelling. We also showed that assuming an average cross section which is significantly wider in respect to its height gives poor results for 2D modelling of piping erosion. This last conclusion is in agreement with the results presented in other earlier studies about piping erosion cross section (Van Beek et al., 2014).

The sewer pipe size and location play an important role in the safety of the flood defence for piping erosion. Both will change the flow patterns and magnitudes inside the aquifer and consequently the exerted pressure gradient inside the erosion channel will be affected as well. In particular, if located after the middle of the flood defence towards the river side. The results for the deterministic assessment show that the most important geometrical aspect for the flood defence safety is the originated gap between the embedded structure and the flood defence base. This gap will determine the portion of flow which will go directly towards the erosion channel. The remaining portion will be forced to go downwards under the structure. In that sense, the size of the structure defines the additional energy loss in the aquifer. In a complementary way it can also be concluded that for the case of deeply embedded structures, no matter their size or

location there is almost no effect in the piping erosion inner pressure as the gap becomes too big and there will be no flow diversion.

In terms of the probabilistic assessments, it is also shown that the uncertainties associated to the sand permeability and water load, have a significant effect in the safety ( $\beta$  index) of the flood defence with the sewer pipe located underneath. The consideration of the soil heterogeneity and water probabilistic distribution influences the increase or reduction of the inner pressure gradient of the erosion channel. This change is relative to the one originated by the embedded structure size and location. Emulation of FEM models proved to be a feasible approach for assessing this kind of complex structures. It was also proven that the method produces the same probabilistic result for non-structural embedment when compared to the revised Sellmeijer limit state equation (Appendix A.5). For realistic values such as the ones measured for the IJkdijk experiment, the structural embedment proved to have significant effects for the commercial sewer pipe diameters used in this study.

### **3.7 Acknowledgements**

“This research is supported by the Dutch Technology Foundation STW, which is part of the Netherlands Organization for Scientific Research (NWO), and which is partly funded by the Ministry of Economic Affairs.” The authors would like to thank STW foundation, Raymond Van der Meij from the Dike Safety department of Deltares, the Integral and sustainable design of Multi-functional flood defences program and the anonymous reviewers who’s comments greatly improved the quality and clarity of the present manuscript.

# Chapter 4

## Wave overtopping probabilistic safety assessment of flood defences with roads on top

### Abstract

Grass cover erosion due to wave overtopping is a major threat to dike safety. Future flood defences will require to withstand more severe storms than the ones used for design at the moment. In the actual state of the art, the effects on the wave overtopping failure mechanism derived from having roads over the crest are not taken into account in the dike probabilistic safety assessments. The present study aimed to include the turbulence effects derived from a road located over the crest of a dike, in the probabilistic assessment of wave overtopping dike failure. This was done by building two different Navier-Stokes computational fluid dynamics models of two different dikes; one with a road on top and one without it. Both models were validated with experimental data collected from real-scale experiments. These models were used to produce training data sets which were later used for constructing emulators (computationally cheaper models). These new emulators allowed to perform various probabilistic scenario analysis. The results showed that the presence of a road reduces the safety against wave overtopping for extreme case storms. The obtained conditional failure probability from a severe storm (100 L/s/m) for a dike with a road and realistic grass quality conditions can be as high as 50.3% whereas is less than 1% for a dike without a road in the same location. In addition, It is also concluded that the spatial grass quality distribution is a more important for determining dike than spatial grass cover thickness distribution.

**This chapter is submitted as:** Aguilar-López, J.P., A. Bomers, Warmink, J.J., Schielen, R.M.J., Hulscher, S.J.M.H., 2016. Wave overtopping probabilistic safety assessment of flood defences with roads on top.

## 4.1 Introduction

Structural embedment of roads on top of dikes will generate stability effects in the flood defence during normal operation and during a flood event (Bomers et al., 2016). Yet, these effects are not explicitly considered in the current probabilistic assessment methods. In the last decades, flood defence design has moved towards a risk-based approach (Vrijling, 2001; Naulin et al., 2015), in order to cope with factors like climate change and especially sea level rise. For the case of grass covered flood defences, this change in climatological conditions represents an increase in erosion rates of the protective grass cover which may lead to an eventual dike breach. With this study it is intended to develop a methodology which allows to include the effects of a road on top of a flood defence in the grass cover failure wave overtopping probabilistic safety assessment.

From a review of the actual state of the art regarding this failure mechanism, it is concluded that most of the research related to grass cover failure on dikes can be classified in: the scouring assessment methods, grass cover resistance and wave overtopping hydrodynamics. Most of the studies found in this categories are concerned about defining deterministic values for the design of standard flood defences which and do not include any non-water retaining additional structures. However, they are used in the present study in order to develop the method. A good methodological starting point for this kind of studies can be found in the study of Lee and Kwon (2009) who presented a reliability assessment for wave overtopping failure estimation based on partial safety factors validated by fully probabilistic Monte Carlo method. This method is based on the classical overtopping approach of defining an allowable overtopping discharge ( $L/s/m$ ). Later studies have shown and stated that overtopping failure is better estimated from individual wave overtopping volumes ( $L/m$ ) (Franco et al., 1994; Van der Meer, 2002; Pullen et al., 2007; Victor et al., 2012). More recently, Dean et al. (2010) tested three different estimation inputs (velocity excess, shear stress excess and work excess) which allow to calculate scouring depths per wave volume. Their results showed that the work excess was the best descriptor from the three tested ones. At the same time Van der Meer et al. (2010) developed the cumulative overload method which relies on the shear stress principle but it does not include the “real” erosion time per wave. This assumption was supported from experimental measurements that resulted in almost constant overtopping times for a conventional flood defence. Additional research has been done, so that this cumulative load method allows include the effects of obstacles and transitions in both hydraulic load and resistance against erosion in the form of calibration coefficients (Steendam et al., 2014; Hoffmans et al., 2015). This

method is suitable for probabilistic assessments of transitions and obstacles, but in its present state, there is still large uncertainty associated and research required for the selection of the coefficients. In addition, the derived effects of the change in the wave overtopping times due to drastic profile irregularities is not taken in this method either. Thornton et al. (2011), implemented both previously mentioned methods and compared them with laboratory experimental measurements. From their results, they concluded that both concepts should be better verified and maybe even unified.

Regarding the grass quality, the earlier study of Verheij et al. (1995) had already recommended grass and soil quality values expressed in terms of their erodability rates which can be estimated as a function of their critical eroding velocity thresholds. Hoffmans et al. (2008) presented their geo-mechanical conceptual approach based on the vertical forces that act upon a turf element model which describe the physical process of grass cover failure. Based on these concept, the work Trung (2014) aimed to determine the grass cover failure of conventional dikes in terms of probabilities while considering their spatial distribution. The method used in this last study is fully probabilistic and could be adapted to more complex dike profiles. Nevertheless, it relies on empirical formulas for estimating the water depths and flow velocities on top of the crest and along the slope. This means that the turbulence derived effects of abrupt geometrical transitions or embedded objects cannot is not explicitly included. Additionally, the resistance of the grass to be eroded is defined by the root tensile strength model from Hoffmans et al. (2008) which is highly demanding in terms of model input.

All Hoffmans et al. (2008), Van der Meer et al. (2010), Trung (2014) and Dean et al. (2010), considered the effects of turbulence but simplified the hydrodynamics of the problem for the sake of calculation simplicity. These effects may be far more important and variable than expected for the case of highly irregular dike profiles. In these cases, detailed hydrodynamics should be included in order to have better understanding of effects derived from the profile irregularities or from the presence of additional embedded structures. Highly turbulent processes are expected in these places. Furthermore, the downstream effects depend on the upstream conditions which are also not explicitly taken into account in all the previously explained methods. Therefore, a more holistic approach such as the ones performed by Quang and Oumeraci (2012) or Kobayashi and Weitzner (2014) becomes more suitable. Both 1D models allowed to simulate the complete time-dependent erosion process of a grassed covered coastal dike. The main drawback of both models is that the effects of turbulence are included as a function of uniform flow models such as Chezy or Manning which are only

applicable for smooth bed slope transitions. When abrupt bottom slope variations are exerted by the flow, the vertical velocity distribution tends to have larger variability (Ribberink, 1998). This variability might result in more turbulent flows, higher energy dissipation and hence more uncertain scouring rates. Consequently, large difference in the resultant scouring profiles is expected when compared to the ones obtained by the uniform flow approaches.

All these previously mentioned challenges can be solved by implementing more detailed hydrodynamic solutions such as computational fluid dynamics (CFD) formulations like RANS  $K-\epsilon$  e.g. Based on this last consideration, Bomers et al. (2016) studied the influence of a road in the scouring patterns of a grass covered dike derived from the wave overtopping process. The CFD simulations used in this study were built based on the real scale experiment results performed with the wave overtopping simulator (Van der Meer et al., 2008), on a riverine dike located next the river Waal in the Netherlands. The CFD results showed that the presence of a road leads to higher scouring depths in places with little to non-existent grass cover. Higher turbulence is observed in these places. This particular model was able to capture the desired effects of turbulent flow, but unfortunately it is computationally prohibitive for probabilistic assessments where large number of simulations are required. Then, emulation of more detailed models becomes a good option for implementing them in the probabilistic safety assessments. Emulation consists in building a computationally inexpensive model, trained with data sets generated from the input-output data sets obtained from more complex models (Castelletti et al., 2012; Razavi, 2012). Hydrodynamic model emulation for example, has proven to be a powerful tool for water level prediction while improving the calculation speed significantly (Duncan et al., 2011; Aguilar-Lopez et al., 2014). For the specific case of reliability of flood defences reliability, emulation has also been implemented in the past for other failure mechanisms (Kingston, 2011; Aguilar-López et al., 2014). For the specific case of wave overtopping, van Gent et al. (2007) used the results of 10,000 physical model tests of different type of coastal defences to train a neural network.

In the present study a methodology was developed which allowed to include the influence of a road and its resultant turbulent effects in the wave overtopping probabilistic safety assessment of grass covered dikes. This is done by emulating the generated shear stress time series produced by two different CFD models; one with a road on top (Bomers et al., 2016) and one fully covered with grass. These emulators are later used for estimating shear stress excess values ( $T$ ) which are required as input for the grass erosion model. Based on the data collected during a real scale wave overtopping experiment and the previously built emulators, erodability curves ( $C_E$ 's)

were built. These functions allowed to generate general curves which are later combined with the emulators for estimating total erosion depths as a function of the overtopped wave volumes. In the end, stochastic variable propagation through the emulators is done so that scoured dike profiles are generated based on an erosion model. These profiles are associated to different storm conditions and different grass qualities in a probabilistic manner. This allowed to compare the results from the dike with a road with respect to the same dike without a road given the same stochastic boundary conditions. The results allowed to answer three main research questions:

1. How does the surface roughness and profile irregularities derived from having a road embedment, influence the occurrence of failure?
2. What is the influence of grass quality in the occurrence of failure?
3. How does the failure probability changes when a road is present with respect to the case when no road is present?

The outline of the present study is organized as follows: The theoretical background of the shear stress excess ( $T$ ) and erosion model used for estimating scouring depths along the profiles is explained in section 4.2. Afterwards, the real scale wave overtopping experiment performed on a Dutch dike located close to the town of Millingen aan de Rijn is explained in detail in section 4.3. All models built for this study are based on this flood defence and validated with the collected results during the experiment. Later the model emulation methodology, the erodability curves ( $G_E$ 's) and their implementation for probabilistic assessment are presented in detail in section 4.4. The results in terms of the effects of turbulence in the shear stress excess variability, the scouring profiles and spatially distributed failure probabilities are presented in section 4.5. The research questions are answered and further discussed in section 4.6 and finally the main conclusions and recommendations of the study are presented in section 4.7.

## 4.2 Theoretical erosion background

### 4.2.1 Shear stress excess ( $T$ )

Most of the overtopping scouring erosion methods are based on a critical threshold value. This defines the limit state for scouring initiation and progression. For the case of grass and soil scouring, the threshold is defined by a critical shear stress constant value ( $\tau_c$ ) which depends on the grass cover quality (Verheij et al., 1995). This limit state represents a reliability concept by itself. However, it does not fully include the

characteristics of the grass cover erosion rate or the “real” erosion time of the erosion process. It only represents the threshold which defines if the process occurs or not. To include these two characteristics (erosion rate and real erosion time), the shear stress excess concept is used in the present study. This value is represented by the capital Greek letter tau ( $T$ ).

It represents the surplus of shear stress during the period of time in one single point over the dike during one single wave in which erosion occurs. It’s only during this period that erosion takes place. Note that for higher values of  $\tau_c$ , the difference between the complete overtopping time  $t_{total}$  and the real erosion time differ significantly. The  $T$  value is calculated for a given point along the profile as the integral of the bottom shear stress function  $\tau(t)$  minus the critical stress threshold  $\tau_c$ , over the erosion time as shown in Figure 4-1. Lower  $\tau_c$  represent lower resistance to erosion and imply longer erosion times.

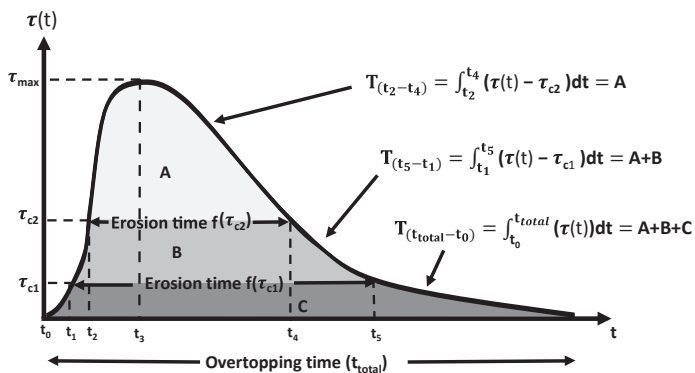


**Figure 4-1 Excess shear stress integral over time for different critical thresholds**

The fact that the erosion times ( $t_{i+1}-t_i$ ) and the total wave overtopping time ( $t_{total}$ ) differ was acknowledged by Hughes (2011), who included the estimation of the erosion excess time by assuming a triangular shape of the wave overtopping discharge hydrograph. However this assumption may be too general for representing the shear stress excess over a highly irregular bottom profile. In addition, the overtopping times change significantly between locations due to the presence of bottom irregularities which may either accelerate or delay the overtopping flows. The advantage of CFD modelling is that these effects are explicitly reflected in the  $\tau(t)$  time series. Furthermore, the upstream hydrodynamic effects are significant for the downstream locations along the dike, which are also reflected in the same time series. This is important in the present study as it is one of the main inputs for calculating the scoured depth per wave.

## 4.2.2 Erosion model as a function of T

The erosion model used in the present study is derived from the time dependent mass erosion rate equation for cohesive soils presented by Partheniades (1965) as:

$$\frac{dm}{dt} + M_p \frac{(\tau - \tau_c)}{\tau_c} = 0 \quad \text{Eq. 4-1}$$

In which  $M_p$  corresponds to the characteristic soil mass transport coefficient,  $\frac{dm}{dt}$  corresponds to the mass transport rate in time,  $\tau_o$  corresponds to the exerted bottom shear stress and  $\tau_c$  corresponds to the critical shear stress threshold.

According to Hoffmans (2012), an equivalent erosional rate strength parameter ( $C_E$ ) for soil and grass together was derived by Verheij et al. (1995) as:

$$C_E \equiv \frac{M_p}{\tau_c} \quad \text{Eq. 4-2}$$

Note that the  $C_E$  parameter is proportional to  $M_p$  and inversely proportional to  $\tau_c$  as shown in Eq. 4-2. Based on this equivalence and by dividing Eq. 4-1 by the dike cover relative density ( $\rho'_{cover}$  [kg/m<sup>3</sup>]), the erosion rate in an specific location for a unitary width of dike can be expressed as:

$$\frac{d\varepsilon}{dt} + \frac{C_E}{\rho'_{cover}} (\tau(t) - \tau_c) = 0 \quad \text{Eq. 4-3}$$

Since neither  $C_E$  or  $\rho'_{cover}$  are dependent of time, they can be taken out of the integral so that the scouring depth due to one single wave ( $\varepsilon$ ) in a particular location can be calculated by integrating Eq. 4-3 as:

$$- \int d\varepsilon = \frac{C_E}{\rho'_{cover}} \int (\tau(t) - \tau_c) dt \quad \text{Eq. 4-4}$$

The integral on the right side of Eq. 4-4 represents the (T) value for a given  $\tau_c$  value. The integral bounds are defined by the specific moments in time where  $\tau(t) \geq \tau_c$ , as erosion will only be possible for this condition (Figure 4-1).

### 4.3 Millingen aan de Rijn Wave Overtopping experiment with a road

Experiments for wave overtopping were conducted on top of a riverine dike along the river Waal nearby Millingen aan de Rijn (The Netherlands) in February and March of 2013 (Verheij et al., 2015). The experiments consisted in releasing random wave volumes ( $V$ ) from wave overtopping simulator WOS (Van der Meer et al., 2010) during a period of time equivalent to the duration of a storm. This device was located on top of the crest of the dike closer to the riverside vertex (Figure 4-2).

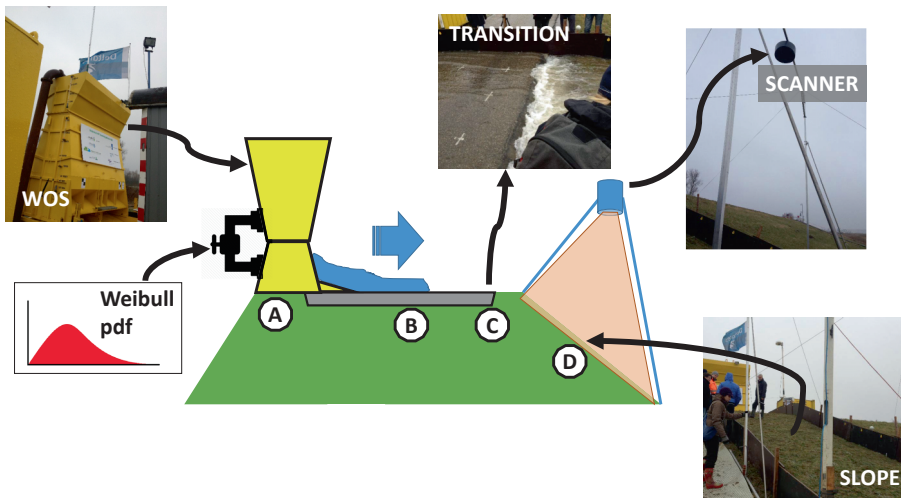


Figure 4-2 Millingen WOS experiment with road on top of the crest

After each simulated storm, the dikes were scanned in order to estimate the scouring depths and spatial scouring patterns. This experiment included a road on top of the dike in order to analyse the effect of transitions in the scouring process due to wave overtopping. The experiment was divided into two parts performed in two adjacent locations. Each test location was 4 meters wide with lateral walls that prevented leakage during the tests.

### 4.3.1 Millingen experiment part I: Scouring measurements

During the first part of the experiment, the WOS was located near the riverside edge of the dike (zone A, Figure 4-2). From this location, a series of volumes were released during a period of time. The released volumes were randomly sampled following a Weibull distribution which represents the stochastic nature of the waves that will eventually overtop the structure during a storm. For the present study, the term “storm” corresponds to a finite set of wave volumes produced from specific storm boundary conditions and which is characterized by an average overtopping discharge expressed in L/s/m. The actual Dutch safety standards for example, allow storms characterized by average overtopping discharges ( $q_m$ ) between 0.1 L/s/m and 10 L/s/m (Pullen et al., 2007). These storm average discharges are conditioned to the relative position of the crest of the dike with respect to the water still level, the dike geometry, dike cover and revetment type. This means that dikes are design for a certain set of storm conditions to ensure a certain maximum average overtopping discharge.

The first part of the experiment was conducted for different consecutive storms as presented in Table 4-1 (Verheij et al., 2015). These storms were generated for a duration of 6 hours and in the meantime, 3D images were taken with a laser scan (Figure 4-2) every 2 hours with an accuracy of 2 mm. For some storms, it was necessary to accelerate or decelerate some of the tests due to the WOS release and pumping constraints. The summary of all the overtopping storms experiments is presented in Table 4-1.

**Table 4-1 Profile scanning times for part I of Millingen experiment**

<b>Storm mean discharge</b>	<b>Storm Interval</b>	<b>Scan moment</b>	<b>Profile scan label</b>
<b><math>q_m</math> [L/s/m]</b>	<b>[min]</b>	<b>[min]</b>	<b>[-]</b>
Initial state	0	0	q0_t0
1	72	72	q1_sc1
10	180	252	q10_sc1
10	180	432	q10_sc2 *
50	60	492	q50_sc1
50	60	552	q50_sc2
50	60	612	q50_sc3
50	60	672	q50_sc4
50	180	852	q50_sc5 *
100	100	952	q100_sc1
100	120	1072	q100_sc2

**\*Note: Profiles used for the present study**

For the initial state scanned profiles of each storm, significant damage due to traffic was already observed inside the transition gaps (zone C, Figure 4-2). This eroded zone increased with each test as bare soil erodes faster the grass. Besides this zone, no significant erosion was observed in the grass cover for the 1 and 10 L/s/m tests. The scan labels presented in Table 4-1 include the average overtopping discharge and the scan number of that experiment.

### **4.3.2 Millingen experiment part II: Flow depths and velocity measurements**

The second part of the experiment consisted on measuring wave depth time series and velocity time series for different wave volumes along the dike profile. Paddle wheel devices were used for measuring velocity and surfboard meters for measuring flow depths in 8 different locations along the crest and landward slope (see Verheij et al. (2015) for more details). In order to exclude the effects on the measurements of the landside road transition and roughness change, a geotextile cover was placed over the transition between the asphalt road and the remaining crest part (Figure 4-2, zone C). Additionally, the WOS was located directly over the road (Figure 4-2, zone B), to avoid the induced effects on the flow measurements from the riverside transition. Velocities and depths time series were measured at least two times for wave volumes ( $V$ ) of 400, 600, 800, 1000, 1500, 2000, 2500, 3000, 4000, 5000 and 5500 L/m. Storms are characterised by their average mean wave overtopping discharge ( $q_m$ ) during the whole storm duration, despite the fact that in reality they are composed of random overtopped wave volumes ( $V$ ) which have variable instantaneous overtopping discharges.

## **4.4 CFD emulation for probabilistic analysis**

The methodology flow chart for building both models, their correspondent emulators and the probabilistic assessment based on them is presented in Figure 4-3. It consists of two CFD models built for producing accurate and detailed time series of the wave overtopping process for each configuration. The first model corresponds to the situation observed in the Millingen dike before the experiment which included an asphalt road. This model is referred to as “Road on crest dike model” (RCDM) in the present study. The second model represents the same dike but without the road on top. This model is referred to as “Grass crest dike model” (GCDM) all along the present study.

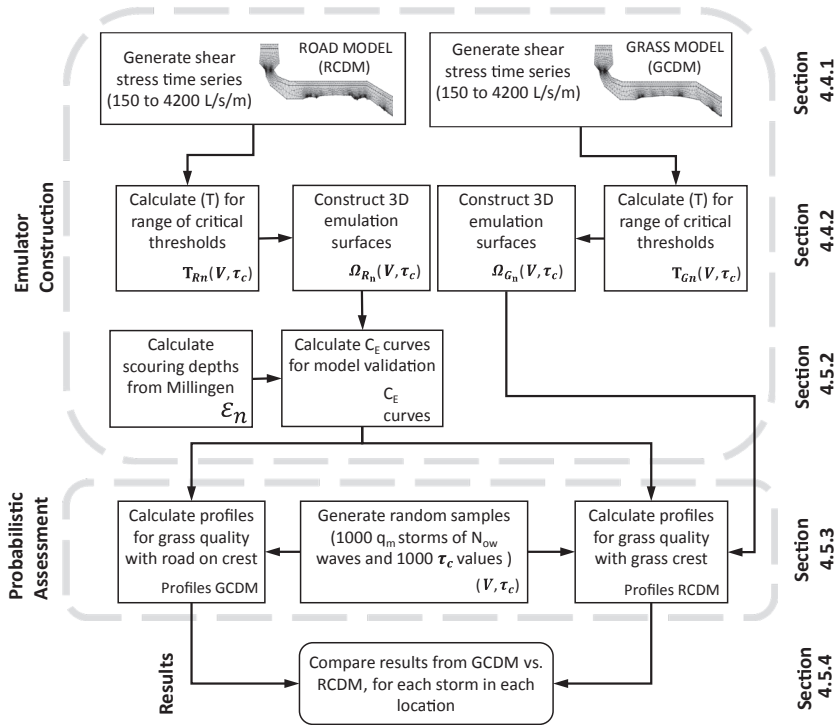


Figure 4-3 Methodology flow chart for emulator construction and probabilistic safety assessment

Afterwards, computationally inexpensive models (emulators) based on the integrated shear stress excess over time (T) concept were built, based on the output produced by the two previously built CFD models. These emulators are capable of estimating T values as a function of combinations of V and  $\tau_c$  values. Their reduced calculation times allowed to implement them for probabilistic failure assessment by combining them with additional grass quality parameters. The erosion model is used for estimating scouring depths in 33 preselected locations along the profiles of both dike conditions with the emulators. Grass erosion resistance curves ( $C_E$ ) required for implementing the erosion model were also built based on the results of the Millingen experiment part I. These curves allow to estimate the erosional rate strength value as a function of the  $\tau_c$  value and the grass quality type (e.g. good, average or poor). These same curves are assumed to be representative of the condition without a road as its presence does not have any influence in their behaviour. Finally, the emulators and the curves are used for generating probabilistic scouring profiles and spatially distributed failure probabilities along the dike by representing their input variables as probabilistic distributions.

## 4.4.1 CFD models

The model from the experiment of Millingen aan de Rijn dike and an additional model with no road were built by using the CFD COMSOL Multiphysics® software for solving 2D Navier-Stokes RANS K- $\epsilon$  formulation for two phases (air/water).

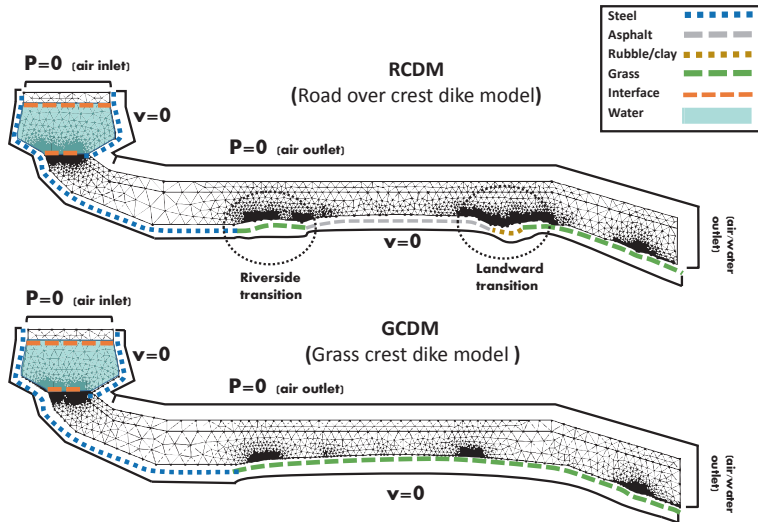


Figure 4-4 CFD models boundary conditions (schematic meshing not in actual size)

The first model (RCDM) originally built by Bomers et al. (2016), was based on the scanned profile obtained as a final condition after the 10 L/s/m experiment (q10\_sc2). This profile includes an asphalt road of 3.1 meters wide with one adjacent eroded transition gap in each side of approximately 0.5 meters each (Figure 4-4). Additionally, 2.5 meters of the landside slope (approx. 1:3) is included.

A second model (GCDM) was generated to recreate a dike which could be tested with the same hydrodynamic conditions, but without including the asphalt road and transition gaps present in the original model. This model was built based on the original Millingen experiment dike profile (q10\_sc2, section 4.3.1) but the transition gaps were removed with a line smoothing procedure and the asphalt cover roughness was replaced by the roughness of grass (Figure 4-4). The rest of the profile remained unmodified with respect to the RCDM. Especially the main height features such as the centerline point elevation, vertex points of both sides of the asphalt cover and vertex points between the crest and lateral slopes. In that way, it was ensured the results remain comparable in terms of the available potential energy in these points for both models. The roughness coefficients used in both models (Table 4-2) were obtained from the reported manning

values by Verheij et al. (2015). The transformation of manning values (n) to sand roughness ( $K_s$ ) values required by COMSOL was done with the equation presented by Marriott and Jayaratne (2010).

**Table 4-2 Roughness coefficients used for both road and crest models**

Surface	Manning's n [s/m <sup>1/3</sup> ]	$K_s$ [m] [m]	Source
Asphalt	0.016	0.0047	(Verheij et al., 2015)
Grass	0.025	0.0680	(Verheij et al., 2015)
Steel	0.017	0.0068	(Te Chow, 1959)
Rubble/Clay	0.025	0.0670	(Te Chow, 1959)
Geotextile*	0.024	0.0660	(Jansen, 2012)

**\* This value was not used as input in any of the two CFD models**

Detailed CFD RANS K- $\epsilon$  simulation has the capability of representing turbulence effects with better accuracy than uniform flow based methods. The main feature of turbulent flow is its capacity to rapidly dissipate kinematic energy (velocity) into internal energy in the form of eddies. Also, air entrapment and flow concentration, are better represented by CFD models and these factors become more important when abrupt geometric bottom changes and local surface roughness variations are present. These effects are explicitly included in the time series of average depth flow velocities, water depths and bottom shear stresses of CFD models.

With this feature in mind, simulations for 150, 400, 700, 1000, 1500, 2500, 3200 and 4500 L/m volume waves (V) were performed for both RCDM and GCDM. The results from the 4500 L/s simulation were discarded as they significantly differ from the measured values during the experiment (see validation plots on appendix A.1 and A.2). From each simulation, shear stress time series were generated in 33 study points along the profiles of both models (Figure 4-5). From now on these locations are referred as STPs. These study points (numbered dots in Figure 4-5) were selected for estimating the erosion resultant depths in places where the bottom slope line segment changed significantly with respect to the previous bottom slope line segment. In this locations it is expected that more turbulence will be generated.

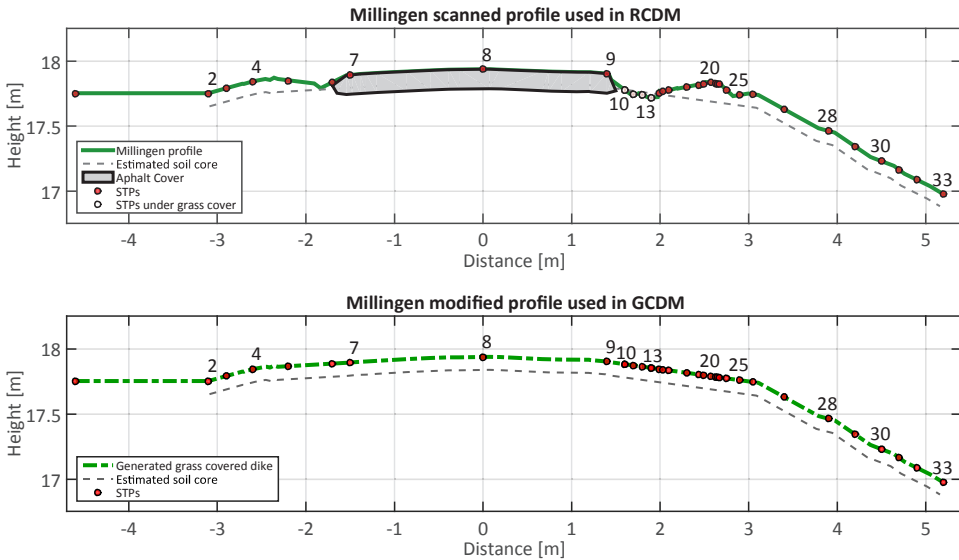


**Figure 4-5 Study points (STPs) location for RCDM and GCDMs**

All 33 STPs are located in the same horizontal position in both RCDM and GCDM. The exact smoothing procedure of the RCDM profile for generating the GCDM profile consisted in placing straight lines between STPs 5 and 7, 9 to 20 and 23 to 26 (Figure 4-5). According to the field measurements presented in Verheij et al. (2015) and Bakker et al. (2013), the average thickness of the grass cover is around 10 cm. Accordingly, a grass soil interface line was defined in both models (lower dashed line in Figure 4-5) as 10 cm offset of the GCDM profile. Points that ended below this line in the RCDM are located inside the clay zone (e.g. STPS 10 to 13 in the RCDM, Figure 4-5).

The RCDM and its validation are presented in the study of Bomers et al. (2016). As the Millingen experiment included a road in the crest, no experimental measurements are available for validating the GCDM. Yet, maximum value data from two other WOS experiments performed in the Vechtdijk in Zwolle (Van der Meer et al., 2012) and the Tholen dijk near Nieuw-Strijen (Verheij et al., 2015) were used. From these data sets, it is concluded that the GCDM model maximum velocities and maximum flow depths are in good agreement with the measurements taken in the Vechtdijk. Additionally, the expected behaviour presented by the GCDM such as lower velocities and larger flow depths with respect to the RCDM gives confidence for using the model in the present study. The validation plots for both RCDM and GCDM are presented in appendix A.1 and A.2.

## 4.4.2 Emulator surfaces construction

From the results of both RCDM and GCDM, bottom shear stress time series are obtained per STP location. Afterwards, each of these time series was integrated in time for one given value of  $\tau_c$  between 1 N/m<sup>2</sup> and 300 N/m<sup>2</sup>, in each STP to obtain a correspondent T value. This same process is repeated for the different simulated wave volumes listed in section 4.4.1. These volumes were selected as intermediate values of ones measured during the Millingen experiment (section 4.3.2). The  $\tau_c$  ranges were defined based on the recommended values for grass and soil presented by Hoffmans (2012). As a result, training data sets of three columns of values (V,  $\tau_c$  and T) in each STP location were obtained. The data sets were later used for training the emulators in each STP location for each of the dike conditions.

Castelletti et al. (2012) classified emulators into two categories; structure-based and data-based. The first category consists in a “manipulation” of the original mathematical structure. The second category reproduces output potential trajectories from relations of input-output scenarios produced by the original model. All 33 emulators built for each dike configuration in this study correspond to the last category. These emulators are based on 3D linear interpolation surfaces (Forrester et al., 2008) further on denoted as  $\Omega_{R_n}$  and  $\Omega_{G_n}$  for each dike model. The Greek letter  $\Omega$  denotes emulator, letters R or G denote either “RCDM” or “GCDM” and the sub index  $n$  denotes the STP location. These emulators were built based on the Matlab® interpolation scientific package and were designed as 3D surfaces for estimating functions in each STP such that  $T_n = f(V, \tau_c)$ . Examples of the emulator generated surfaces of RCDM and GCDM in locations 8 and 28 ( $\Omega_{R_8}, \Omega_{G_8}, \Omega_{R_{28}}, \Omega_{G_{28}}$ ) are presented in Figure 4-6.

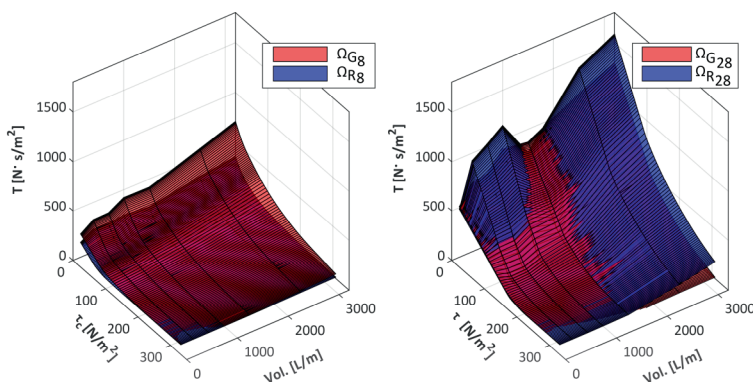


Figure 4-6 3D linear interpolation surfaces for locations before and after the landward transition

The  $T$  values used for the emulator training were calculated from integrating the positive differences between  $\tau_c$  and the time series  $\tau(t)$  produced from the RCDM and GCDM in each STP. Note that the intersection between  $\tau(t)$  and  $\tau_c$  is used to define the integration bounds. Then, the erosion time effects on these  $T$  values is implicitly included as the integration is done between these two time bounds as shown in Figure 4-1. Hence, each emulator can be assumed to be equivalent to the solution of the excess shear stress integrals for one single wave present in the right side of Eq. 4-4, as presented in Eq. 4-5 and Eq. 4-6 for both GCDM and RCDM respectively.

$$\Omega_{G_n}(V, \tau_c) \approx \int (\tau_{G_n}(V, t) - \tau_c) dt \quad \text{Eq. 4-5}$$

$$\Omega_{R_n}(V, \tau_c) \approx \int (\tau_{R_n}(V, t) - \tau_c) dt \quad \text{Eq. 4-6}$$

These emulators are valid for estimating the  $T$  values of any given  $V$  value between 150 and 3200 L/s and for any given  $\tau_c$  value between 1 and 300 N/m<sup>2</sup>. Note that the surfaces generated for the STP8 in both models ( $\Omega_{R_8}$ ,  $\Omega_{G_8}$ ) before the landward transition, are located one above the other one (Figure 4-6) which reflects the effects of the surface roughness. For surfaces located after the transition (e.g.  $\Omega_{R_{28}}$ ,  $\Omega_{G_{28}}$  in Figure 4-6), an erratic intersection behaviour of the surfaces is observed as a consequence of the more turbulent flow.

### 4.4.3 $C_E$ functions

In this study, the  $C_E$  coefficient is expressed as a function of the  $\tau_c$  as shown in Eq. 4-2 and not as a constant value as presented by Verheij et al. (1995). By assuming that  $C_E$  as a function of  $\tau_c$  it is ensured that the grass quality is reflected in both the threshold and the difficulty to erode the cover and that Eq. 4-2 remains valid. These functions were built by using the previously built emulators (section 4.4.2), the WOS released volume list from the experiment and the q10\_sc2 and q50\_sc5 scanned profiles (Figure 4-7 upper plot). This two scans represent the initial and final state of the 50 L/s/m storm experiment. Based on this last information, the scouring depths ( $\varepsilon$ ) values per location (Figure 4-7 lower plot) at the end of the 50 L/s/m storm experiment were obtained in each STP by subtracting both profile scans.

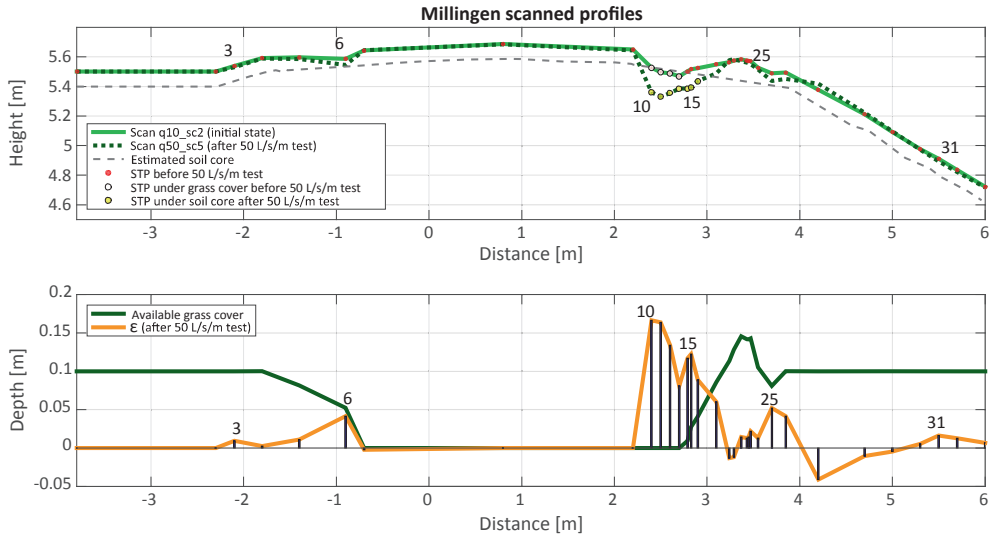


**Figure 4-7 Scouring depths (e) calculated from profiles q10\_sc2 and q50\_sc5 profiles**

The 50 L/s/m storm results were chosen for building the  $C_E$  functions as the previous experiments did not result in significant scouring and consequently the grass cover was still in good conditions. Locations such as STPs 18, 19 and 27, 28 and 29 where accretion was observed, were discarded as the erosion model assumes that all material is fully washed to the downstream part.

For the remaining locations, the  $C_E$  functions were calculated as:

$$C_{En}(\tau_c) = \rho'_{cover} \frac{-\int d\varepsilon}{\Omega_{Rn}(V, \tau_c)} \quad \text{Eq. 4-7}$$

This equation was obtained by substituting Eq. 4-6 in Eq. 4-4. With this equation,  $C_E$  curves for each SPT were built as a function of a  $\tau_c$  range between 1 and 300 N/m<sup>2</sup> in steps of 1 N/m<sup>2</sup>. In each step, the actual release list of the 50 L/s/m was used as input for the RCDM emulators in order to obtain a cumulative value of  $T$  for evaluating Eq. 4-7. The  $\varepsilon$ 's calculated previously (Figure 4-7 lower plot) are equivalent to the solution of the negative integral present in this same equation in each location.

Different submerged cover densities ( $\rho'_{cover}$ ) are required for each  $C_E$  curve depending whether the profile bottom is located on the grass cover or inside the soil core. For determining these density values of each type of cover (grass or soil), the results of the measurements of a complete grass cover block (grass, roots and soil) reported by Piontkowitz (2009) were used as reference. They correspond to a saturated sample

extracted from a Danish dike which was composed of 0.17 meters of soil and 0.03 meters of grass with a total average density of 1870 kg/m<sup>3</sup>. For this study, we assumed a reference saturated density value of soil ( $\rho_{cover_{soil}}$ ) of 2000 kg/m<sup>3</sup>. Based on these values, it is estimated that the saturated density of grass solely ( $\rho_{cover_{grass}}$ ) is 1100 kg/m<sup>3</sup>. Based on these values, the resultant  $C_E$  curves obtained by the use of Eq. 4-7 are presented in section 4.5.2.

#### 4.4.4 Probabilistic safety assessment

In general, failure mechanisms can be expressed as a limit state equation in the form of:

$$Z = R(x_1, x_2, x_3 \dots x_n) - S(y_1, y_2, y_3 \dots y_n) \quad \text{Eq. 4-8}$$

where the variable  $S$  represents the solicitation load,  $R$  represents the resistance of the structure against such load and  $x_n$  and  $y_n$  are the variables used to estimate each term. The  $Z$  term represents the marginal resistance which defines the state of the system as safe when positive and in failure when equal or less than zero. Wave overtopping failure is a major threat to flood defence safety as once the grass cover is completely lost, the rapid scouring process of the soil core may originate a dike breach. Hence for the present study, failure is defined as the complete loss of the available grass cover in each location. In other words, the dike is assumed to be in failure state once one or more of the STP's grass cover is completely lost.

Hence, the dike grass cover limit state is obtained by rearranging Eq. 4-4 and making it equal to the marginal strength term ( $Z$ ) as:

$$Z_{wo} = [- \int d\varepsilon] - \frac{C_E(\tau_c)}{\rho'_{cover}} \int (\tau(V, t) - \tau_c) dt \quad \text{Eq. 4-9}$$

Analogously to Eq. 4-8, the first integral presented in square brackets represents the resistance term ( $R$ ). The second integral represents the solicitation term ( $S$ ). The failure state ( $Z \leq 0$ ) is determined by the total available grass cover thickness ( $\varepsilon$ , Figure 4-7) in each STP location which is equivalent to the solution of the negative integral of  $d\varepsilon$ , inside squared brackets of Eq. 4-9.

The  $\varepsilon$  values in each location and their corresponding emulators were replaced in Eq. 4-9 so that the limit state equation of the grass cover for both RCDM and GCDM in each location could be evaluated. For failure to occur it is required that several overtopped waves scour the grass cover as grass can be quite resistant to erosion. Then, a single cumulative shear stress excess value is calculated from the total number of

overtopped waves equal to  $N_{ow}$  during one single storm. This value is randomly sampled for several storms and in that manner a probabilistic distribution of the  $S$  term is obtained. For each storm, a  $\tau_c$  value is also randomly sampled and in that manner the  $R$  term can also be represented as a stochastic random variable. In this manner the resultant limit state equations per STP in the GCDM and RCDM are:

$$Z_R = \varepsilon_{R_n} - \frac{C_E(\tau_c)}{\rho'_{cover}} \sum_{i=1}^{N_{ow}} \Omega G_n(V, \tau_c) \quad \text{Eq. 4-10}$$

$$Z_G = \varepsilon_{G_n} - \frac{C_E(\tau_c)}{\rho'_{cover}} \sum_{i=1}^{N_{ow}} \Omega R_n(V, \tau_c) \quad \text{Eq. 4-11}$$

The failure probabilities are estimated as  $P_{R}(Z_R \leq 0)$  and  $P_{IG}(Z_G \leq 0)$ . This probability is estimated via a Monte Carlo simulation for 3% error (1000 samples required). For a probabilistic failure assessment, all variables involved in the model should be defined either as stochastic or deterministic depending on the modelling choices. For the present study, the critical grass cover thickness values ( $\varepsilon$ ) in each STP location in the GCDM and RCDM were assumed to be constant and equal to the difference in elevation between the profile and the soil core line (dashed lines in RCDM and GCDM on Figure 4-5). The cover submerged densities ( $\rho'_{cover}$ ) were assumed to be constant as well (values presented in section 4.4.3).

The overtopping volume ( $V$ ) and critical shear stress threshold ( $\tau_c$ ) are assumed to be the only stochastic random variables for the probabilistic analysis. For  $V$ , the two parameter (a and b) Weibull distribution was adopted for the random sample generation (Van der Meer et al., 1994). The exceedance cumulative function of this distribution is expressed as:

$$P_V = P(\underline{V} \leq V) = 1 - \exp\left[-\left(\frac{V}{a}\right)^b\right] \quad \text{Eq. 4-12}$$

Hughes et al. (2012) improved the estimation of the shape parameter (b) for wave overtopping by fitting an empirical equation to different experimental results as presented in Eq. 4-13. Both unmodified scale (a) and shape (b) parameters presented in their study were adopted for the distribution fitting and random sampling of  $V$  as presented in Eq. 4-13 and Eq. 4-14:

$$a = \left( \frac{1}{\Gamma(1 + \frac{1}{b})} \right) \cdot \left( \frac{q_m T_m}{P_{ov}} \right) \quad \text{Eq. 4-13}$$

$$b = \left[ \exp \left( -0.6 \frac{R_c}{H_{m0}} \right) \right]^{1.8} + 0.64 \quad \text{Eq. 4-14}$$

Where  $q_m$  represents the storm overtopping average discharge expressed in [L/s/m],  $P_{ov}$  represents the overtopping probability (dimensionless),  $R_c$  represents the dike free crest height expressed in [m],  $T_m$  represents the mean wave period expressed in [s] and  $H_{m0}$  represents the incident energy based significant wave height expressed in [m]. For flood defences, the average overtopping discharge  $q_m$  is also used for characterizing storm conditions in overtopping events (Pullen et al., 2007). This value corresponds to the accumulated overtopped volumes during the storm event. Dutch guidelines define the allowable average overtopping discharge depending on the type and state of the structure. For dikes, the allowable overtopping discharge values range between 0.1 and 10 L/s/m depending on the cover and/or outer slope revetment (Van der Meer, 2002). This range plus four larger storm conditions were tested and their characteristic values are presented in Table 4-3:

**Table 4-3 Storm boundary conditions for riverine dike**

	Mean overtopping discharge $q$ (L/s/m)						
	0.1	1	10	20	50	75	100
<b>R<sub>c</sub> [m]</b>	2.99	2.20	1.40	1.17	0.85	0.71	0.61
<b>Outer Slope [-]</b>	1:3	1:3	1:3	1:3	1:3	1:3	1:3
<b>N<sub>w</sub> [-]</b>	6545	6545	6545	6545	6545	6545	6545
<b>N<sub>ow</sub> [-]</b>	65	458	2291	3142	4451	4974	5367
<b>P<sub>ov</sub> [-]</b>	1%	7%	35%	48%	68%	76%	82%
<b>V<sub>max</sub> [L/m]*</b>	209	460	943	1266	1910	2350	2719

Note \*: Maximum tentative volume from Weibull distribution (Eurotop; (Pullen et al., 2007))

For each storm condition, one thousand storms composed of  $N_{ow}$  values for  $V$  were generated via random sampling from the Weibull fitted distribution (Eq. 4-12, Eq. 4-13 and Eq. 4-14). All the storms tested in this study (presented in Table 4-3) corresponded to typical wave conditions ( $H_s = 1$  m. and  $T_p = 4$  s.) of flood defences located in riverine areas such as the one in Millingen (Van der Meer et al., 2010). For simplification of the problem,  $H_{m0} = H_s$  and  $T_p = 1.1T_m$  can be used as a approximated values (Van der Meer, 2002).

For the  $\tau_c$  random variable, there is no available literature to our knowledge that studied or suggest the stochastic nature of this variable in particular for grass. However, from the values reported in Verheij et al. (2015), an equivalence curve between critical erosion velocities ( $U_c$ ) and  $\tau_c$  was built as shown in Figure 4-8:

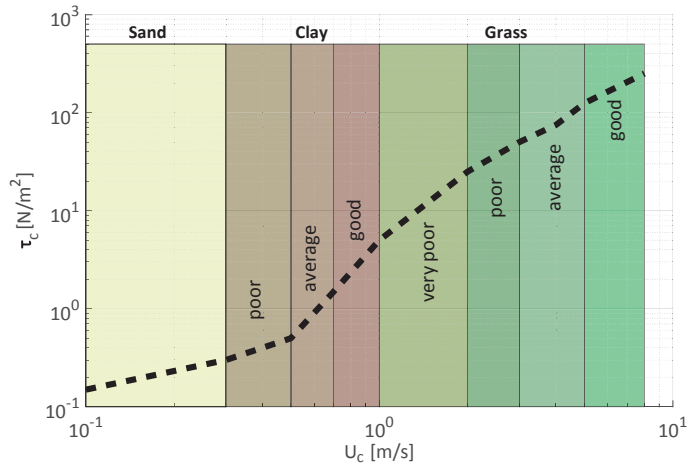


**Figure 4-8 Critical velocity vs critical shear stress threshold equivalence curve from (Hoffmans, 2012)**

The work of Trung (2014) was used for defining the stochastic distributions for the  $U_c$  of grass and soil. His work concluded that  $U_c$  can be represented by a log-normal distribution for the grass cover and by an extreme generalized distribution (e.g. Weibull) for bare soil locations. This last type of distribution requires additional information (e.g. shape and location parametrization) which could not be estimated from the experimental data collected during the Millingen experiment. Hence, a log-normal distribution is also assumed for the bare soil spots as presented in Table 4-4.

**Table 4-4 Stochastic random variables of cover quality used as input for CE calculation**

		Clay $U_c$		Grass $U_c$	
		Good	Poor	Average	Good
Distribution	[-]	Log-norm	Log-norm	Log-norm	Log-
mean	[m/s]	0.85	3	4	6.5
C.V.	[-]	0.1	0.3	0.3	0.3
QCF	[-]	[-]	1.5	1	0.1

This assumption will not affect the results significantly as failure is defined by the complete scouring of the grass cover only. Finally, the  $U_c$  random samples were transformed into critical stress threshold with the curve presented in Figure 4-8. In consequence, the  $C_E$  function will be represented as a stochastic variable as it depends on the value of  $\tau_c$ . Based on the indicative average values of  $\tau_c$  presented by Hoffmans (2012) it was possible to define mean values of  $U_c$  per grass and soil qualities (Table 4-4). The coefficients of variation were estimated based on the results presented by Trung (2014). The grass quality correction factor (QCF) is obtained by estimating the value which shifts the average grass quality function  $C_E$  until the quality values suggested by Verheij et al. (1995) are intersected.

## 4.5 Results

### 4.5.1 Effects on the excess shear stress

In order to analyse the effects of roughness and bottom slope changes derived from the hydrodynamics only (research question 1), the shear stress excess results were analysed first. To do this, the average  $T$  value ( $\bar{T}$ ) per location from the Millingen experiment was calculated for each of the 33 locations in both RCDM and GCDM based on the input list of released volumes by the WOS for the 50 L/s/m test. We refer to the calculated  $T$  values here as “potential” because of the  $\tau_c$  value used in each of the locations is set to zero and no cover density or erodability constants were included. In other words, only the summatory functions present in Eq. 4-10 and Eq. 4-11 were analysed. In addition, the 95% confidence intervals for all  $T$  values from the experiment were calculated for each location as well as shown in Figure 4-9. The ratio between the  $\bar{T}$  values of the RCDM and GCDM in all locations is also presented in a third lower plot in the same figure.

The first observation from these results was that the  $\bar{T}$  values in the lower part of the landward slope (between STPs 26 and 33) were larger in the RCDM with respect to the GCDM. This behaviour was surprising as the landward transition gap was expected to be a great energy loss for the flow. If this hypothesis was correct, the downstream  $\bar{T}$  values obtained in the RCDM should be lower than the ones obtained in the GCDM.

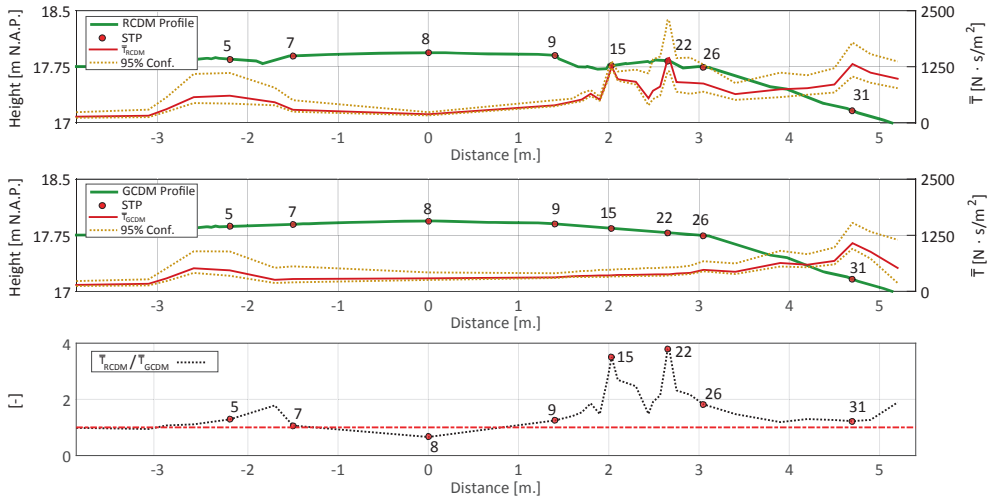


**Figure 4-9 Mean values of  $\bar{T}$  and confidence intervals of RCDM and GCDM**

The second observation was that it was possible to identify the effects of surface roughness and bottom surface irregularities separately. On one hand, the  $\bar{T}$  values increase significantly after STP 9 were evident abrupt bottom changes are present in the RCDM case. In particular, for the STP's 15, 22 and 31 were four times larger values are obtained on the RCDM with respect to the GCDM (see the lower plot, Figure 4-9). On the other hand, the mean shear stress excess in the centerline location (STP8) is lower in the RCDM case. This effect can be attributed to the smoother surface. Note that this point (STP8), the bottom slope is almost identical in both GCDM and RCDM.

Except for STP8, all locations present equal or larger  $\bar{T}$  values in the RCDM with respect to the GCDM. From a probabilistic point of view this means that on average, the probability of scouring in these locations will always be higher if grass quality and cover thickness are constant along both profiles. Furthermore, the 95% confidence bounds show wider spreading widths with respect to the mean values in all locations after STP 15 in the RCDM case. This higher variability of single wave  $T$  values is correlated to higher turbulence in these locations. In that same manner, it can be observed that in places where bottom slope changes are minimal (e.g. STP8), less spreading of the confidence bounds is observed which means that there is less turbulence.

## 4.5.2 $C_E$ curves from Millingen measurements

The  $C_E$  curves obtained from the experiment data are presented in Figure 4-10. This figure only includes the resulting  $C_E$  curves for STP's located after the asphalt cover (STP's > 9) where scouring was observed as these locations will certainly be influenced by the presence of the road. They are plotted with thinner dashed lines for STP's inside gap, thick continuous lines for STP's located over the dike vertex and thick dashed lines for STP's located along the landward slope. The indicative interval values suggested in the study of Verheij et al. (1995) are also included in the figure. They are represented by black horizontal bars. An additional side plot is built for the  $C_E$  curves obtained for STP's inside the gap where no grass cover was initially available.

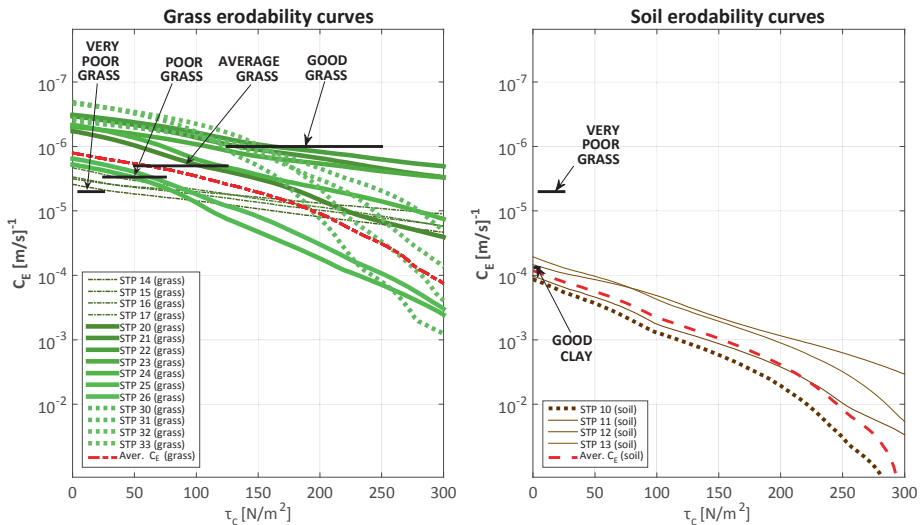


Figure 4-10  $C_E$  curves for each STP for grass and clay

In the figure it can be observed that for STP's located closer to the road (STP's 14 to 17 plotted as thin dashed lines in Figure 4-10) correspond to grass qualities between the very poor and poor grass quality. For STP's located over the vertex plotted as continuous thicker lines (STP's 20 to 26), average and good grass qualities are obtained, besides STP 25 and 26. For the remaining locations along the landward slope (STP > 29 plotted as thick dashed lines), the grass quality is mostly good.

These results are in good agreement with the findings for grass quality reported by Verheij et al. (2015). For the STP's located initially in the soil zone, good clay quality values were obtained (right plot of Figure 4-10). In addition, grass and clay quality average curves ( $\overline{C_E}$ ) were built by averaging all the  $C_E$  curves per type of cover (read

dashed line, Figure 4-10). In the case of the grass cover, the  $\overline{C_E}$  curve intersects the suggested range for average quality from Hoffmans (2012). Two additional grass quality  $C_E$  curves (poor and good) were deducted by multiplying the same  $\overline{C_E}$  curve by a factor. These factors were deducted by ensuring that the new curve intersects the midsection of the correspondent  $C_E$  grass quality reference value (Black indicative lines on Figure 4-10). The estimated QCF values for these other two grass qualities were presented in Table 4-4. Even though this new set of curves (poor, average and good) were deducted from the road on crest experiment we assume that they are also representative for the case were no road is present on top of the dike.

### 4.5.3 Scouring depth profiles

All the results obtained for the storms of  $q_m$  0.1, 1.0 and 10 L/s/m were omitted from this study as almost no scouring was obtained with 1000 samples. Hence, only the resulting scouring profiles for the largest 4 storms presented in Table 4-3 were analysed. Each profile was produced by plotting the mean value of the final scouring depths obtained from each of the 1000 storms per storm condition (Table 4-3). These values are equivalent to the mean value of the probability density function obtained for the second term of Eq. 4-10 and Eq. 4-11 for the 1000 generated storms in each STP. The profiles were only analysed for the STPs locations after the asphalt cover as they will certainly be influenced by the presence of the road. The first results correspond to simulations where the grass cover was assumed to have good grass quality along the whole profile as shown in Figure 4-11.

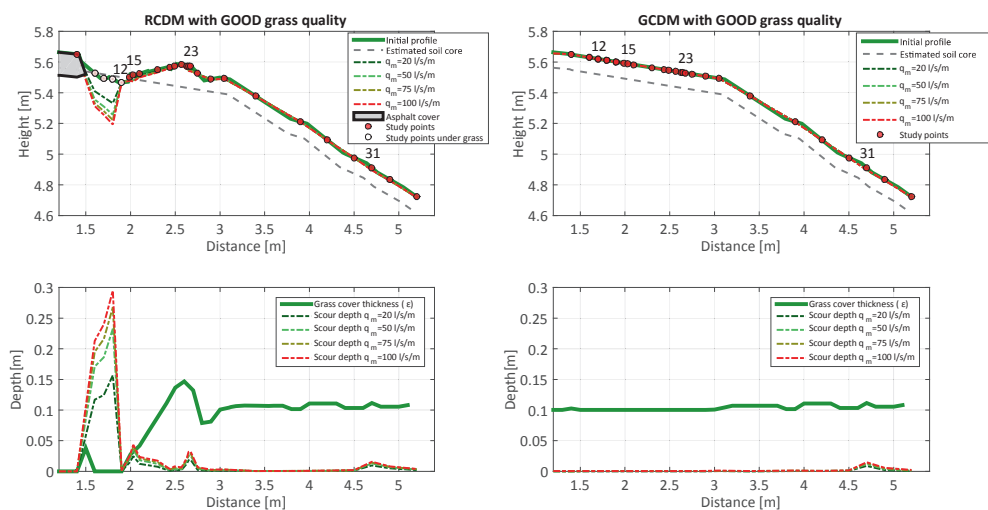
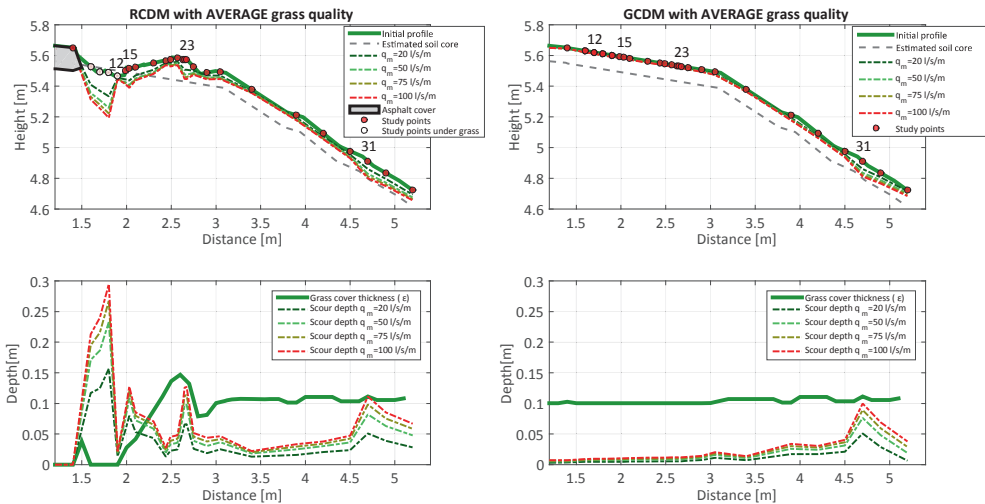


Figure 4-11 Results of scouring profiles for different storms on good grass quality

These results show that for this grass quality, the maximum scouring depths are less than 0.05 meters along the whole dike profile for all storms. The scouring magnitude of both models in the lower part on STP 31 is almost identical. This means that when the grass cover is strong, the effect of the road is almost negligible and will only affect the less resistant zones such as the bare soil spots. A failure point for all storms larger than 20 L/s/m is observed on the STP 15, just beside the bare soil zone where not much grass cover was left. During the scouring process, it is expected that this kind of zone fails first due to the combination of thinner grass cover and high turbulent flows (Figure 4-9). For the case of the average grass quality (Figure 4-12), the scouring depths increase significantly and there is also an additional failure spot located in STP 31 for the 100 L/s/m.



**Figure 4-12 Results of scouring profiles for different storms on average grass quality**

This failure is only observed for the dike with a road on top. The results show that despite the existence of a transition gap in the right side of the road (additional energy loss), the additional energy available due to the presence of a smoother surface might cause a failure downstream (STP 31).

A new significant scouring zone is also observed in the transition between bare soil (inside the gap, STP12) and the dike crest vertex (STP23). These “most probable” failure spots coincide to locations where the profile present an adverse slope. From these results, the most interesting finding is that STP23 represents a weak spot in the profile despite the fact that the available grass cover is even thicker than most of the other locations. This can be explained based on the results presented in Figure 4-9 were STP23 corresponds to one of the most turbulent locations. Again, this result supports

the importance of including high geometrical detail and turbulence effects in the model used for safety assessment.

For the case where poor grass cover quality is assumed along the whole profile (Figure 4-13), the scouring trend is very similar to the average grass quality results but the scouring depths become significantly deeper. Failure spots are identified in STP 31 for the GCDM for the 75 and 100 L/s/m storms. For the RCDM, the STPs 23, 24, 25 and 31 result in failure for the 75 and 100 L/s/m storms and very close to failure for the 50 L/s/m storm in the STPs 23 and 31.

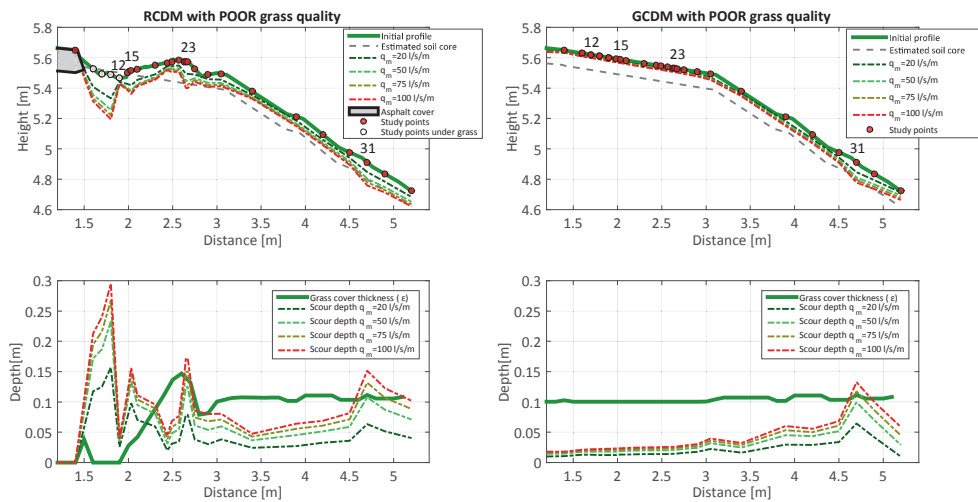


**Figure 4-13 Results of scouring profiles for different storms on poor grass quality**

For a more realistic analysis, the grass qualities of each point were replaced by one of the three qualities used in the previous analysis that seems closer to the local condition per STP found in section 4.5.2. The resultant scouring profiles (Figure 4-14) become safer in the lower part of the slope (STP 31) for both RCDM and GCDM. However, failed locations were identified in STPs 15 and 16.

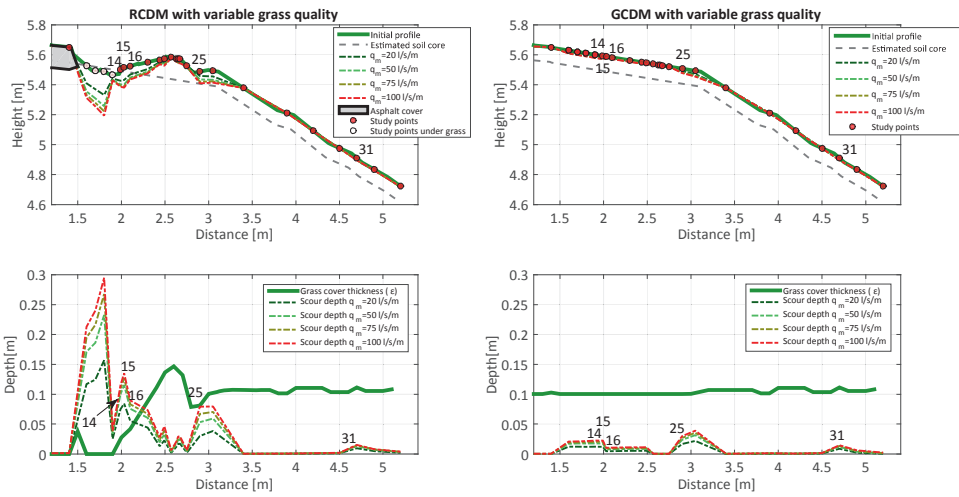


**Figure 4-14 Results of scouring profiles for different storms with spatial distribution the Millingen dike**

For the 100 L/s/m storm profile, it can be observed how STP 25 is very close to failure as the scouring depth is very close to the available grass cover thickness (lower RCDM plot in Figure 4-14). This location corresponds to the most prone to fail spot in the GCDM given the poor grass quality present in that particular location.

#### 4.5.4 Probability of failure

The scouring profiles are plotted based on the mean scouring values obtained after the dike was exposed to all the 1000 simulated storms. Yet, the probability of failure in each location is estimated as the number of times that the obtained scouring depth per storm is larger than the available cover thickness, divided by the total number of simulations (1000 in our case). Each of this estimated failures is conditioned to the overtopping probability related to each storm (see Table 4-3). This “conditional” probabilities for both RCDM and GCDM are presented in Figure 4-15. For this study, any failure probability larger that 0.99 is assumed as an already failed spot. This value was assumed since STPs 10, 11, 12 and 13 (located in bare soil) presented values above 0.99 and had already failed before routing the different storms.

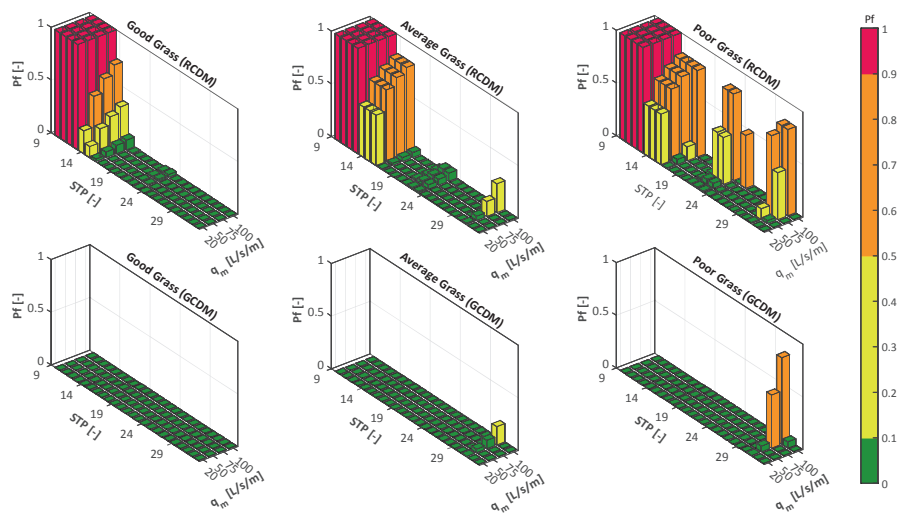


**Figure 4-15 Failure probabilities per storm along the right side of the profile in each STP for different grass qualities**

For the good grass quality configuration, the most probable location for the failure to occur corresponds to STP14 (disregarding the STP's 10 to 13 which were in a failure state already) of the RCDM which will always fail before any other downstream location disregarding the storm. An interesting observation is that this spot shows a lower  $\bar{T}$  value with narrow confidence bounds (less turbulent flow), with respect to other STPs located further from the road (Figure 4-9). As this scenario corresponds to a dike completely covered in good grass quality, the failure can be attributed due to the small thickness of the grass cover in this spot.

When grass quality is decreased to average, STPs 14, 15 and 16 present significantly high probability of failing ( $P_f > 0.5$ ) for storms with average discharges larger than 50 L/s/m. A remarkable finding from this configuration is how the average scouring depth obtained in STPs 23 and 31 seems to be very close to failure (Figure 4-12), and yet the probability results show that both points have less than 50% probability of failing for the largest storm (Figure 4-15). This means that for average grass quality, this point will certainly present deep scouring depths but is very unlikely to fail completely. The remaining locations of both RCDM and GCDM with good and average grass quality, show a low chance of failure ( $P_f < 0.001$ ). From all previous results, it can be stated that the RCDM dike will fail first in the locations inside the transition gap just after the bare soil locations despite the grass quality, as both average scouring depth and probabilities are significantly high ( $P_f > 0.5$ ).

For the model with poor grass quality all along the profile, three different potential failure zones are observed (Figure 4-15); one inside the ditch where grass cover was available before the storm, a second one on the vertex between the crest and the slope and a third one along the slope.

The results for this last configuration show that the probability of failure along the landward slope are almost identical for both RCDM and GCDM for the case of the largest storm. Yet for lower storms ( $q_m < 75$  L/s/m), the probability of failure in this part of the dike are always higher in the RCDM. It is also observed on STP25, that a sudden potential failure spot is created for storms with  $q_m$  larger than 50 L/s/m. It is described as sudden because the failure probability was less than 10% for lower storms with poor grass quality also. This can be explained due to the high turbulent flows expected in this location (see Figure 4-9). This feature makes the failure estimation more “volatile” with respect to the increase of  $q_m$ . This may be reaffirmed by the fact there is good grass cover thickness available in that same location. This same phenomenon becomes more evident for the assessment performed with the more realistic spatial grass quality distribution observed in the Millingen experiment explained in section 4.5.3 in which a sudden failure spot is observed in STP25 for a 100 L/s/m storm (see Figure 4-16).

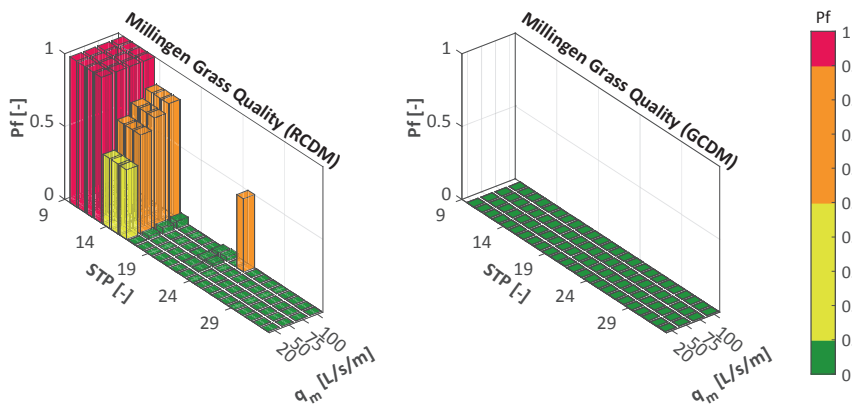


**Figure 4-16 Failure probabilities per storm in each STP for Millingen dike realistic grass qualities**

These results show that for the RCDM, there is a chance of failure higher than 50% for the largest storm in STP25. Based on all previous analysis, STP25 presented a high  $\bar{T}$  value and highly turbulent flow (Figure 4-9) combined with poor grass quality (Figure 4-10) and medium grass cover thickness ( $\varepsilon = 7.8$  cms). All of these characteristics indicate that STP25 represents a highly potential failure spot on the RCDM.

For the GCDM with variable grass quality, all estimated failure probabilities were close to zero. This result does not imply that the dike is 100% safe in this spots. It only means the failure probabilities are so small ( $P_f < 0.001$ ) with respect to the ones obtained in the other locations and therefore the 1000 Monte Carlo assessment is not enough to explore the tail of the distribution while ensuring the same standard error ( $> 3\%$ ). The spatially distributed failure probabilities become useful not only to determine the most prone to failure location but to prioritize the dike zone maintenance frequency.

## 4.6 Discussion

The literature states that dikes tend to fail more frequently on locations closer to the toe (Trung, 2014). This is expected as they represent a location with an abrupt slope change in which the flow will reach very velocities. In this study, the results showed that for the initial part of the landward slope in both models, higher scouring depths, and higher failure probabilities were obtained when a road is present. If this trend remained for the rest of the profile until the toe, it is expected that the presence of a road would also exacerbate the scouring process in the toe zone. Furthermore, the results show that the probability of failure when a road is present are always higher along the simulated dike section, with respect to the case where no road is present for all storms and grass qualities tested.

A remarkable characteristic of this method is that the values obtained in each location are conditional to the upstream and the downstream locations. This means that the turbulence effects are also captured in the emulators as they are trained based on the time series of the CFD models. These simple and yet powerful surrogates allow implementing probabilistic modelling by making the required simulations computationally feasible. Yet, the emulators will only include as many characteristics as the modeller is capable of including while being constraint by the chosen emulation technology. With that being said, it is also acknowledged that scouring is a highly time-dependent process which means that the dike profile changes in time and consequently the hydrodynamics change in time as well. In that sense the emulators built for this study become more uncertain for larger storms as the probability of significant change in the dike profile become larger. Still, the results of the present study are in good agreement with the scouring results obtained after the 50 L/s/m test in Millingen. Note that the resultant profiles are a function of the emulators which use a set of 1000 storms generated independently from the set of volumes used in the Millingen experiment and yet result in very similar scouring patterns with to one observed during the Millingen experiment. This proves that despite the fact that the profiles were not updated after

each wave scouring, the shear stress stochastic nature is fairly represented by the emulators.

In the present study and the one presented by Bomers et al. (2016), the influence of the road in the turbulent flow is characterized by two main features. The first one is the influence of a smoother surface (asphalt cover profile the road) which changes the hydrodynamics given the different superficial energy losses. The second is the generated turbulence and friction losses derived from abrupt changes in the bottom surface like for example the lateral transition gaps beside road.

From the hydrodynamic point of view, a smoother surface located over the crest of the dike increases the average probability of failure in the downstream locations as less energy is dissipated with respect to grass covered crest. Therefore, higher flow velocities are expected in the landward slope. For the case of abrupt irregularities such as the lateral transition gap, it is expected that a localized energy loss due to turbulence is generated in this zone. Yet, this same turbulence increases the probability of having higher scouring on this same location. Then, as energy was dissipated upstream, the probability of scouring on the downstream zones are reduced as well. This energy trade-off between crest and slope depends on the initial amount of available energy in the flow (wave volume), the surface roughness dissipation rate (road surface roughness) and the amount of energy transformed in terms of turbulence which is a function of the geometrical irregularities.

In terms of the grass quality, the results show that it is a very sensitive variable for determining the scouring patterns along the dike profile. From all tested grass quality configurations, it was observed that when a road is present, the scoured profiles always increase in depth as the grass quality decreases. Yet, the presence of a good grass quality makes the erosion depths almost negligible even for the strongest storm (100 L/s/m). When lower grass qualities are present, the road derived turbulent effects become more important and potential scouring depths become more significant along the crest, vertex and even in the lower part of the slope. Nevertheless, grass quality is also spatially distributed. Poor to average grass qualities were mostly obtained along the crest (Figure 4-10). This spatial variation could also be attributed to the deterioration effect due to the traffic along the crest of the dike. Hence, one can imply that having a road might deteriorate the nearby grass quality and therefore increase the probability of failure in these areas. Nevertheless, the results show that grass quality is not necessarily correlated to the available grass cover thickness which is another factor that determines the resistance to erosion. An example of this can be found for STP's 21 and 26 where  $\varepsilon$  is

greater than 0.10 meters for both locations and still the estimated grass qualities was good and poor.

For the failure probabilities, the grass quality has a more significant effect when a road is present. This is concluded from the failure probability obtained in the RCDM with realistic grass quality distribution where the failure probability is 51% with a poor grass quality in STP 25. For the same location in the model and tested in the same conditions, the failure probability is close to zero by just changing the grass quality to average. This is not the case when the road is not present as the failure probabilities for both grass qualities in the same location are both close to zero.

When including the variability in the spatial distribution of the grass quality along the profile, the resulting failure locations show that the safety assessment cannot be done solely from the hydrodynamic point of view as they differ to the ones expected by using highest  $\bar{T}$  values only. These spots are failing always despite the magnitude of the storm. Additionally, the RCDM realistic model also presents 61% probability of failing in the landward vertex (STP 25, Figure 4-16 Failure probabilities per storm in each STP for Millingen dike realistic grass qualities) during the most severe storm whereas the realistic GCDM has almost 0 chances of failing in this same location. This spatial variability can be attributed to the presence of a road, which explains the decay in the grass quality in the location just beside it. Note that, for the realistic condition (Millingen grass quality) poor grass quality is obtained just beside the bare soil zone just beside the road.

All previous explanations show why the road affects the failure probabilities. Yet, the most important question is by how much it affects them. In this aspect it can be observed that:

1. For the case where good grass quality is uniformly distributed along both dike conditions, the failure probabilities in the RCDM are always higher than the ones obtained in the GCDM. There is only one zone of potential failure in the RCDM. From this zone, the location which is most prone to fail is STP14 with failure probabilities that range between 0.21 for a 20 L/s/m to 0.73 for the 100 L/s/m storm.
2. For the average grass quality, the obtained failure probabilities for the RCDM are always higher in all locations with respect to the ones obtained for the GCDM. For the RCD, three different failure prone zones ( $P_f > 0.1$ ) are identified. The most prone failure zone is located inside the transition gap, in which failure probabilities range between 0.47 and 0.82. For the GCDM, the

most failure prone location corresponds to the landward slope with failure probabilities ranging between 0.006 and 0.17.

3. For the poor grass cover condition, the RCDM presents high probability ( $P_f > 0.5$ ) of failing in three different zones. In the first zone which corresponds to the transition gap, the failure probabilities range between 0.48 and 0.82 whereas for the GCDM are less than 0.01. For the vertex zone, the failure probabilities of the RCDM range between 0.005 and 0.81 whereas the GCDM present failure probabilities which are less than 0.01. For the last to zone both RCDM and GCDM present failure prone zones. For the RCDM, the failure probabilities range between 0.008 and 0.81. The same range is found for the GCDM but in a smaller zone of influence. Based on the maximum values it can be stated that the probability of failure are similar for both conditions for large storms but the RCDM will present more failure prone locations.
4. For the models in which a more realistic grass quality spatial variation is taken into account, is observed that the probability of failure of the RCDM model are always higher and much more significant when compared to the ones obtained in the GCDM. This is explained due to the fact that the worst grass quality is located on the crest for both models but for the RCDM the turbulence effects are milder. This is also reflected in the failure probabilities of the transition gap zone in which the RCDM presents failure probabilities that range between 0.47 and 0.80 whereas for the GCDM the failure probabilities are less than 0.001.

These results become even more relevant for the case of dike concepts such as the unreachable dike and the multi-functional flood defence which are conceived to withstand even more extreme conditions in order to cope with climate change (Van Loon-Steensma and Vellinga, 2014)).

## 4.7 Conclusions

This study shows that for the Millingen dike, the presence of a road reduces the safety margins with respect to a dike with no road on top. Using a novel emulation method, we were able to assess the spatially distributed probability of failure of a dike with and without a road. Based on the results of the present study, the answer to the three main research questions are:

1. Surface roughness and profile irregularities represent a change in the amount of turbulence in the flow. Yet the former one represents a less uncertain gradual change (either increase or decrease depending on the surface) in turbulence whereas the latter one represents a sudden and highly uncertain change in the amount of turbulence. Hence, it is expected that localized irregularities have a higher probability of scouring if no dike cover resistance information was included in the analysis. Additionally, the presence of a smoother surface over the crest such as asphalt also increases the probability of scouring along the slope as less energy is dissipated during the overtopping process when compared to a dike covered in a rougher surface such as grass.
2. Grass cover quality is a spatially distributed variable and therefore the probability of failure of the dike is spatially distributed as well. The results for grass quality are in agreement with the ones observed in the field and also with the recommended values in the literature for the erodability coefficients. Nevertheless, the failure probability is not only dependent on the grass quality but also the available grass thickness. With these two considerations in mind, it is expected that the presence of a road diminishes both grass quality and grass cover thickness in the adjacent zones next to the asphalt cover. Hence, the probability of failing first on these “weak spots” is higher when compared to other locations along the profile. In addition, good grass quality must be ensured when a road is present to achieve the same failure probabilities in the vertex and along the crest. This means that maintenance is essential for dikes that have a road on top.
3. The dike with a road is always less safe than a dike without a road in relation to wave overtopping grass cover erosion failure. Especially, in the zones where higher initial deterioration is observed such as the immediate locations next to the road. The probability of failure of these locations is significantly higher with respect to the rest of the dike as they tend to have less grass cover available.

For locations close to the landward vertex, the failure probabilities are also significantly higher when roads are present as asphalt is a smoother surface which dissipates less energy and the vertex represent an abrupt bottom slope change. For the case of the landward slope location, the probability of failure when a road is present are also higher with respect to the dike without a road as less energy has been dissipated over the asphalt cover on the crest which results in higher flow velocities in the former case. However, if good grass quality is present as for the Millingen dike, both failure probabilities differ but remain lower than 1%.

## **4.8 Acknowledgements**

This research is supported by the Dutch Technology Foundation STW, which is part of the Netherlands Organization for Scientific Research (NWO), and which is partly funded by the Ministry of Economic Affairs. The authors would like to thank STW foundation, Dr. Jan Ribberink from Twente Univeristy, Gosse-Jan Steendam from INFRAM, Andre van Hoven from Deltares and Dr. Jentsje Van der Meer from Van der Meer Consulting B.V. for providing the data, and the Integral and sustainable design of Multi-functional flood defences program for the help and support.

# Chapter 5

## Discussion

Chapters 2, 3, and 4 allowed to determine qualitatively and quantitatively, the derived effects in the failure probability of the two selected erosion-based failure mechanisms from three different design choices. Nevertheless, other aspects of these studies such as their applicability and the implication of the assumptions taken for building the models are further discussed in the present chapter. As a final analysis, this chapter includes the analysis of the change in safety due to the most realistic choices estimated in Chapters 2, 3, and 4. The analysis is also performed via a simplified fault tree analysis in order to make the choices comparable in terms of component level safety.

### **5.1 Applicability of correlation modelling for piping erosion MFFD design (Chapter 2)**

One of the most efficient countermeasures for increasing the flood defence reliability in terms of piping erosion is to increase the potential seepage length. This is one of the most important concepts for developing flood defence concepts such as the Delta dike, the Unbreachable dike, the Robust dike or the MFFD's (Silva and Van Velzen, 2008; Van Loon-Steensma and Vellinga, 2014). In Chapter 3, the influence of correlation in the safety assessment of a conventional flood defence was shown. Yet, it is also important to prove by how much this design choice affects the dimensioning of an MFFD during the design stage. A numerical fictitious case was investigated in the study of Aguilar-López et al. (2015), in order to determine the implication of correlation between  $K$  and  $d_{70}$  in the pre-dimensioning of the MFFD for achieving different safety targets. The seepage design length was estimated to determine the available space inside a future MFFD for a certain target safety value and consequently the allowable size of future functions.

**Example case:** A hypothetical MFFD is going to be designed for a flood defence cross section of the ring 16 located below the Utrecht Province. The statistical distributions of the soil parameters (Table 5-1) are assumed equal to the ones used in the VNK study (VNK2 et al., 2014) for dike ring 16 in a location where a strengthening measure against piping was recommended.

**Table 5-1 Stochastic Soil properties of hypothetical case (C.V. stands for coefficient of variation)**

Var.	Unit	Dist. Type	Mean	C.V.
$\eta$	[-]	Constant	0.25	-
$\gamma_{\text{sand}}$	[N/m <sup>3</sup> ]	Normal	26.5	1%
$\gamma_w$	[N/m <sup>3</sup> ]	Constant	9.81	-
$\theta$	[deg.]	Constant	37	-
$d_{70}$	[m]	Log-normal	3.33e-4	15%
$d_{70m}$	[m]	Constant	2.08e-4	-
$K$	[m/s]	Log-normal	3.00e-4	100%
$D$	[m]	Log-normal	65	10%
$mp$	[-]	Log-normal	1	12%
$L^*$	[m]	Log-normal	70+ $\Delta$	10%
$H^{**}$	[m]	Gumbel	a=4.357 b=0.288	
$h_b$	[m]	Normal	0.5	10%
$d$	[m]	Log-normal	7.5	30%

\* $\Delta$  is equivalent to steps of 10 meter variation in until a final width of 250 meters.

\*\*Obtained values from the fitting are estimated as annual maximum

Based on the results obtained in section 2.5, a Clayton Copula is assumed for the correlation modelling as it was shown to represent the relation between  $d_{70}$  and  $K$  better than the other two Copula functions tested. Different MFFD designs (required seepage lengths, see Figure 2-1) are assessed for different degrees of correlation between  $K$  and  $d_{70}$ . This will allow to obtain design curves in which the target safety is estimated as a function of the degree of correlation and the design seepage length.

For the present example, the Unbreachable dike safety level proposed by Silva and Van Velzen (2008) is taken as the required target reliability for MFFD's as there is no guidelines that allow to define the target safety values for MFFD's at the moment. The Unbreachable dike concept defines that the required safety level of "The dike of the future" should be at least 100 times smaller than the required annual target failure probability of a traditional Dutch flood defence. Note that this required value is defined for the total aggregated failure probability of the whole defence. This means that it includes the combined effect of uplift/piping with other failure mechanisms that can be triggered during a flood event and in different representative cross sections.

It is also assumed that the occurrence of other failure mechanisms (e.g. overtopping or slope stability) are independent of each other and that the whole defence has the same representative cross section. In the old Dutch safety standards where each ring was supposed to have the same target failure probability (see section 1.3.5), the dike ring 16 was required to have a total failure probability of  $5E-4$  1/year.

The results from the VNK project safety assessment for the Dike ring 16, showed that 79.4% of the total estimated failure probability of this ring could be attributed solely to the uplift/piping failure mechanisms in this particular ring. Therefore, the minimum annual estimated reliability index for uplift/piping would be:

- **MFFD-VNK:**  $(5e-4 \cdot 0.794) / 100 = 3.97E-6$  or  $\beta = 4.467$

According to the new Dutch flood risk legislation (WBI-2017, 2015), the percentage of the maximum allowable contribution from the uplift/piping mechanism to the system's overall probability of failure is 24% (see Table 1-1). This allows calculating the target safety for MFFD flood defences as:

- **MFFD-TARGET:**  $(5e-4 \cdot 0.24) / 100 = 1.2E-6$  or  $\beta = 4.72$

Based on the Sellmeijer revised limit state equation, the MFFD design results obtained for the different degrees of correlation are presented in Figure 5-1.

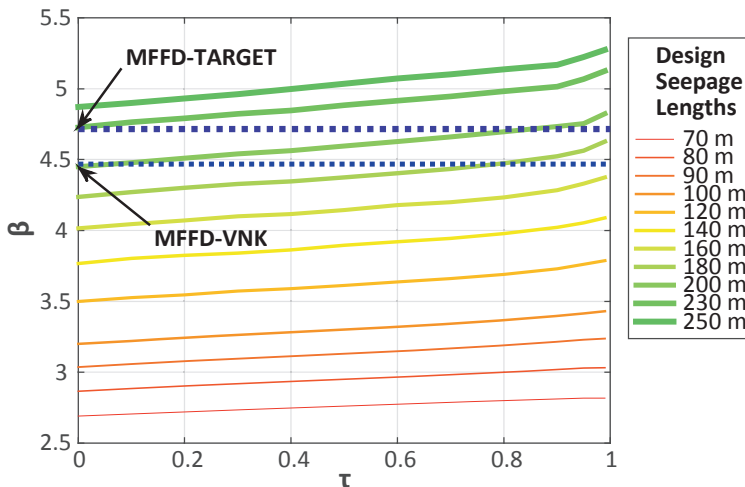


Figure 5-1  $\beta$  indexes of different designs for varying correlation degrees ( $\tau$ )

The horizontal purple dashed lines corresponds to the required target safety values based on the results of the VNK project and the maximum allowable failure probability Dutch guidelines. If a similar correlation degree as the one estimated for the Lekdijk

MFFD ( $\tau = 0.692$  - section 2.4, dashed brown line on Figure 5-1) was assumed for the hypothetical MFFD, approximately 180 meters of width would be required in order to cope with the target reliability index estimated from the VNK project results ( $\beta = 4.467$ ). When assumed uncorrelated ( $\tau = 0$ ), a 200 width MMFD will be required instead for the same target reliability.

Note that the slope of each design seepage length function becomes steeper for wider defences. This effect makes correlation inclusion even more important for the design defences with higher target reliability indexes such as massive MFFD's like the Arakawa river (see section 1.1). For a future MFFD for which the contribution to the total failure is required to be even lower (24%) than the one obtained in the VNK (79.4%), the required design widths are even larger. When assuming the variables fully uncorrelated, the flood defence will require a minimum width of 230 meters. If the two main variables are correlated to a similar degree to the one found in Chapter 2 ( $\tau = 0.692$ ) it will only require approximately 200 meters.

Such a difference in a longitudinal structure such as a flood defence has a large effect in its financial feasibility. From these results, it is intuited that robust soil investigation may be much cheaper in comparison with the cost of the over dimensioning error that one may incur when assuming the variables completely uncorrelated. However, the assumption of the variables to be uncorrelated is derived from the fact that the  $d_{70}$  distribution must only represent the uncertainty distribution associated with the most superficial part of the aquifer while the K value is representative of the whole aquifer. While this assumption is correct, there are other considerations like the geological profile of the foundation, the soil deposition process and the localized permeability effect in the upper aquifer which may show that this assumption is not always true. While correlation may not always have the same amount of importance in all cases, it is recommended to at least make a sensitivity analysis of its potential effects on the structural reliability so that its proper investigation may result in more cost effective MFFD designs and more accurate assessments. The results obtained in Chapter 2 like the Clayton copula choice and the correlation values can be easily implemented during the design stage for determining if more robust soil investigation is needed.

## 5.2 Applicability of the fictitious permeability method (Chapter 3)

The limit state concept based on the fictitious permeability modelling approach presented in Chapter 3 is bounded by the following 5 main assumptions:

1. The process can be modelled in 2DV.
2. The flow inside the erosion channel is laminar (Poiseuille flow).
3. The erosion channel has progressed already until the middle of the flood defence.
4. The aquifer is confined (built on an impermeable basin).
5. The model is valid for probabilistic assessment.

Each of these assumptions is influenced by the inclusion of structures embedded underneath the flood defence. The implications with respect to the model and probabilistic assessment are further explained as follows:

1. The process can be modelled in 2DV: Piping erosion is a three dimensional problem which is often modelled in two dimensions (Van Beek, 2015). The main implication of this assumption is that the water flow that contributes to the sediment transport inside the 3D erosion channel is larger than the one estimated in a 2DV condition. This is due to the additional contribution from the side wall of the channel in terms of flow. Hence, larger pressure gradients are exerted inside the erosion channel than the ones estimated from the 2DV approach. This was acknowledged by Vandenboer et al. (2014a) who also recognized that piping erosion meandering patterns increased with respect to the experimental model width, which shows that this process should be represented as three dimensional. Following the same line of reasoning, the inclusion of embedded structures may reduce the pressure gradients even more than what was estimated in chapter 3 due to their extension and orientation with respect to the erosion channel. Nevertheless, these effects are included by calibrating the equivalent erosion channel size so that an equivalent pressure gradient is achieved. In this study, a recommended circular shaped channel size with an equivalent diameter of 8.2 times the  $d_{70}$  grain size is proven to be a good initial choice which is also in agreement with the experimental findings.

2. The flow inside the erosion channel is laminar (Poiseuille flow): The pressure line inside the erosion channel may be represented as a straight line as the Sellmeijer model assumes a laminar flow regime inside the erosion channel. Hence, the pressure gradient inside the equivalent erosion channel is assumed to be constant all along its length. Additional pressure losses are originated due to the inclusion of an embedded structure, which will affect this pressure gradient as a function of the embedment position and size. Such effects are not represented in the original Sellmeijer limit state equation unless the hydraulic conductivity representative value is modified. This modification may even increase the uncertainty of the estimation derived from the Sellmeijer limit state equation. With the methodology presented in Chapter 3, such effects are already included in the original FEM model results and consequently in the emulators training data set. In addition, it is possible to determine if the equivalent flow velocities inside the erosion channel corresponds to the laminar regime which makes it an even more robust method for assessing if the model is implemented in a feasible range of pressure gradients. This check was not performed in Chapter 3 as the validation was performed against the obtained failure probability from Sellmeijer's modified equation.
  
3. The erosion channel has progressed already until the middle of the flood defence: The Sellmeijer limit state concept assumes that the critical point in which erosion will continue is located most of the time in a longitudinal position which is equivalent to half of the potential seepage length of the flood defence for aquifers of infinite depth (Sellmeijer, 1988). Given the 3 meter depth of the Ijkdijk foundation aquifer, this assumption may not be applicable. However, the present study aims to determine the failure probability of the system conditioned to a critical head value. In our case, the head value is set equal to the one observed during the real scale experiment (2.1 meters). Afterwards, the erosion channel size is determined so that the two forces limit equilibrium is satisfied while imposing the critical head boundary conditions. This ensures that the critical pressure gradient inside the erosion channel is estimated correctly. The ideal situation will have been that every single stochastic run would have been coupled with an iterative routine so that the correct erosion channel size was found for each head. In that way not only the failure probability would have been correctly estimated but also the probability of other potential critical heads. In the end this would have resulted in two exact probability density functions instead of one skewed as shown in Figure 3-10.

The method presented in this thesis maintained this limit state definition so that the results obtained while including the embedments remain comparable with the case in which no structural embedment was present. With the present methodology, it can be determined if the pressure loss induced by the embedded structure reduces the probability of the erosion channel to progress for any predefined erosion channel length. This is not possible to achieve with the actual Sellmeijer limit state equation as this equation is calibrated for erosion propagation of a channel with the tip located in the exact middle of the estimated seepage length. With this in mind, we also acknowledge that the Sellmeijer numerical solution will also allow to determine the critical erosion length.

4. The aquifer is confined (built on an impermeable basin): The case study that was modelled in the Chapter 3 represents the original conditions of the IJkdijk piping erosion experiment. This experiment was founded inside a geotextile covered basin which made it impermeable. In real situations, this is not always the case as aquifers may also be significantly deeper and unconfined. Yet, the results presented in Chapter 3 (see Figure 3-7) show that the aquifer depth is only important for erosion progression until a threshold which is determined by the hydraulic conductivity of the aquifer. It is expected that the influence of the structural embedment is also determined by this threshold. This means that with the method presented in Chapter 3, it is also possible to define a safety depth threshold disregarding the structural embedment size. If the aquifer is confined by an impermeable layer which defines an aquifer depth smaller than the threshold, the effects may be greater than if embedded in shallower areas depending on the size of the embedment. These effects cannot be captured by the limit state equation which proves the importance of assessing the embedment effects with higher detailed models.
5. The model is valid for probabilistic assessment: In the present study, it was possible to validate the failure probability if no embedment was included. For the embedment case, it was not possible as this structure's effects cannot be included in any of the Sellmeijer limit state equations. However, it was observed that the failure probability value estimated by the Sellmeijer modified limit state two forces equation (Appendix A.5) is almost identical to the one predicted with the fictitious permeability method (Figure 3-10), but significantly different from the one estimated from the revised (re-calibrated) version used in Chapter 2. Note that there are three different Sellmeijer limit state equation versions; the original 4

forces, the modified (two forces) and the revised (also two forces but corrected see Sellmeijer et al. (2011)). The difference between the two last versions is that the revised was recalibrated by including additional factors which relate the  $d_{70m}$  reference values used in the experimental setup with the  $d_{70}$  value used for the assessment. In addition, this factor is powered to a 0.4 exponent which resulted from a multivariate analysis. It is acknowledged by the authors of this adaptation (Sellmeijer et al., 2011), that the origin of the exponent has no physical foundation and that it is recommended to use this latter version within a recommended range of grain sizes. This warning is often disregarded in reliability studies that use this version. This is not a problem for the method presented in this thesis as the FEM model is fully derived based on the physical representation of the problem.

From these observations it can be recommended that:

- a) The revised Sellmeijer equation implementation for safety the assessment may be improved by the use of truncated stochastic probabilistic distributions or at least a previous filtering of the results of the variable random sampled tail values. This will ensure that the equation is used for the correct ranges of applicability. To our knowledge it is not clear if this procedure is done in the actual safety assessments. The use of truncated water level fitting and sampling has not been found in literature or tested in this study and it is expected to be a good explanation of the difference between field, experimental and modelling probabilistic performance.
- b) Both original and modified Sellmeijer limit state equations were obtained by curve fitting procedures. For the original version, a remarkable 3% accuracy was achieved as stated in the original work of Sellmeijer (Sellmeijer, 1988). However, this performance is also required for defining the threshold values of  $F_G$ ,  $F_S$  and  $F_R$  of the newer 2 forces limit state equation. At the moment it is still unclear for us what are these thresholds for the two forces revised version as no literature could be found about this matter. If these studies exist, it is also important to know what is the performance of the equation for inputs which result in  $F_G$ ,  $F_S$ , and  $F_R$  values located outside these bounds. Particularly for the implementation of this latest Sellmeijer version in the future Dutch probabilistic safety assessments. These required bounds are obtained by comparing the results of the original Sellmeijer numerical model (e.g. MSeep software) with respect to the obtained values from the fitted limit state function for the same inputs. In a later stage, these values were validated with

experimental data (see, Van Beek (2015)). Hence it can be assumed that the fictitious permeability method presented in this thesis is also applicable for probabilistic assessments in wider ranges as no curve fitting was included. One can argue that emulation is a fitting method as well but note that the performance of these methods and especially neural network technologies have proven to be significantly more powerful than curve fitting. This is acknowledged by Sellmeijer himself (Sellmeijer, 2006). Nevertheless, it is evident that the method presented in this thesis still lacks from the experimental validation. Yet, this can also be done with the same data collected and presented in the work of Van Beek (2015) plus additional experiments that include structural embedments.

- c) If the computational burden associated with the complete Sellmeijer numerical model represents the major constraint for deriving new curve fittings that may include the effects of structural embedments, the present method may overcome this obstacle with the implementation of the emulators. In particular for artificial neural network based models which are capable of capturing highly non-linear processes with high accuracy. Their potential for estimating piping erosion progression was already acknowledged and tested by Sellmeijer himself (Sellmeijer, 2006).

As a final remark, it is also acknowledged that any increase of inflow inside the aquifer may also increase the probability of piping erosion failure to occur (or any slope stability type of failure). This might be the case in which an embedded sewer or water supply pipe is broken due to excessive tensile stresses triggered by a flood event. In that case, the conditional probability of piping erosion due to a pipe leakage should be reflected in the failure scenario represented in the fault tree of the flood defence. Note that this case represents how the reliability of the additional structure affects the whole component reliability. This is out of the scope of this thesis which aimed to investigate how the presence embedded structures affect the likelihood of the physical processes involved in a certain failure mechanism.

## 5.3 Applicability of the shear stress excess method (Chapter 4)

The applicability of the limit state concept based on the shear stress excess concept for estimating the safety of grass cover against wave overtopping of MFDD's is based on the following 5 main assumptions:

1. The process can be modelled in 2DV
2. Overtopped wave volumes are represented by a Weibull distribution.
3. Water depth and velocity time series are representative.
4.  $C_E$  are functions instead of constants
5. The model is valid for probabilistic assessment.

Each of these assumptions is influenced by the inclusion of structures founded over the crest of the flood defence. The implications of the model and probabilistic assessment are further explained as follows:

1. The process can be modelled in 2DV: the erosion process is related to two dimensional superficial stresses which may be assessed by a unitary width approach without having a major repercussion in the scouring depth. This type of approach has proven to relate well with experimental measurements for processes in which one dimension of the domain is significantly greater than the expected flow depths such as rivers and channels. It is also expected that flood defences with roads on top have representative cross sections of long segments of flood defence in which an additional dimension will not add more information to the scouring process. In this sense, it is expected that three dimensional effects are not necessarily essential. Still, the study of Oaks et al. (2011) suggests that there is no sufficient knowledge of the derived effects on failure due to wave overtopping from a three dimensional perspective over the flood defence transitions. For a road over the defence, the most immediate transition which may require a 3D assessment is the access ramp that derives from the road at one or both sides of the flood defences. These locations represent high uncertainty scoring points given the combination of structural embedment and three dimensional derived hydrodynamic effects (see (Oaks et al., 2011)). In this case, the appropriate 3D representation of the hydrodynamics is recommended for accurately modelling the process for scouring in this complex transitional locations.

2. Overtopped wave volumes are represented by a Weibull distribution: Wave overtopping is the subsequent process after wave run-up. This means that the wave overtopping is conditional to the wave-run up process (Pullen et al., 2007). From a probabilistic point of view, the wave overtopping process corresponds to low frequency events of the wave run-up distribution which are composed of “un-broken” waves which may rise until the upper boundary of the flood defence. For deep water conditions, these wave heights are often assumed to follow a Rayleigh type of stochastic distribution (Van der Meer, 2002). For shallow water conditions, the wave height distributions on shallow foreshores do not follow such a distribution due to the limited depth and distance for wave breaking. Based on this condition, Battjes and Groenendijk (2000) proposed a Weibull composite distribution which can be fitted as a function of the local wave height distribution, bottom slope and total wave energy. For the particular case of individual wave volumes probabilistic distribution fitting, the studies of Van der Meer and Janssen (1994), Hughes and Nadal (2009), Victor et al. (2012) and Pan et al. (2015) included the flood defence geometry and crest freeboard in the estimation of the fitting parameters for the Weibull distribution of the overtopped volumes. In the present study, it was not studied the derived effects from the inclusion of an additional structure located in the riverside slope which may also influence the likelihood of other failure mechanisms. Yet, the inclusion of such a structure in this location will certainly have a direct impact on the estimated values of the Weibull wave overtopping distribution. A first approximation to the problem may be tackled by using the average slope, berm and element roughness factors included in the report of Van der Meer (2002). Still, it is unclear if a larger and more complex structure such as a pipe, a road or a structure founded over the riverside slope may be represented with these tools. For a simpler case as the one presented in in Chapter 4, the assumption of a Weibull distribution for the overtopped single volume remains valid as no additional structure besides the road is included in the flood defence. Then, the main source of uncertainty for this assumption is related to the boundary conditions represented by the significant wave height and wave peak period. The wave overtopping simulator experiments (and the numerical experiments presented in chapter 4) are performed based on volume release lists which are fitted based on the expected significant wave height and peak period of an average riverine flood defence ( $H_m=1$  m.,  $T_m=4$  s., (Van der Meer et al., 2010; Hoffmans, 2015)). In case the distribution fitting is changed but is still related to the stochastic nature of the

volumes that already overtopped the flood defence, the method presented in this thesis remains applicable as the shear stress excess is estimated by wave independently from the overtopping distribution.

3. Water depth and velocity time series are representative: The present methodology assumes that the simulated volumes that exit the WOS are representative of the real conditions of a wave that overtops the flood defence. This was first checked in a qualitative way by comparing the shapes of the resulting velocity and water depth time series with the study of Hughes and Nadal (2009). Based on their results it was observed that velocity profiles are characterized by initial sharp peaks whereas flow depths present a round shape around the peak area. This behaviour was also noted in the results of the simulations used for the time series validation presented in appendix A.3. In addition, the maximum peak values and overtopping times were also checked based on the measured values during the Millingen experiment. From all validations, it is concluded that both hydrodynamic expected behaviour and numerical values are in good agreement while capturing the effects of the embedded structure. The inclusion of other structures in the model such as barriers or drains may have different results which are cumbersome to validate. Nevertheless, it is acknowledged that for implementing the method presented in this research, the simulation of the wave overtopping simulator may be replaced by a cosine defined boundary condition which may reduce the calculation costs significantly.
4.  $C_E$  are functions instead of constants: Based on measured values, most of the literature recommends the erodability proportional factors (Eq. 4-2) instead of functions of the critical shear stress as shown in Figure 4-10. However, the present study assumes that the value of the erosional rate strength coefficient  $C_E$  which is a characteristic of the grass cover must change when the critical shear stress threshold changes  $\tau_c$ . The reason for this assumption based on the fact that the high values of  $\tau_c$  which define the start of erosion of the grass cover may only be surpassed by high values of exerted surface tension. This values are directly related to high flow velocities. The increase in velocity must also increase the mass erosion transport rate of the soil. This is not possible to include in the scouring model if the  $C_E$  values remain constant and independent of the  $\tau_c$ . In addition, the  $C_E$  coefficient is defined as the ratio between the soil mass transport coefficient  $M_p$  and the critical shear stress threshold  $\tau_c$ .

However it is also acknowledged that the curves presented in Chapter 4 in Figure 4-10, present values of  $\tau_c$  for grass qualities that will never be achieved. The reason for this is that these curves were used for the stochastic grass quality modelling which required extrapolation of the  $C_E$  for the  $\tau_c$  random variable. Hence, it is recommended to investigate the use of truncated stochastic distributions so that this extrapolated values are not sampled during the Monte Carlo simulations.

5. The model is valid for probabilistic assessment: The main weakness of the method presented in this research for probabilistic assessment is that the emulators are trained based on shear stress excess values estimated from the initial bottom profile of the modelled flood defences. In reality, the bottom profile is evolving due to the erosion generated wave after wave and slowly drifting. When embedded structures are present, this effect becomes even more significant as they are often built with materials which are expected to be more resistant than grass or soil, e.g. concrete, metal or polymers. As these materials erode much slower, the error is not evenly distributed resulting in an overestimation of the erosion depths or in erroneous weak spot estimation. Yet, the results of the 100L /s/m simulation were compared to the obtained results for the Millingen experiments and it was concluded that the error was not significant. Hence, it is expected that the profile updating will only become an important issue for low grass quality cover defences exposed to large storms. As a final remark, the study for estimating the influence factors of the hydraulic cumulative load method presented by Hoffmans (2015) for assessing flood defences with non-water retaining objects resulted in similar orders of magnitude. This means that the present method may be useful to further study and improve the hydraulic cumulative load method based on numerical simulations instead of using the wave overtopping simulator only.

## 5.4 Effects derived from other structural embedments

Based on the location considerations, the case of the influence of a building in the inner slope stability failure mechanism will complete the set of most feasible MFFD's found in the actual Dutch landscape. In the actual Dutch assessment guidelines, the embedment of buildings and other structures in the flood defences have qualitative assessment guidelines which evaluate the influence in the safety of the flood defences depending on characteristics such as the dimensions, foundation depth and the state of

the structure among others (VTV2006, 2007). These methods result in approval of disapproval and required measures for improving the flood defence safety but none of them allow to determine the probability of failure of the representative cross section.

The case of inner slope stability with a house embedment is studied by Ilieş et al. (2015) who showed that the structural embedment may increase the slope stability safety also based on limit equilibrium methods. For the specific case of slope stability of flood defences, a first attempt to quantify the derived effects in the reliability from a building embedment was done by Jongerius (2016). In his MSc research, he aimed to estimate the failure probability conditioned to the collapse of the embedded structure. His results showed that the resultant  $\beta$  indexes from the combined collapse of dike and structure are significantly higher with respect to the probability of collapse of the same flood defence without an embedded building. This is in dis-agreement with the conclusions of Ilieş et al. (2015) as he shows that structural embedment can also have a beneficial effect due to the loading reduction of the soil slope. Nevertheless, the chosen simulation models (Bishop limit equilibrium) of both studies might not be robust enough for estimating the effects derived from the phreatic line abutment or the inner contact lateral forces. For conventional flood defences, the work of Melnikova et al. (2015) concluded that the safety factors obtained from simplified assumptions of the inner pore pressure distributions assumed in limit equilibrium methods may result in safety overestimations of 22% and above with respect to finite element methods safety assessment. Furthermore, finite element models are capable of determining the deformations in the system without any assumption about the failure surface or interslice forces (Griffiths and Lane, 1999). This becomes an important characteristic for combined structures (soil and masonry) as their effect in the failure surface is not correctly represented in the limit equilibrium methods. Limit equilibrium models are developed as a representation of an elastoplastic type of failure whereas buildings are often constructed with elasto-brittle types of materials. Hence, the limit state of this kind of structures is better defined in terms of displacement instead of the safety factors of the limit equilibrium method. Nevertheless, it is expected that the failure probabilities of this kind of systems are very low for the case of slope stability as buildings are often founded in the passive zone of the slip surface which increases the resistance to rotational displacements.

For the case of the trees, the most immediate failure could be derived from the inner slope stability. During storms, trees exert significant torsional forces in their roots due to wind currents. These torsional moments affect the forces equilibrium when trees are founded inside the dike slopes or crest. Studies which are not specifically related to

flood defences but study the effects of roots in the stabilization of soil slopes have shown that the additional tensile resistance due to the root intrusion may increase the safety factor against slope stability (Nakamura et al., 2007). The study by Zanetti et al. (2011) acknowledged the importance of preserving the trees alive when present as in the case in which the roots decompose, they may originate seepage passages for piping erosion and loss of bearing capacity. Other studies have stated that the erosive rates around objects like trees tend to differ in unknown ways making their location potential weak spots for the flood defences (Steendam et al., 2014; Hoffmans et al., 2015).

Studies for assessing the effects on the slope stability safety derived from structural embedments for non-flood defence case studies are presented by (Paul and Kumar, 1997; Roy and Mandal, 2009; Ilieş et al., 2015). The results are useful for extrapolating a general conclusion but the main effects exerted by the flood defences like the phreatic level abutment and the lack of a robust foundation require a deeper analysis. For the particular case of embedded buildings in flood defences, Jongerius (2016) proposed in his Master's research an interesting reliability method in which limit equilibrium methods are coupled with mechanical properties of masonry elements for defining the boundary conditions of a slope stability model. This approach is implemented in a Bayesian probabilistic method in order to estimate the failure likelihood of the flood defence. The results show that the failure probability of the flood defence is increased when the building is present. Nevertheless, the Bishop modelling choice of both studies and the obtained failure probability values of the later one are doubtful.

For the case of pipelines and cables, the inner slope stability and the piping erosion failure mechanisms are the most influenced by their embedment. Safety zones in the cross-sectional profile are defined based on the expected influence they might have in the different failure mechanisms (Hoffmans and Knoeff, 2012). For slope stability failure in particular, the MSc. research of Groot (2015) showed that the location and size of pipelines inside the flood defences may have either beneficial or disadvantageous effects. Still the effects of contact between soil and pipe in the soil resistance and the fluctuation of the soil saturation inside the flood defence are recommended for further improving this study. For the specific case of reliability assessment of pipelines, Sanders and Wiggers (2015) presented a semi-probabilistic method in which the influence on failure during a flood event due to a pipeline rupture may induce an eventual dike breach. The main drawback of the method is that it assumes that the probability of the pipeline failure is independent of the effects of the water level fluctuation. This assumption may result in an underestimation of the rupture probability itself as during

flood events, the embed structures exert an additional buoyancy effect due to the groundwater change which is considered one of the most important effects for pipeline safety (Zangenehmadar and Moselhi, 2016).

As presented in this thesis, the largest contribution to failure is expected from failure mechanisms which involve erosive processes. With this in mind, it is expected that the presence of light poles, staircases, access ramps and any other non water retaining objects will also increase the probability of localized erosion spots and seepage paths due to increase in turbulence around these objects. The emulation approach and erosion estimation presented in this thesis for both piping erosion and wave overtopping may be a good starting point for developing an assessment method for these small structures.

## **5.5 Applicability of emulation techniques for safety assessments**

The study of Gomes and Awruch (2004) showed that reliability assessments in level III with neural networks are capable of achieving comparable levels of accuracy with a crude Monte Carlo assessment based on the original models. They also require less runs for generating the training sets compared to the required number of runs required during the iteration process of a FORM or SORM implementation of the same model. From this thesis, it may also be added that the neural network emulation will also allow assessing different scenarios without retraining the models again if the generalization and extrapolation capacity of the emulators is tested beforehand. This is a very helpful approach for systems with numerous cross sections.

All along the present thesis it has been shown how emulation techniques allow implementing level III reliability methods for structural failure estimation of MFFD's. Nevertheless, emulation remains an approximation of the multivariate joint distribution and consequently, it can be argued that such method should be classified as a level II method. Reliability methods are only concerned about the way of estimating the structural safety indistinctly from the models used for generating the multivariate distributions. For example, a level II method can be implemented based on a simple equation or a complex finite element model. The emulation methods presented in this thesis were performed for the models related to the load term only (e.g. pressure inside the erosion channel of Chapter 3 and wave induced shear stress of Chapter 4) and no approximations of the limit state function were required. Furthermore, the models for estimating the resistance remained unmodified and no transformation of the input variables or assumptions about the limit state functions were needed. Moreover, the

failure probability is estimated via Monte Carlo until a low standard error is achieved which shows that the actual method can be considered as a level III assessment.

## **5.6 MFFD's safety assessment in an international context**

The present thesis is mostly framed in a Dutch context as robust and extensive research and policy is available for design and assessment of conventional flood defences. Moreover, target safety values are included in the national legislation which allows estimating to ensure that a design or an existent structure aligns with the required national safety standards. For other countries like the U.K. and the U.S., governments have already started to improve their safety systems based on structural reliability and cost-benefit optimizations approaches. In a more advance situation, Japan has already implemented a couple of massive MFFDs inside the flood defence system of the city of Tokyo. Nevertheless, this is not an international common scenario in which flood defence systems with structural embedments are present in all low lying countries in which urban and rural developments are threatened by flooding events.

The methods presented in this thesis are applicable in any international context in which the structural reliability needs to be assessed. In addition, they also allow to include recommended values such as the ones of the EUROCODE or any other as their development was fully based on the conceptualization of the failure mechanisms. For the European context, the structural codes such as the EUROCODE include information about the recommended values for geotechnical variable uncertainties and model choices based on the reliability assessment method associated level. This information allows to design safe structures in a probabilistic way despite the fact that no legislative target safety values may be elaborated for a certain country.

## **5.7 Quantification of the effect of the design choices in the MFFD safety**

In order to quantify the effects of the different design choices on the flood defence reliability, the resultant  $\beta$  indexes by section are calculated. Based on the failure budget target safety values presented in Table 1-1 (WBI-2017, 2015), a simplified fault tree is proposed as shown in Figure 5-2 for evaluating the total safety in a component level (dike section).

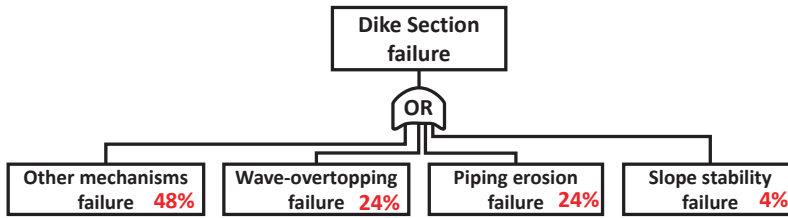


Figure 5-2 Fault tree with allocated failure budgets

For each analysis presented in Chapters 2, 3 and 4, a failure probability was estimated for only one specific failure mechanism affected by a certain design choice. This value represents the probability of failing by one specific failure mechanism disregarding any other failure mechanism. However, the complete assessment is done by assessing all other possible failure mechanisms. For this reason, it is assumed that for the remaining failure mechanisms included in the proposed fault tree, their failure probabilities are equal to their maximum allowable failure target value. In other words, they are assumed to be equal to their corresponding percentage (see Figure 5-2) of the predefined maximum allowable failure probability per section (WBI-2017, 2015). In this manner it is possible to estimate the total failure probability in each case while considering all possible mechanisms. This allows to compare the effects of the structural inclusion in terms of the total safety value.

Note that, the proposed fault tree is defined by a single “or” gate which means that each failure mechanism contributes to the failure independently if the other one occurs or not. Hence, the dike section failure is estimated as the sum of the failure probabilities of each failure mechanism. The procedure is explained in the following example.

#### Total safety calculation example:

The *total target safety value* of a particular section is defined as 0.01 [1/year]. The estimated piping erosion failure probability of a certain design choice was found to be equal to 0.025 [1/year]. The resultant total failure probability of this section while including the other failure mechanisms according to the fault tree presented in Figure 5-2 is calculated as:

$$P_{f_{\text{dike section}}} = 0.01 \cdot (1 - 0.24) + 0.025 = 0.0326.$$

The estimated total failure probabilities are also expressed in terms of their equivalent  $\beta$  indexes. As it was presented in Chapters 2, 3 and 4, a benchmark case was always assessed so that the increase or decrease in safety derived from the design choice could be quantified. This is done by estimating the percentual change in the  $\beta$  indexes between

the design choice and benchmark case. The  $\beta$  indexes are used instead of probabilities as these last ones vary by different orders of magnitude which makes them difficult to compare in percentual terms. The influence in the total safety results are presented in Table 5-2.

**Table 5-2 Safety change assessment by design choice**

Case	Failure mechanism	Failure Budget	Target $P_f$ /section	$P_f$ /mech	$P_f$ /section	$\beta_{mech}$	$\beta_{section}$	$\Delta\beta_{mech}$	$\Delta\beta_{section}$
	H	[/years]	[/years]	[/years]	[/years]	H	H	[%]	[%]
K and $d_{70}$ 100% uncorrelated	Piping   Uplift	0.24	5.00E-04	3.71E-03	4.09E-03	<b>2.677</b>	<b>2.645</b>	-	-
	Piping   Uplift	0.24	5.00E-04	1.14E-03	1.52E-03	<b>3.051</b>	<b>2.964</b>	14.0%	12.1%
K and $d_{70}$ 100% correlated	Piping   Uplift	0.24	5.00E-04	1.19E-03	1.57E-03	<b>3.038</b>	<b>2.954</b>	13.5%	11.7%
	Piping   Uplift	0.24	5.00E-04	2.01E-03	2.39E-03	<b>2.877</b>	<b>2.821</b>	7.4%	6.7%
No sewer pipe embedded ( $CV_k$ 1.0 D = 5.0m)	Piping	0.24	1.00E-02	1.82E-01	1.89E-01	<b>0.910</b>	<b>0.881</b>	-	-
	Piping	0.24	1.00E-02	1.48E-01	1.56E-01	<b>1.043</b>	<b>1.011</b>	14.7%	14.7%
Sewer pipe embedded in front ( $CV_k$ 1.0 D = 5.0m)	Piping	0.24	1.00E-02	1.34E-01	1.41E-01	<b>1.110</b>	<b>1.075</b>	22.0%	22.0%
	Piping	0.24	1.00E-02	1.48E-01	1.56E-01	<b>1.043</b>	<b>1.011</b>	14.7%	14.7%
Sewer pipe embedded in the middle ( $CV_k$ 1.0 D = 5.0m)	Erosion   Overtopping	0.24	5.00E-04	9.60E-04	1.34E-03	<b>3.102</b>	<b>3.002</b>	-	-
	Erosion   Overtopping	0.24	5.00E-04	1.34E-02	1.38E-02	<b>2.213</b>	<b>2.202</b>	-28.7%	-26.6%
Sewer pipe embedded in the back ( $CV_k$ 1.0 D = 5.0m)	Erosion   Overtopping	0.24	5.00E-04	9.60E-04	1.34E-03	<b>3.102</b>	<b>3.002</b>	0.0%	0.0%
	Erosion   Overtopping	0.24	5.00E-04	9.60E-04	1.34E-03	<b>3.102</b>	<b>3.002</b>	0.0%	0.0%

The table includes the target failure probability for each dike section, the estimated failure probability of obtained in each chapter case, the total estimated failure probability by section (calculated as shown in the example), the equivalent  $\beta$  indexes of both failure mechanism and section and their correspondent percentual safety change with respect to the reference case. Before analysing the results presented in Table 5-2 it's important to take into consideration that:

1. For the first case study, the inclusion of correlation will always improve the estimated safety value no matter the choice of copula model or degree of correlation. However, this design choice should be seen as a way to reduce uncertainty instead of a choice for improving safety as the correlation degree cannot be changed physically.
2. For the second case study, it should be taken into account that the IJkdijk experiment was intentionally designed to fail which explains the significantly low  $\beta$  indexes presented in Table 5-2. In addition, no impermeable blanket was present in the experiment which explains why the assessment does not include the likelihood of uplift.
3. All cases included in this thesis were intentionally selected with high probability of failure and therefore none of them comply with the current or former Dutch safety standards.
4. The boundary conditions and flood defence of each case study are different and therefore they should not be compared against each other. Yet, the increase or decrease in safety is calculated with respect to their benchmark case study. If the benchmark case was unified, it is expected that the safety change will not remain constant but the sign of the safety change will. This last characteristic defines whether the design choice is beneficial or not for the flood defence safety.

When compared on the component level (by section, Table 5-2), the results show that the design choice which affects safety is the placement of roads with average grass quality on top of the flood defence. The safety can be reduced as much as 26.6 % for the studied case tested in very extreme storm conditions.

The design choice that improves safety is the location of pipes in the middle of the seepage length. This may increase the safety of flood defences by as much as 22% for the studied case.

The reduction of uncertainty derived from the inclusion of correlation between  $K$  and  $d_{70}$  is may have a positive effect in the estimated safety of as much as 6.7%. This result suggests that correlation assessment becomes profitable for MFFD's in which the resultant reduction of the dimensions may represent a significant reduction cost of the design as shown in section 5.1.

From the results it can also be stated that the positive or negative results of structural embedment are relative to the total target safety value defined for the cross section as they are relative to the other failure mechanisms.

## **5.8 Additional effects from the design choices**

Additional effects derived from embedding hard structures under flood defences were also found in Chapter 3. A sewer pipe located under a riverine flood defence showed that the structural embedment has considerable effect in the equivalent hydraulic conductivity value of the whole system. This shows that the embedment not only has an effect in the physical process but also in the associated stochastic distribution of the  $K$  variable. In detail, embedded structures represent an obstacle for the groundwater flow which may reduce (or increase in some cases) the pressure gradient inside the erosion channel. This can be interpreted as a change in the probabilistic distribution of the equivalent permeability of the foundation aquifer. The correct probabilistic representation of these effects in the stochastic distribution of the hydraulic conductivity becomes a cumbersome task when implementing empirical models for the safety assessment. Therefore, is more practical to represent them as an additional and independent term on the resistance side of the limit state equation, especially when assessing the structures with simplified limit state equations such as Bligh, Lane or Sellmeijer.

For the case of the road on top of the defence, there is an additional effect derived the presence of the road due to its use. From the results of the study, it was observed that the presence of the road was correlated to lower grass quality locations just after the side ditches. This is explained by the traffic over the road which increases the deterioration rates along these zones. These spatial effects are not included in the actual representation of the failure mechanism as it is assumed a generalized grass quality along the entire profile. For the present case study, detailed information was available to determine which coefficient of erodability function ( $C_E$ , section 4.4.3) may be associated with each location along the profile. It is acknowledged that this information may be difficult to have during the design or assessment of the MFFD. In those cases,

deterioration can still be represented with a lower quality CE function from the 3 different quality functions presented in section 4.5.2.

It is also expected that the associated uncertainty of the embedment materials may have significant effects on the failure mechanism of piping erosion or any other mechanism in which seepage triggers the failure such as pipe leakage or relief wells. If that was the case, inflow towards the inner voids of the structural embedment or outflows from them may change the pressure distributions of the flood defence foundation in unknown ways. Depending on how important these inflows may be with respect to the aquifer flow, the likelihood of the piping erosion may change. In such cases, inflow-outflow stochastic functions along the embedment boundary condition are more realistic.

For the derived effects of the structural embedment of buildings inside flood defences, no study was done in the present thesis. Yet, it is expected that the inclusion of structures will even improve the safety in terms of slope stability as masonry structures will increase the resistance against mass displacement and reduce the triggering force of this mechanism if located in the passive zone of the failure. However, the obtained improvement from embedding this structures is not significantly important when assessed in a component safety level as the expected failure probabilities due to this failure mechanism are low. This statement is supported by the associated budget coefficient ( $\omega = 0.04$ , see Table 1-1) defined for the maximum allowable failure probabilities in the latest statutory budget (WBI-2017, 2015).

# Chapter 6

## Conclusions and recommendations

From the infinite but plausible number combinations of design uncertainties/choices, three different cases were assessed for solving each of the three research questions.

### 6.1 Research question 1

*How does correlation between  $K$  and  $d_{70}$  influence the probabilistic design and assessment of a multifunctional flood defence?*

From the physical point of view, the ideal condition for piping to occur is a flood defence founded over an aquifer with a high hydraulic conductivity composed of mostly small grain sizes. These two conditions ensure high inflows towards and inside of the erosion channel and low resistance for the particles to be transported. However, this condition is contradictory as the presence of finer grains will inevitably reduce the hydraulic conductivity value of the aquifer. This results in lower pressure gradients inside the erosion channel with respect to the previously mentioned “ideal condition”. However, when  $K$  and  $d_{70}$  variables are sampled independently during the stochastic process, the “ideal condition” is sampled as well.

From the correlation function testing presented in Chapter 2, a Clayton type of copula resulted in the best fit for the field data. This function allows to have higher left tail dependence of variables which means that the chances of sampling low grain sizes and low hydraulic conductivity values at the same time are higher. Hence, it also reduces the chances of sampling combinations of low grain sizes and high hydraulic conductivity values. Then the question is: “why is this important for multifunctional flood defences?”. The answer is derived from two of the main advantages of multifunctionality; the space optimization and the reduction in failure likelihood. As low failure probabilities are desired, the omission of correlation results in more conservative and over-dimensioned multifunctional flood defence designs. The implicit costs of these extra dimensions may either determine the financial feasibility the project or reduce the number of potential uses to be allocated. Furthermore, it may even restrict

the type of uses as larger multifunctional flood defences require more profitable uses to make the projects financially feasible. These side effects become even more important for large multifunctional flood defences as the error in the dimensioning increases with respect to the increase in its desired target safety as shown in section 5.1.

## 6.2 Research question 2

*How does an embedded pipe under a multifunctional flood defence influence the probabilistic design and assessment of the piping erosion failure mechanism?*

From the results of Chapter 3 it is concluded that structural embedments inside the aquifer will always decrease the flood defence piping erosion failure probability with respect to the case in which no structural embedment is present. This conclusion becomes even more important for multifunctional flood defences as one of their main goals is the function integration. This means that commercial and residential uses may be part of the flood defence which require to be connected to the main water supply and sewer drainage systems.

From a physical point of view, the embedment of pipes forces the flow to divert in two portions; one portion goes over the pipe and the other one goes underneath. This is equivalent to a reduction of the average hydraulic conductivity of the aquifer. In other words, the embedded structure represents an additional pressure loss inside the aquifer flow. This loss is dependent on the size and location of the pipe with respect to the bottom of the multifunctional flood defence as this distance defines the proportions of flow diversion. This diversion increases the flow path length of the portion diverted underneath which results in a reduction of the pressure gradient inside the erosion channel. In consequence, the inclusion of the pipe also reduces the probability of piping erosion to progress. This effect is even more important for configurations in which the sewer pipe is founded in a shallow depth and its size is significantly large with respect to the total aquifer depth as the pressure losses become larger.

From a probabilistic point of view, the inclusion of impermeable structures (ground water flow obstacles) will always represent a reduction in the average system hydraulic conductivity which consequently will result in a lower piping erosion failure probability. If multifunctional flood defences are required to be assessed based on simplified models of the Sellmeijer concept (e.g. original, modified and revised limit state equations) in which the embedment effects are not explicitly included, the associated stochastic distributions and deterministic variables that describe the system should be modified to

reflect these effects. It is of paramount importance to stress that these conclusions only explain the effects on the piping erosion failure mechanism and they should be used for the assessment of this failure mechanism only. The likelihood of other failure mechanisms may either increase or decrease due to the structural embedments in unknown ways. The study of these effects were out of the scope of the present thesis.

### 6.3 Research question 3

*How does the presence of a road on top of the crest of a multifunctional flood defence influence the probabilistic design and assessment for the wave overtopping grass cover erosion failure mechanism?*

For the case study with the road embedded over the crest of the flood defence, the results presented in Chapter 4 show that the inclusion of roads over MFFDs reduces the safety against grass cover erosion from wave overtopping. Especially for large storms which may be expected in the future due to effects like sea level or other climate change effects.

From a physical point of view, the energy loss due to superficial roughness and the erosion resistance associated with the grass quality are the two features that influence grass cover failure due to wave overtopping the most. From the side of the superficial roughness, it can be divided into two classes; the first is associated to the roughness on a small scale derived from the superficial roughness inherent to the material and the second one to a larger scale roughness originated from abrupt bottom slope changes. Both characteristics contribute to energy dissipation but the latter one contributes the most to the formation localized turbulent zones along the MFFD profile. The inclusion of a smoother surface such as asphalt rather than plain grass represents a lower energy dissipation rate. Hence, locating a road over the crest of the multifunctional flood defence will result in faster overtopping waves over that specific surface cover. This is not a problem for the much more erosion resistant asphalt cover but it is a significant change for the less resistant grass cover located immediately afterwards along the side slope. Consequently, from a probabilistic point of view, the lower material roughness of the road increases the probability of scouring on the grass cover subsequent locations.

From the geometrically induced bottom roughness, the observed erosive effects are localized and correlated to higher turbulence points. For a convex bottom form for example such as the lateral transition gap of a road, it is expected that a large amount of energy will be dissipated once the overtopped volume arrives at this point. This

expected effect is beneficial for the downstream grass cover as a reduction in the velocity is desirable. However, this energy dissipation is obtained by an increase in the kinematic turbulent energy. This increase is explained by the formation of local turbulent eddies which induce higher bottom shear stresses and consequently deeper erosion cuts. Such localized and high stresses will not be exerted if a flat bottom surface was located in the same place. The presence of these convex shaped zones are commonly found on current flood defences with roads on top, as they are exposed to higher rates of traffic which will induce this sort of irregularities along the profile. In the case of a future multifunctional flood defence in which wider roads may also be included, the inherent superficial roughness may become more important than the geometrical induced roughness. This shows how the design choice related to size is also important for the present failure mechanism. Traffic will also reduce the quality of the erosion resistance of grass which represents the second most important characteristic for grass cover erosion safety.

From a probabilistic point of view, the uncertainty associated with the grass quality and spatial distribution has great importance in the safety of multifunctional flood defences. The results showed that for the same storm, grass quality and cover thickness will not only determine the scouring depths but also the number of failure prone locations along the dike. In addition, the inclusion of a road or any other structure will also have an important effect in the stochastic nature of the occurrence of the bottom shear stresses.

## 6.4 Synthesis

From all three case studies presented in this thesis, it was concluded that the size and location of the embedded structure underneath the MFFD has the most beneficiary effect for safety (the only one with positive sign in the percentual change of safety, see Table 5-2). It was reiteratively observed that this design choice always improved the defence safety when probabilistically assessed. Nevertheless, the importance in the safety increase is conditioned to the aquifer depth and the hydraulic conductivity stochastic distribution. This effect is a direct impact in the equivalent hydraulic conductivity of the whole aquifer. This finding is very important as it means that the implementation of the newest Sellmeijer limit state equation in cases in which an embedment is present may only underestimate the MFFD safety against piping erosion resulting in conservative conclusions only. In relation to the safety at a component level (by cross section), the embedment of pipes also shows that it may result in a significant safety increase in safety as long as the other failure mechanisms comply with their suggested maximum allowable probabilities.

Despite the fact that the importance of the inclusion of the correlation effect between the grain size and the aquifer hydraulic conductivity proved to be less significant in terms of added safety, it is expected that the combination of both design choices (embedment and correlation) will improve the safety of the system even further.

For the case of grass cover failure due to wave overtopping, it is concluded that the inclusion of roads represents the most unsafe design choice of all the three studied cases. Nevertheless, this effect was only studied for the case of design storms which are greater than the ones allowed by the actual Dutch legislation ( $q_m \leq 10$  L/s/m). The main problem with this design choice is not the structural embedment itself but the associated traffic which may affect dike profiles and erosion resistance of the grass cover. For the case of multifunctional flood defences, it is expected that not only the traffic will increase but also the road width. In that case, the expected effects in safety are even greater.

In the present thesis it was explained why multifunctional flood defences cannot be assessed by the actual methods as they are not capable of including the effects of structural embedments. This restriction obliges the designer to implement more complex models in order to capture the additional effects. These models are generally computationally expensive and not flexible for multiple scenario assessment. The emulation techniques presented in this thesis proved to be powerful tools which allow perform probabilistic design and assessment of multifunctional flood defences with multiple scenarios while including the detail obtained from more complex numerical models. In addition, they reflect potential improvement for the current probabilistic assessment tools as they can easily be included disregarding the reliability method to be used.

## 6.5 Final Recommendations

1. The present study shows how the Clayton Copula fits best to the potential correlation function. While it is acknowledged that having a large set of field samples to determine the significance of the estimated correlation degree, it is highly recommended that correlation inclusion is implemented during the design process in the form of a sensitivity tool. This can be done based on the method presented in Chapter 2 by changing the degree of correlation and observing the change in failure probability. This will allow determining if a robust field campaign for correlation assessment may improve the assessment.

2. For structures embedded under the MFFD's it is important to include the effects of the reliability of the embedment in the fault tree scenario as the likelihood of failure may increase. Hence, it is recommended to further study this reliability problem by assessing the probability of failure of the embedment itself in combination with the method presented in this thesis.
3. While the results of the present thesis show that the embedment of structures is always beneficiary for the piping erosion safety, it is also acknowledged that seepage along hard structures is a major treat for these structures. For this reason, it is recommended to:
  - a) Further study the derived effects in safety from the inclusion of hard structures underneath MFFD's for other failure mechanisms such as seepage, uplift, and slope stability.
  - b) Further study the derived effects in safety from the inclusion of hard structures and correlation assessment. From the results of this thesis, it is expected that this kind of assessment may reduce the MFFD's costs.
4. A significant amount of research has been done in the world and in particular in the Netherlands about grass quality, tensile resistance and erosive resistance of grass. Given the new Dutch policy which aims to move towards a more risk based legislation, it is highly recommended to develop knowledge about the associated uncertainties of this grass characteristic so that they can be implemented in probabilistic designs and assessments of conventional flood defences and MFFD's.
5. Emulation techniques proved to be quite efficient for probabilistic assessments of particular scenarios. It is recommended to further research the possibility of developing them for ensuring large generalization capacities so that they can be implemented in complete system assessments without having to retrain them for every specific case. This can be done by sampling the stochastic variables as uniform distributions.
6. Further investigation over the effects in the flood safety reliability derived from the stochastic nature assumptions and/or choices of the variables and model simplification is recommended. Especially, for failure mechanisms in which the loads or resistance values are obtained from unreal sample combinations.

# References

- Aguilar-Lopez, J.P., Van Andel, S.J., Werner, M., Solomatine, D.P., 2014. Hydrodynamic and water quality surrogate modelling for reservoir operation 11th IWA/IAHR International Conference on Hydroinformatics New York City, USA.
- Aguilar-López, J.P., Warmink, J.J., Schielen, R.M.J., Hulscher, S.J.M.H., 2014. Data-driven surrogate models for flood defence failure estimation: "Jarillon de Cal", 11th IWA/IAHR International Conference on Hydroinformatics, New York City, USA.
- Aguilar-López, J.P., Warmink, J.J., Schielen, R.M.J., Hulscher, S.J.M.H., 2015. Correlation effect in probabilistic design against piping erosion in multi-functional flood defences. In: Schweckendiek, T. (Ed.), International Conference of Geotechnical Safety and Risk (ISGSR2015). IOS Press BV - Amsterdam, Rotterdam, The Netherlands, pp. 239-244. DOI:10.3233/978-1-61499-580-7-239
- Aguilar-López, J.P., Warmink, J.J., Schielen, R.M.J., Hulscher, S.J.M.H., 2016a. Piping erosion safety assessment of flood defences founded over sewer pipes. *European Journal of Environmental and Civil Engineering*: 1-29. DOI:10.1080/19648189.2016.1217793
- Aguilar-López, J.P., Warmink, J.J., Schielen, R.M.J., Hulscher, S.J.M.H., 2016b. Soil stochastic parameter correlation impact in the piping erosion failure estimation of riverine flood defences. *Structural Safety*, 60: 117-129. DOI:10.1016/j.strusafe.2016.01.004
- Allsop, N., Kortenhaus, A., Morris, M., 2007. Failure mechanisms for flood defence structures. FLOODsite project report T04\_06\_01.
- Arangio, S., 2012. Reliability based approach for structural design and assessment: performance criteria and indicators in current European codes and guidelines. *International Journal of Lifecycle Performance Engineering*, 1(1): 64-91.
- Attoh-Okine, N.O., 2013. Pair-copulas in infrastructure multivariate dependence modeling. *Construction and Building Materials*, 49(0): 903-911. DOI:10.1016/j.conbuildmat.2013.06.055
- Bakker, J., Melis, R., Mom, R., 2013. Factual Report: Overslagproeven Rivierenland, INFRAM, The Netherlands.
- Barlow, R.E., 2004. Fault Tree Analysis, *Encyclopedia of Statistical Sciences*. John Wiley & Sons, Inc. DOI:10.1002/0471667196.ess0766.pub2
- Battjes, J.A., Groenendijk, H.W., 2000. Wave height distributions on shallow foreshores. *Coastal Engineering*, 40(3): 161-182. DOI:10.1016/S0378-3839(00)00007-7
- Bear, J., Buchlin, J.M., Von Karman Institute for Fluid Dynamics., 1991. Modelling and applications of transport phenomena in porous media. Theory and applications of transport in porous media. Kluwer Academic Publishers, Dordrecht ; Boston, 380 pp.
- Bear, J., Verruijt, A., 1987. Modeling groundwater flow and pollution, 2. Springer Science & Business Media.
- Beijersbergen, J.A., Spaargaren, G.R., 2009. Vuistregels voor het beheerdersoordeel bij de toetsing van niet-waterkerende objecten (Definitief), Zuid-Holland Afdeling Water Den Haag, The Netherlands.
- Bersan, S., Jommi, C., Koelewijn, A., Simonini, P., 2013. Applicability of the fracture flow interface to the analysis of piping in granular material, COMSOL Conference 2013, Rotterdam

- Billar, B., Gunes Corlu, C., 2012. Copula-based multivariate input modeling. *Surveys in Operations Research and Management Science*, 17(2): 69-84. DOI:10.1016/j.sorms.2012.04.001
- Bligh, W., 1910. Dams, barrages and weirs on porous foundations. *Engineering News*, 64(26): 708-710.
- Bomers, A., Aguilar-López, J.P., Warmink, J.J., Hulscher, S.J.M.H., 2016. Modelling erosion development during wave overtopping of an asphalt road covered dike, FLOODrisk2016 - 3rd European Conference on Flood Risk Management, Innovation, Implementation and Integration, Lyon, France.
- Brasor, P., 2010. Flood control: Destroying neighborhoods to save them (Arakawa Teibo). In: Tsubuku, M. (Ed.), *Yen For living Blog*, Japan Times.
- Brooks, R.J., Tobias, A.M., 1996. Choosing the best model: Level of detail, complexity, and model performance. *Mathematical and Computer Modelling*, 24(4): 1-14. DOI:10.1016/0895-7177(96)00103-3
- Bucher, C., Most, T., 2008. A comparison of approximate response functions in structural reliability analysis. *Probabilistic Engineering Mechanics*, 23(2-3): 154-163. DOI:10.1016/j.probengmech.2007.12.022
- Calle, E.O.F., Weijers, J.B., 1994. Technisch rapport voor controle op het mechanisme piping bij rivierdijken, Deltares (Geodelft), Delft, The Netherlands
- Castelletti, A., Galelli, S., Ratto, M., Soncini-Sessa, R., Young, P.C., 2012. A general framework for Dynamic Emulation Modelling in environmental problems. *Environmental Modelling & Software*, 34: 5-18. DOI:10.1016/j.envsoft.2012.01.002
- Chapuis, R.P., 2012. Predicting the saturated hydraulic conductivity of soils: a review. *Bull Eng Geol Environ*, 71(3): 401-434. DOI:10.1007/s10064-012-0418-7
- Chen, N., Gunzburger, M., Hu, B., Wang, X., Woodruff, C., 2012. Calibrating the exchange coefficient in the modified coupled continuum pipe-flow model for flows in karst aquifers. *Journal of Hydrology*, 414-415: 294-301. DOI:10.1016/j.jhydrol.2011.11.001
- Chen, X., Hofland, B., Altomare, C., Suzuki, T., Uijttewaal, W., 2015. Forces on a vertical wall on a dike crest due to overtopping flow. *Coastal Engineering*, 95: 94-104. DOI:10.1016/j.coastaleng.2014.10.002
- Chen, X., Hofland, B., Uijttewaal, W., 2016. Maximum overtopping forces on a dike-mounted wall with a shallow foreshore. *Coastal Engineering*, 116: 89-102. DOI:10.1016/j.coastaleng.2016.06.004
- Cho, S.E., 2009. Probabilistic stability analyses of slopes using the ANN-based response surface. *Computers and Geotechnics*, 36(5): 787-797. DOI:10.1016/j.compgeo.2009.01.003
- Chojaczyk, A.A., Teixeira, A.P., Neves, L.C., Cardoso, J.B., Guedes Soares, C., 2015. Review and application of Artificial Neural Networks models in reliability analysis of steel structures. *Structural Safety*, 52, Part A: 78-89. DOI:10.1016/j.strusafe.2014.09.002
- Danka, J., Zhang, L., 2015. Dike failure mechanisms and breaching parameters. *Journal of Geotechnical and Geoenvironmental Engineering*, 141(9): 04015039.
- Dean, R.G., Rosati, J.D., Walton, T.L., Edge, B.L., 2010. Erosional equivalences of levees: Steady and intermittent wave overtopping. *Ocean Engineering*, 37(1): 104-113. DOI:10.1016/j.oceaneng.2009.07.016
- Diamantidis, D., 1987. Reliability assessment of existing structures. *Engineering Structures*, 9(3): 177-182.

- Diermanse, F.L.M., Geerse, C.P.M., 2012. Correlation models in flood risk analysis. *Reliability Engineering & System Safety*, 105(0): 64-72. DOI:10.1016/j.res.2011.12.004
- Dobrić, J., Schmid, F., 2007. A goodness of fit test for copulas based on Rosenblatt's transformation. *Computational Statistics & Data Analysis*, 51(9): 4633-4642. DOI:10.1016/j.csda.2006.08.012
- Dodge, M.M., 1876. *Hans Brinker: Or The Silver Skates; a Story of Life in Holland*. Scribner, Armstrong & Company.
- Duncan, A., Chen, A.S., Keedwell, E., Djordjevic, S., Savic, D., 2011. Urban flood prediction in real-time from weather radar and rainfall data using artificial neural networks.
- El Shamy, U., Aydin, F., 2008. Multiscale modeling of flood-induced piping in river levees. *Journal of geotechnical and geoenvironmental engineering*, 134(9): 1385-1398.
- Elishakoff, I., 2012. *Safety factors and reliability: friends or foes?* Springer Science & Business Media.
- Forrester, A., Sobester, A., Keane, A., 2008. *Engineering design via surrogate modelling: a practical guide*. John Wiley & Sons.
- Förster, U., Van den Ham, G., Calle, E., Kruse, G., 2012. *Onderzoeksrapport: Zandmeevoerende Wellen*. Report.
- Franco, L., De Gerloni, M., Van der Meer, J., 1994. Wave overtopping on vertical and composite breakwaters. *Coastal Engineering Proceedings*, 1(24).
- Genest, C., Rémillard, B., Beaudoin, D., 2009. Goodness-of-fit tests for copulas: A review and a power study. *Insurance: Mathematics and Economics*, 44(2): 199-213. DOI:10.1016/j.insmathco.2007.10.005
- Gomes, H.M., Awruch, A.M., 2004. Comparison of response surface and neural network with other methods for structural reliability analysis. *Structural Safety*, 26(1): 49-67. DOI:10.1016/S0167-4730(03)00022-5
- Griffiths, D., Lane, P., 1999. Slope stability analysis by finite elements. *Geotechnique*, 49(3): 387-403.
- Grimaldi, S., Serinaldi, F., 2006. Asymmetric copula in multivariate flood frequency analysis. *Advances in Water Resources*, 29(8): 1155-1167.
- Groot, T., 2015. *Macro-stability safety assessment for flood defenses with buried pipes* (MSc. Thesis), University of Twente, Enschede, The Netherlands, 90 pp.
- Hasofer, A., 1974. Reliability index and failure probability. *Journal of Structural Mechanics*, 3(1): 25-27.
- Hasofer, A.M., Lind, N.C., 1974. Exact and invariant second-moment code format (for reliability analysis in multivariate problems). American Society of Civil Engineers, Engineering Mechanics Division, *Journal*, 100: 111-121.
- Hewlett, H., Boorman, L.A., Bramley, L., 1987. *Design of reinforced grass waterways*. Construction Industry Research and Information Association.
- Hoffmans, G.J.C.M., 2012. The influence of turbulence on soil erosion, 10. Eburon Uitgeverij BV.
- Hoffmans, G.J.C.M., 2014a. An overview of piping models. In: Liang Cheng, S.D., and Hongwei An (Ed.), *7th International Conference on Scour and Erosion*. CRC Press 2014, Perth, Australia, pp. 3-18. DOI:10.1201/b17703-3

- Hoffmans, G.J.C.M., 2014b. An overview of piping models, Scour and Erosion: Proceedings of the 7th International Conference on Scour and Erosion, Perth, Australia, 2-4 December 2014. CRC Press, pp. 3.
- Hoffmans, G.J.C.M., 2015. Effect van Invloedsfactoren op Toetsing/Ontwerp: Voorstel voor implementatie, Deltares.
- Hoffmans, G.J.C.M., Akkerman, G.J., Verheij, H., Van Hoven, A., Van der Meer, J., 2008. The erodibility of grassed inner dike slopes against wave overtopping. ASCE, Proc. ICCE 2008: 3224-3236.
- Hoffmans, G.J.C.M., Knoeff, H., 2012. Achtergrondrapportage Technisch deel VTV. 1204143-001-GEO-0019.
- Hoffmans, G.J.C.M., van Hoven, A., Harderman, B., Verheij, H., 2015. Erosion of grass covers at transitions and objects on dikes. In: Cheng, L., Drapper, S., An, H. (Eds.), 7th International Conference on Scour and Erosion. Taylor and Francis Group, Perth, Australia.
- Hughes, S.A., 2011. Adaptation of the Levee Erosional Equivalence Method for the Hurricane Storm Damage Risk Reduction System (HSDRRS), DTIC Document.
- Hughes, S.A., Nadal, N.C., 2009. Laboratory study of combined wave overtopping and storm surge overflow of a levee. *Coastal Engineering*, 56(3): 244-259. DOI:10.1016/j.coastaleng.2008.09.005
- Hughes, S.A., Thornton, C.I., Van der Meer, J.W., Scholl, B.N., 2012. Improvements in describing wave overtopping processes. *Coastal Engineering Proceedings*, 1(33): 35.
- Hurtado, J.E., 2013. Structural reliability: statistical learning perspectives, 17. Springer Science & Business Media.
- Ilieș, N.-M., Moldovan, I.-M., Moldovan, S.-V., 2015. Improving the Stability of Slopes with the Aid of Underground Houses. *Procedia Technology*, 19: 363-370.
- Jansen, R.B., 2012. Advanced dam engineering for design, construction, and rehabilitation. Springer Science & Business Media.
- Jianhua, Y., 1998. FE Modelling of Seepage in Embankment Soils with Piping Zone. *Chinese Journal of rock mechanics and engineering*(1998-12).
- Johnson, P.A., Gleason, G.L., Hey, R.D., 1999. Rapid assessment of channel stability in vicinity of road crossing. *Journal of Hydraulic Engineering*, 125(6): 645-651.
- Jongejan, R.B., Calle, E.O.F., 2013. Calibrating semi-probabilistic safety assessments rules for flood defences. *Georisk: Assessment and Management of Risk for Engineered Systems and Geohazards*, 7(2): 88-98.
- Jongejan, R.B., Maaskant, B., 2013. Applications of VNK2, a fully probabilistic risk analysis for all major levee systems in The Netherlands. *Comprehensive flood risk management*. Taylor & Francis Group, London.
- Jongejan, R.B., Maaskant, B., Ter Horst, W., Havinga, F., Roode, N., Stefess, H., 2013. The VNK2 project a fully probabilistic risk analysis for the major levee systems in the Netherlands In: Takeuchi, A.C.K. (Ed.), 5th International Conference on Flood Management (ICFM5). IAHS, Tokyo, Japan, pp. 480.
- Jongerius, Y.R., 2016. Reliability of a dike influenced by a building: Development of a probabilistic method for slope stability of a dike containing a building inside the soil profile (MSc. Thesis), TU Delft, Delft University of Technology, 210 pp.
- Jonkman, S., Brinkhuis-Jak, M., Kok, M., 2004. Cost benefit analysis and flood damage mitigation in the Netherlands. *Heron*, 49 (1).

- Kanning, W., 2012. *The Weakest Link: Spatial Variability in the Piping Failure Mechanism of Dikes* (PhD Thesis), TU Delft, The Netherlands, 235 pp.
- Kanning, W., Van Baars, S., Van Gelder, P.H.A.J.M., Vrijling, J.K., 2007. Lessons from New Orleans for the design and maintenance of flood defence systems, *Proc. ESREL*.
- Karadeniz, H., Vrouwenvelder, T., 2003. SAFERELNET Task 5.1 Overview reliability methods.
- Kaunda, R.B., 2015. A neural network assessment tool for estimating the potential for backward erosion in internal erosion studies. *Computers and Geotechnics*, 69: 1-6. DOI:10.1016/j.compgeo.2015.04.010
- Kind, J., 2011. *Maatschappelijke kosten-batenanalyse Waterveiligheid 21e eeuw*. Deltares, Delft: 1204144-006.
- Kingston, G.B.R., Mohammadreza; Gouldby, Ben P. ;Van Gelder, P.H.A.J.M., 2011. Computational intelligence methods for the efficient reliability analysis of complex flood defence structures. *Structural Safety*, 33(1): 64-73. DOI:10.1016/j.strusafe.2010.08.002
- Klijn, F., Kreibich, H., De Moel, H., Penning-Rowsell, E., 2015. Adaptive flood risk management planning based on a comprehensive flood risk conceptualisation. *Mitigation and Adaptation Strategies for Global Change*, 20(6): 845-864.
- Knoeff, H., Ellen, G.J., 2011. *Verkenning deltadijken*. Deltares.
- Kobayashi, N., Weitzner, H., 2014. Erosion of a seaward dike slope by wave action. *Journal of Waterway, Port, Coastal, and Ocean Engineering*, 141(2): 04014034.
- Koduru, S.D., Haukaas, T., 2010. Feasibility of FORM in finite element reliability analysis. *Structural Safety*, 32(2): 145-153. DOI:10.1016/j.strusafe.2009.10.001
- Koelwijjn, A., De Vries, G., Van Lottum, H., Förster, U., Van Beek, V., Bezuijen, A., 2014. Full-scale testing of piping prevention measures: three tests at the IJkdijk. *Proceedings of the Physical Modeling in Geotechnics*: 891-897.
- Koelwijjn, A.R., 2009. *SBW Hervalidatie piping E. Evaluatie 0,3d rekenregel*. 1 001453-002-GE0-0001, Deltares, Netherlands.
- Kuijken, W., 2015. *Deltaprogramma 2015*, Deltacommissaris.
- Lachouette, D., Golay, F., Bonelli, S., 2008. One-dimensional modeling of piping flow erosion. *Comptes Rendus Mécanique*, 336(9): 731-736. DOI:10.1016/j.crme.2008.06.007
- Lane, E.W., 1935. Security from under-seepage-masonry dams on earth foundations. *Transactions of the American Society of Civil Engineers*, 100(1): 1235-1272.
- Lee, C.-E., Kwon, H.J., 2009. Reliability analysis and evaluation of partial safety factors for random wave overtopping. *KSCE Journal of Civil Engineering*, 13(1): 7-14. DOI:10.1007/s12205-009-0007-x
- Li, D., Chen, Y., Lu, W., Zhou, C., 2011. Stochastic response surface method for reliability analysis of rock slopes involving correlated non-normal variables. *Computers and Geotechnics*, 38(1): 58-68. DOI:10.1016/j.compgeo.2010.10.006
- Liedl, R., Sauter, M., Hückinghaus, D., Clemens, T., Teutsch, G., 2003. Simulation of the development of karst aquifers using a coupled continuum pipe flow model. *Water Resources Research*, 39(3): n/a-n/a. DOI:10.1029/2001WR001206
- Link, L.E., 2010. The anatomy of a disaster, an overview of Hurricane Katrina and New Orleans. *Ocean Engineering*, 37(1): 4-12. DOI:10.1016/j.oceaneng.2009.09.002
- Lominé, F., Scholtès, L., Sibille, L., Poullain, P., 2013. Modeling of fluid–solid interaction in granular media with coupled lattice Boltzmann/discrete element methods: application

- to piping erosion. *International Journal for Numerical and Analytical Methods in Geomechanics*, 37(6): 577-596.
- Lopez De La Cruz, J., Calle, E., Schweckendiek, T., 2011. Calibration of piping assessment models in the Netherlands, *Proceedings of the 3rd International Symposium on Geotechnical Safety and Risk, ISGSR 2011, Munich, Germany, 2-3 June 2011*. Bundesanstalt für Wasserbau.
- Low, B.K., 2014. FORM, SORM, and spatial modeling in geotechnical engineering. *Structural Safety*, 49(0): 56-64. DOI:10.1016/j.strusafe.2013.08.008
- Lü, Q., Low, B.K., 2011. Probabilistic analysis of underground rock excavations using response surface method and SORM. *Computers and Geotechnics*, 38(8): 1008-1021. DOI:10.1016/j.compgeo.2011.07.003
- Marriott, M.J., Jayaratne, R., 2010. Hydraulic roughness—links between Manning’s coefficient, Nikuradse’s equivalent sand roughness and bed grain size.
- Mazzoleni, M., Barontini, S., Ranzi, R., Brandimarte, L., 2014. Innovative Probabilistic Methodology for Evaluating the Reliability of Discrete Levee Reaches Owing to Piping. *Journal of Hydrologic Engineering*.
- Melnikova, N.B., Jordan, D., Krzhizhanovskaya, V.V., 2015. Experience of using FEM for real-time flood early warning systems: Monitoring and modeling Boston levee instability. *Journal of Computational Science*, 10: 13-25. DOI:10.1016/j.jocs.2015.04.033
- Moellmann, A., Vermeer, P.A., Huber, M., 2011. A probabilistic finite element analysis of embankment stability under transient seepage conditions. *Georisk: Assessment and Management of Risk for Engineered Systems and Geohazards*, 5(2): 110-119. DOI:10.1080/17499511003630520
- Morris, M., Allsop, W., Buijs, F., Kortenhaus, A., Doorn, N., Lesniewska, D., 2008. Failure modes and mechanisms for flood defence structures.
- Mott, R.L., Noor, F.M., Aziz, A.A., 2006. *Applied fluid mechanics*. Pearson Prentice Hall.
- Muzychka, Y., Yovanovich, M., 2009. Pressure drop in laminar developing flow in noncircular ducts: A scaling and modeling approach. *Journal of Fluids Engineering*, 131(11): 111105.
- Nakamura, H., Nghiem, Q., Iwasa, N., 2007. Reinforcement of tree roots in slope stability: A case study from the Ozawa slope in Iwate Prefecture, Japan, *Eco-and Ground Bio-Engineering: The Use of Vegetation to Improve Slope Stability*. Springer, pp. 81-90.
- Naulin, M., Kortenhaus, A., Oumeraci, H., 2015. Reliability-based flood defense analysis in an integrated risk assessment. *Coastal Engineering Journal*, 57(01): 1540005.
- Nelsen, R.B., 2006. *An introduction to copulas*. Springer series in statistics. Springer, New York, xiii, 269 p. pp.
- Nicholls, R.J., Marinova, N., Lowe, J.A., Brown, S., Vellinga, P., De Gusmao, D., Hinkel, J., Tol, R.S., 2011. Sea-level rise and its possible impacts given a ‘beyond 4 C world’ in the twenty-first century. *Philosophical Transactions of the Royal Society of London A: Mathematical, Physical and Engineering Sciences*, 369(1934): 161-181.
- Oaks, D., Edge, B., Lynett, P., 2011. Evaluation of the Structure of Levee Transitions on Wave Run-Up and Overtopping by Physical Modeling. *Journal of Waterway, Port, Coastal, and Ocean Engineering*, 138(1): 53-62.
- Ojha, C.S.P., Singh, V.P., Adrian, D.D., 2008. Assessment of the role of slit as a safety valve in failure of levees. *International Journal of Sediment Research*, 23(4): 361-375. DOI:10.1016/S1001-6279(09)60007-X

- Pan, Y., Kuang, C., Li, L., Amini, F., 2015. Full-scale laboratory study on distribution of individual wave overtopping volumes over a levee under negative freeboard. *Coastal Engineering*, 97: 11-20.
- Partheniades, E., 1965. Erosion and deposition of cohesive soils. *Journal of the Hydraulics Division*, 91(1): 105-139.
- Paul, D.K., Kumar, S., 1997. Stability analysis of slope with building loads. *Soil Dynamics and Earthquake Engineering*, 16(6): 395-405. DOI:10.1016/S0267-7261(97)00008-0
- Piontkowitz, T., 2009. EroGRASS: Failure of grass cover layers at seaward and shoreward dike slopes. Design, construction and performance, Danish Coastal Inspectorate.
- Piotrowski, A.P., Napiorkowski, J.J., 2013. A comparison of methods to avoid overfitting in neural networks training in the case of catchment runoff modelling. *Journal of Hydrology*, 476: 97-111. DOI:10.1016/j.jhydrol.2012.10.019
- Pontillo, M., Schmocker, L., Greco, M., Hager, W.H., 2010. 1D numerical evaluation of dike erosion due to overtopping. *Journal of Hydraulic Research*, 48(5): 573-582. DOI:10.1080/00221686.2010.507005
- Pullen, T., Allsop, N., Bruce, T., Kortenhuis, A., Sch, H., Van der Meer, J., 2007. Eurotop: Wave overtopping of sea defences and related structures: assessment manual.
- Pyayt, A.L., Mokhov, I.I., Lang, B., Krzhizhanovskaya, V.V., Meijer, R.J., 2011. Machine learning methods for environmental monitoring and flood protection. *World Academy of Science, Engineering and Technology*, 5: 82-85.
- Quang, T.T., Oumeraci, H., 2012. Numerical modelling of wave overtopping-induced erosion of grassed inner sea-dike slopes. *Natural hazards*, 63(2): 417-447.
- Razavi, S.T., Bryan A.; Burn, Donald H.;, 2012. Review of surrogate modeling in water resources. *Water Resources Research*, 48(7): W07401. DOI:10.1029/2011WR011527
- Ribberink, J.S., 1998. Bed-load transport for steady flows and unsteady oscillatory flows. *Coastal Engineering*, 34(1): 59-82.
- Rijkswaterstaat, 2007. HR2006 Hydraulische Randvoorwaarden primaire waterkeringen voor de derde toetsronde 2006-2011. Ministerie van Verkeer en Waterstaat, Directoraat-Generaal Rijkswaterstaat, Delft, The Netherlands.
- Rosas, J., Lopez, O., Missimer, T.M., Coulibaly, K.M., Dehwah, A.H., Sesler, K., Lujan, L.R., Mantilla, D., 2014. Determination of hydraulic conductivity from grain-size distribution for different depositional environments. *Ground water*, 52(3): 399-413. DOI:10.1111/gwat.12078
- Roy, S., Mandal, N., 2009. Modes of hill-slope failure under overburden loads: Insights from physical and numerical models. *Tectonophysics*, 473(3-4): 324-340. DOI:10.1016/j.tecto.2009.03.005
- Samardzioska, T., Popov, V., 2005. Numerical comparison of the equivalent continuum, non-homogeneous and dual porosity models for flow and transport in fractured porous media. *Advances in Water Resources*, 28(3): 235-255. DOI:10.1016/j.advwatres.2004.11.002
- Sanders, M.P.M., Wiggers, A.G., 2015. Semi-probabilistic safety assesment of pipelines near levees. In: Schweckendiek, T. (Ed.), *Geotechnical Safety and Risk conference V*. IOS Press BV, Rotterdam, Netherlands. DOI:10.3233/978-1-61499-580-7867
- Schoefs, F., Le, K.T., Lanata, F., 2013. Surface response meta-models for the assessment of embankment frictional angle stochastic properties from monitoring data: An

- application to harbour structures. *Computers and Geotechnics*, 53(0): 122-132. DOI:10.1016/j.compgeo.2013.05.005
- Scholz, F.W., Stephens, M.A., 1987. K-Sample Anderson-Darling Tests. *Journal of the American Statistical Association*, 82(399): 918-924. DOI:10.2307/2288805
- Schüttrumpf, H., Oumeraci, H., 2005. Layer thicknesses and velocities of wave overtopping flow at seadikes. *Coastal Engineering*, 52(6): 473-495.
- Schweckendiek, T., Vrouwenvelder, A.C.W.M., Calle, E.O.F., 2014. Updating piping reliability with field performance observations. *Structural Safety*, 47(0): 13-23. DOI:10.1016/j.strusafe.2013.10.002
- Sellmeijer, J.B., 1988. On the mechanism of piping under impervious structures (PhD Thesis). PhD Dissertation Thesis, TU Delft, Delft University of Technology.
- Sellmeijer, J.B., 2006. Numerical computation of seepage erosion below dams (piping). In: Gouda (Ed.), *Third International Conference on Scour and Erosion 2006*. CUR Bouwn & Infra, 2006, Amsterdam, The Netherlands, pp. 596-601. .
- Sellmeijer, J.B., de la Cruz, J.L., Van Beek, V.M., Knoeff, H., 2011. Fine-tuning of the backward erosion piping model through small-scale, medium-scale and IJkdijk experiments. *European Journal of Environmental and Civil Engineering*, 15(8): 1139-1154. DOI:10.1080/19648189.2011.9714845
- Sellmeijer, J.B., Koenders, M.A., 1991. A mathematical model for piping. *Applied Mathematical Modelling*, 15(11–12): 646-651. DOI:10.1016/S0307-904X(09)81011-1
- Shamekhi, E., Tannant, D.D., 2015. Probabilistic assessment of rock slope stability using response surfaces determined from finite element models of geometric realizations. *Computers and Geotechnics*, 69: 70-81. DOI:10.1016/j.compgeo.2015.04.014
- Silva, W., Van Velzen, E., 2008. De dijk van de toekomst?: quick scan doorbraakvrije dijken, Rijkswaterstaat, Waterdienst.
- Sklar, A., 1959. Fonctions de Répartition à n Dimensions et Leurs Marges. *Publications de l'Institut de Statistique de L'Université de Paris*, 8: 229–231.
- Solomatine, D., See, L., Abraham, R., 2009. Data-driven modelling: concepts, approaches and experiences, *Practical hydroinformatics*. Springer, pp. 17-30.
- Stalenberg, B., Kikumori, Y., 2008. Urban flood control on the rivers of Tokyo metropolitan. *Urban Water in Japan*, Taylor & Francis Group, London, UK: 119-141.
- Steenberghen, H.M., Lassing, B.L., Vrouwenvelder, A.C.W.M., Waarts, P., 2004. Reliability analysis of flood defense systems HERON: Special issue - Risk based water defence, 49(1).
- Stendam, G.J., Van Hoven, A., Van der Meer, J., Hoffmans, G., 2014. Wave overtopping simulator tests on transitions and obstacles at grass covered slopes of dikes *Coastal Engineering Proceedings*, 1(34): 79.
- STOWA, 2000. Handleiding voor beplanting op nabij primaire waterkeringen, Utrecht, The Netherlands.
- Sundar, V.S., Shields, M.D., 2016. Surrogate-enhanced stochastic search algorithms to identify implicitly defined functions for reliability analysis. *Structural Safety*, 62: 1-11. DOI:10.1016/j.strusafe.2016.05.001
- Te Chow, V., 1959. *Open channel hydraulics*. McGraw-Hill, London, U.K.
- Terzaghi, K., Peck, R.B., Mesri, G., 1996. *Soil mechanics in engineering practice*. John Wiley & Sons.

- Thoft-Cristensen, P., Baker, M.J., 2012. Structural reliability theory and its applications. Springer Science & Business Media.
- Thornton, C., Van der Meer, J., Hughes, S., 2011. Testing levee slope resiliency at the new Colorado State University wave overtopping test facility, Proc. Coastal Structures. ASCE Yokohama, Japan, pp. 167-178.
- Trung, L., 2014. Overtopping on grass covered dikes: resistance and failure of the inner slopes. TU Delft, Delft University of Technology.
- Van Baars, S., Van Kempen, I., 2009. The causes and mechanisms of historical dike failures in the Netherlands. E-Water Official Publication of the European Water Association.
- Van Beek, V.M., 2015. Backward erosion piping: initiation and progression (PhD Thesis). PhD Dissertation Thesis, TU Delft, Delft University of Technology, 263 pp.
- Van Beek, V.M., Knoeff, H., Sellmeijer, J.B., 2011. Observations on the process of backward erosion piping in small-, medium- and full-scale experiments. European Journal of Environmental and Civil Engineering, 15(8): 1115-1137. DOI:10.1080/19648189.2011.9714844
- Van Beek, V.M., Vandenboer, K., Bezuijen, A., 2014. Influence of sand type on pipe development in small- and medium-scale experiments, Scour and Erosion: Proceedings of the 7th International Conference on Scour and Erosion, Perth, Australia, 2-4 December 2014. CRC Press, pp. 111.
- Van der Meer, J.W., 2002. Technical report wave run-up and wave overtopping at dikes, Rijkswaterstaat, DWW.
- Van der Meer, J.W., 2009. Coastal flooding: A view from a practical Dutchman on present and future strategies. In: Samuels P., H.S., Allsop W., Harrop J. (Ed.), European Conference on Flood Risk Management Research and Practice (FLOODRISK2008). Taylor and Francis, Oxford.
- Van der Meer, J.W., Hardeman, B., Steendam, G.J., Schuttrumpf, H., Verheij, H.J., 2010. Flow depths and velocities at crest and landward slope of a dike, in theory and with the wave overtopping simulator. Coastal Engineering Proceedings, 1(32): 10.
- Van der Meer, J.W., Janssen, J., Hydraulics, D., 1994. Wave run-up and wave overtopping at dikes and revetments. Delft Hydraulics.
- Van der Meer, J.W., Janssen, J.P., 1994. Wave run-up and wave overtopping at dikes and revetments. Delft hydraulics.
- Van der Meer, J.W., Steendam, G.J., de Raat, G., Bernardini, P., 2008. Further developments on the wave overtopping simulator, ASCE, proc. ICCE, pp. 2957-2969.
- Van der Meer, J.W., Van Hovern, A., Paulissen, M., Steendam, G.J., Verheij, H.J., Hoffmans, G.J.C.M., Kruse, G.A.M., 2012. Handreiking Toetsen Grasbekledingen op Dijken tbv het opstellen van het beheerdersoordeel (BO) in de verlengde derde toetsronde, Rijkswaterstaat, waterdienst.
- Van der Most, H., Táncoz, I., De Bruijn, K., Wagenaar, D., 2014. New Riskbased standards for flood protection in the Netherlands, Proceedings of the ICFM6 conference, pp. 16-18.
- Van Esch, J.M., Sellmeijer, J.B., Stolle, D., 2013. Modeling Transient Groundwater Flow and Piping under Dikes and Dams, 3rd International Symposium on Computational Geomechanics (ComGeo III).
- Van Gelder, P., 2000. Statistical methods for the risk-based design of civil structures. TU Delft, Delft University of Technology.

- van Gent, M.R.A., van den Boogaard, H.F.P., Pozueta, B., Medina, J.R., 2007. Neural network modelling of wave overtopping at coastal structures. *Coastal Engineering*, 54(8): 586-593. DOI:10.1016/j.coastaleng.2006.12.001
- Van Loon-Steensma, J.M., Vellinga, P., 2014. Robust, multifunctional flood defenses in the Dutch rural riverine area. *Nat. Hazards Earth Syst. Sci.*, 14(5): 1085-1098. DOI:10.5194/nhess-14-1085-2014
- Van, M.A., Koelewijn, A.R., Barends, F.B., 2005. Uplift phenomenon: model, validation, and design. *International Journal of Geomechanics*, 5(2): 98-106.
- Van Noortwijk, J.M., Vrouwenvelder, A.C.W.M., Calle, E.O.F., Slijkhuis, K.A.H., 1999. Probability of dike failure due to uplifting and piping. In: Kafka, G.I.S.a.P. (Ed.), *The 10th European Conference on Safety and Reliability (ESREL)*. Taylor & Francis, Munich-Garching, German, pp. 1616.
- Van Ree, C.C.D.F., Van, M.A., Heilemann, K., Morris, M.W., Royet, P., Zevenbergen, C., 2011. FloodProBE: technologies for improved safety of the built environment in relation to flood events. *Environmental Science & Policy*, 14(7): 874-883. DOI:10.1016/j.envsci.2011.03.010
- Van Veelen, P., Voorendt, M., van der Zwet, C., 2015. Design challenges of multifunctional flood defences. A comparative approach to assess spatial and structural integration. *Research in Urbanism Series*, 3(1): 275-292.
- Vandenbergh, S., Verhoest, N.E.C., De Baets, B., 2010. Fitting bivariate copulas to the dependence structure between storm characteristics: A detailed analysis based on 105 year 10 min rainfall. *Water Resources Research*, 46(1): n/a-n/a. DOI:10.1029/2009wr007857
- Vandenboer, K., Bezuijen, A., Van Beek, V., 2014a. 3D character of backward erosion piping: Small-scale experiments, *Scour and Erosion: Proceedings of the 7th International Conference on Scour and Erosion, Perth, Australia, 2-4 December 2014*. CRC Press, pp. 81.
- Vandenboer, K., Van Beek, V., Bezuijen, A., 2014b. 3D finite element method (FEM) simulation of groundwater flow during backward erosion piping. *Frontiers of Structural and Civil Engineering*, 8(2): 160-166. DOI:10.1007/s11709-014-0257-7
- Vellinga, P., Marinova, N., Van Loon-Steensma, J.M., 2009. Adaptation to climate change: A framework for analysis with examples from the Netherlands. *Built Environment (1978-)*: 452-470.
- Verheij, H.J., Hoffmans, G.J.C.M., Hardeman, B., Paulissen, M., 2012. Erosion at transitions in landward slopes of dikes due to wave overtopping, *ICSE 6: Proceedings of the 6th International Conference on Scour and Erosion, Paris, France, 27-31 August 2012*. Société Hydrotechnique de France (SHF).
- Verheij, H.J., Hoffmans, G.J.C.M., van der Meer, J., 2015. Evaluation and Model Development, *Grass Erosion Test at the Rhine dike, Deltares, Delft, Netherlands*.
- Verheij, H.J., Meijer, D.G., Kruse, G.A.M., Smith, G.M., Vesseur, M., 1995. *Onderzoek naar de sterkte van graszoden van rivierdijken, Deltares (WL)*.
- Victor, L., Van der Meer, J.W., Troch, P., 2012. Probability distribution of individual wave overtopping volumes for smooth impermeable steep slopes with low crest freeboards. *Coastal Engineering*, 64: 87-101. DOI:10.1016/j.coastaleng.2012.01.003

- Vienken, T., Dietrich, P., 2011. Field evaluation of methods for determining hydraulic conductivity from grain size data. *Journal of Hydrology*, 400(1-2): 58-71. DOI:10.1016/j.jhydrol.2011.01.022
- VNK2, 2014. De veiligheid van Nederland in kaart: Eindrapportage VNK, Rijkswaterstaat, projectbureau VNK.
- VNK2, Vergouwe, R., M.C.J., v.d.B., P., v.d.S., 2014. VNK2: Overstromingsrisico dijkkring 16 Alblasserwaard en de Vijfheerenlanden, Rijkswaterstaat WVI, The Netherlands
- Voortman, H.G., Vrijling, J.K., 2004. Optimal design of flood defence systems in a changing climate. *Heron*, 49 (1).
- Vorogushyn, S., Merz, B., Apel, H., 2009. Development of dike fragility curves for piping and micro-instability breach mechanisms. *Natural Hazards and Earth System Sciences*, 9(4): 1383-1401.
- Vrijling, J.K., 2001. Probabilistic design of water defense systems in The Netherlands. *Reliability Engineering & System Safety*, 74(3): 337-344. DOI:10.1016/S0951-8320(01)00082-5
- Vrijling, J.K., 2010. piping: Realiteit of rekenfout?, Rijkswaterstaat, Waterdienst.
- Vrijling, J.K., Van Hengel, W., Houben, R.J., 1998. Acceptable risk as a basis for design. *Reliability Engineering & System Safety*, 59(1): 141-150. DOI:10.1016/S0951-8320(97)00135-X
- Vrouwenvelder, A.C.W.M., 2001. The fundamentals of structural building codes, *Structural Engineering, Mechanics and Computation, Proceedings of the International Conference on Structural Engineering, Mechanics and Computation 2–4 April 2001, Cape Town, South Africa*, pp. 183-193.
- Vrouwenvelder, A.C.W.M., 2002. Developments towards full probabilistic design codes. *Structural Safety*, 24(2–4): 417-432. DOI:10.1016/S0167-4730(02)00035-8
- Vrouwenvelder, A.C.W.M., 2006. Spatial effects in reliability analysis of flood protection systems *Second International Forum on Engineering Decision Making, Lake Louise Canada*.
- Vrouwenvelder, A.C.W.M., Calle, E.O.F., 2003. Measuring spatial correlation of soil properties. *Heron*, 48(4): 297-311.
- VTV2006, M.v.V.e.W., 2007. Voorschrift toetsen op veiligheid: primaire waterkeringen voor de derde toetsronde 2006–2011 (VTV2006). Ministerie van Verkeer en Waterstaat, Den Haag.
- Vukovic, M., Soro, A., 1992. Determination of hydraulic conductivity of porous media from grain-size composition. *Water Resources Publications, Littleton, Colo.*, v, 83 p. pp.
- Wainwright, J., Mulligan, M., 2005. *Environmental modelling: finding simplicity in complexity*. John Wiley & Sons.
- Wang, D.Y., Fu, X.D., Jie, Y.X., Dong, W.J., Hu, D., 2014. Simulation of pipe progression in a levee foundation with coupled seepage and pipe flow domains. *Soils and Foundations*, 54(5): 974-984.
- WBI-2017, 2015. WBI-2017 - OI2014v3 Handreiking ontwerpen met overstromingskansen: Veiligheidsfactoren en belastingen bij nieuwe overstromingskansnormen, Rijkswaterstaat WVL.
- Weigao, W., 2015. Slope Stability Assessment Based on Limit Analysis, *Geotechnical Safety and Risk V, Rotterdam, The Netherlands*, pp. 263. DOI:10.3233/978-1-61499-580-7-263

- White, C.M., 1940. The Equilibrium of Grains on the Bed of a Stream. *Proceedings of the Royal Society of London. Series A, Mathematical and Physical Sciences*, 174(958): 322-338. DOI:10.2307/97393
- Yazdi, J., Salehi Neyshabouri, S.A.A., 2014. Adaptive surrogate modeling for optimization of flood control detention dams. *Environmental Modelling & Software*, 61: 106-120. DOI:10.1016/j.envsoft.2014.07.007
- Yen, B.-C., 1988. Stochastic methods and reliability analysis in water resources. *Advances in water resources*, 11(3): 115-122.
- Zanetti, C., Vennetier, M., Mériaux, P., Royet, P., Provansal, M., 2011. Managing woody vegetation on earth dikes: risks assessment and maintenance solutions. *Procedia Environmental Sciences*, 9: 196-200.
- Zangenehmadar, Z., Moselhi, O., 2016. Prioritizing deterioration factors of water pipelines using Delphi method. *Measurement*, 90: 491-499. DOI:10.1016/j.measurement.2016.05.001
- Zhang, J., Chen, H.Z., Huang, H.W., Luo, Z., 2015. Efficient response surface method for practical geotechnical reliability analysis. *Computers and Geotechnics*, 69(0): 496-505. DOI:10.1016/j.compgeo.2015.06.010
- Zhou, X.-j., Jie, Y.-x., Li, G.-x., 2012. Numerical simulation of the developing course of piping. *Computers and Geotechnics*, 44: 104-108. DOI:10.1016/j.compgeo.2012.03.010
- Zwanenburg, C., Van Duinen, A., Rozing, A., 2013. Technisch rapport macrostabiliteit, Deltares.

# Appendices

## A.1 GCDM Crest validation

For the validation of the RCDM by Bomers et al. (2016), a set of measurements taken by the measuring devices SB1, PW1 and PW2 (see (Verheij et al., 2015)) located at the midpoint of the road are taken as reference (see Figure A.1).

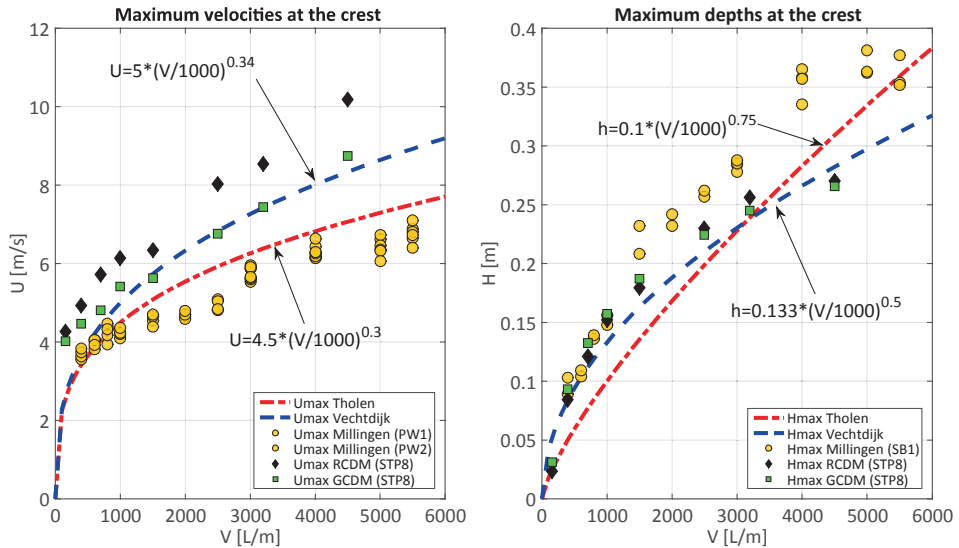


**Figure A.1 Validation of crest maximum velocity and maximum flow depths at PW1, SB1, and STP8**

The location where these measurements were taken, correspond to the exact STP8 location on both RCDM and GCDM. In addition, the fitted curves for the results of the WOS experiments of the Tholen dike and the Vecht dike are also included in Figure A.1 for the validation of the GCDM. The maximum values obtained for different wave volumes are plotted as squares for the GCDM case and diamonds for the RCDM case. The RCDM results differ significantly with respect to the measurements performed in Millingen (round dots) and the fitted curve of Tholen dijk. These last results were expected as according to the Millingen experiment report (Verheij et al., 2015), a geotextile cover was placed between the midpoint of the road and the foreland slope to cover the damaged transition. This choice was not included in the RCDM as its bottom profile corresponds to the q10\_sc2 scan without the geotextile. As asphalt is a much smoother surface than geotextile (see Table 4-2), the results of the RCDM result in higher velocities and lower depths with respect to the measurements from the Millingen

experiment part II. Additionally, it was also reported that the water depth measurements recorded by the SB1 meter were larger than expected when compared to the obtained values of other experiments. However, The results obtained for the GCDM in terms of flow depths and velocities, are in good agreement with the ones fitted for the Vechtdijk experiment (upper dashed line). Furthermore, they also show lower velocities and larger flow depths with respect to the RCDM as the grass is significantly rougher than asphalt. This result was also expected and shows how important is to include the surface roughness effects in the wave overtopping safety assessment.

## A.2 Landward slope validation

The second set of measuring devices (SB4 and PW4) during the Millingen experiment were located in the slope almost one meter further from the vertex of the crest and landward slope. This location corresponds to the STP28 in both RCDM and GCDM. The validation results for both models base on this location is presented in Figure A.2.

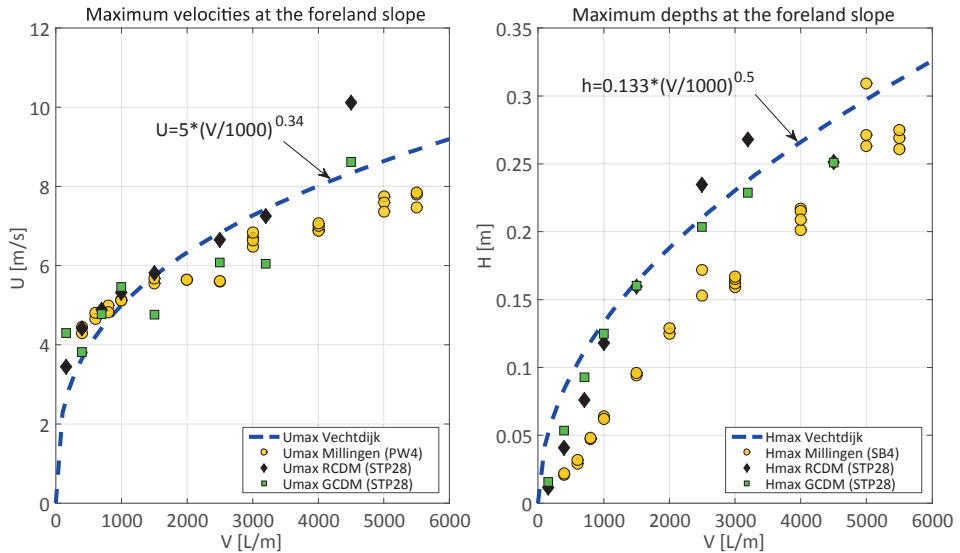


Figure A.2 Validation of slope maximum velocity and maximum flow depths at PW4, SB4, and STP28

The velocity measurements from Millingen and the results from the RCDM and GCDM show a fair agreement for waves with volumes which are less than 3500 L/m. In the case of the flow depths, both GCDM and RCDM differ significantly from the recorded values during the experiment. Again these differences could be attributed to the Geotextile upstream effects. The measuring devices accuracy should also be included in this analysis but unfortunately, it was not available in the literature. Nevertheless, the models results show good agreement and expected behaviour with respect to the fitted curve for the slope measurements in the Vechtdijk presented in (Van der Meer et al., 2010). Nevertheless, the results obtained for wave volumes greater than 3500 L/m are further discarded as they present an erratic behaviour.

### A.3 Overtopping times validation

Waves of 150, 400, 700, 1000, 1500, 2500, 3200 and 4500 L/m were simulated in both RCDM and GCDM.

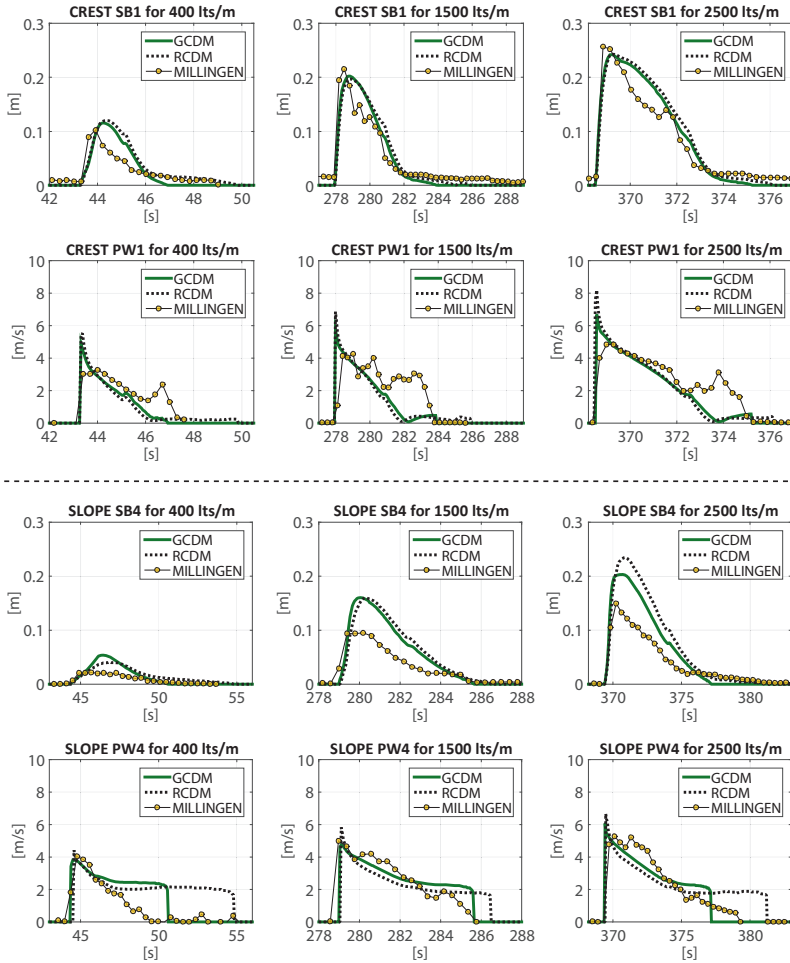
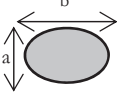


Figure A.3 Validation of overtopping times for different wave volumes

The overtopping times coincide for the case of the flow depth measured time series but not for the velocity time series. This result is interesting as it shows that there is a discrepancy originated from the precision of both SB and PW meters.

## A.4 Friction loss coefficients ( $\beta_{fi}$ ) for different cross sections

Table A.1 Different cross section parameters used for fictitious permeability calculation with their corresponding  $\beta_{fi}$  (Bersan et al., 2013; Muzychka & Yovanovich, 2009)

Channel Cross section	$b/a$	$D_h$	$\beta_{fi}$
Square 	1	$a$	56.92
Rectangular 	16	$\frac{4ab}{(2a + 2b)}$	85.58
Circular 	1	$a$	64.00
Ellipsoid 	16	$\frac{2ba(64 - 16(\frac{b-a}{b+a})^2)}{(b+a)(64 - 3(\frac{b-a}{b+a})^4)}$	76.77
Fracture 	$\infty$	$2a$	96.00

## A.5 Sellmeijer modified limit state function 2011

In 2011 the original equation was modified and calibrated based on the two forces approach explained previously in section 3.3.2. However, this equation is not corrected by the scaling factors presented as an end result in (H. Sellmeijer et al., 2011). The updated expressions are presented in equations A1 to A5 as:

$$Z_{\text{Sellmeijer}} = H_c - (H - h_b - 0.3d) \quad \text{A1}$$

$$H_c = m_p (F_G) (F_R) (F_S) L \quad \text{A2}$$

$$F_S = \frac{d_{70}}{\sqrt[3]{\left(\frac{\nu K}{g}\right) L}} \quad \text{A3}$$

$$F_R = \eta \frac{\gamma'_s}{\gamma_w} \tan(\theta) \quad \text{A4}$$

$$F_G = 0.91 \left(\frac{D}{L}\right)^{\left(\frac{0.28}{\left(\left(\frac{D}{L}\right)^{2.8} - 1\right)} + 0.04\right)} \quad \text{A5}$$

**Table A.2 Sellmeijer 2011 revised equation nomenclature:**

<b>Z<sub>p</sub></b>	[m]	Residual resistance (Limit State)
<b>η</b>	[-]	White's sand packing coefficient (0.25)
<b>γ'<sub>s</sub></b>	[kN/m <sup>3</sup> ]	Unitary weight of submerged sand particles
<b>γ<sub>w</sub></b>	[kN/m <sup>3</sup> ]	Unitary weight of water
<b>θ</b>	[deg]	Bedding angle of sand grains
<b>d<sub>70</sub></b>	[m]	70 percent quintile value grain size distribution of sand layer
<b>d<sub>70m</sub></b>	[m]	Calibration reference value (2.08 x 10 <sup>-4</sup> m)
<b>ν</b>	[m <sup>2</sup> /s]	Kinematic viscosity of water at 20 °C
<b>K</b>	[m/s]	Hydraulic conductivity of sand
<b>g</b>	[m/s <sup>2</sup> ]	Gravitational acceleration (9.81m/s <sup>2</sup> )
<b>D</b>	[m]	Average thickness of sand aquifer
<b>m<sub>p</sub></b>	[-]	Modelling uncertainty factor
<b>H<sub>c</sub></b>	[m]	Critical hydraulic head difference
<b>F<sub>R</sub></b>	[-]	Resistance factor
<b>F<sub>S</sub></b>	[-]	Scale factor
<b>F<sub>G</sub></b>	[-]	Geometric factor
<b>L</b>	[m]	Seepage length from entrance point to sand boil water exit
<b>H</b>	[m]	Water level in the foreside of the flood defence
<b>h<sub>b</sub></b>	[m]	Water level at hinter side outflow point
<b>d</b>	[m]	Impermeable layer thickness at the sand boil exit point

# List of Figures

Figure 1-1 “Super Levee” board in Oshima Komatsugawa Park, Tokyo (Japan Times, (Brasor, 2010)).....	2
Figure 1-2 House and road in the Lekdijk in Vianen – Utrecht province .....	3
Figure 1-3 Schematics of the most dominant failure mechanisms.....	4
Figure 1-4 Fault tree of flood defence .....	12
Figure 1-5 New flood standards by segment according to the .....	14
Figure 1-6 Influence zones of structural embedments.....	16
Figure 1-7 Design choices.....	18
Figure 1-8 General thesis research methodology.....	25
Figure 2-1. PE process under flood defence .....	31
Figure 2-2. a) $d_{70}$ vs $K$ and b) marginal probabilities $U(d_{70})$ vs $V(K)$ .....	43
Figure 2-3. Generated empirical probability contours (dashed) vs Gumbel, Gauss and Clayton copula probability contours with rank correlation coefficient $\tau=0.692.44$	
Figure 2-4. SAPE of the three different copula functions.....	45
Figure 2-5. Root mean square errors for different Kendall’s rank correlation coefficients estimated from the 76 samples. ....	46
Figure 2-6. Generated copula samples of $d_{70}$ representative grain size diameter versus hydraulic conductivity for different correlation degrees (Kendall’s tau coefficient).....	48
Figure 2-7. Probability density functions of LSE for different copulas with different correlation.....	49
Figure 2-8. PE/Uplift $\beta$ index of the Lekdijk flood defence as a function of rank correlation coefficient ( $\tau$ ) with 95% confidence bounds .....	50
Figure 3-1 IJkdijk cross section for piping erosion test (not in scale) .....	63
Figure 3-2 Methodology flow chart.....	64
Figure 3-3 IJkdijk cross section and boundary conditions of FEM models with and without embedded sewer pipe.....	65
Figure 3-4 Two forces grain equilibrium model inside the erosion channel. ....	69
Figure 3-5 Required erosion channel height (in terms of $ng$ ), for different cross section geometries. ....	74
Figure 3-6 Required erosion channel height (in terms of $ng$ ), for different aquifer permeability ( $k$ ) values. ....	76
Figure 3-7 Required erosion channel height (in terms of $ng$ ), for different aquifer depths. ....	77

Figure 3-8 Stability factor as a function of location for a) 0.5 m diameter, b) 0.8 m diameter, c) 1.0 m diameter, d) 1.2 m diameter .....	78
Figure 3-9 ANN emulator architectures R2.....	81
Figure 3-10 a) PDF of Z for the Sellmeijer revised equation (Thick black line), FEM (Thin blue line) and Emulator (Dashed line). b) CDF of Z for the Sellmeijer revised equation (Thick black line), FEM (Thin blue line) and Emulator (Dashed line). .....	82
Figure 3-11 Failure probabilities as a function of the main random variables with different CV .....	83
Figure 3-12 $\beta$ indexes for different aquifer depths and permeability CV's .....	85
Figure 4-1 Excess shear stress integral over time for different critical thresholds .....	94
Figure 4-2 Millingen WOS experiment with road on top of the crest.....	96
Figure 4-3 Methodology flow chart for emulator construction and probabilistic safety assessment .....	99
Figure 4-4 CFD models boundary conditions (schematic meshing not in actual size) .....	100
Figure 4-5 Study points (STPs) location for RCDM and GCDMs.....	102
Figure 4-6 3D linear interpolation surfaces for locations before and after the landward transition .....	103
Figure 4-7 Scouring depths (e) calculated from profiles q10_sc2 and q50_sc5 profiles .....	105
Figure 4-8 Critical velocity vs critical shear stress threshold equivalence curve from (Hoffmans, 2012) .....	109
Figure 4-9 Mean values of T and confidence intervals of RCDM and GCDM.....	111
Figure 4-10 CE curves for each STP for grass and clay .....	112
Figure 4-11 Results of scouring profiles for different storms on good grass quality .	113
Figure 4-12 Results of scouring profiles for different storms on average grass quality .....	114
Figure 4-13 Results of scouring profiles for different storms on poor grass quality .	115
Figure 4-14 Results of scouring profiles for different storms with spatial distribution the Millingen dike .....	116
Figure 4-15 Failure probabilities per storm along the right side of the profile in each STP for different grass qualities .....	117
Figure 4-16 Failure probabilities per storm in each STP for Millingen dike realistic grass qualities.....	118
Figure 5-1 $\beta$ indexes of different designs for varying correlation degrees ( $\tau$ ).....	127
Figure 5-2 Fault tree with allocated failure budgets.....	142

# List of Tables

Table 1-1. Failure probability budget factors per failure mechanism (WBI-2017, 2015)	13
Table 1-2. Failure mechanisms modelling studies with different complexities	19
Table 2-1. Copula families and generator functions	36
Table 2-2. Equivalence expressions between dependence Copula generator parameters and Kendall's ranking correlation coefficient ( $\tau$ )	37
Table 2-3. Input data for stochastic failure estimation of PE	40
Table 2-4. Kendall's correlation coefficient between variables	42
Table 2-5 Anderson Darling test results for the three Copula fittings	47
Table 2-6 Obtained Standard deviation of $Z_p$ for different rank correlation copulas	48
Table 3-1 IJkdijk experiment 3 parameters and results	63
Table 3-2 Prior distributions of random variables for FEM models and Sellmeijer limit state equation	73
Table 3-3 Validation results of emulators ( $\Omega$ ) versus FEM output as a function of different number of hidden layers (H.L.)	84
Table 4-1 Profile scanning times for part I of Millingen experiment	97
Table 4-2 Roughness coefficients used for both road and crest models	101
Table 4-3 Storm boundary conditions for riverine dike	108
Table 4-4 Stochastic random variables of cover quality used as input for CE calculation	109
Table 5-1 Stochastic Soil properties of hypothetical case (C.V. stands for coefficient of variation)	126
Table 5-2 Safety change assessment by design choice	143



# List of Symbols

## Abbreviations

AD <sup>2</sup>	Two sample Anderson-Darling value for normally distributed variables
AD <sup>2</sup> <sub>kn</sub>	Two sample Anderson-Darling value for general distributions
ANN	Artificial neural network
ASD	Allowable stress design
CDF	Cumulative density function
CFD	Computational fluid dynamics
FEM	Finite element model
GCDM	Grass crest dike model
LSD	Limit state design
LSE	Limit state equation
PDF	Probability density function
PW	Paddle wheel meter
QCF	Grass quality correction factor
RANS	Reynolds average Navier-Stokes model
RCDM	Road on crest dike model
RMSE	Root mean squared error
SAPE	Spatial absolute percentual error
SB	Surf Board meter
SF	Safety Factor
STP	Study point
VNK	Veiligheid Nederland in Kaart - ( <i>Dutch safety mapping</i> )
WOS	Wave overtopping simulator

## Roman

$a$	Erosion channel height (Chapter 3)	[m]
$a$	Minor geometrical dimension (Chapter 3)	[m]
$a$	Weibull fit scale parameter (Chapters 2, 3 and 4)	[-]
$b$	Weibull fit shape parameter (Chapters 2, 3 and 4)	[-]
$b$	Major geometrical dimension (Chapter 3)	[m]
$C(u,v)$	Joint copula function of $u$ and $v$	[-]
$C_E$	Coefficient of erosion	[s/m]
$\overline{C_E}$	Mean erodability coefficient	[s/m]
$C_{emp}$	Empirical copula function	[-]

$C_{family}$	Copula function for any given family	[-]
CV	Coefficient of variation	[-]
$CV_k$	Hydraulic conductivity coefficient of variation	[-]
D	Average thickness of sand layer	[m]
d	Impermeable layer thickness at the sand boil exit point (Chapter 2)	[m]
d	Generalized representative size of grain (Chapter 3)	[m]
$d_{10}$	10 <sup>th</sup> Percentile representative size of grain	[m]
$d_{60}$	60 <sup>th</sup> Percentile representative size of grain	[m]
$d_{70}$	70 <sup>th</sup> Percentile representative size of grain	[m]
$d_{70m}$	70 <sup>th</sup> Percentile calibration reference value (2.08 x 10 <sup>-4</sup> m)	[m]
$D_h$	Hydraulic diameter	[m]
$d_m$	Representative grain diameter	[m]
f	Flow friction factor	[-]
$F_G$	Geometric factor	[-]
$F_R$	Resistance factor	[-]
$F_S$	Scale factor	[-]
$F_X(x)$	Cumulative distribution function of the random variable x	[-]
$F_{XY}(x,y)$	Joint cumulative distribution function of the random variable x and y	[-]
$F_Y(y)$	Cumulative distribution function of the random variable y	[-]
g	Gravitational acceleration (9.81m/s <sup>2</sup> )	[m/s <sup>2</sup> ]
h	Water pressure head	[m]
H	Water level in the riverside of the flood defence	[m]
$h_b$	Water level at hinter side outflow point	[m]
$H_c$	Critical PE resistance head	[m]
$H_S$	Significant wave height	[m]
i	i <sup>th</sup> value	[-]
j	j <sup>th</sup> value	[-]
k	Intrinsic permeability	[m <sup>2</sup> ]
K	Hydraulic conductivity of sand	[m/s]
$K_s$	Equivalent sand roughness	[m]
L	Seepage length from entrance point to sand boil water exit	[m]
m	mass	[kg]
$M_{ij}$	Number of observations of the i <sup>th</sup> sample larger than the k <sup>th</sup> value	[-]
$M_p$	Soil mass transport coefficient	[kg/(m <sup>2</sup> .s)]
$m_p$	Piping modelling uncertainty factor	[-]
n	Soil porosity	[-]

N	Number of random samples	[-]
n	Manning roughness coefficient	[s/m <sup>1/3</sup> ]
n <sub>g</sub>	Number of grains coefficient	[-]
N <sub>ow</sub>	Number of overtopping waves	[-]
N <sub>w</sub>	Number of waves	[-]
p	Pressure head	[m]
P	Pressure head boundary condition	[m]
P <sub>f</sub>	Probability of failure	[1/year]
P <sub>fpe</sub>	Probability of failure due to piping erosion	[1/year]
P <sub>fpe/uplift</sub>	Probability of failure due to piping erosion given uplift failure	[1/year]
q <sub>m</sub>	Storm average overtopping discharge per unit of width	[L/s/m]
R	Resistance term of the reliability limit state function	[variable]
R <sub>c</sub>	Dike free crest height	[m]
Re	Reynolds number	[-]
S	Load term of the generalized limit state function	[-]
t	time	[s]
T <sub>p</sub>	Peak period	[s]
U	Transformed dimensionless random variable of x	[-]
U <sub>c</sub>	Critical erosion velocity	[m/s]
u	Marginal probability value of variable x (Chapter 2)	[-]
u	Horizontal Darcyan flow velocity (Chapter 3)	[m/s]
V	Transformed dimensionless random variable of x (Chapter 2)	[-]
V	Wave volume per unit of width (Chapter 4)	[L/m]
V <sub>max</sub>	Maximum wave volume per unit of width	[L/m]
v	Marginal probability value of variable y (Chapter 2)	[-]
v	Velocity boundary condition (Chapter 3)	[m/s]
X	Horizontal sewer pipe coordinate	[m]
X <sub>n</sub>	Stochastic random variable of the resistance term	[-]
x <sub>n</sub>	Deterministic variable of the resistance term	[-]
Y	Vertical sewer pipe coordinate	[m]
Y <sub>n</sub>	Stochastic random variable of the load term	[-]
y <sub>n</sub>	Deterministic random variable of the load term	[-]
Z	Reliability term of the generalized limit state function	[-]
Z <sub>G</sub>	Reliability term of wave overtopping limit state of GCDM	[m]
Z <sub>p</sub>	Limit state residual resistance for Sellmeijer limit state equation	[m]
Z <sub>R</sub>	Reliability term of wave overtopping limit state of RCDM	[m]
Z <sub>Sellmeijer</sub>	Reliability term from Sellmeijer modified function	[m]
Z <sub>wo</sub>	Reliability term of wave overtopping limit state equation	[m]

## Greek

$\alpha$	Correlation parameter for Archimedean copula functions	[-]
$\beta$	Reliability index	[m]
$\beta_{fi}$	Geometrical cross section laminar flow factor	[-]
$\varepsilon$	Grass cover thickness	[m]
$\varepsilon_G$	Cover thickness at grass crest model study point	[m]
$\varepsilon_R$	Cover thickness at road on crest model study point	[m]
$\theta$	General correlation copula variable (Chapter 2)	[-]
$\theta$	Bedding angle of sand grains of Sellmeijer's limit state	[deg]
$\Phi$	Normal distribution	[-]
$\gamma$	Soil volumetric weight	[kN/m <sup>3</sup> ]
$\gamma'_s$	Unitary weight of submerged sand particles	[kN/m <sup>3</sup> ]
$\gamma_w$	Water volumetric weight	[kN/m <sup>3</sup> ]
$\mu$	Water dynamic viscosity	[kg.s/m]
$\eta$	White's sand drag force factor (0.25)	[-]
$\Omega$	Pressure gradient Emulation function	[m/m]
$\omega$	Failure budget coefficient	[-]
$\Omega_G$	Emulation function of shear stress excess of GCDMI study point	[N.s/m <sup>2</sup> ]
$\Omega_R$	Emulation function of shear stress excess of RCDM study point	[N.s/m <sup>2</sup> ]
$\phi$	Soil repose angle	[deg.]
$\theta$	Bedding angle of sand grains of Sellmeijer's limit state	[deg.]
$\rho$	Water density	[kg/m <sup>3</sup> ]
$\rho$	Pearson's correlation coefficient	[-]
$\rho'_{cover}$	Submerged cover density	[kg/m <sup>3</sup> ]
$T$	Shear stress excess	[N.s/m <sup>2</sup> ]
$\tau$	Kendall's correlation coefficient (Chapter 2)	[-]
$\tau$	Shear stress (Chapter 4)	[N/m <sup>2</sup> ]
$\tau_G$	Shear stress in time of grass crest model study point	[N/m <sup>2</sup> ]
$\tau_R$	Shear stress in time for the road on crest model study point	[N/m <sup>2</sup> ]
$\tau_c$	Critical shear stress	[N/m <sup>2</sup> ]
$\tau_{max}$	Maximum shear stress	[N/m <sup>2</sup> ]
$\bar{\tau}$	Average shear stress excess	[N/m <sup>2</sup> ]
$\nu$	Kinematic viscosity of water at 20 °C	[m <sup>2</sup> /s]

# List of Publications

## Peer-reviewed journal articles

- Aguilar-López, J.P., Warmink, J.J., Schielen, R.M.J., Hulscher, S.J.M.H., 2016a. Piping erosion safety assessment of flood defences founded over sewer pipes. *European Journal of Environmental and Civil Engineering*: 1-29. DOI:10.1080/19648189.2016.1217793
- Aguilar-López, J.P., Warmink, J.J., Schielen, R.M.J., Hulscher, S.J.M.H., 2016b. Soil stochastic parameter correlation impact in the piping erosion failure estimation of riverine flood defences. *Structural Safety*, 60: 117-129. DOI:10.1016/j.strusafe.2016.01.004
- Aguilar-López, J.P., A. Bomers, Warmink, J.J., Schielen, R.M.J., Hulscher, S.J.M.H., 2016. Wave overtopping probabilistic safety assessment of flood defences with roads on top. Submitted for publication
- Bomers, A., Aguilar-López, J.P., Warmink, J.J., Hulscher, S.J.M.H., 2016. Modelling effects of an asphalt road at a dike crest on erosion patterns during wave overtopping. Submitted for publication

## Conferences proceedings

- Bomers, A., Aguilar-López, J.P., Warmink, J.J., Hulscher, S.J.M.H., (2016). Modelling erosion development during wave overtopping of an asphalt road covered dike (Conference Paper), FLOODrisk2016 - 3rd European Conference on Flood Risk Management, Innovation, Implementation and Integration, Lyon, France
- Aguilar López, J.P., Warmink, J.J., Schielen, R.M.J. & Hulscher, S.J.M.H. (2015). Correlation effect in probabilistic design against piping in multi-functional flood defences, doi: 10.3233/978-1-61499-580-7-239. In T. Schweckendiek, A.F. van Tol, D. Peereboom, A. van Staveren & P.M.C.B.M. Cools (Eds.), *Geotechnical Safety and Risk V* (pp. 239-244). Amsterdam, The Netherlands

- Aguilar López, J. P., Warmink, J. J., Schielen, R. M. J., and Hulscher, S. J. M. H. (2015), Surrogate modelling for failure probability estimation of multifunctional flood defences (Conference Paper) 36<sup>th</sup> IAHR2015 World Congress - Den Haag- The Netherlands.
- Aguilar López, J. P., Warmink, J. J., Schielen, R. M. J., and Hulscher, S. J. M. H. (2014). Data-driven surrogate models for flood defence failure estimation: "Jarillon de Calí" (Conference Paper). 11th IWA/IAHR International Conference on Hydro informatics, New York City, UA.
- Aguilar López, J. P., Van Andel, S. J., Werner, M., and Solomatine, D. P. (2014), Hydrodynamic and water quality surrogate modelling for reservoir operation (Conference Paper). 11th IWA/IAHR International Conference on Hydro informatics New York City, USA.
- Aguilar López, J. P., Warmink, J. J., Schielen, R. M. J., and Hulscher, S. J. M. H. (2013), Flood defence design parameters correlation influence on failure probability - Case study of piping (Conference Paper). 3rd IAHR Europe Congress - Water Engineering and Research Porto, Lisbon.

## MSc thesis supervision

- Bomers, A. – Road impact on erosion development during overtopping flood events (2015), – University of Twente
- Groot, T. - Macro-stability safety assessment for flood defences with buried pipes (2015), University of Twente
- Kramer, R. - Piping under transient conditions: investigation of time-dependent erosion under dikes (2014), University of Twente

# Acknowledgments

I firmly believe that our main purpose and what gives meaning to life is to help others achieve what they think they can achieve on their own. Despite the fact that this book has only my name on the cover, I could have not finished this book without:

- The guidance, support and enthusiasm of Professor Suzanne Hulscher and Dr. Ralph Schielen who always reminded me the importance of my research topic.
- My daily supervisor Dr. Jord Warmink who always had time for me and for reading thoroughly my “short” and “synthetic” paper drafts. But more important, who picked me up at the train station on day one with a box of food for the first days which shows the kind of human being he is.
- The enormous help of Raymond van der Meij from Deltares since day one to the point he ended up being appointed as “Project user” without previous notice.
- My office mate Joep, who later ended up being my good friend, band mate (both Swafflers and Kapsalons) but more important my *homie* who also “had love for the streets”. Cause every Friday should be a “Kanye Friday!”
- My personal Dutch teacher and good friend Lianne, who always was kind enough to laugh about my jokes and who made the office a nicer place to be.
- Dr. Leonardo A.K.A. “Dr. Mojo” and family (Loreto, Pelusa and Blanquita) who took care of me whenever I was home alone by having me over for a nice dinner and more than few drinks. But more important, who kindly listened to my stories despite they were a bit “exaggerated”.
- My good friend Àngels (and her “Churri” Rotman) who always had a “piti” and a “ya estas! no te falta nada!” whenever the path seemed dark.
- My good friend Filipe (and his lovely wife Stephanie), who always took care of the Waaier menu so we don’t miss “Shoarma day” and kept always the band on tempo with his awesome drumming.
- The university but non-work related friends like Nico, Caro Kreidler, Dani-Renata (the last two with a dash as they cannot be separated), Marcela, Ana Paula, Ivo, Marina, Enrique, Nico-Chile, Nekane, Lissy, Vamsy, Diego (Pasto), Javi, Caro Valladares, Enrico, Sergio, Marina, and Adriana (Yes! you the angry chamita from Venezuela) who made Twente an ever nicer place to be.
- My good friends Gerard (his family) and Nilo who are part of my small family of the Netherlands. You are what we call in Colombia “el compadre y la comadre”.
- Julieta my good friend from the NS train company with whom I developed a really nice friendship (and the Lego Game) and with whom I shared long talks about life, politics, wine and thoughts that came into her mind in her last trip to Mongolia.
- Denic, Kathalijne, Jan, Pieter, Bas, Arjen, René and Joanne who helped me every time I was “in a pickle” and greeted me with a nice “Goedemorgen”.

- My three amazing MSc. students (Anouk, Tijmen and Renier) who helped me with my research. Literally, I could not have done it without you guys.
- The MFFD research group and specially Baukje and Trudes for being the glue of the group.
- My former PhD colleagues (Suleyman, Eric, Olav, Geert, Isaac, Louisa, Caroline, Wenlong, Abebe, Hatem, La, Michiel, Pim, Koen, John, Johan, Pepijn, Valesca, Hero, Rick and Joep).
- Anke, Joke, Monique and Brigitte who always helped me with everything I needed while offering a nice smile and who never got annoyed by all my questions (I hope).
- Always counted on the daily Dutch practice small talk of the lovely Anne-Marie and Marieke in the cafeteria and who spoiled me with the occasional “wij zijn gesloten maar...” coffee after 16:00.
- All my family back in Colombia, specially Jairo, Nohora, Cata and “Cintura de Mico” who have always made their home my home.
- Juliette my step sister with whom we have shared this adventure since day one. Thanks for everything and that also includes you Yared my good friend (Haile Selassie ... I)
- All the nice friends from UNESCO-IHE (Saul, Assiyeh, Sergio, Carola, Jeniffer, Neiler, Juan Carlos, Angelica, Mauri, Veronica, Patricia, Ana, Aleyda, Arlex and Nora).
- To my new Boss, Thom who has been very supportive in this final stage of my PhD.
- The VL crew back in Colombia who I miss so much.
- Fabio (and Mechy) and Naty who more than friends are brothers to me.

With that being said, I would like to dedicate this book to:

- My Mother who has been an inspiration to achieve everything I wanted in life and who always took care that me and my brother never forgot that people is the only and most important thing in life. My father who has been always an inspiration of how the passion for what you do will take you to unimaginable places in life. To both of you, thanks for being my best friends.
- To my brother Cesar (and Yuka and Tonka) because since we were kids you have always take care of me and because you still do. When I grow up, I want to be like you.
- To my beautiful Mireia who is a daily source of inspiration of how to be unstoppable. I admire you so much like you cannot imagine. You are the best thing that has happened to me. Te vull molt ♥ !

*El pensamiento currambero  
Es pensamiento rebelde  
Optimo, optimo, optimo positivo ,  
Buen voltaje y amor...  
Bacaneria total !*

*Humberto Pernet, 2004.*

## About the Author

Juan Pablo Aguilar López was born on the 9<sup>th</sup> of December of 1981 in the city of Bogotá in Colombia. He obtained his civil engineering degree in 2005 from the Colombian school of engineering “Julio Garavito”. In 2007, he finished his research on culvert scale modeling for peak discharge estimation for which he obtained the post-degree title of water resources specialist from the same institution. Later on, he moved to Delft where he obtained his MSc. degree in Hydro-informatics from the Unesco-IHE institute in 2011. His research topic consisted in the development of a multi-purpose reservoir operation optimization method in combination with a water quality emulator based forecasting system. By mid-2012, Juan Pablo started his PhD at the University of



Twente, on the influence of structural embedments in the probabilistic safety assessment of multi-functional flood defences. At the moment (2016), Juan Pablo is appointed as Post-doc fellow researcher of the Technical University of Delft for the European DOMINO project for developing a fibre optics based sensor for flood defence monitoring. Juan Pablo has also worked as a consultant in multiple flood management consultancy projects in the areas of hydraulics, hydrology and geotechnics. His main research interest is the development of artificial intelligence model emulators for forecasting, early warning and reliability assessment of water related systems. He is also the guitar player and lead singer of the Punk rock cover band “De Kapsalöns”. He enjoys cooking and baking and not taking himself too seriously.

